

NONLINEAR AND DISTRIBUTED SENSORY ESTIMATION

A Dissertation

by

SURANTHIRAN SUGATHEVAN

Submitted to the Office of Graduate Studies of  
Texas A&M University  
in partial fulfillment of the requirements for the degree of

DOCTOR OF PHILOSOPHY

May 2004

Major Subject: Mechanical Engineering

NONLINEAR AND DISTRIBUTED SENSORY ESTIMATION

A Dissertation

by

SURANTHIRAN SUGATHEVAN

Submitted to Texas A&M University  
in partial fulfillment of the requirements  
for the degree of

DOCTOR OF PHILOSOPHY

Approved as to style and content by:

---

Suhada Jayasuriya  
(Chair of Committee)

---

Shankar P. Bhattacharyya  
(Member)

---

Alexander G. Parlos  
(Member)

---

Won-jong Kim  
(Member)

---

Dennis O'Neal  
(Head of Department)

May 2004

Major Subject: Mechanical Engineering

## ABSTRACT

Nonlinear and Distributed Sensory Estimation. (May 2004)

Suranthiran Sugathevan, B.S., University of Peradeniya, Sri Lanka;

M.S., University of Cambridge, England

Chair of Advisory Committee: Dr. Suhada Jayasuriya

Methods to improve performance of sensors with regards to sensor nonlinearity, sensor noise and sensor bandwidth are investigated and new algorithms are developed. The necessity of the proposed research has evolved from the ever-increasing need for greater precision and improved reliability in sensor measurements. After describing the current state of the art of sensor related issues like nonlinearity and bandwidth, research goals are set to create a new trend on the usage of sensors.

We begin the investigation with a detailed distortion analysis of nonlinear sensors. A need for efficient distortion compensation procedures is further justified by showing how a slight deviation from the linearity assumption leads to a very severe distortion in time and in frequency domains. It is argued that with a suitable distortion compensation technique the danger of having an infinite bandwidth nonlinear sensory operation, which is dictated by nonlinear distortion, can be avoided. Several distortion compensation techniques are developed and their performance is validated by simulation and experimental results. Like any other model-based technique, modeling errors or model uncertainty affects performance of the proposed scheme, which leads to the innovation of robust signal reconstruction. A treatment for this problem is given and a novel technique, which uses a nominal model instead of an accurate model and produces the results that are robust to model uncertainty, is developed.

The means to attain a high operating bandwidth are developed by utilizing sev-

eral low bandwidth pass-band sensors. It is pointed out that instead of using a single sensor to measure a high bandwidth signal, there are many advantages of using an array of several pass-band sensors. Having shown that employment of sensor arrays is an economic incentive and practical, several multi-sensor fusion schemes are developed to facilitate their implementation.

Another aspect of this dissertation is to develop means to deal with outliers in sensor measurements. As fault sensor data detection is an essential element of multi-sensor network implementation, which is used to improve system reliability and robustness, several sensor scheduling configurations are derived to identify and to remove outliers.

To Almighty Bhagavan Sri Sathya Sai Baba

## ACKNOWLEDGMENTS

This dissertation is the conclusion of three years of research in the Department of Mechanical Engineering at Texas A&M University. Many people have helped me over the past three years and it is my great pleasure to take this opportunity to express my gratitude to them all.

Firstly, I would like to express my sincere gratitude to my advisor, Professor Suhada Jayasuriya, for giving me the opportunity to pursue a doctoral research program in nonlinear sensors and sensor arrays. His expertise, constant support, encouragement, guidance and the beautiful insight of control theory have proved invaluable in every step of this work.

I am grateful to Professors Bhattacharyya, Parlos and Won-jong Kim for agreeing to serve on my degree committee and some useful suggestions. I would also like to thank Professors Chan and Fleming for the useful discussions.

I would like to thank Ukpai Ukpai and May Douglas Conrad for their help in setting up the experiment and Esteban Irigoyen for proofreading some of my papers.

The support received from the National Science Foundation under Grant No. CMS-0097719 is gratefully acknowledged.

I save my last special thanks for Anusha who has offered unconditional love and support through the most difficult time of this process.

## TABLE OF CONTENTS

CHAPTER		Page
I	INTRODUCTION . . . . .	1
	A. Motivation . . . . .	1
	B. Objectives . . . . .	10
	C. Dissertation Overview . . . . .	11
II	PRELIMINARIES . . . . .	13
	A. Definitions and Theorems . . . . .	13
III	LITERATURE REVIEW . . . . .	17
	A. Nonlinear Distortion Analysis and Signal Reconstruction . . . . .	17
	B. Conditioning of Distorted Measurements . . . . .	19
	1. Signal Conditioning . . . . .	19
	2. Filtering . . . . .	19
	3. Smoothing . . . . .	20
	C. Multiple Sensor Fusion Techniques . . . . .	20
	1. Estimation Methods . . . . .	25
	a. Linear Weighted Averaging . . . . .	25
	b. Kalman Filtering . . . . .	25
	c. Least Square Estimation . . . . .	26
	2. Classification Methods . . . . .	26
	3. Inference Methods . . . . .	27
	4. Artificial Intelligence Methods . . . . .	27
	a. Dempster-Shafer Theory . . . . .	27
	b. Fuzzy Logic . . . . .	28
	c. Neural Networks . . . . .	28
IV	CONDITIONING OF DISTORTED SENSOR MEASUREMENTS . . . . .	29
	A. Nonlinear Distortion Analysis . . . . .	29
	B. Recovery of Band-limited Signals . . . . .	34
	C. Recovery of Corrupted/Noisy Band-limited Signals . . . . .	39
	D. Effect of Modeling Errors . . . . .	43
	E. Recovery of Signals Corrupted by Non-stationary Noise . . . . .	45
	1. Wavelets and Filter Banks . . . . .	45

CHAPTER	Page
2. Removal of Noise in Sensor Output . . . . .	47
F. Recovery of Chirp Signals . . . . .	50
1. Reconstruction of Bandlimited Chirp Signals . . . . .	50
2. Example 1 . . . . .	51
3. Example 2 . . . . .	53
G. Recovery of Signals Using Nominal Sensor Model . . . . .	55
H. Signal Recovery in Discrete Domain . . . . .	59
1. Signal Recovery Procedure . . . . .	63
2. Special Case: Negative Gradients . . . . .	68
I. Signal Recovery with Non-monotonic Sensor Function . . . . .	69
J. Recovery of Signals Distorted by Non-invertible Sensor Nonlinearity . . . . .	71
1. Motivation . . . . .	71
2. Non-quadratic Regularization . . . . .	74
3. Optimization of Non-quadratic Cost Functions . . . . .	80
4. Illustrative Example . . . . .	81
V FUSION OF DISTORTED MULTI-SENSOR MEASUREMENTS	87
A. Fusion of Distorted Multi-sensor Data by Sensor Scheduling	87
1. Example 1 . . . . .	90
2. Implementation Scheme . . . . .	93
3. Example 2 . . . . .	100
B. Fusion of Distorted Data by Continuous Optimization . . . . .	105
1. Implementation Scheme . . . . .	107
2. Example 1 . . . . .	110
3. Example 2 . . . . .	111
4. Example 3 . . . . .	113
C. Effective Sensor Fusion by Confidence Measures . . . . .	114
1. Characterization of Sensor Measurements . . . . .	114
2. Multi-sensor Fusion . . . . .	117
3. Fusion Rule . . . . .	118
4. Illustrative Example . . . . .	119
VI ATTAINING HIGH OPERATING BANDWIDTH BY SEN- SOR ARRAYS . . . . .	123
A. Implementation of Sensor Arrays . . . . .	123
B. Sensor Arrays . . . . .	124
C. Multi-sensor Fusion in Sensor Arrays . . . . .	128



CHAPTER	Page
D. Design of Compensators by Frequency Domain Methods . . .	130
E. Design of Compensators by Optimization . . . . .	134
F. Implementation of Sensors Array by Feedback Mechanisms	137
VII RESULTS AND ANALYSIS . . . . .	143
A. Signal Conditioning . . . . .	143
1. Nonlinear Filtering Example: A Computer Simulation	143
2. Experimental Demonstration of Performance of the Nonlinear Filtering Algorithm . . . . .	149
3. Nonlinear Filtering Algorithm as a Distortion Com- pensation Technique . . . . .	153
4. Recovery with Monotonic Nonlinear Sensor Function .	156
5. Recovery of Distorted Signals in Non-stationary Noisy Environments . . . . .	167
a. Simulation Results . . . . .	168
b. Experimental Results . . . . .	174
6. Signal Recovery Using Nominal Sensor Model . . . . .	180
7. Recovery with Non-monotonic Nonlinear Sensor . . . .	184
8. Recovery of Signals Distorted by Non-invertible Sensor Nonlinearity . . . . .	188
a. Simulation Example 1 . . . . .	188
b. Simulation Example 2 . . . . .	194
B. Fusion of Distorted Multi-sensor Data . . . . .	204
1. Fusion of Distorted Data by Sensor Scheduling . . . .	205
2. Fusion of Distorted Data by Continuous Optimization	212
3. Effective Sensor Fusion by Confidence Measures . . . .	216
C. Sensor Arrays: Illustrative Examples . . . . .	224
1. Design of Sensor Arrays by Frequency Domain Methods	224
2. Design of Sensor Arrays by Optimization . . . . .	229
3. Design of Sensor Arrays from Realistic Sensor Models	232
4. Implementation by Feedback Mechanisms . . . . .	237
VIII SUMMARY AND CONCLUSIONS . . . . .	244
A. Summary and Conclusions . . . . .	244
B. Directions for Future Work . . . . .	250
REFERENCES . . . . .	253
VITA . . . . .	269

## LIST OF TABLES

TABLE		Page
I	Effects of Penalty Weights on Optimal Solution: Quadratic Cost Case	86
II	Effects of Penalty Weights on Optimal Solution: Non-quadratic Cost Case . . . . .	86
III	Signal Data for Examples 1 & 2 . . . . .	110
IV	Sensor Schedule (Example 1) . . . . .	111
V	Sensor Schedule (Example 2) . . . . .	112
VI	Signal Data for Example 3 . . . . .	113
VII	Sensor Schedule (Example 3) . . . . .	114

## LIST OF FIGURES

FIGURE		Page
1	Comparison of Linear and Nonlinear Characteristics . . . . .	4
2	Representation of the Proposed Nonlinear Sensor Distortion Compensation . . . . .	7
3	Sensor Array with Low Bandwidth Pass-band Sensors . . . . .	10
4	Basic Signal Recovery Setup . . . . .	35
5	Recovery of Signals Corrupted by Noise . . . . .	36
6	Effect of $\alpha$ on Weight $\frac{\alpha}{1-r}$ . . . . .	38
7	Signal Recovery Setup That Incorporates Noise Removal . . . . .	40
8	Practical Implementation of Threshold Filtering . . . . .	41
9	Decomposition and Reconstruction in Wavelet Packets . . . . .	47
10	Signal Recovery Setup That Incorporates Non-stationary Noise . . . . .	49
11	Wavelet Filtering of Noise . . . . .	49
12	Nonlinear Sensor Used in Example 1 . . . . .	52
13	Chirp Signal . . . . .	53
14	Spectrum of Chirp Signal . . . . .	54
15	Time Frequency Map Obtained Using Continuous Wavelet Transform . . . . .	55
16	Solution to the Recursive Equation (Example 2) . . . . .	56
17	Uncertain Sensor Model . . . . .	57
18	Proposed Approach . . . . .	58

FIGURE	Page
19	A General Setup . . . . . 59
20	Nonlinear Sensor Function (Approximated) . . . . . 61
21	Non-monotonic Nonlinear Sensor Function . . . . . 70
22	Comparison of Optimal Solutions Obtained with Quadratic and Non-quadratic Cost Functions . . . . . 73
23	Effect of Weight on Non-quadratic Penalty on Optimal Solutions . . . 75
24	Effect of Adding a Quadratic Penalty Function . . . . . 76
25	Effect of Penalty Function Weight on the Optimal Solution-Quadratic Penalty Case . . . . . 77
26	Effect of Adding a Non-Quadratic Penalty . . . . . 78
27	Effect of Penalty Function Weight on the Optimal Solution-Non- Quadratic Penalty Case . . . . . 79
28	Optimal Solutions for High and Low Weights on Non-Quadratic Penalty 80
29	Comparison of Penalty Function Values When the Variable Is of High Value . . . . . 81
30	Approximating a Convex Function by a Linear Piece-wise Function . . 82
31	Approximating a Non-convex Function by a Linear Piece-wise Function 82
32	Multi-Sensor Data Fusion Setup . . . . . 88
33	Two-Sensor Data Fusion Setup . . . . . 90
34	Optimization Setup to Find $\Phi^*$ . . . . . 94
35	Branch and Bound Tree Structure . . . . . 98
36	Optimization Setup to Find $\Lambda_i^*$ . . . . . 107
37	Assigning “Confidence Measure” to Sensor Data . . . . . 115
38	Calculation of $\alpha_{ij}$ . . . . . 119

FIGURE	Page
39	Sensor Array Configuration . . . . . 125
40	Sensor Array with Low Pass-band Sensors . . . . . 125
41	Sensor Array with Two Sensors . . . . . 126
42	Ideal Sensor Array . . . . . 127
43	Another Ideal Sensor Array . . . . . 127
44	Sensor Array as a Stand-alone Process . . . . . 130
45	Multi-sensor Data Fusion Setup in Sensor Arrays . . . . . 130
46	Ideal Frequency Response of the Sensors and Compensators Integrated Setup . . . . . 131
47	Multi-sensor Data Fusion Setup in Sensor Arrays with Uncertain Sensor Models . . . . . 132
48	Expected Frequency Response of the Sensors and Compensators Integrated Setup . . . . . 133
49	Feasible Region of $I(j\omega)$ in Nichols Chart . . . . . 135
50	Identifying Different Confidence Regions in a Sensor Array . . . . . 136
51	Sensor Array with Different Confidence Regions . . . . . 136
52	Sensor Arrays . . . . . 138
53	Frequency Responses of Sensors . . . . . 139
54	Multi-sensor Data Fusion by Feedback Mechanisms . . . . . 140
55	Sensor Function . . . . . 144
56	Original Signal Used for Computer Simulation . . . . . 145
57	Distorted Version of Signal Shown in Fig. 56 . . . . . 146
58	Filtered Signal Obtained Using the Ideal Low Pass Filter . . . . . 147

FIGURE	Page
59	Frequency Spectrum of Recovered Signal . . . . . 148
60	Implementing Signal Recovery Scheme . . . . . 148
61	Nonlinear Diode Circuit . . . . . 149
62	Model Identification Scheme . . . . . 150
63	Signal Recovery Implementation Scheme Based on Fuzzy Model . . . 150
64	Input Voltage, $v_{in}$ . . . . . 151
65	Distorted Voltage Output, $v_{out}$ . . . . . 152
66	Recovered Signal and Error Values . . . . . 153
67	Nonlinear Sensor Used by Frank . . . . . 154
68	Bandlimited Input Signal . . . . . 155
69	Distorted Signal . . . . . 156
70	Compensated Signal . . . . . 157
71	Comparison of Linear and Nonlinear Sensor Functions . . . . . 158
72	Input Signal Used in Subsection 4 . . . . . 159
73	Spectrum of Input Signal Shown in Fig. 72 . . . . . 160
74	Sensor Noise . . . . . 161
75	Spectrum of Sensor Noise Shown in Fig. 74 . . . . . 162
76	Spectrum of the Linear Sensor Output . . . . . 163
77	Spectrum of the Nonlinear Sensor Output . . . . . 164
78	Filtered Sensor Output Obtained by Removing High Harmonics . . . 165
79	Reconstructed Signal . . . . . 166
80	Spectrum of Recovered Signal Shown in Fig. 79 . . . . . 167

FIGURE	Page
81	Input Signal, $y$ . . . . . 169
82	Nonlinear Sensor, $g$ . . . . . 170
83	Sensor Output, $w$ . . . . . 171
84	Filter Bank Setup . . . . . 171
85	Decompositions of Low Pass Filter Output . . . . . 172
86	Reconstruction to Obtain Denoised Estimate . . . . . 173
87	Signal Recovered Using the Iterative Algorithm . . . . . 174
88	Actual Input Signal, $v_{in}$ . . . . . 175
89	Acquired Output, $v_{out}$ . . . . . 176
90	Corrupted Output, $v_n$ . . . . . 177
91	Filter Bank Setup . . . . . 177
92	Decompositions of Low Pass Filter Output . . . . . 178
93	Reconstruction to Obtain Denoised Estimate . . . . . 179
94	Unknown Signal Recovered by Solving the Iterative Algorithm . . . . . 180
95	Actual and Nominal Sensor Models . . . . . 181
96	Sensor Input . . . . . 182
97	Sensor Output . . . . . 183
98	Recovered Signal Using Nominal Sensor Model . . . . . 184
99	Input Signal Used in Subsection 7 . . . . . 185
100	Non-monotonic Nonlinear Sensor . . . . . 186
101	Distorted Sensed Signal . . . . . 187
102	Recovered Signal from the Distorted Sensor Output . . . . . 188

FIGURE	Page
103	Signal to Be Estimated . . . . . 189
104	Sensor Output before Low Pass Filtering, $w$ . . . . . 190
105	Non-invertible Nonlinear Sensor . . . . . 191
106	Signal Recovered by Optimizing Quadratic Error Function, $J_{e_1}$ . . . . . 192
107	Signal Recovered by Optimizing Quadratic Cost Function, $J_{q_1}$ . . . . . 193
108	Signal Recovered by Optimizing Non-quadratic Cost Function, $J_{n_1}$ . . . . . 194
109	Signal to Be Measured . . . . . 195
110	Spectrum of the Signal to Be Measured . . . . . 196
111	Signal Output Before Low Pass Filtering . . . . . 197
112	Spectrum of the Sensor Output before Low Pass Filtering . . . . . 198
113	Signal Recovered by Optimizing Quadratic Cost Function, $J_{q_2}$ . . . . . 199
114	Signal Recovered by Optimizing Non-quadratic Cost Function, $J_{n_2}$ . . . . . 200
115	Spectrum of Signal Recovered by Optimizing Quadratic Cost Function, $J_{q_2}$ . . . . . 201
116	Spectrum of Signal Recovered by Optimizing Non-quadratic Cost Function, $J_{n_2}$ . . . . . 202
117	Signal Recovered by Quadratic Criteria ( $J_{q_2}$ )(after Filtering out Insignificant Frequency Components) . . . . . 203
118	Signal Recovered by Non-quadratic Criteria, ( $J_{n_2}$ ) (after Filtering out Insignificant Frequency Components) . . . . . 204
119	Original Signal $y$ Used to Demonstrate the Sensor Scheduling Scheme . . . . . 205
120	Sensor Data 1 Used to Demonstrate Sensor Scheduling Scheme . . . . . 206
121	Sensor Data 2 Used to Demonstrate Sensor Scheduling Scheme . . . . . 207
122	Sensor Data 3 Used to Demonstrate Sensor Scheduling Scheme . . . . . 208



FIGURE	Page
123	Nonlinear Sensor Function . . . . . 209
124	Filtered Signal $z$ of Nonlinear Sensor Shown in Fig. 123 . . . . . 210
125	Optimal Sensor Schedule, 0 and 1 Are Used to Denote off and on Positions Respectively . . . . . 211
126	Fused Signal $y_r$ . . . . . 212
127	Original Signal $y$ . . . . . 213
128	Sensor Data 1 . . . . . 214
129	Sensor Data 2 . . . . . 214
130	Sensor Data 3 . . . . . 215
131	Known Nonlinear Sensor Function . . . . . 215
132	Filtered Signal $z$ of Nonlinear Sensor Shown in Fig. 131 . . . . . 216
133	Optimal Sensor Schedule, 0 and 1 Are Used to Denote off and on Positions Respectively . . . . . 217
134	Estimated Signal $v_f$ . . . . . 218
135	Original Signal $y$ Used to Demonstrate Sensor Fusion Algorithm . . . 219
136	Nonlinear Sensor $S_1$ . . . . . 219
137	Nonlinear Sensor $S_2$ . . . . . 220
138	Sensor Data $v_1$ . . . . . 220
139	Sensor Data $v_2$ . . . . . 221
140	Filtered Signal $z_1$ . . . . . 221
141	Filtered Signal $z_2$ . . . . . 222
142	Confidence Measures for Sensor Data 1 . . . . . 222
143	Confidence Measures for Sensor Data 2 . . . . . 223

FIGURE	Page
144	Correct Samples of Sensor Data 1 . . . . . 223
145	Correct Samples of Sensor Data 2 . . . . . 224
146	Fused Signal Obtained Using the Confidence Measure Based Sensor Fusion Algorithm . . . . . 225
147	Magnitude Plot of Sensors, $S_1, S_2, S_3$ . . . . . 226
148	Phase Angle Plot of Sensors, $S_1, S_2, S_3$ . . . . . 227
149	Bode Plot of $I(j\omega)$ . . . . . 228
150	Frequency Response of $I(j\omega)$ in Nichols Chart . . . . . 229
151	Frequency Responses of Sensors $S_1$ and $S_2$ . . . . . 230
152	Frequency Responses of Compensators $P_1$ and $P_2$ . . . . . 231
153	Frequency Response of $I(j\omega)$ . . . . . 232
154	Fusion of Low and High Frequency Data . . . . . 233
155	Frequency Responses of Realistic Sensors $S_1$ and $S_2$ . . . . . 234
156	Frequency Response of Compensator $P_1$ . . . . . 235
157	Frequency Response of Compensator $P_2$ . . . . . 236
158	Frequency Response of Integrated Set up $I(j\omega)$ . . . . . 237
159	Sensor Fusion Setup . . . . . 238
160	Multi-sensor Data Fusion Simulation Setup . . . . . 239
161	Original Signal Considered for Demonstration . . . . . 240
162	Low Frequency Sensor Output . . . . . 241
163	High Frequency Sensor Output . . . . . 242
164	Fused Signal Obtained Using the Closed Loop Control . . . . . 243

## NOMENCLATURE

## Symbols

$\in$	element of
$\subset$	subset of
$\forall$	for all
$\exists$	there exists
$\diamond$	end of discussion
$.*$	denotes the term by term multiplication
$E$	Metric Space
$E^n$	$n$ -dimensional, real Euclidean Space
$L^2(-\infty, \infty)$	finite energy space
$l^p, 1 \leq p < \infty$	Set of all sequences $x = \{\xi_v\}$ with $\sum_{v=1}^{\infty}  \xi_v ^p < \infty$
$l^\infty$	Set of all bounded sequences $x = \{\xi_v\}$
$\mathbb{R}$	the real numbers
$\mathbb{R}^{m \times n}$	real matrices with $m$ rows and $n$ columns
$d(x, y)$	the distance $ x - y $ in $E$
$\overline{f(\cdot)}$	complex conjugate of a function $f(\cdot)$
$f(t)$	continuous-time function defined over a subset of $\mathbb{R}$
$f[k]$	discrete-time function defined over a subset of integers
$\mathcal{F}$	Fourier Transform
$\mathcal{F}^{-1}$	Inverse Fourier Transform
$I_n$	$n \times n$ identity matrix
$[m_{ij}]$	a matrix with $m_{ij}$ as its $i$ -th row and $j$ -th column element
$diag(m_1, \dots, m_n)$	an $n \times n$ diagonal matrix with $m_i$ as its $i^{th}$ diagonal element
$M^{-1}$	inverse of the matrix $M$
$M^T$	transpose of the matrix $M$
$\overline{M}$	complex conjugate of the matrix $M$

## Acronyms

DFT	Discrete Fourier Transform
IDFT	Inverse Discrete Fourier Transform
MIMO	Multiple-Input, Multiple-Output
QFT	Quantitative Feedback Theory
SISO	Single-Input, Single-Output

## CHAPTER I

### INTRODUCTION

#### A. Motivation

Sensors are essential for monitoring and controlling of industrial processes. Often the success of such processes heavily depends on the quality and reliability of the sensors utilized. There is an ever-increasing need for greater precision in sensor measurements and processing of signals from all types of sensors is becoming increasingly critical. In order to achieve this, new sensor technologies must be adapted and demands on signal processing, digital communication and local intelligence expanded. These requirements make it imperative that the sensor and its associated electronics be viewed as an integrated system and increasingly this system needs to be intelligent or smart.

As the density of the transistors on a chip is continuously increasing while the cost is decreasing, the intelligent sensor approach to compensate the sensor defects is becoming an established alternative to traditional methods. To address the need for intelligent sensor systems several approaches are available to sensor manufacturer or system integrator [1]. Such a methodology should provide the system intelligence and allow for data storage as well as software routines for the sensor to perform in-module sensor calibration, digital compensation, and self-validation. The current status of intelligent sensor has evolved from derision to acceptance in less than two decades. The technologies such as microcomputers and integrated circuits have promoted the progress considerably. As sensor systems get more intelligent, the distinction between a sensor and an instrument, between an intelligent sensor and a smart sensor, is

---

The journal model is *IEEE Transactions on Automatic Control*.

becoming more blurred. Although the demand for high accuracy, high reliability, low cost and compactness has been constantly increasing for the last two decades, much research is still to be done. The current trend toward the intelligent and smart sensors is to integrate 1) a sensing element that can be made in a standard process, and 2) electronic circuits to fully and periodically calibrate and compensate the sensor.

The conventional industrial practice corrects or recalibrates sensors and measuring instruments according to a fixed schedule (calibration interval). It can be time-consuming when the schedule is very tight or even can provide a false control when the schedule is relaxed. It has no information about the history data, re-calibration and overall suggestion. The self-calibration means that the sensor can monitor the measuring condition by a confidence test to decide whether a new calibration is needed or not. For a real time confidence test, a stimulus is looped back with a measurement and gets the level of confidence. The confidence is used to judge whether the system is still performing satisfactorily or not. If not, a calibration procedure is required to recover the sensor performance.

Some of the common unwanted effects found in classical sensors are [2]:

1. nonlinearity
2. noise
3. time (or frequency) response
4. parameter drift
5. cross sensitivity

Methods dealing with these issues have been widely studied in the literature and fall into four main classes of technique [1]:

1. Structural Compensation
2. Tailored Compensation
3. Monitored Compensation

#### 4. Deductive Compensation

However, the techniques available to compensate the effects of sensor nonlinearity are relatively crude. These techniques include the use of diode networks that are used to realize reciprocal characteristics and linearization processes such as Look-up Tables or polynomials. Despite being a dominant impediment, issues related to sensor nonlinearity have not received much attention. The fact that none of the available techniques can compensate the effects the sensor nonlinearity efficiently affects the use of sensory systems in two ways. For linear sensors, this will result in inaccurate sensor measurements. For primary nonlinear sensors, their use may be ignored. However, the use of primary nonlinear sensors may not be completely ignored or sensors are only allowed to work in a range where the linearity assumption is valid. However, the use of nonlinear sensors can be advantageous or may be the only option available. For example, an image sensor usually has a nonlinear characteristic that can be modelled as point-wise (memory-less) nonlinearity. Another example is photographic film [3]. Due to the well known nonlinear relationship between the incoming light exposure and the silver density deposited on the film, the widely assumed linear relationship between the blurred image and the “ideal” scene does not hold in the case of scanned photographic images. This problem is of great interest in many real-life applications, since the photographic film continues to be a very widely used image recording medium.

Noise and dynamic range are common measures often used to determine sensor performance. With lower noise, the sensor measurement is more reliable when used to characterize a physical variable. Dynamic range determines how much of the total input energy is captured by the sensor. For example, in Charge-Coupled Device (CCD) cameras, a linear image sensor is used to capture the image. The output voltage varies linearly with the input light energy. If the light energy doubles, the

output voltage doubles. The sensor may not tolerate a very high voltage output, which limits the maximum amount of light energy they can accumulate. This limit usually referred to as “Well Capacity” can be increased if the sensor is developed in such a way that its output varies nonlinearly with its input. This fact is evident in Fig. 1 as the range covered by the nonlinear sensor is greater than that by the linear sensor. Logarithmic nonlinear sensor characteristic is used in High Dynamic Range Complementary Metal-Oxide Semiconductor (CMOS) Sensors to increase the dynamic range [4].

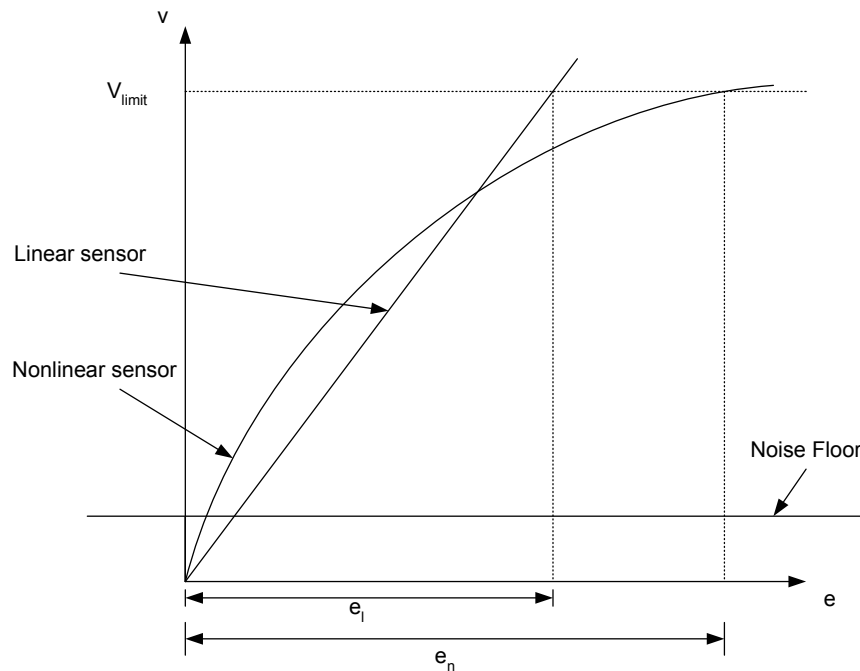


Figure 1: Comparison of Linear and Nonlinear Characteristics

Noise is inevitable with sensor measurement. When a signal is measured through a sensor, there is a tendency for the low amplitude part of the signal to be corrupted by sensor noise. Referring to Fig. 1, the actual data within the noise floor may not be distinguishable due to sensor noise. This situation may get worsened if the signal



amplification due to sensor is not sufficient. In the case of linear sensors, having a high gradient within the noise floor may not always be possible as higher slope will result in lower dynamic range. An effective tradeoff between the signal amplification and dynamic range coverage may not be made. However, with nonlinear sensors both objectives can easily be achieved. The nonlinear sensor may be designed such that the slope of the function within the noise floor is chosen as high as required. The gradient of the sensor function outside the noise floor can be adjusted so as to meet the dynamic range requirement and the maximum output voltage limit. With this sensor characteristic, a suitable frequency transform localizes the noise into a few isolated regions, which can then be eliminated using a threshold estimator.

Sensors are often designed in such a way to preserve linearity so that they can be reliably calibrated. Achieving a true input-output linearity is very difficult and not cost effective since nonlinearity is present in some form in almost all physical devices. In practice, several signal conditioning devices are used to compensate the distortion caused by nonlinearity and to achieve linearity. For example, the high-end device Maxim Integrated Product, MAX1457, linearizes a sensor output by establishing 120 piecewise-linear segments, drawing on data stored in EEPROM. Furthermore, achieving linearity seems to be the prime objective of most sensor manufacturers and enormous resources are invested for related research. In addition, expensive periodic calibration procedures may be required to preserve linearity from time to time. The difficult task of achieving linearity and the trouble of periodic maintenance can be simplified if nonlinearity is considered as one of the features of a sensor. For example, a low cost oxygen sensor that is used for closed-loop active combustion control in automobiles [5] displays nonlinear characteristics and the cost of the linear oxygen sensor (Wide Band Oxygen Sensor) is much higher than that of the nonlinear sensor.

Fiber optic displacement sensors, which are widely used to obtain approximate

displacement measurements at very low cost [6], and the Hercules Orthoflex capacity sensor, a biosensor that is used to measure the pressure between the foot and shoe [7] are some other well-known nonlinear sensors widely used in practice. Efficient noise removal and wider dynamic range can be achieved if these sensors are designed as alluded to earlier.

Despite several advantages in using nonlinear sensors, distortion caused by nonlinearity may appear at first as the main factor discouraging their use. In this dissertation, this problem is investigated in detail and it is shown that a robust signal recovery setup that reconstructs the original signal from the distorted sensor output will guarantee that nonlinear distortion will not be a problem. It is also shown that a unique signal recovery is possible when the nonlinear sensor is designed to satisfy certain requirements. It is emphasized that utilizing certain characteristics of nonlinear sensor functions, it is possible to compensate nonlinear distortion and to remove sensor noise by a few step iterative process. The successful development of the real time recovery procedure will support the use of nonlinear sensors and improve the accuracy in sensor measurements. It can then be implemented in a hardware unit or DSP chip. The combination of a nonlinear sensor and the hardware unit or DSP chip will do the required job that is currently done by a linear sensor with nonlinearity and other expensive distortion compensation devices whose performance may not always be guaranteed. The proposed distortion compensation setup is illustrated in Fig. 2.

In the above discussion, we considered a class of sensors that are memory-less and whose dynamics can be ignored. However, certain applications, for example, control of dynamical systems require that sensors with a reasonable bandwidth be used. The success of such application is heavily dependent upon the quality and reliability of the sensors utilized including sensor bandwidth. The sensors are often used to measure the information and the necessary control actions are generated based

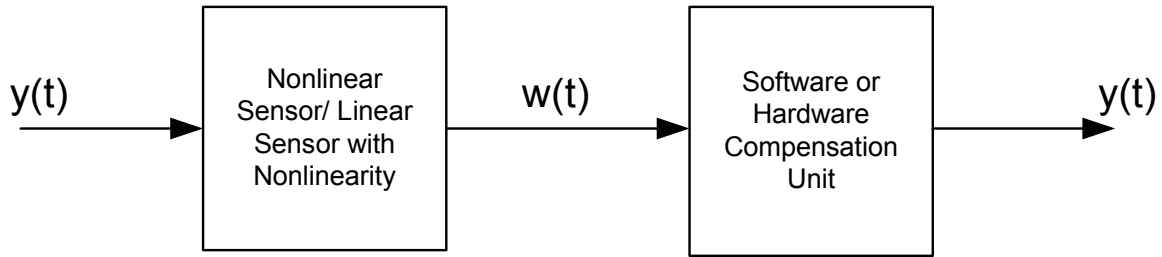


Figure 2: Representation of the Proposed Nonlinear Sensor Distortion Compensation

on the feedback provided by sensor measurements. Precise control of processes has become increasingly important to ensure high performance and reliability. Sensory systems are used widely in many applications, and high reliability of the system, which is a crucial factor in achieving high product yield, is heavily dependant on the accuracy of sensed signals. However, uncertainty caused by sensor noise and failure and insufficient sensor bandwidth may seriously degrade reliability. Sensor bandwidth plays a vital role in the success of a control system as it dictates the extent to which information about a system can be reliably extracted for further signal processing and interpretation. However, the cost of implementing feedback becomes a direct function of how large the required bandwidth is.

In the design of feedback systems it is important to keep the bandwidth of the controller small enough to guarantee the performance needs which are typically at low frequencies. Of course if there are sensors with very large bandwidth then the controller design problem does not become a major concern. However, such sensors are obviously very expensive because they must work with signals over a spectrum consistent with the sensor bandwidth. It is best to use just enough controller bandwidth so that sensors with sufficiently low bandwidth can be incorporated into the closed loop system. As an example, having large margins of stability implies suppres-

sion of the closed loop resonances at frequencies around the bandwidth frequency, but a serious drawback generally arises in the form of an increase of sensor noise response at the plant input.

Even though designing and implementing of high bandwidth sensors is very expensive and difficult, having a high sensor bandwidth is advantageous and necessary in many control applications. For example, the spacecraft attitude needs to be measured at sufficiently high bandwidth to take full advantage of line-of-sight type instruments and fast steering mirrors [8]. Other applications include laser marking, trimming and writing, high speed printing, as well as use in imaging systems, astronomy, and disturbance simulation [9]. However, expanding the bandwidth of sensors is neither practical nor economically feasible.

The high bandwidth sensors are very expensive because they must work with signals over a spectrum consistent with the sensor bandwidth. It is often necessary to detect signals whose spectrum span over a wide range. The use of a single sensor is likely to be neither a practical nor economically feasible option for the foreseeable future. Furthermore, there is no single sensor currently available that would provide both the accuracy and the bandwidth needed for the measurement. In addition, the design of a sensor that can accurately pick up low frequency signals as well as high frequency signals in the same time frame may not be feasible. For example, a common problem associated with high bandwidth sensors is their inability to accurately register slow-varying motion (low-frequencies). Consider the case where accelerometers are used to sense angular jitter [8]. Then, rapid motion would yield large accelerometer outputs, while slow motion would generate small acceleration signals. If the accelerometers are selected so that they have enough sensitivity to measure slow motion, they are likely to saturate under rapid motion. Conversely, if they are scaled not to saturate under rapid motion, they would lack the resolution to detect slow motion.

This creates problems when trying to resolve attitude angles over a wide range of frequencies. Similarly, other high-bandwidth sensor types (like the ADS and quartz gyros) do not have near DC response. This creates an analogous problem as that associated with accelerometers. Therefore, other sensing means needs to be developed. One of the goals of this dissertation is to develop means for producing accurate high as well as low frequency measurements using a smart and low cost integrated sensory system.

Instead of using a single sensor to obtain both high and low frequency measurements, we point out there are many advantages of using an array of several sensors. The idea is to divide the required sensor bandwidth into several frequency segments and organize a sensor network that consists of low pass-band sensors such that each sensor is restricted to cover a particular frequency segment. The proposed sensor array configuration is schematically shown in Fig. 3. This allows us to take full advantage of cheap and low bandwidth sensors whose performance is optimum only in the given bandwidth. For example, angular displacement sensors and quartz rate sensors are good high frequency sensors but have a poor near-DC response whereas accelerometers and gyroscopes have good low frequency responses but are likely to saturate under rapid motion. Combining these sensors in an array as described would be a cost effective alternative to a very expensive, high bandwidth sensor design. Multi-sensor data can then be fused intelligently to obtain the required measurement. This requires that efficient multi-sensor fusion and sensor scheduling algorithms be developed to blend the multi-source measurements for off-line as well as real time applications. If used in feedback control systems, this approach would enable the designer to devise several low bandwidth controllers each utilizing sensors of much smaller bandwidth.

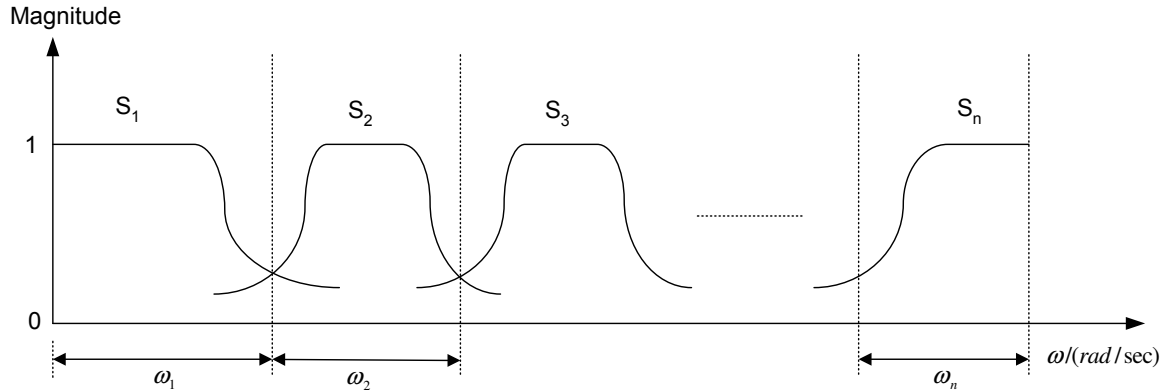


Figure 3: Sensor Array with Low Bandwidth Pass-band Sensors

## B. Objectives

The main goal of the proposed investigation is to develop and implement a new generation of smart sensory systems that would enhance capabilities and add intelligence in existing systems with regard to design, performance, cost, sensor bandwidth, sensor nonlinearity and measurement noise. The proposed research is aimed at achieving this goal by meeting the following objectives:

1. To utilize certain characteristics of nonlinear sensor function for the improvement of sensory systems performance by making it less sensitive to measurement noise and increasing its dynamic input range.
2. To develop robust and stable signal recovery schemes that include nonlinear distortion compensation and noise removal procedures and implement them in real time applications.
3. To devise several intelligent and efficient multi-sensor fusion procedures to facilitate the design and implementation of sensor arrays.

4. To develop sensor scheduling algorithms and faulty sensor detection schemes to optimize the use of multiple sensors and to reduce the cost of sensory operation.

### C. Dissertation Overview

The remaining chapters of this dissertation are organized as follows.

Chapter II presents some important definitions and theorems that are used in this dissertation. Chapter III aims at providing the reader with some background information and related previous work. Commonly used signal reconstruction and multi-sensor fusion methods are presented and their practicality is briefly discussed. Chapter IV is concerned with the recovery of band-limited signals from the distorted nonlinear sensor measurements. A detailed nonlinear distortion analysis is given to point out the need for an efficient signal conditioning scheme to improve accuracy of sensor measurements. A recursive signal conditioning scheme is developed and its limitations are discussed. A novel approach that uses non-quadratic optimization to recover the signals distorted by non-invertible sensor nonlinearity is also proposed. Chapter V details the multi-sensor fusion schemes developed in this dissertation. The problem of fusing distorted multi-sensor data is considered and several data fusion techniques are developed. The main purpose of this chapter is to identify the faulty sensor measurements and to optimize the number of sensors used in a process. Chapter VI is devoted to the development and implementation of sensor arrays. A new and efficient approach that uses the idea of organizing many low bandwidth pass-band sensors in a distributed sensor array to attain a high operating bandwidth is proposed. Having emphasized the necessity for a suitable sensor fusion method to implement the proposed approach, several multi-sensor schemes are developed. The proposed methods are different from the traditional sensor data fusion methods

in the sense that the frequency responses of the multi-sensors are shaped by means of compensators in the proposed approach rather than sensor data association as done in traditional methods. In Chapter VII, experimental and simulation results are presented to validate the methods developed in this dissertation. The results are analyzed and their significance is discussed. Chapter VIII concludes the dissertation with a summary of results, an outline of its contributions to the research community and practitioners, and several suggestions for future research.



## CHAPTER II

## PRELIMINARIES

This chapter presents some basic theorems that will be used later in this dissertation.

## A. Definitions and Theorems

The norm of a function ( $\|\cdot\|$ ) is simply a measure of the distance of the function to the origin (i.e., 0). In other words, we can use the norm  $\|f - g\|$  to measure the difference between two functions  $f$  and  $g$ . The norm of a function can be calculated in a variety of ways. For example, the finite energy space  $L^2(-\infty, \infty)$  uses the following definition for the norm [10].

**Definition 1** *The norm of a function,  $f(t) \in L^2(-\infty, \infty)$  is defined by,*

$$\|f(t)\| = \left[ \int_{-\infty}^{\infty} |f(t)|^2 dt \right]^{\frac{1}{2}} \quad (2.1)$$

The finite energy space  $L^2(-\infty, \infty)$  requires that all functions that belong to this space have finite energy. The following definition states this fact in mathematical notation [11].

**Definition 2** *A signal is a function  $f(t) \in L^2(-\infty, \infty)$*

$$\|f(t)\|^2 = \int_{-\infty}^{\infty} |f(t)|^2 dt < \infty \quad (2.2)$$

We use the following convention for Fourier Transform and its inverse (in one dimension).

**Definition 3 *Fourier Transform:*** *The Fourier Transform of a finite-energy function  $f(t) \in L^2(\mathbb{R})$  of a real variable  $t$  is defined by:*

$$\mathcal{F}\{f(t)\} = \int_{-\infty}^{\infty} f(t)e^{-j\omega t} dt \quad (2.3)$$

where  $\omega$  is frequency in rad/sec.  $\mathcal{F}\{f(t)\}$  is also known as the spectrum of  $f(t)$ .

**Definition 4 Inverse Fourier Transform:** The Inverse Fourier Transform ( $\mathcal{F}^{-1}\{.\}$ ) recovers the function  $f(t)$  from its Fourier Transform  $\mathcal{F}\{f(t)\}$ .

$$\mathcal{F}^{-1}\{\mathcal{F}\{f(t)\}\} = f(t) = \frac{1}{2\pi} \int_{-\infty}^{\infty} \mathcal{F}\{f(t)\}e^{j\omega t} d\omega \quad (2.4)$$

A useful theorem named Parseval's Theorem or Identity that relates the time and frequency domain functions is stated next [10].

**Theorem 1 Parseval's Theorem** states that

$$\int_{-\infty}^{\infty} |f(t)|^2 dt = \frac{1}{2\pi} \int_{-\infty}^{\infty} |\mathcal{F}\{f(t)\}|^2 d\omega \quad (2.5)$$

**Theorem 2 Plancherel's Theorem** [12]: Using the above Parseval's Identity, it can be shown that [10] two functions,  $f(t)$  and  $g(t) \in L^2(-\infty, \infty)$ , are related to their Fourier Transforms  $\mathcal{F}\{f(t)\}$  and  $\mathcal{F}\{g(t)\}$  by,

$$\int_{-\infty}^{\infty} f(t)\overline{g(t)} dt = \frac{1}{2\pi} \int_{-\infty}^{\infty} \mathcal{F}\{f(t)\}\overline{\mathcal{F}\{g(t)\}} d\omega \quad (2.6)$$

**Definition 5 Band-limitedness:** A signal  $f(t)$  is bandlimited with frequency band  $(-\Omega, \Omega)$  if its Fourier Transform  $\mathcal{F}\{f(t)\}$  vanishes for  $|\omega| > \Omega$ .

**Definition 6** The **bandwidth** of a signal is a measure of the range of frequencies present in the signal. More technically, bandwidth is the width of the range of frequencies that an electronic signal occupies on a given transmission medium.

**Definition 7** The **bandwidth** of a device is the range of frequencies over which a particular instrument is designed to function within specified limits.

The bandwidth of a device is given by  $f_1 - f_2$  Hz where frequencies  $f_1$  and  $f_2$  are such that the frequency response of the device,  $G(f)$ , satisfies the following:

$$|G(f)| < 1 \quad \text{for } f \notin [f_1, f_2] \quad (2.7)$$

**Definition 8 Convexity:** A nonempty set  $X \in E^n$  is said to be convex if for any two points  $x_1, x_2 \in X$  the line segment joining  $x_1$  and  $x_2$  is contained in  $X$ , that is, if [13]

$$\lambda x_1 + (1 - \lambda)x_2 \in X \quad \text{for every } \lambda \in [0, 1]$$

**Definition 9 Linearity:** A function  $f : X \rightarrow E^m$ , with  $X \subset E^n$ , is said to be linear if for all  $x_1, x_2 \in X$  and for all real scalars  $\alpha_1$  and  $\alpha_2$  [13]

$$f(\alpha_1 x_1 + \alpha_2 x_2) = \alpha_1 f(x_1) + \alpha_2 f(x_2). \quad (2.8)$$

**Definition 10 Convex Function:** A function  $f : X \subset E^1$ , with  $X$  a convex subset of  $E^n$ , is said to be convex if for any two points  $x_1$  and  $x_2$  in  $X$  and any real  $\lambda$ ,  $0 \leq \lambda \leq 1$ , we have

$$f(\lambda x_1 + (1 - \lambda)x_2) \leq \lambda f(x_1) + (1 - \lambda)f(x_2). \quad (2.9)$$

If strict inequality holds in Equation (2.9) for all  $x_1 \neq x_2$  in  $X$  and for all  $0 < \lambda < 1$ , then  $f(\cdot)$  is said to be strictly convex [13].

**Definition 11 Concave Function:** A function  $f : X \subset E^1$ , with  $X$  a convex subset of  $E^n$ , is called concave (strictly concave) if  $-f(\cdot)$  is convex (strictly convex) [13].

**Definition 12 Convergence:** The convergence of the sequence  $\{x_k\}$  to  $x$  means

that the distance  $|x_k - x|$  of the  $k$ -th term  $x_k$  from the limit  $x$  will be arbitrarily small when  $k$  increase beyond all limits [14].

**Definition 13 Lipschitz-condition:** A function  $g$  maps the interval  $[a, b]$  into itself and it is said to satisfy a Lipschitz-condition with a Lipschitz-constant  $q < 1$  if there exists a number  $q$  with  $0 \leq q < 1$  such that

$$|g(x) - g(y)| \leq q|x - y| \quad \forall x, y \in [a, b]. \quad (2.10)$$

**Theorem 3 Banach's Fixed Point Theorem [14]:** If  $A$  is a contracting self-map of the complete metric space  $E$ , then the Equation  $(x = Ax)$  has exactly one solution in  $E$ . This solution can be obtained by iteration: if one chooses an arbitrary point  $x_0$  in  $E$  and sets  $x_{n+1} := Ax_n$ ,  $n = 0, 1, 2, \dots$ , then  $\{x_n\}$  converges to  $x$ . Furthermore the error estimate

$$d(x, x_n) \leq \frac{q^n}{1 - q} d(x_1, x_0)$$

is valid.

## CHAPTER III

### LITERATURE REVIEW

Before devising a suitable plan to achieve the objectives posed in Chapter I, we will first gather the relevant background information. This chapter summarizes the previous work on signal reconstruction methods, nonlinear sensors, distortion compensation and multi-sensor data fusion.

#### A. Nonlinear Distortion Analysis and Signal Reconstruction

Nonlinear distortion is a well-known problem in communication networks where devices like compander are used to transmit signal data [15]. Several distortion compensation techniques for these devices have been proposed in the literature. Zames [16] showed nonlinear distortion can be compensated using an invertible nonlinear filtering technique. Beurling (as cited in [17]) proved the existence of a bandlimited solution to the nonlinear filtering problem. An iterative scheme to obtain such a solution is given and convergence requirements are derived in [11]. The problem of recovering band-limited signals under considerably weaker conditions is investigated in [15]. A technique based on Orthogonal Polynomial Inverses to compensate nonlinear distortion is derived in [18].

Compensation of linear and nonlinear distortions due to sensor nonlinearity by a digital post processing technique using several FIR filters is proposed in [19]. The use of Tikhonov's operators to compensate the effects of static nonlinearities in the presence of noise is detailed in [20]. In [21], Scheoukens *et al* proposed an approach to deal with nonlinear distortion in a linear modeling framework in which a nonlinear system is replaced by a linear system and a nonlinear noise source. The asymptotic behavior of nonparametric and parametric frequency domain identification methods

to model linear dynamic systems in the presence of nonlinear distortions under some general conditions for random multi-sine excitations is presented in [22]. A broad class of iterative signal restoration techniques, which can be applied to remove the effects of many different types of distortions are given in [23].

Nonlinear distortion is also a serious problem in audio engineering. For example, nonlinearity of magnetic recorder distorts the input sound while recording. A method to restore nonlinearly distorted magnetic recordings is presented in [24]. A histogram-equalization method to restore amplitude-distorted speech is developed in [25]. In this method, a histogram of the input signal is modeled, the distribution function of the modeled input signal is compared to a reference distribution function and the mismatch can be used to describe the distorting nonlinearity and its inverse as an amplitude map, which corrects the distorted signal. Nonlinearities in horn loudspeakers are modeled by electromechanical-acoustical analogous circuits and the methods to identify the dominant nonlinearity from the nonlinearly distorted measurements are given in [26].

Though nonlinear distortion is a serious issue with the use of almost all real sensors, these issues have not received much attention in the literature. Noise related issues have been paid much attention to [27]. However, a systematic methodology to address nonlinear distortion related issues is yet to be developed. This dissertation is devoted to fill this gap and to provide a methodology to improve accuracy and reliability of sensor measurements.

## B. Conditioning of Distorted Measurements

### 1. Signal Conditioning

The manipulation of the output of a sensor to prepare it for further processing and use is generally known as signal conditioning[28]. Common types of signal conditioning includes the following:

1. Signal conversion
2. Isolation
3. Multiplexing
4. Attenuating
5. Amplifying
6. Filtering
7. Transducer Excitation
8. Linearizing
9. Signal Reproduction
10. Smoothing

### 2. Filtering

Filtering is the process by which the frequency content of a signal is altered. In other words, it is a process that selectively lowers the power content of specific signal frequencies. Filtering is one of the commonly used signal processing techniques. The classical filtering techniques assume that the signal content of a signal is clearly distinct from the remainder of the signal in the frequency domain. Filters alter the frequency content of a signal. The term “filtering” is also used to denote the signal conditioning operation done in real time.

### 3. Smoothing

Smoothing is the manipulation of a signal to make it fit a particular model or pattern. In practice, signal smoothing is a form of filtering. Specifically, it is low pass filtering. In fact, if we compare, in the frequency domain, the characteristics of a Butterworth low-pass filter and spline smoothing, they are very similar [29]. The term “smoothing” is also used to denote the off-line signal conditioning operation.

#### C. Multiple Sensor Fusion Techniques

Multiple sensor data fusion is the uniting or blending of several sensor data into a whole single data set. Several specific advantages obtained by using more than one source of data in seeking some typical conclusions are improved system reliability and robustness, increased confidence, reduced ambiguity, shorter response time, improved resolution, extended coverage and in some cases, reduced cost of operation [30]. The fusion of redundant information can reduce overall uncertainty and thus serves to increase the accuracy of process measurements. Complementary measurements from multiple sensors allow certain features of the environment to be perceived that may not be possible or feasible with a single sensor. For example, the use of a single sensor may not be practical when the sensor is employed to detect high bandwidth signals. The high bandwidth sensors are very expensive because they must work with signals over a spectrum consistent with the sensor bandwidth. In this case, an array of several low bandwidth sensors could be employed to cover the required high bandwidth. The individual measurements can then be combined to yield the required inference.

Sensor data fusion has been a promising research topic for quite some time and it has been used widely in a variety of applications that include robotics, medical applications such as electric wheel chair, remote sensing, monitoring and control of



manufacturing processes, automated target recognition, guidance of autonomous vehicles, battlefield surveillance and automatic threat recognition systems. A good review of the multi-sensor fusion techniques and commonly used sensor fusion techniques can be found in [31] [32], [33], [34], [35].

Tenney and Sandell [36] were among the first to study how distributed sensors may be used for the detection problems. Their analysis, deemed since then to be pioneering work in the field, follows classical Bayesian theory and offers decentralized statistical binary hypothesis testing at each of the individual sensors in the distributed network to determine the optimal local detection rules. Kushner and Pacut [37] reported on their simulation efforts involving to sensors and made a comparative analysis of the decentralized detection problem with two observers against the traditional detection problem based on a single observer. Teneketzis and Varaiya [38] tackled what they termed the decentralized quickest detection problem. The problem posed is that of two detectors that while making independent observations must decide on a binary state change of a Markov chain. Tsitsiklis and Athans [39] reported a study on the computational complexity of discrete models of some basic decentralized detection/decision problems.

Chair and Varshney [40] attempted the development of an optimal global decision rule through the weighting of the independent optimal decisions of the individual sensors by their reliability rates, given in terms of false alarm and miss rates. Hoballah and Varshney discussed the use of the Neyman-Pearson criterion for deriving the optimal decision with distributed sensors and a central fusion unit in [41]. Thomopoulos and Okello [42] dealt with the problem of detection with mismatched sensors. This addresses a very specific type of problem, one in which the two sensors each have certain blind spots. This study is not of a general nature due to numerous assumptions made in the analysis. However, some of the concepts may have applications in other

specific contexts.

Izzo and Paura [43], in their comments on the optimal detection study by Reibman and Nolte [44], focused their attention on the problem of the computational complexity of deriving the general solution, which involves highly nonlinear coupled equations. The constant false alarm rate (CFAR) problem in the distributed sensor environment was studied by Barkat and Varshney [45]. In this study, the scope for adaptive threshold techniques instead of the preestablished thresholds used in the earlier studies in order to assure a detection with constant false alarm rate was examined. A study of correlated noise in a distributed detection system was reported in [46]. This study assumes that the local sensors have the same operating points and that the distribution of sensor observations is a symmetric function. A study on optimum decision space partitioning in multi-sensor environments, which investigates the benefits of transmitting reliability data in addition to the traditional decision-only transmission assumed between the local sensors and the central processor in many of the previous studies was presented in [47].

A method that does not assume availability of any probabilistic descriptions ( probability density functions and the like) of the target data environment was presented in [48]. In this way, this method differs from other traditional approaches and more or less corresponds to nonparametric training approaches in the classic pattern recognition field. Hoballah and Varshney [49] dealt with the problem of deriving a global decision by combining local binary decisions through a Bayesian formulation. This method involves a computational challenge for large values of number of sensors considered, especially when one considers that in realistic military environments where real time detection decisions are crucial. A study on a distributed  $m$ -ary hypotheis-testing problem with correlated observation is presented in [50]. In this study, each of the local processors is assumed to be transmitting any one of a

predefined set of messages, on the basis of its own local processing, to a central fusion processor wherein these messages are fused with with its own inputs to arrive at the overall decision.

Three specific schemes for fusing information namely 1) fusion of observations, 2) fusion of local decisions, 3) fusion of probabilities are reported in [51]. Unlike most of earlier studies, this attempts to relate the analysis to nonmilitary applications. A method of fusion of evidence based on fuzzy integrals is presented in [52]. This method combines objective evidence with subjective interpretation on the reliability of the source of such evidence. Wang and Cai [53] adapted the sample matrix inversion (SMI) procedure to tackle the problem of adaptive signal detection in multiband sensor environments. The SMI procedure uses two (primary and secondary) noise- and interference-inclusive data sets, with the signal being present only in the so-called primary input. The secondary input is the basis for the estimation of the covariance matrix of the inference and noise. and this estimate is used in place of the unknown covariance matrix in the primary data containing the signal to set the optimal detection thresholds.

A new study on distributed detection with decision feedback was presented in [54]. The central decision of the fusion processor is communicated back to the local sensors to influence subsequent decisions on a new observation. According to the author, the feedback leads to consistency in an asymptotic sense; that is, asymptotically all the local sensors have to agree among themselves and hence with the central fusion processor. A study in which each local processor, or decision maker, is assumed to receive an observation and transmit a binary message to its successor was presented in [55]. The last decision maker makes the final decision as to which the hypothesis is true, which essentially represents the configuration of multi-sensors in series. The asymptotic performance of a class of multi-sensor memoryless detection

system was investigated in [56]. Some results in distributed nonparametric detection are discussed in [57].

The problem of signal detection amid the combination of clutter and thermal noise was considered in [58]. It presents adaptive threshold techniques designed to maintain a constant false alarm rate through a cell-averaging approach. In this study, two different sensor network topologies, parallel and tandem, are considered. The study on hardware complexity, defined as number of sensors of distributed detection systems was reported in [59]. This study compares two specific schemes, namely, 1) an optimal parallel-sensor centralized architecture, 2) a suboptimal binary distributed detection architecture. In the former scheme, the data measurements themselves are transmitted to the centralized decision processor for derivation of the globally optimal decision. In the latter scheme, each sensor has its own local decision processor that minimizes the local Bayes risk and transmits only a binary decision to the central processor for minimization of the global risk.

A study on optimum fusion of correlated local decisions was presented in [60]. The system considered in this work consists of a central fusion unit and a number of local detectors with each local detector making its own binary-hypothesis-based decision using its own set of observations. A normative Bayesian model consisting of a primary decision-maker and two expert assistants organized in a hierarchical team structure for tackling the binary hypothesis testing problem was presented in [61]. An alternative approach to the design of decentralized Bayesian detection systems was presented in [62]. The practical problem of CFAR detection in clutter environments is addressed by Donohue and Bilgutay [63] in their study on OS characterization as a means of modeling the clutter statistics. The problem of distributed detection by a team of sensors in tandem with each sensor/decision-maker sending a binary message based on its observations to the succeeding one is considered in [64]. Kam, Zhu and

Gray [65] discuss the problem of optimal data fusion of correlated local decisions in multi-sensor systems.

The multi-sensor fusion algorithms can be broadly classified into four categories [31], which are:

1. Estimation Methods
2. Classification Methods
3. Inference Methods
4. Artificial Intelligence Methods

A brief discussion of the above methods is presented next.

### 1. Estimation Methods

#### a. Linear Weighted Averaging

One of the common method of fusing or combining information received by multiple sensors is to take the weighted average of the various sensor data to arrive at a composite fused value. The well known advantages of this techniques are simple, easy to use and most importantly real time implementable.

#### b. Kalman Filtering

Kalman filtering [66] provides another fusion method, which generates the estimates of the required data. The estimates are optimal in a statistical sense. It is a linear systems technique that works well for reconstructing the environment, when the data is corrupted by measurement noise only. It is different from conventional filtering methods in that it uses an explicit (probabilistic) system model. The system model is represented by a state vector to be estimated, a known state transition matrix, and an additive zero mean white noise process with known covariance matrix. This

approach is useful when the state vector can be identified and related to its previous values through a state transition matrix. The Kalman filter has found widespread application in data fusion problems. For example, Durrant-Whyte has demonstrated in many occasions how Kalman Filter can be used to solve some challenging multi-sensor fusion problems encountered in robotic and vehicle applications [67], [68], [69], [70], [71]. Other areas of application include target detection, collision avoidance, automatic target recognition, multi-target tracking, etc. [33], [72], [73], [74], [75]. A detailed discussion on target association and track-to-track fusion methods can be found in [76], [77], [78], [79].

### c. Least Square Estimation

Least squares methods fuse data by searching for solutions, which minimize the squared error between the observed data and the predicted data. A weighted least squares method to compute the position and orientation parameters of an object from sparse contact point tactile data is presented in [80]. A least approach is used to fuse multi-sensor data to determine the pose of a known object in [81].

## 2. Classification Methods

Cluster method that include hierarchical agglomerative, hierarchical divisive and iterative partitioning methods tries to establish geometrical relationships on a set of sample data in a training process [82]. It is considered a powerful tool to classify multi-sensor data and the classification is done by unsupervised or self-organized learning algorithms such as learning vector quantization, K-means clustering etc. [83]. In the clustering methods, the distance between two clusters are optimized or adjusted to reach the final decision.

### 3. Inference Methods

The Bayesian inference fusion methods allow the multi-sources to be united according to the rules of probability theory [84]. Dempster-Shafter evidential reasoning, which is an extension to the Bayesian approach makes explicit any lack of information concerning a proposition's probability by separating firm support for the proposition from just its plausibility. A generalized evidence processing that unifies the Bayesian and Dempster-Shafter evidential reasoning to perform sensor fusion at the level of evidence is proposed in [85].

### 4. Artificial Intelligence Methods

The artificial intelligence methods use a priori set of training data to establish a inference system and the applicable rules are identified by searching the complete set of rules [86],[31]. Artificial Intelligence Techniques such as Neural Networks and Fuzzy Logic have sufficient degrees of freedom to fit complex nonlinear relationships with the necessary precautions to properly generalize. Some of the artificial intelligence methods are briefly discussed in here.

#### a. Dempster-Shafer Theory

Dempster-Shafer (DS) theory of evidence is based on the notion of assigning *beliefs* and *plausibilities* to the possible interpretations of observed multi-sensor data. A survey and taxonomy of various belief fusion operators are presented in [87]. It also provides a guide for choosing an appropriate operators for belief combination. Dempster-Shafer theory is applied for data fusion in [88] and [89].

### b. Fuzzy Logic

Fuzzy Logic has been used by many researchers and practitioners for fusing multi-sensor data. A modular fuzzy control architecture where the control function is broken down into multiple local agents, each of which samples a subset of a large sensor input space is presented in [90]. Runkler [91] describes model based fusion using a fuzzy model of the functional dependence between the sensor signals.

### c. Neural Networks

Neural Networks are used in data mining [92], classification [93], and in robotics to map multi-sensor data space into actions for providing a real-time connection between sensing and action. Lee [94] describes sensor fusion and planning using a perception-action network, which consists of a number of heterogenous computational units, representing feature transformation and decision-making for actions.

Even though the above techniques have been proven to conduct sensor fusion at different levels, there is still a need for a generic multi-sensor fusion tool. Taking weighted average of the multi-source information may not always yield a reliable measurement, especially when one or more of the sensors are faulty. Kalman filtering cannot be used if the model of the process is not available. Furthermore, such an approach is very sensitive to outliers in the data; they can completely throw off the estimate of the system state vector [95]. Other techniques must be used to filter the outliers from the data. The artificial intelligence methods require an extensive training of the system be performed prior to the actual experiment.



## CHAPTER IV

## CONDITIONING OF DISTORTED SENSOR MEASUREMENTS

This chapter details the nonlinear distortion analysis, development of signal recovery schemes, the discussion on how modeling errors and sensor noise affect the proposed methods and the recommendations to improve the accuracy of the signal reconstructed. A shorter version of this work can also be found in [96], [97], [98], [99], [100], [101]. A detailed analysis of distortion caused by sensor nonlinearity is given in section A. A discussion on how bandlimited signals can be reconstructed from the low pass filtered version of the distorted nonlinear sensor output is documented in section B. Section C extends the signal recovery procedure to a more general problem that involves measurement noise. The effects of modeling errors or model uncertainty on the outcome of the signal recovery procedure is analyzed in section D. The problem recovering distorted signals in non-stationary noisy environments is studied in section E. Considered in section F is the problem of recovering non-stationary signal from distorted nonlinear sensor measurements. A robust signal recovery scheme that uses a nominal sensor model instead of an accurate model is discussed in section G. Section H is concerned with the recovery of distorted signals in discrete domain. The signal recovery problem with non-monotonic nonlinear sensor function is considered in section I. The problem of recovering signals distorted by non-invertible sensor nonlinearities is considered in section J.

## A. Nonlinear Distortion Analysis

When a band limited signal is measured through a sensor, it is known that the low amplitude part of the signal is often indistinguishable due to corruption by noise whereas the high amplitude part may get distorted by sensor nonlinearity. Typically

only the mid range of amplitude of a signal is reproduced accurately. The nonlinear distortion of a band-limited signal manifests itself as high and low frequency foreign components in its frequency spectrum. For example, consider the measurement of a bandlimited signal

$$y = a_1 \cos(\omega_1 t) + a_2 \cos(\omega_2 t)$$

by a nonlinear sensor, which is characterized by

$$w = c_1 y + c_2 y^2$$

where  $w$  is the sensor output. The corresponding sensed signal would be

$$\begin{aligned} w = & d_0 + d_1 \cos(\omega_1 t) + d_2 \cos(\omega_2 t) + d_3 \cos[(\omega_1 - \omega_2)t] + d_4 \cos[(\omega_1 + \omega_2)t] \\ & + d_5 \cos(2\omega_1 t) + d_6 \cos(2\omega_2 t) \end{aligned}$$

Though the spectrum of signal,  $y$ , has only two frequency components  $\omega_1$  and  $\omega_2$ , the output spectrum consists of more than two frequency components  $\omega_1$ ,  $\omega_2$ ,  $(\omega_1 - \omega_2)$ ,  $(\omega_1 + \omega_2)$ ,  $2\omega_1$  and  $2\omega_2$ . Obviously, sensor nonlinearity destroys the property of band-limitedness. Thus, if the signals are being measured through a nonlinear sensor, which is characterized by a function  $g(\cdot)$ , the sensed signal  $g(y(t))$  will get distorted, even though the original  $y(t)$  would not have been. It is shown in [102] that to recover a band-limited signal  $y(t)$  with band limit  $-\Omega$  to  $\Omega$  from the distorted signal  $g(y(t))$ , it is not necessary to know the complete spectrum of  $g(y(t))$  but only that part of its spectrum that lies in the frequency band  $[-\Omega, \Omega]$ . Ignoring sensor noise, the original signal  $y(t)$  can be recovered from its distorted version if  $g(0) = 0$  and

$$0 < \frac{dg(y)}{dy} < \infty \quad \text{or} \quad -\infty < \frac{dg(y)}{dy} < 0 \quad \forall y \quad (4.1)$$

We will now generalize nonlinear sensor distortion by considering a nonlinear

sensor, which is characterized by an  $n^{\text{th}}$  order polynomial  $g(\cdot)$ ,

$$g(y) = a_1y + a_2y^2 + \cdots + a_ny^n \quad (4.2)$$

Assuming that  $g(y)$  is continuous and differentiable, condition (4.1) can be rewritten in terms of the coefficients of the above polynomial as follows.

$$0 < a_1 + 2a_2y + 3a_3y^2 + \cdots + na_ny^{n-1} < \infty, \quad \forall y \quad (4.3)$$

It can be shown that condition (4.3) will be satisfied if

$$a_1 + 3a_3|y|^2 + 5a_5|y|^4 + \cdots > 2a_2|y| + 4a_4|y|^3 + 6a_6|y|^5 \cdots \quad (4.4)$$

$\forall y$ .

Next consider the measurement of a band-limited continuous signal  $y = \cos(\omega t)$ .

The sensed signal  $w$  would be:

$$\begin{aligned} w &= g(y) \\ &= a_0 + a_1\cos(\omega t) + a_2\cos^2(\omega t) + a_3\cos^3(\omega t) + \cdots + a_n\cos^n(\omega t) \end{aligned} \quad (4.5)$$

To identify the frequency content of the signal,  $w$ , we will expand the above trigonometric power series using the following identities:

$$\begin{aligned} \cos^2(\omega t) &= \frac{1}{2} + \frac{1}{2}\cos(2\omega t) \\ \cos^4(\omega t) &= \frac{3}{8} + \frac{1}{2}\cos(2\omega t) + \frac{1}{8}\cos(4\omega t) \\ &\vdots \\ \cos^{2m}(\omega t) &= \frac{1}{2^{2m}} {}^{2m}C_m + \frac{1}{2^{2m-1}} \sum_{k=0}^{m-1} {}^{2m}C_k \cos[2(m-k)\omega t] \end{aligned}$$

and

$$\begin{aligned}
\cos^3(\omega t) &= \frac{3}{4}\cos(\omega t) + \frac{1}{4}\cos(3\omega t) \\
\cos^5(\omega t) &= \frac{10}{16}\cos(\omega t) + \frac{5}{16}\cos(3\omega t) + \frac{1}{16}\cos(5\omega t) \\
&\vdots \\
\cos^{2m+1}(\omega t) &= \frac{1}{4^m} \sum_{k=0}^m {}^{2m+1}C_k \cos[(2m+1-2k)\omega t]
\end{aligned}$$

Depending on whether  $n$  is odd or even, the expressions for the sensor output,  $w$ , will be as follows.

**Case 1:  $n$  is even**

$$w = e_0 + e_1\cos(\omega t) + e_2\cos(2\omega t) + e_3\cos(3\omega t) + \cdots + e_n\cos(n\omega t) \quad (4.6)$$

where

$$\begin{aligned}
e_0 &= \frac{1}{2}a_2 + \frac{3}{8}a_4 + \cdots + \frac{{}^nC_{\frac{n}{2}}}{2^n} a_n \\
e_1 &= a_1 + \frac{3}{4}a_3 + \cdots + \frac{{}^{n-1}C_{\frac{n}{2}-1}}{4^{\frac{n}{2}-1}} a_{n-1} \\
e_2 &= \frac{1}{2}a_2 + \frac{1}{2}a_4 + \cdots + \frac{{}^nC_{\frac{n}{2}-1}}{2^{n-1}} a_n \\
&\vdots \\
e_{n-1} &= \frac{1}{4^{\frac{n}{2}-1}} a_{n-1} \\
e_n &= \frac{1}{2^{n-1}} a_n
\end{aligned}$$

**Case 2:  $n$  is odd**

$$w = d_0 + d_1\cos(\omega t) + d_2\cos(2\omega t) + d_3\cos(3\omega t) + \cdots + d_n\cos(n\omega t) \quad (4.7)$$

where

$$\begin{aligned}
d_0 &= \frac{1}{2}a_2 + \frac{3}{8}a_4 + \cdots + \frac{{}^{n-1}C_{\frac{n-1}{2}}}{2^{n-1}} a_{n-1} \\
d_1 &= a_1 + \frac{3}{4}a_3 + \cdots + \frac{{}^nC_{\frac{n-1}{2}}}{4^{\frac{n-1}{2}}} a_n \\
d_2 &= \frac{1}{2}a_2 + \frac{1}{2}a_4 + \cdots + \frac{{}^{n-1}C_{\frac{n-3}{2}}}{2^{n-2}} a_{n-1} \\
&\vdots \\
d_{n-1} &= \frac{1}{2^{n-2}} a_{n-1} \\
d_n &= \frac{1}{4^{\frac{n-1}{2}}} a_n
\end{aligned}$$

Using (4.4), the following inequalities can be derived:

$$e_1 > e_0, e_2, e_3, \dots, e_n \quad (4.8)$$

$$d_1 > d_0, d_2, d_3, \dots, d_n \quad (4.9)$$

The above results lead to the following conclusion:

*If a bandlimited continuous signal with finite frequency components is measured through this nonlinear sensor, then the spectrum of the sensed signal will have more frequency components than that of the original signal. However, the original frequency components dominate the output spectrum. That is, the strengths of the original frequency components in the output spectrum are greater than the strength of any other foreign frequency spike.*

If the spectrum of the original signal consists of multiple frequency components, then the expressions for the sensor output,  $w$ , will slightly differ from those derived

for the single frequency case. For example, let  $y$  be

$$y = s_1 \cos(\omega_1 t) + s_2 \cos(\omega_2 t) \quad (4.10)$$

Then the expression for the corresponding sensor output would be,

$$\begin{aligned} w = & h_1 \cos(\omega_1 t) + h_2 \cos(\omega_2 t) + h_3 \cos[(\omega_1 - \omega_2)t] + h_4 \cos[(\omega_1 + \omega_2)t] \\ & + h_5 \cos[(2\omega_1 - \omega_2)t] + h_6 \cos[(\omega_1 - 2\omega_2)t] + h_7 \cos(2\omega_1 t) + h_8 \cos(2\omega_2 t) + \dots \end{aligned} \quad (4.11)$$

It is again observed that the amplitudes of the original frequency components are greater than that of any other frequency component when condition (4.4) is satisfied. In addition to the high harmonics, the following low frequency components can also be seen in the output spectrum due to intermodulation:  $|\omega_1 - \omega_2|$ ,  $|2\omega_1 - \omega_2|$ ,  $|\omega_1 - 2\omega_2|$ ,  $|2\omega_1 - 2\omega_2|$ ,  $|3\omega_1 - 3\omega_2|$ ,  $\dots$  and so on.

If none of the above intermodulation frequencies is equal to  $\omega_1$  and  $\omega_2$ , then the amplitude ratio of the original frequencies is preserved even after the nonlinear distortion, that is,

$$\frac{s_1}{s_2} = \frac{h_1}{h_2}.$$

We will next present the distortion compensation techniques and explain how the actual data can be recovered from the distorted and noisy nonlinear sensor measurement.

## B. Recovery of Band-limited Signals

As shown in Fig. 4, to preserve the exact band-limitedness of signals, an ideal low pass filter should be used, which is given by

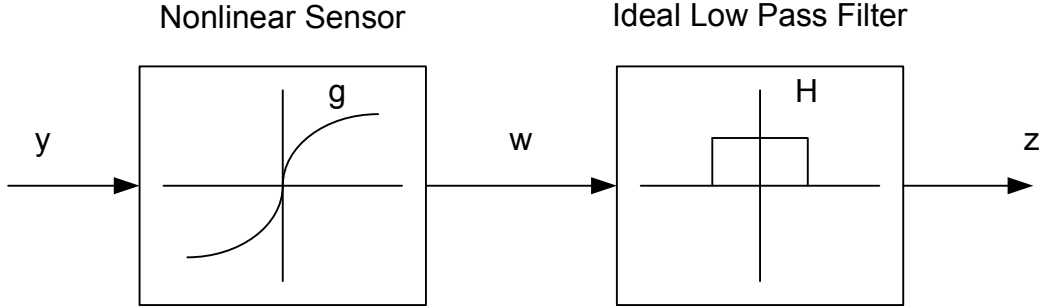


Figure 4: Basic Signal Recovery Setup

$$\mathcal{H}(w) = \begin{cases} 1 & |\omega| \leq \Omega \\ 0 & \text{otherwise} \end{cases}$$

It is shown in [96] that the iterative scheme given by

$$y_{k+1}(t) = y_k(t) + \alpha z(t) - \alpha \mathcal{F}^{-1}\{\mathcal{H}\mathcal{F}\{g(y(t))\}\} \quad (4.12)$$

converges to  $y(t)$  if  $r = \max_y |1 - \alpha \frac{dg(y)}{dy}| < 1$ , where  $z(t)$  is the filtered signal,  $\alpha$  is the convergence parameter,  $\mathcal{F}$  is Fourier Transform and  $\mathcal{F}^{-1}$  is Inverse Fourier Transform.

With a suitable choice of  $\alpha$  and conditions (4.1), it can be shown that the convergence requirement  $r < 1$  is satisfied [102, 96]. The converged solution  $y$  is given by

$$y = y + \alpha z - \alpha \mathcal{F}^{-1}\{\mathcal{H}\mathcal{F}\{g(y)\}\} \quad (4.13)$$

or

$$z = \mathcal{F}^{-1}\{\mathcal{H}\mathcal{F}\{g(y)\}\} \quad (4.14)$$

Next, it is shown that this user-defined convergence parameter,  $\alpha$ , should be carefully chosen because any inappropriate choice may generate misleading results. To

derive the correct range of  $\alpha$ , suppose that the nonlinear sensor function is monotonic with positive gradients, *i.e.*  $0 < \frac{dg(y)}{dy} < \infty \quad \forall y$ . In this case, it can be easily shown that the convergence requirement  $r = \max_y |1 - \alpha \frac{dg(y)}{dy}| < 1$  will be satisfied if  $0 < \alpha < \frac{2}{\max\{\frac{dg(y)}{dy}\}}$ .

The above iterative procedure, which assumes no or high frequency noise will not converge to  $y$  if the sensor output  $w_n$  is corrupted by noise  $n$  as shown in Fig. 5. The effect of noise is considered next.

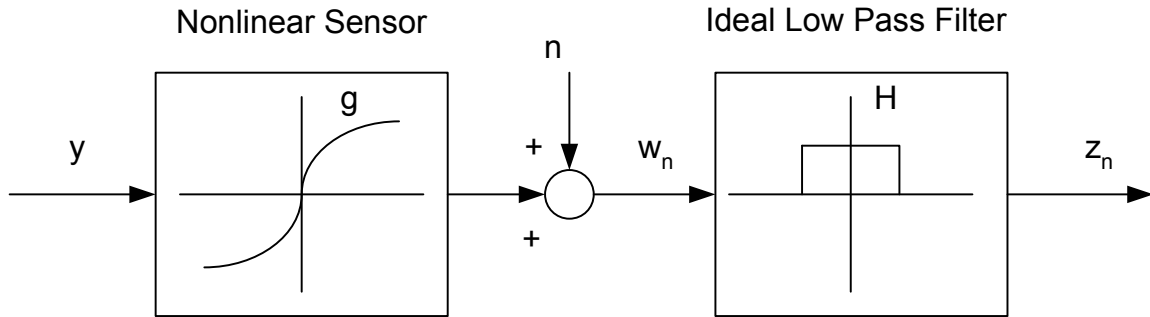


Figure 5: Recovery of Signals Corrupted by Noise

Let  $z_n$  be the filtered output of the setup shown above. If convergence requirements are met, the algorithm still converges to a solution  $y_n$ , which is given by

$$y_n = y_n + \alpha z_n(t) - \alpha \mathcal{F}^{-1}\{\mathcal{HF}\{g(y_n)\}\} \quad (4.15)$$

Subtracting Equations (4.13) and (4.15) and taking the norm on both sides of the resultant equation yields

$$\begin{aligned} \|y - y_n\| &\leq \alpha \|z - z_n\| + \\ &\|(y - y_n) - \alpha \mathcal{F}^{-1}\{\mathcal{HF}\{g(y)\}\} + \alpha \mathcal{F}^{-1}\{\mathcal{HF}\{g(y_n)\}\}\| \end{aligned} \quad (4.16)$$

Throughout this subsection, unless otherwise stated norm  $\|\cdot\|$  refers to:



$$\|f(t)\| = \left[ \int_{-\infty}^{\infty} |f(t)|^2 dt \right]^{\frac{1}{2}}$$

As signals  $y$  and  $y_n$  are band-limited with band  $[-\Omega, \Omega]$ ,

$$\begin{aligned}
& \|(y - y_n) - \alpha \mathcal{F}^{-1}\{\mathcal{H}\mathcal{F}\{g(y)\}\} + \alpha \mathcal{F}^{-1}\{\mathcal{H}\mathcal{F}\{g(y_n)\}\}\|^2 \\
&= \|(y - y_n) - \mathcal{F}^{-1}\{\mathcal{H}\mathcal{F}\{\alpha g(y) - \alpha g(y_n)\}\}\|^2 \\
&= \|\mathcal{F}^{-1}\{\mathcal{H}\mathcal{F}\{(y - y_n) - [\alpha g(y) - \alpha g(y_n)]\}\}\|^2 \\
&= \|\mathcal{H}\mathcal{F}\{(y - y_n) - [\alpha g(y) - \alpha g(y_n)]\}\|^2 \\
&= \frac{1}{2\pi} \int_{-\infty}^{\infty} |\mathcal{H}\mathcal{F}\{(y - y_n) - [\alpha g(y) - \alpha g(y_n)]\}|^2 dw \\
&= \frac{1}{2\pi} \int_{-\Omega}^{\Omega} |\mathcal{F}\{(y - y_n) - [\alpha g(y) - \alpha g(y_n)]\}|^2 dw \\
&\leq \|\mathcal{F}\{(y - y_n) - [\alpha g(y) - \alpha g(y_n)]\}\|^2 \\
&= \|(y - y_n) - [\alpha g(y) - \alpha g(y_n)]\|^2 \\
&= \int_{-\infty}^{\infty} |y - y_n|^2 \left| 1 - \alpha \frac{g(y) - g(y_n)}{y - y_n} \right|^2 dt \\
&\leq \max_y \left| 1 - \alpha \frac{dg(y)}{dy} \right|^2 \|y - y_n\|^2 \\
&= r^2 \|y - y_n\|^2
\end{aligned} \tag{4.17}$$

Using Equation (4.17), Equation (4.16) can be written as:

$$\|y - y_n\| \leq \alpha \|z - z_n\| + r \|y - y_n\|$$

That is,

$$\|y - y_n\| \leq \frac{\alpha}{1 - r} \|z - z_n\| \tag{4.18}$$

According to Equation (4.18), if noise is present, then the filtered signal may not be equal to  $z$  and the recovery algorithm may not converge to the correct solution. It should be noted that if noise has only high frequency components, then the ideal low pass filter can remove noise completely. In that case,  $z = z_n$  and therefore the original

signal will be recovered. We will not consider this special case, which is obviously trivial. However, it is worth noting here that at least a part of noise will be removed by the low pass filter.

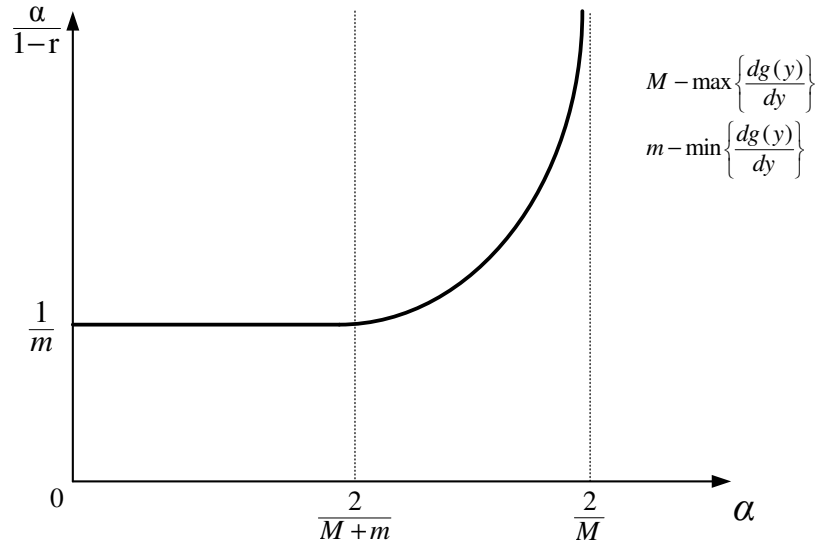


Figure 6: Effect of  $\alpha$  on Weight  $\frac{\alpha}{1-r}$

The convergence accelerator  $\alpha$  determines the rate of convergence of the iterative scheme given by Equation (4.12) and the degree of stability of this algorithm. The relationship between the weighting  $\frac{\alpha}{1-r}$  and the convergence accelerator,  $\alpha$  is plotted in Fig. 6. Referring to Equation (4.18) and Fig. 6, the norm of errors due to noise ( $\|y - y_n\|$ ) has an upper bound, which can be optimized by choosing  $\alpha$  to be within 0 and  $\frac{2}{M+m}$  and the optimum value is  $\frac{1}{m}\|z - z_n\|$ . This proves stability of the recovery algorithm. Furthermore, if the error bound given in Equation (4.18) is acceptable for certain applications, then the recovery algorithm could be used to recover signals that are subject to noise. However, in certain applications that require precision in sensor measurements, the above error bound may not be tolerable. In this case, additional procedures should be included to tackle sensor noise. How this can be done

is discussed in the next section.

### C. Recovery of Corrupted/Noisy Band-limited Signals

If a nonlinear sensor is designed such that it supports the recovery requirements as given in Equation (4.1) and has a very high gradient within the noise floor so that the actual sensor data can be distinguishable from sensor noise, then it is possible to remove noise completely and the original signal can be uniquely recovered from the filtered signal.

By transforming the distorted and noisy sensor output  $w_n = g(y) + n$  to the frequency domain, noise components can be identified as relatively low strength spikes. As shown in Fig. 7, a suitable threshold filter could be used to remove these spikes. In practice, threshold filtering can be accomplished by a threshold comparator as shown in Fig. 8.

The filtered signal  $z_d$  can be used to recover the original signal using the following iterative scheme:

$$y_{k+1} = y_k + \alpha z_d - \alpha \mathcal{F}^{-1}\{\mathcal{HTF}\{g(y_k)\}\} \quad (4.19)$$

where  $\mathcal{T}$  is the threshold filtering operation defined by,

$$\mathcal{T}(v) = \begin{cases} 1 & |v| \geq \delta \\ 0 & \text{otherwise} \end{cases} \quad (4.20)$$

where  $\delta$  is the threshold, and  $|v|$  is the amplitude of a frequency spike.

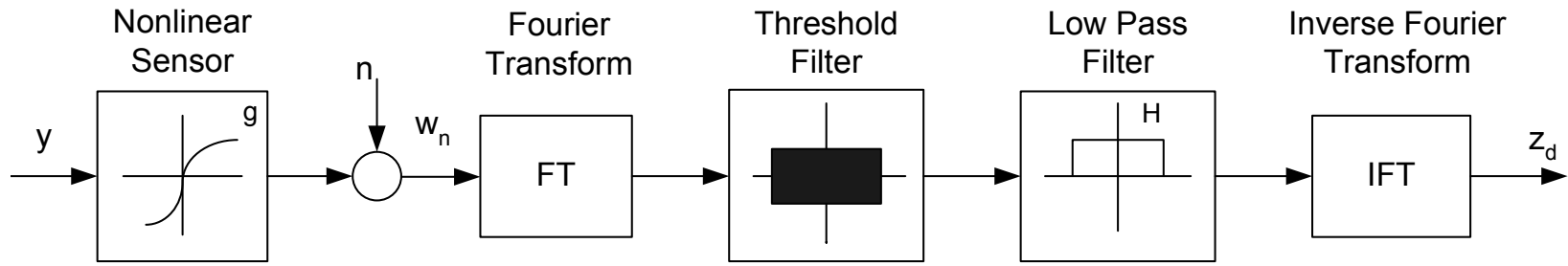


Figure 7: Signal Recovery Setup That Incorporates Noise Removal

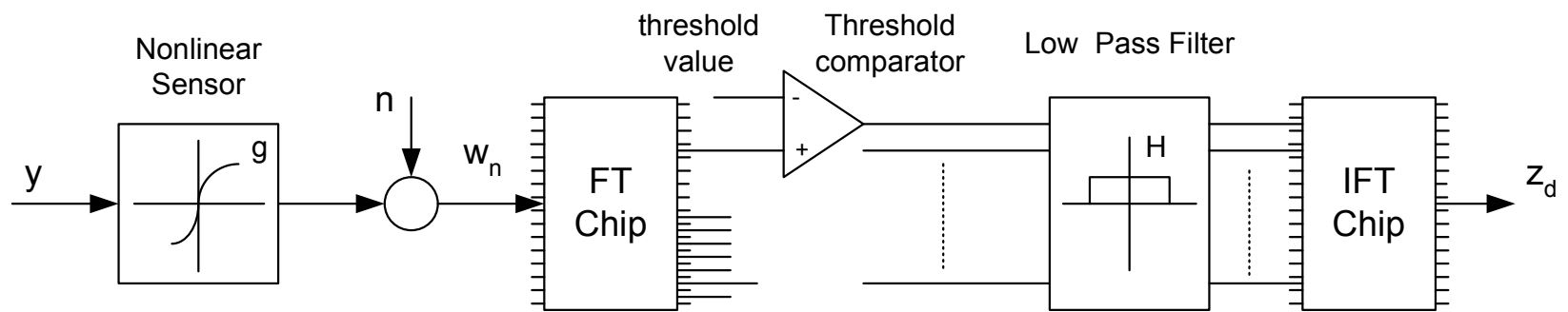


Figure 8: Practical Implementation of Threshold Filtering

The threshold filtering operation is done in the frequency domain. For a signal that has a finite number of frequency spikes, this operation is carried out as follows.

$$\mathcal{TF}\{g(y_k)\} = \mathcal{T} .* \mathcal{F}\{g(y_k)\}$$

where  $.*$  is the term by term multiplication. When each term of  $\mathcal{F}\{g(y_k)\}$  is multiplied by the appropriate term of the threshold filter defined by Equation (4.20), the low strength frequency components will be eliminated.

The important steps involved in the recovery process are summarized in the following algorithm:

**Algorithm 1** *Recovery of Corrupted Signals*

**Step 1** *[Acquiring Sensor Data] Acquire sensor data  $w_n$ .*

**Step 2** *[Obtaining Output Spectrum] Using the Fourier Transform, obtain the frequency spectrum of sensor data  $w_n$ .*

**Step 3** *[Filtering out Noise] Design a threshold filter to remove the low strength frequency spikes.*

**Step 4** *[Removing High Harmonics] Pass the cleaned signal through an ideal low pass filter and use the Inverse Fourier Transform to transform it back to the time domain.*

**Step 5** *[Recovering the Original] Use the iterative scheme given in Equation (4.19) to recover the original signal from the filtered signal.*

If the convergence requirements are satisfied, the algorithm will converge to a solution, which is given by

$$\begin{aligned}
z_d &= \mathcal{F}^{-1}\{\mathcal{HT}[\mathcal{F}\{g(y)\}]\} \\
&= \mathcal{N}(y)
\end{aligned}$$

where  $\mathcal{N}$  is a cascaded nonlinear operation of  $\mathcal{H}, \mathcal{T}$  and  $g(\cdot)$ . An underlying assumption behind this recovery scheme is that no original information within the frequency band  $[-\Omega, \Omega]$  is lost by the nonlinear transformation  $\mathcal{N}$ . In addition, if the nonlinear function has a very high slope near zero, the iterative schemes (4.12) and (4.19) are identical as the threshold operator  $\mathcal{T}$  simply removes noise  $n$  and reproduce signal  $g(y)$  from the corrupted signal  $g(y) + n$ . If noise is not completely removed by this process, the true signal may not be recovered and the error in the recovered signal will be characterized by Equation (4.18).

#### D. Effect of Modeling Errors

It is emphasized that a unique signal recovery is possible only if the exact sensor function  $g(\cdot)$  is fed to the iterative process. In practice, modeling errors are inevitable and the exact sensor function is difficult if not impossible to obtain. Investigated next is how the modeling errors affect the (converged) solution. Let  $g_a(\cdot)$  be the available model. The filtered signal obtained using  $g_a(\cdot)$  is given by

$$z_a = \mathcal{F}^{-1}\{\mathcal{HF}\{g_a(y)\}\} \quad (4.21)$$

The expression for the ideally filtered signal would be

$$z = \mathcal{F}^{-1}\{\mathcal{HF}\{g(y)\}\} \quad (4.22)$$

The following inequality can be obtained using the previously proven result given

in Equation (4.18).

$$\|y - y_a\| \leq \frac{\alpha}{1-r} \|z - z_a\| \quad (4.23)$$

Substituting for  $z$  and  $z_a$  using the expressions (4.21) and (4.22), we obtain

$$\|y - y_a\| \leq \frac{\alpha}{1-r} \|\mathcal{F}^{-1}\{\mathcal{HF}\{g(y)\}\} - \mathcal{F}^{-1}\{\mathcal{HF}\{g_a(y)\}\}\| \quad (4.24)$$

But

$$\|\mathcal{F}^{-1}\{\mathcal{HF}\{g(y)\}\} - \mathcal{F}^{-1}\{\mathcal{HF}\{g_a(y)\}\}\| = \|\mathcal{HF}\{g(y)\} - \mathcal{HF}\{g_a(y)\}\| \quad (4.25)$$

Using

$$\begin{aligned} \int_{-\infty}^{\infty} |\mathcal{HF}\{g(y)\} - \mathcal{HF}\{g_a(y)\}|^2 dw &= \int_{-\Omega}^{\Omega} |\mathcal{HF}\{g(y)\} - \mathcal{HF}\{g_a(y)\}|^2 dw \\ &\leq \int_{-\infty}^{\infty} |\mathcal{F}\{g(y)\} - \mathcal{F}\{g_a(y)\}|^2 dw \end{aligned}$$

we obtain

$$\|\mathcal{HF}\{g(y)\} - \mathcal{HF}\{g_a(y)\}\| \leq \|\mathcal{F}\{g(y)\} - \mathcal{F}\{g_a(y)\}\| \quad (4.26)$$

Using Expressions (4.25) and (4.26), Expression (4.24) can be written as:

$$\|y - y_a\| \leq \frac{\alpha}{1-r} \|\mathcal{F}\{g(y)\} - \mathcal{F}\{g_a(y)\}\| \quad (4.27)$$

Using the fact

$$\|\mathcal{F}\{g(y)\} - \mathcal{F}\{g_a(y)\}\| = \|g(y) - g_a(y)\|$$



the expression for the error signal (4.27) becomes

$$\|y - y_a\| \leq \frac{\alpha}{1-r} \|g(y) - g_a(y)\| \quad (4.28)$$

The above expression shows that the maximum error is proportional to modeling error or uncertainty. Referring to Fig. 6, this error can be optimized with a proper choice of the convergence accelerator  $\alpha$ . The weighting  $\frac{\alpha}{1-r}$  will be minimum when  $0 < \alpha < \frac{2}{M+m}$ . This proves that the algorithm is stable with respect to sensor model error.

#### E. Recovery of Signals Corrupted by Non-stationary Noise

In this section, it is discussed how accuracy of recovered signal can be improved when sensor measurements are subject to unknown non-stationary noise. Numerous applications ranging from underwater acoustics to cellular communications in which sensor measurements are subject to non-stationary noise exist in practice [103]. The fact that the wavelet transform localizes the event on the time-frequency plane by a projection of the transient signal on to the basic wavelets at different scale or resolution makes the wavelet based denoising methods very efficient in dealing with such transient noise effects.

##### 1. Wavelets and Filter Banks

From the mathematical definition of continuous wavelet transform (CWT) [10], a time domain function  $f(t)$  can be represented or approximated by many translated and scaled versions of a particular (basic) wavelet,  $\psi(t)$ ,

$$(W_\psi f)(a, b) = \int_{-\infty}^{\infty} f(t) \frac{1}{\sqrt{|a|}} \overline{\psi\left(\frac{t-b}{a}\right)} dt \quad (4.29)$$

where  $W_\psi f$  is the transformation coefficient that is a function of the scaling and translation parameters,  $a$  and  $b$  respectively and  $\overline{\psi(\cdot)}$  is a complex conjugate of  $\psi(\cdot)$ . Since  $b$  is a parameter of time and  $a$  carries the spectral details of the wavelet function, wavelet transformation reveals both the time and spectral information of  $f(t)$  through fitting of the many different scaled and translated versions of the basic wavelet to  $f(t)$ . The Discrete Wavelet Transform (DWT), which is defined below is a fast algorithm that computes digitally the transform coefficients on the dyadic scale by setting  $a = 2^{-j}$  and  $b = ka$ .

$$(W_\psi f)(2^{-j}, k2^{-j}) = 2^{-j/2} \int_{-\infty}^{\infty} f(t) \psi(2^j t - k) dt \quad (4.30)$$

The DWT algorithms decomposes the spectrum of a signal by digital filtering and downsampling into components in octave frequency sub-bands. As shown in Figure 9 (where  $\downarrow 2$  denotes decimation or downsampling,  $\uparrow 2$  denotes interpolation or upsampling and  $h_0, h_1, g_0$  and  $g_1$  are filters designed to attain the required decomposition and a perfect reconstruction), this multi-resolution decomposition of a signal into its coarse and detail components is useful for denoising. If the frequency change of an event is too small, the wavelet packet transform (WPT) that consists of several sub-bands may be used to refine the indication. If the spectra of two different signatures are too close for the DWT algorithm to resolve, the WPT can refine a wavelet sub-band into two wavelet-packet sub-band with finer spectral distinction. The decomposed data can be processed to remove noise. The perfect reconstruction properties of the DWT algorithms assure the user of recovering the processed original function from the sample values.

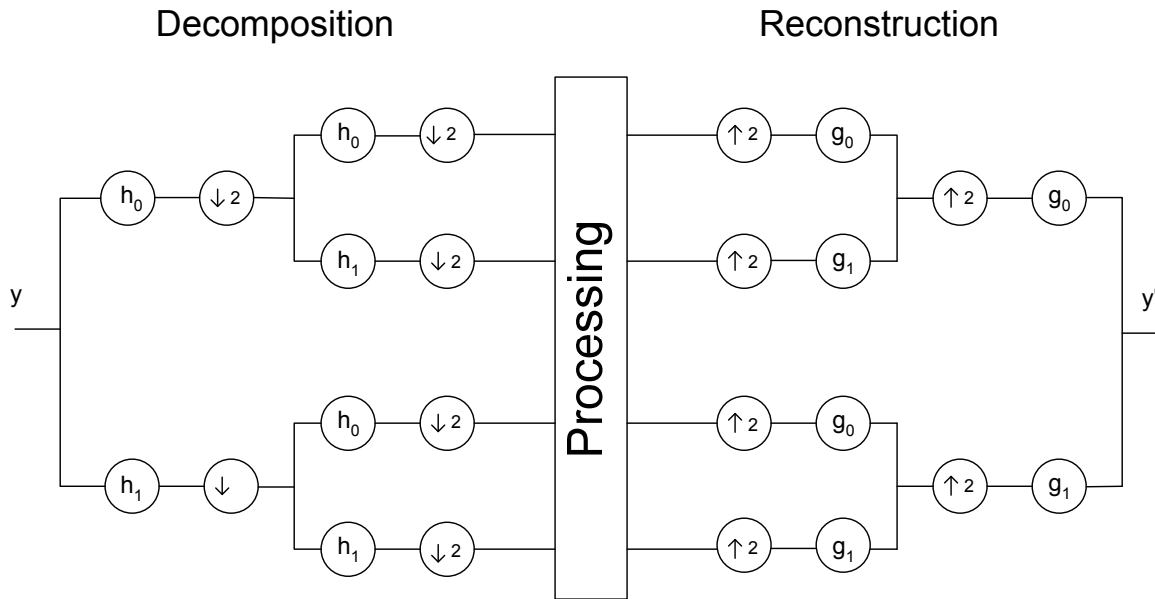


Figure 9: Decomposition and Reconstruction in Wavelet Packets

## 2. Removal of Noise in Sensor Output

Filtering of noise is done by the decomposition and reconstruction processes using the Filter Bank setup shown in Figure 9. The number of sub-bands required will be decided based on how complicated or noisy is the signal data. The coarsest approximation of the signal together with the details at every level completely represent the original signal.

As shown in Figure 9, the basic steps in the wavelet filtering process are:

1. Decompose a complicated noisy signal into simpler ones using the DWT.
2. Process the decomposed components using standard signal filtering techniques to identify and remove noise.
3. Reconstruct the denoised estimate using the Inverse Discrete Wavelet Transform (IDWT).

The processing of noise can be done in many ways. Thresholding is one of the most commonly used processing tools in wavelet signal processing. It is widely used in noise reduction, signal and image compression, and sometimes in signal reconstruction [10]. We consider two simple thresholding methods [104] here. (1) hard thresholding, (2) soft thresholding.

Hard thresholding is done by setting a signal or coefficient value to zero when it is below a preset value. That is,

$$y = \begin{cases} x & |x| \geq \sigma \\ 0 & |x| < \sigma, \end{cases} \quad (4.31)$$

where  $\sigma$  is the threshold value.

Soft thresholding is defined as

$$y = \begin{cases} \text{sgn}(x)f(|x| - \sigma) & |x| \geq \sigma \\ 0 & |x| < \sigma. \end{cases} \quad (4.32)$$

Implementation of the hard and soft thresholding methods are quite simple: The magnitude of each coefficient is subtracted from the threshold, if the difference is negative, the coefficient is set to zero and if it is positive no change is applied to the coefficient.

To identify and remove non-stationary noise in the low pass filter output,  $z$  (as in Figure 10), we will use the setup shown in Figure 11, where  $v$  is the denoised estimate of the low pass filter output.

Now, in order to reconstruct the sensor input,  $y$ , we will replace signal,  $z$ , in the recursive equation (4.12) by the denoised signal,  $v(t)$ , and obtain the following modified iterative equation,

$$y_{k+1}(t) = y_k(t) + \alpha v(t) - \alpha \mathcal{F}^{-1}\{\mathcal{H}\mathcal{F}\{g(y_k(t))\}\}. \quad (4.33)$$

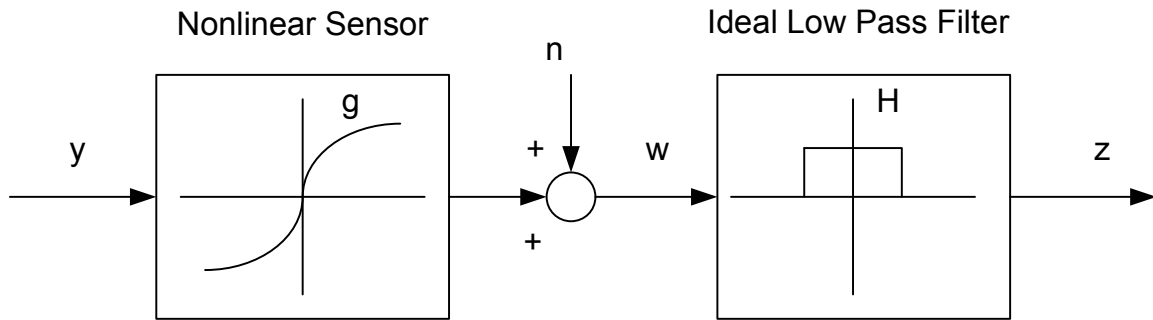


Figure 10: Signal Recovery Setup That Incorporates Non-stationary Noise

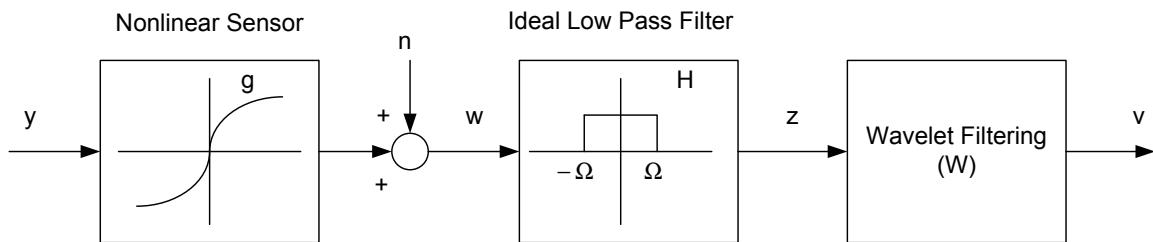


Figure 11: Wavelet Filtering of Noise

If noise is not completely removed by the wavelet filtering method, then the signal recovered by solving Equation (4.33) will have errors. Let  $y_w$  be the recovered signal in this case. It can be shown that [98]  $y_w$  is related to the actual sensor input  $y$  by,

$$\|y - y_w\| \leq \frac{\alpha}{1 - r} \|z - v\| \quad (4.34)$$

With an efficient denoising, the upper bound of the errors due to unfiltered noise described by Equation (4.34) can be reduced.

Furthermore, as  $\|z - v\| < \|z - z_n\|$  in general, it is expected that signal recovered using the iterative equation (4.33) will be more accurate than that obtained by solving Equation (4.12).

## F. Recovery of Chirp Signals

The above iterative scheme will fail to reconstruct signal,  $y$  if it is a non-stationary or chirp signal. As frequency content of a chirp signal varies with time, the above Fourier Transform based algorithm will not be able to analyze or process it efficiently. This is due to the fact that transforming back and forth from frequency domain to time domain does not preserve the Time-Frequency information. We will use a simple example to illustrate this point.

### 1. Reconstruction of Bandlimited Chirp Signals

The Signal Reconstruction Scheme was developed in the preceding sections bearing in mind that signals considered are bandlimited and stationary. In practice, it is difficult to make the separation of stationary and non-stationary or chirp signals as they are bound to be mixed. For example, almost all biological signals are chirp. ECG (electrical activity of the heart and electrocardiograph), EEG (electrical activity of the brain and electroencephalograph) and EMG (electrical activity of the muscles and electromyogram) are a few applications worth noting. In order to correctly identify the chirp signals, the stationarity assumption has to be eliminated or necessary modifications to the proposed algorithm have to be done.

The use of Fourier Transform in the proposed signal recovery methods has many disadvantages. A serious drawback is its inability to accurately interpret the time-frequency information of a chirp signal. The frequency spectrum obtained using Fourier Transform does not usually display the true frequency content of a chirp signal. As frequency content of a chirp signal changes with time, the frequency spectrum may not always be useful and frequency domain data processing may not yield accurate results. A simple example is presented next to illustrate this point.

## 2. Example 1

Let us consider a nonlinear sensor that is characterized by the function shown in Figure 12. Now pass a band-limited chirp signal shown in Figure 13 through this sensor and filter it using an ideal low pass filter. The frequency spectrum of the chirp signal ( $y$ ) obtained using Fourier Transform is shown in Figure 14. All signals considered are assumed to be of finite duration and are sampled at 1025 Hz. Figure 15 shows the Time-Frequency Map of the chirp signal obtained using Continuous Wavelet Transform. It is evident from this figure that signal,  $y$ , is bandlimited with a maximum frequency of 70 Hz. In order to recover the signal,  $y$ , using the signal recovery procedure described by Equation (4.12), an ideal low pass filter of very high band width, say about 400 Hz has to be used. Referring to the spectrum of  $y$  shown in Figure 14, the input signal has frequencies across the entire frequency spectrum and the use of the ideal low pass filter whose cut-off frequency is less than the bandwidth of the entire spectrum will only result in the removal of actual sensor data. An accurate signal recovery may not be possible in this case.

Implementing a very high bandwidth ideal low pass filter may not be always feasible as this will result in an infinite bandwidth sensor operation. Intuitively, it is argued that the hassle of frequency domain processing may be avoided if signal processing is done only in the time domain, instead of back and forth transformation from time domain to frequency domain. In fact, this can be made feasible by using the following convolution identity.

$$\mathcal{F}^{-1}\mathcal{H}\mathcal{F}\{g(y)\} = \int_{-\infty}^{\infty} g(y(\tau)) \frac{\sin[\Omega(t - \tau)]}{\pi(t - \tau)} d\tau$$

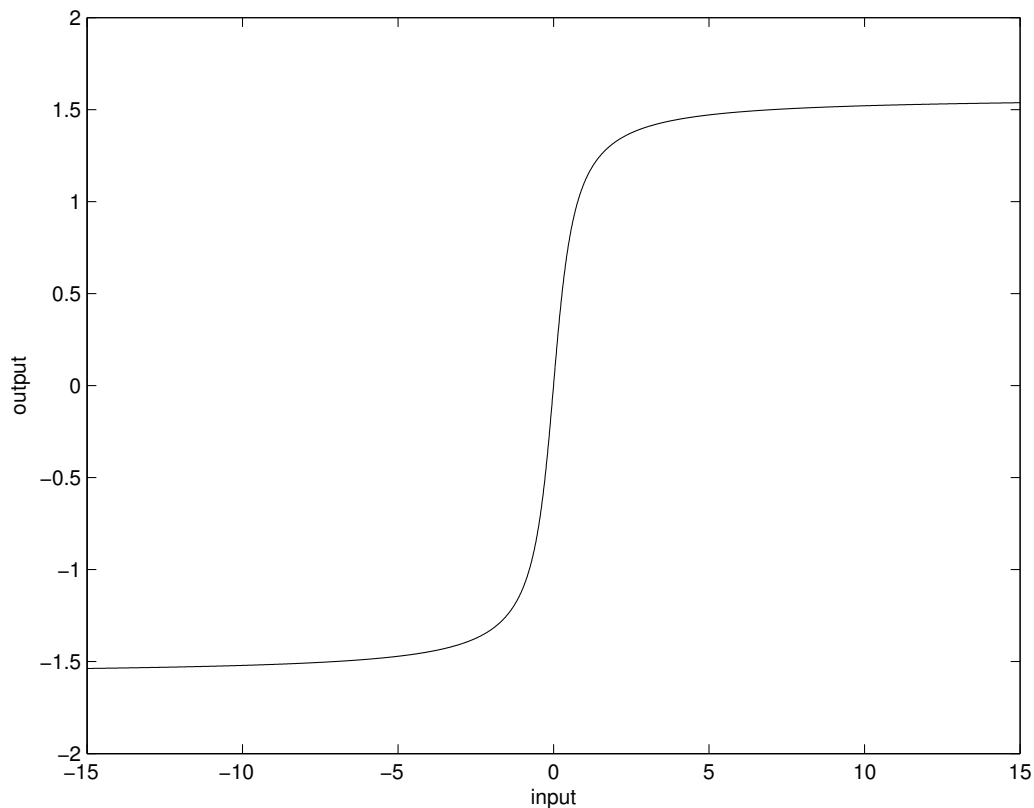


Figure 12: Nonlinear Sensor Used in Example 1

Using the above convolution integral, the iterative signal recovery scheme described by Equation (4.12) is modified as follows.

$$v_{k+1}(t) = v_k(t) + \alpha z(t) - \alpha \int_{-\infty}^{\infty} g(v_k(\tau)) \frac{\sin[\Omega(t - \tau)]}{\pi(t - \tau)} d\tau \quad (4.35)$$

Iterative algorithm given by Equation (4.35) does not require any frequency domain transformation as signal processing is done only in the time domain. Therefore, it can preserve Time-Frequency Information of a chirp signal and should successfully recover the chirp signals from their distorted versions. The only disadvantage is that the threshold filtering procedure described in Section 3 is inapplicable. This is because the threshold filtering operation is done in the frequency domain and the recovery



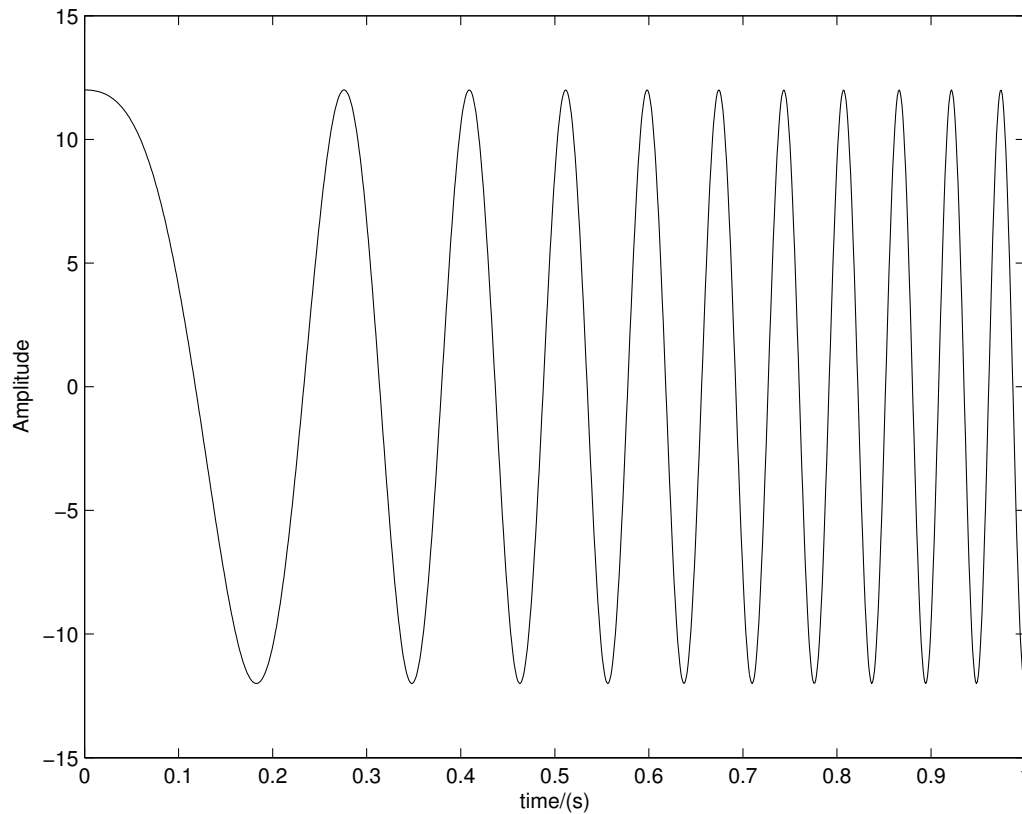


Figure 13: Chirp Signal

procedure of Equation (4.35) does not allow frequency domain processing. It is noted that the ideal low pass filter implemented through its time domain coefficients will remove high frequency sensor noise. Another example is presented next to support this method.

### 3. Example 2

Consider again the same nonlinear sensor and the chirp signal used in Example 1. Applying the recursive scheme of Equation (4.35), we obtain the signal shown in Figure 16, which is, in fact, the original chirp signal. To implement the recovery

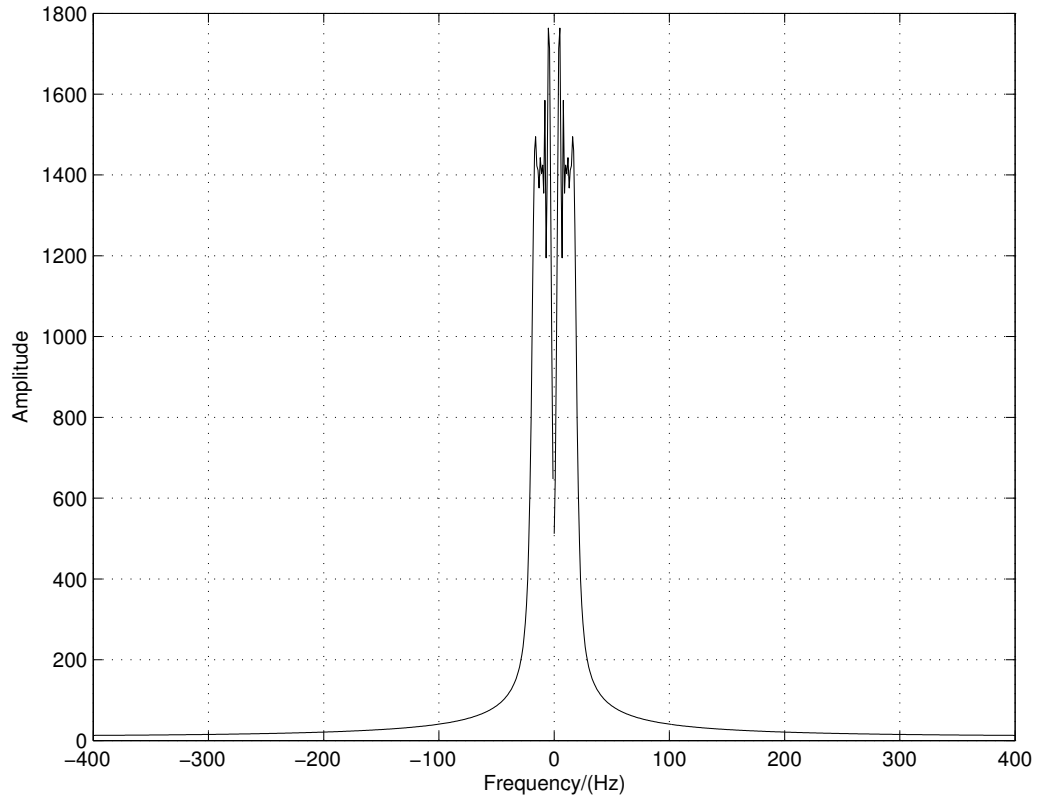


Figure 14: Spectrum of Chirp Signal

scheme described by Equation (4.35) for practical problems in Matlab platform, the following algebraic loop is used.

$$v_{k+1}(t) = v_k(t) + \alpha z(t) - \alpha \text{conv} \left\{ g(v_k(t)), \frac{\sin \Omega t}{\pi t} \right\}$$

where *conv* is a Matlab Command used to convolve two signals and the cut-off frequency of the ideal low pass filter,  $\Omega$ , is chosen to be 70 Hz.

This example validates the proposed claim.

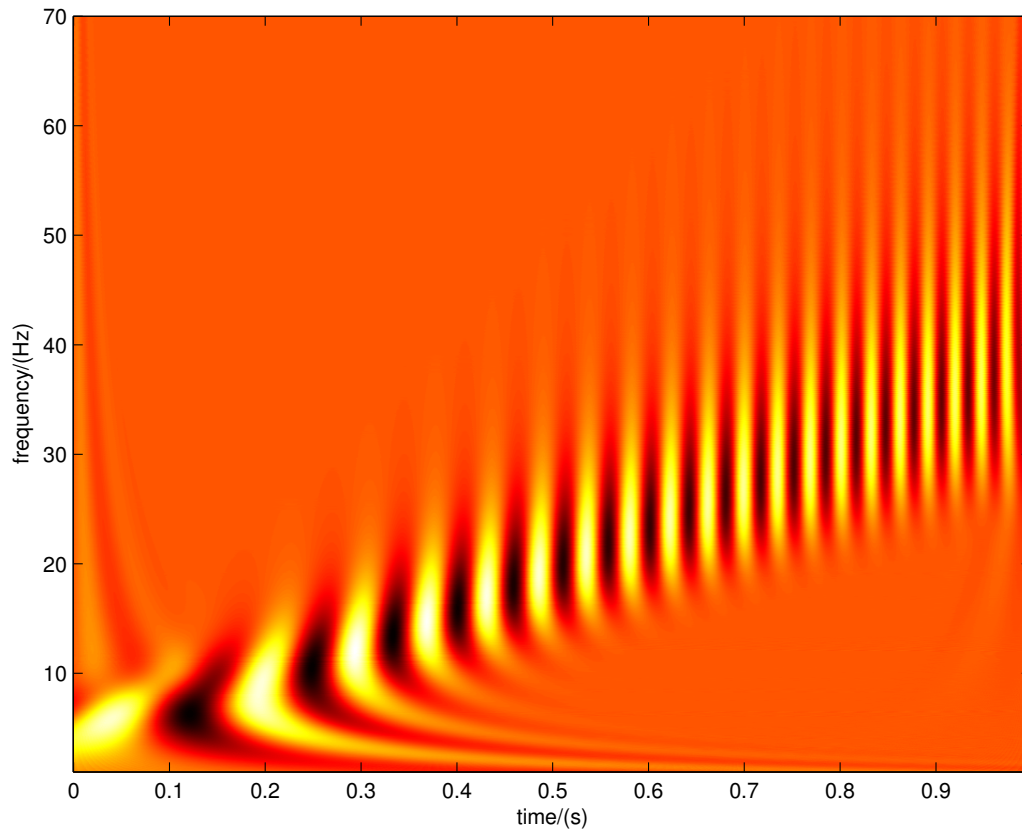


Figure 15: Time Frequency Map Obtained Using Continuous Wavelet Transform

### G. Recovery of Signals Using Nominal Sensor Model

It is noted that accurate signal recovery is possible only if the exact sensor model is known. Though the error that occurs due to model uncertainties can be minimized up to a certain extent, it cannot be completely removed. Most sensors are sensitive to physical parameters such as temperature. Therefore, expensive and time consuming periodic calibration and maintenance are necessary to preserve the true input output relationship. If it is possible to interpret a physical variable using a nominal sensor model instead of an accurate sensor model, it would be considered advantageous in many aspects. In this section, such an approach is proposed.

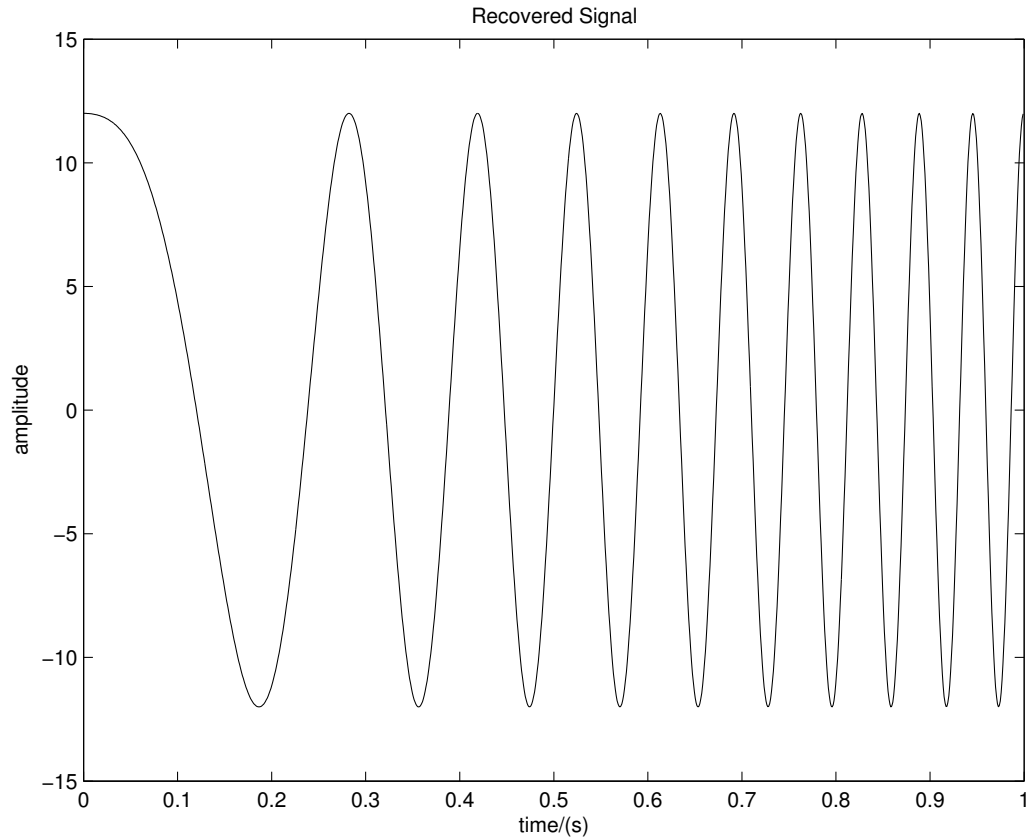


Figure 16: Solution to the Recursive Equation (Example 2)

Consider a nonlinear sensor model shown in Fig. 17. Let  $G$  be the nominal nonlinear sensor function matrix and  $\Delta$  be the uncertainty matrix. The actual sensor model  $G_a$  is,

$$G_a = G + \Delta \quad (4.36)$$

Suppose that Nonlinear Filtering Setup schematically shown in Fig. 4 and the Iterative Equation (4.12) are used to recover the original signal. The original signal,  $y$  and the sensor output,  $w$  are related by,

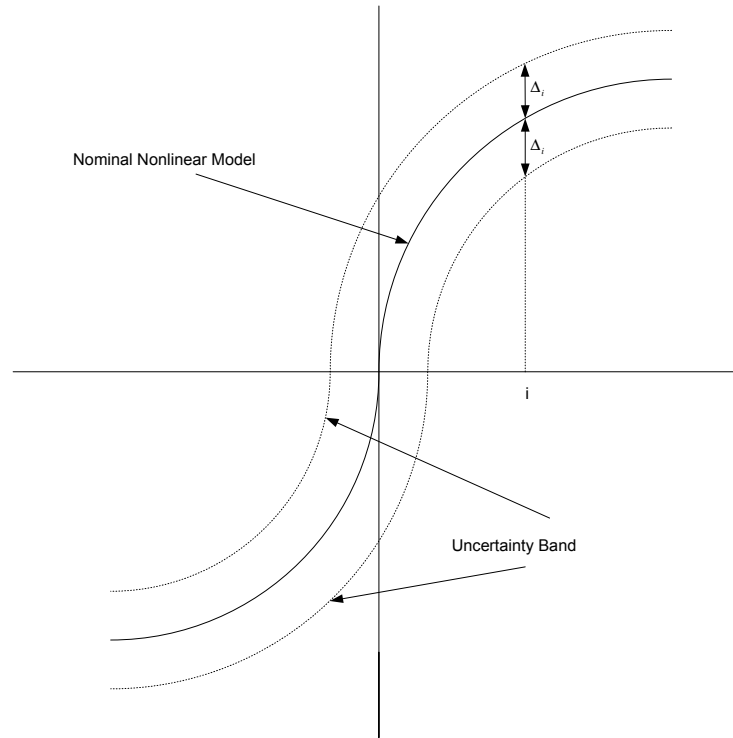


Figure 17: Uncertain Sensor Model

$$\begin{aligned}
 w &= G_a y + n \\
 &= (G + \Delta)y + n \\
 &= Gy + \Delta y + n \\
 &= Gy + n_g
 \end{aligned} \tag{4.37}$$

where  $n$  is measurement noise  $n_g = \Delta y + n$ .

The nominal sensor model,  $G$  is supposed to preserve the original information whereas the model uncertainty,  $\Delta$  would generate noise-like signal,  $\Delta y$ . The idea behind the proposed approach is schematically shown in Fig. 18 in which the nominal

model is assumed to be linear.

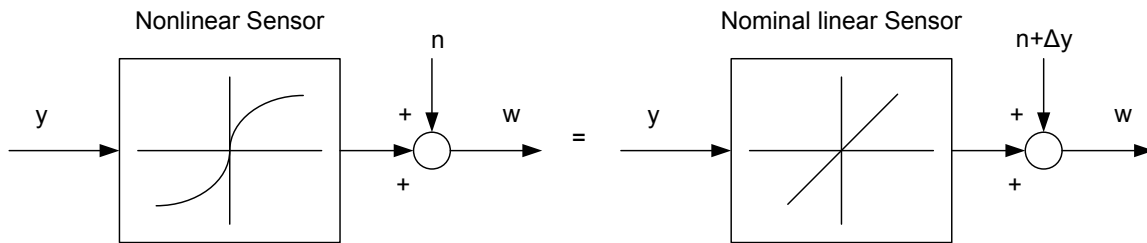


Figure 18: Proposed Approach

In general, the nominal sensor model may not be linear especially when the input signal consists of multiple frequency components. This is because the nonlinear sensor function may amplify multiple frequency components differently, which may not be equivalently represented by a linear function. However, a linear piece-wise function may be used as a nominal sensor model. In most cases, identifying a suitable nominal sensor model may be easier than the tedious actual sensor model identification. For example, assuming that  $g(0) = 0$ , the Taylor Series Expansion of function,  $g(y)$  about the origin can be written using the standard notation as follows.

$$\begin{aligned} g(y) &= g'y + \frac{1}{2!}g''y^2 + \frac{1}{3!}g^3y^3 + \frac{1}{4!}g^4y^4 + \dots \\ &= a_1y + a_2y^2 + a_3y^3 + a_4y^4 + \dots \end{aligned}$$

The above series can be divided into two as shown below.

$$g(y) = \underbrace{a_1y + a_3y^3 + \dots}_G + \underbrace{a_2y^2 + a_4y^4 + \dots}_\Delta$$

The even power terms do not preserve the original frequency information and may be considered to generate noise-like signals. The model identification process is

now simplified because it is only necessary to identify the coefficients of odd power terms.

In summary, the robust signal recovery procedure with a nominal model will be successful only if

1.  $\Delta y$  is a noise-like signal and does not contain the original frequency components.
2. the nominal model,  $G$ , is such that the original information does not get lost by the nonlinear transformation,  $Gy$ .
3. noise-like signal,  $\Delta y + n$  can be filtered.

#### H. Signal Recovery in Discrete Domain

Consider a general sensor set-up shown in Fig. 19. A band-limited signal  $y(t)$  is measured through a nonlinear sensor whose characteristics are described by a function  $g(\cdot)$ . It can be easily shown that the spectra of the original signal and the distorted signal are not the same. The output of the sensor is then sent through a non-ideal low pass filter whose time domain function is  $h(t)$ .

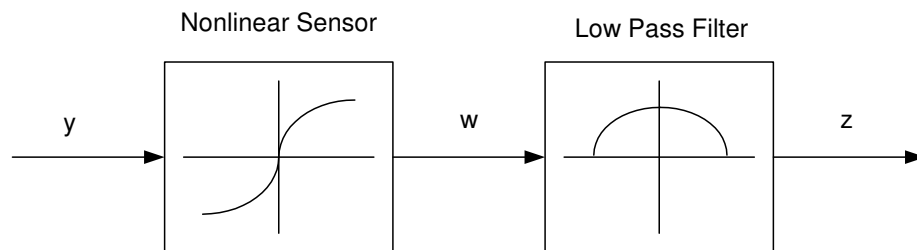


Figure 19: A General Setup

Let  $z(t)$  be the output of the low pass filter. The pass-band of the low pass filter is set to allow only frequencies that are in the bandwidth of the signal. It can be shown that under certain conditions the part of the spectrum outside the frequency

band of the original signal does not contribute towards the original sensor recovery and can be discarded with no effect. Analysis suggests that if this were not the case, then a sensor with a larger bandwidth would be needed and the sensor recovery idea would not do any good.

It will be shown later that a sensor model may not be known *a priori* to recover the signal with reasonable accuracy. But if the nonlinear sensor model is readily available or can be estimated with reasonable accuracy, then a unique sensor recovery may be possible. We will next derive sufficient conditions for this to happen.

Suppose that  $g(\cdot)$  is described by a linear piecewise function as shown in Fig. 20. Without loss of generality, it is assumed that  $g(\cdot)$  is symmetric about the origin and its gradients  $K_i \geq 0$ . The negative gradient case is discussed separately in Section 4. Even though the nonlinear sensor function is assumed to be known, it may not be used to deduce the original signal from the sensed signal directly. This point is evident from Equation (4.38). As the sensor output is a function of the original signal as well as measurement noise, direct evaluation of the original signal from the sensed signal may not yield accurate results. As emphasized in section 1, this is one of the reasons why the use of look-up tables or calibration curves is not recommended.

The discretized values of the original signal and the sensor output are related by

$$w = Gy + n \tag{4.38}$$

where  $n$  is high frequency measurement noise and matrix  $G$  is composed of the gradients of the linear piecewise function ( $K_i$ 's) shown in Fig. 20, and has the following form for a particular input  $y(t)$ ,



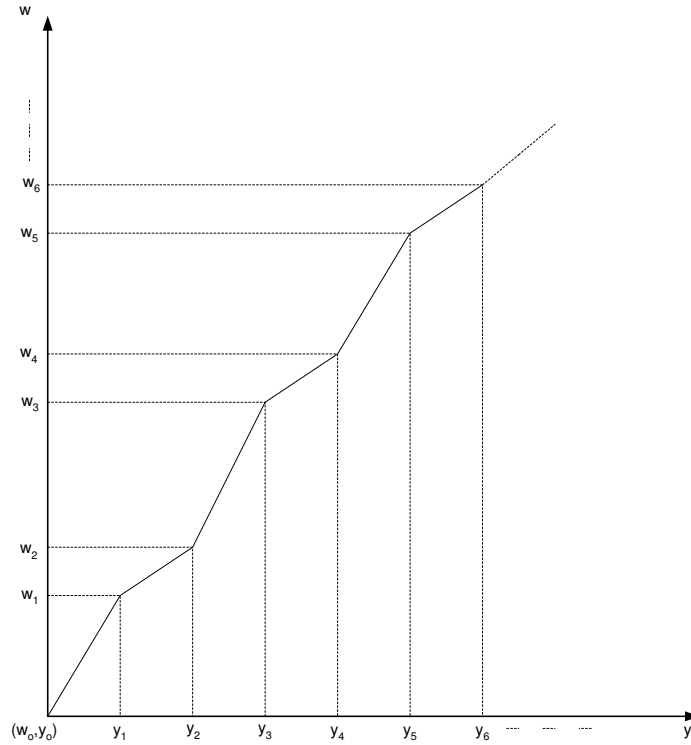


Figure 20: Nonlinear Sensor Function (Approximated)

$$G = \begin{pmatrix} 1 & 0 & 0 & 0 & \dots & 0 \\ 0 & K_1 & 0 & 0 & \dots & 0 \\ 0 & K_1 - K_2 & K_2 & 0 & \dots & 0 \\ \vdots & \vdots & \vdots & \vdots & \ddots & \vdots \\ 0 & K_1 - K_2 & K_2 - K_3 & K_3 - K_4 & \dots & K_{n-1} \end{pmatrix} \quad (4.39)$$

It is noted that matrix  $G$  is not constant and its entries must be compatible with the order the input samples are received. The samples of the filter output,  $z(t)$  can be calculated using the following convolution formula [105],

$$z_k = \sum_{i=0}^{n-1} w_i h_{k-i} \quad (4.40)$$

which can also be written in matrix form as follows:

$$z = Fw \quad (4.41)$$

where

$$F = \begin{pmatrix} h_0 & 0 & 0 & 0 & \dots & 0 \\ h_1 & h_0 & 0 & 0 & \dots & 0 \\ h_2 & h_1 & h_0 & 0 & \dots & 0 \\ \vdots & \vdots & \vdots & \vdots & \ddots & \vdots \\ h_{n-1} & h_{n-2} & h_{n-3} & h_{n-4} & \dots & h_0 \end{pmatrix} \quad (4.42)$$

Referring to Equations (4.38) and (4.41) the filtered signal,  $z$  and the original signal,  $y$  can now be related by,

$$z = FGy \quad (4.43)$$

Note that high frequency noise does not appear in Equation (4.43).

Now, the signal recovery problem reduces to finding a solution to Equation (4.43). If the matrix  $FG$  has an inverse, then the original signal can be directly obtained by  $y = (FG)^{-1}z$ . But, this may not be feasible if the dimension of the matrix is very high. For instance, if the incoming signal has  $10^6$  samples, then in order to reproduce the original signal a matrix of dimension  $10^6 \times 10^6$  needs to be inverted. Obviously, it is unrewarding to attempt to compute the inverse of this matrix. Another practical difficulty with this inversion process is that even if the matrix to be inverted is singular, round-off errors quickly destroy the singularity, and numerically one can “invert” a singular matrix. And therefore inverting a matrix may not always give reliable and accurate results. These observations emphasize the necessity for a systematic and efficient procedure to solve Equation (4.43). In the next section, we will discuss how such a solution procedure could be developed and derive sufficient conditions for the existence of a unique signal recovery.

### 1. Signal Recovery Procedure

By introducing a scalar  $\alpha$ , Equation (4.43) can also be written as,

$$y = (I - \alpha FG)y + \alpha z \quad (4.44)$$

To solve Equation (4.44) means to find a fixed point of map  $A: \mathbb{R}^n \rightarrow \mathbb{R}^n$  defined by:

$$A(y_1, y_2, \dots, y_n) := \left( \sum_{k=1}^n b_{1k}y_k + \alpha z_1, \dots, \sum_{k=1}^n b_{nk}y_k + \alpha z_n \right)$$

where  $B = (I - \alpha FG)$  and  $b_{ij}$  is its  $ij^{th}$  element.

Equation (4.44) has a unique solution if  $A$  is a contracting self-map of the complete metric space  $E$  and this solution can be obtained by iteration [14]. And the following iterative equation could be used to find the solution if it exists:

$$y_{k+1} = (I - \alpha FG)y_k + \alpha z \quad (4.45)$$

As stated above, a unique solution to Equation (4.44) exists if  $A$  is a contracting map. To be able to apply the fixed-point theorem, we have to make first a complete metric space out of  $\mathbb{R}^n$ . For this purpose, we define the following three metrics, which transform  $\mathbb{R}^n$  into the metric spaces  $l^p(n)$ .

Consider two points  $x$  and  $y$  of  $\mathbb{R}^n$ :  $x = (x_1, x_2, \dots, x_n)$  and  $y = (y_1, y_2, \dots, y_n)$ .

**For  $p=1$ :**  $d(x, y) := \sum_{v=1}^n |x_v - y_v|$

**For  $p=2$ :**  $d(x, y) := (\sum_{v=1}^n |x_v - y_v|^2)^{\frac{1}{2}}$

**For  $p=\infty$ :**  $d(x, y) := \max_{v=1}^n |x_v - y_v|$

For the cases  $p=1,2$  and  $\infty$ , let us now write down the conditions which tell us that  $A$  is contracting.

**For  $p=1$ :**

$$\begin{aligned} d(Ax, Ay) &= \sum_{i=1}^n \left| \sum_{k=1}^n b_{ik}(x_k - y_k) \right| \\ &\leq \sum_{i=1}^n |b_{ik}| |x_k - y_k| \\ &= \sum_{k=1}^n |x_k - y_k| \sum_{i=1}^n |b_{ik}| \end{aligned}$$

and

$$d(Ax, Ay) \leq \left( \max_{k=1}^n \sum_{i=1}^n |b_{ik}| \right) d(x, y)$$

**For  $p=2$ :**

$$\begin{aligned} d(Ax, Ay) &= \sqrt{\sum_{i=1}^n \left( \left| \sum_{k=1}^n b_{ik}(x_k - y_k) \right|^2 \right)} \\ &\leq \sqrt{\sum_{i=1}^n \left( \sum_{k=1}^n |b_{ik}|^2 \sum_{k=1}^n |x_k - y_k|^2 \right)} \end{aligned} \tag{4.46}$$

and

$$d(Ax, Ay) \leq \left( \sqrt{\sum_{i,k=1}^n |b_{ik}|^2} \right) d(x, y)$$

**For  $p=\infty$ :**

$$\begin{aligned}
d(Ax, Ay) &= \max_{i=1}^n \left| \sum_{k=1}^n b_{ik}(x_k - y_k) \right| \\
&\leq \max_{i=1}^n \left( \sum_{k=1}^n |b_{ik}| \max_{k=1}^n |x_k - y_k| \right)
\end{aligned}$$

and

$$d(Ax, Ay) \leq \left( \max_{i=1}^n \sum_{k=1}^n |b_{ik}| \right) d(x, y)$$

Therefore, the map  $A$  is contracting if one of the numbers,  $\max_{k=1}^n \sum_{i=1}^n |b_{ik}|$ ,  $\sqrt{\sum_{i,k=1}^n |b_{ik}|^2}$ ,  $\max_{i=1}^n \sum_{k=1}^n |b_{ik}|$  is less than one.

Let us now summarize this result in the following theorem.

**Theorem 4** *The original signal,  $y$  (Fig. 19) may be uniquely recovered from the filtered signal,  $z$ , if one of the following numbers is less than one:*

$$\begin{aligned}
&\max_{k=1}^n \sum_{i=1}^n |(I - \alpha FG)_{ik}|, \quad \sqrt{\sum_{i,k=1}^n |(I - \alpha FG)_{ik}|^2}, \\
&\max_{i=1}^n \sum_{k=1}^n |(I - \alpha FG)_{ik}|
\end{aligned}$$

**Proof:** It is straightforward from the previous development.  $\diamond$

It is noted that the choice of  $\alpha$  plays a crucial role toward unique signal recovery. Even though the sensor characteristics support the unique signal recovery, a wrong choice of  $\alpha$  may restrict the successful signal recovery and lead to incorrect conclusions. In addition, matrices  $F$  and  $G$  need to satisfy certain conditions, which are not evident in Theorem 4. And therefore, it would be useful if the conditions were stated in terms of  $F, G$  and  $\alpha$ .

The conditions for unique signal recovery can be stated in terms of matrices  $F$  and  $G$  and  $\alpha$  by considering the three numbers given in Theorem 4. Alternatively, we could simplify this process by making some reasonable assumptions.

Assume that the gradients of the sensor function are such that  $|K_i - K_{i+1}| < \epsilon$

for some  $\epsilon > 0$  and  $K_i \gg \epsilon \forall i$ . Under these assumptions, the matrix  $G$  of Equation (4.39) will have the following form:

$$G = \begin{pmatrix} K_1 & \epsilon & \epsilon & \epsilon & \dots & \epsilon \\ \epsilon & K_2 & \epsilon & \epsilon & \dots & \epsilon \\ \epsilon & \epsilon & K_3 & \epsilon & \dots & \epsilon \\ \vdots & \vdots & \vdots & \vdots & \ddots & \vdots \\ \epsilon & \epsilon & \epsilon & \epsilon & \dots & K_{n-1} \end{pmatrix} \quad (4.47)$$

where  $\epsilon$  is either 0 or  $|K_i - K_{i+1}|$ .

Now, using matrices  $F$  and  $G$  given in Equations (4.42) and (4.47) respectively, we could form the matrix,  $I - \alpha FG$  as:

$$I - \alpha FG \approx \begin{pmatrix} 1 - \alpha h_0 K_1 & 0 & 0 & 0 & \dots \\ -h_1 K_1 & 1 - \alpha h_0 K_2 & 0 & 0 & \dots \\ -h_2 K_1 & -h_1 K_2 & 1 - \alpha h_0 K_3 & 0 & \dots \\ \vdots & \vdots & \vdots & \vdots & \ddots \end{pmatrix} \quad (4.48)$$

As  $I - \alpha FG$  is lower triangular, the convergence requirements can also be stated in terms of diagonal elements. This is because the diagonal elements are the eigenvalues of a lower triangular matrix, and the matrix convergence is guaranteed if the maximum absolute value of the eigenvalues (or the spectral radius) is less than 1. Let  $K_p$  be  $\max_{i=1}^n K_i$ .

Sufficient conditions for the unique signal recovery can be easily derived and are summarized in the following Theorem.

**Theorem 5** *The original signal,  $y$  (Fig. 19) may be uniquely recovered from the filtered signal,  $z$  if*

$$\frac{g(x_i) - g(x_{i+1})}{x_i - x_{i+1}} \neq 0 \quad \forall i \quad \text{provided}$$

1.  $h(t=0) \neq 0$

2.  $0 < \alpha < \frac{2}{h_0 K_p}$

**Proof:** It is clear that when the gradient of the sensor function is zero, the spectral radius of  $I - \alpha FG$  becomes 1. This violates the convergence requirement and therefore, the original signal may not be recovered. Similar argument is valid to prove that  $h_0 \neq 0$  is also a necessary condition for signal recovery. The sufficient condition that the spectral radius must be less than one for convergence yields the condition on  $\alpha$ .  
 $\diamond$

When the above conditions are satisfied, the iterative procedure given in Equation (4.45) could be used to find  $y$ . It is noted that the derivation of matrices may become tedious, especially when the dimension is very high. Instead an equivalent iterative scheme could be used to solve for  $y$ :

$$y_{k+1} = y_k + y_0 - \alpha IDFT\{DFT(g(y_k)) \cdot * DFT(h_k)\} \quad (4.49)$$

where  $y_0 = \alpha z$ .

By summarizing the above results, we formally state the important steps involved in the signal recovery process in the following algorithm:

**Algorithm 2 (Signal Recovery Procedure)**

**Step 1** Choose  $\alpha$  such that it falls in the safety range ( $0 < \alpha < \frac{2}{h_0 K_p}$ ) and pick the starting value of the iterative scheme given by Equation (4.49) as  $\alpha z$ .

Repeat the following steps for all  $k$  until  $|y_{k+1} - y_k| < \gamma$ , where  $\gamma$  is a user-defined stopping criterion.

**Step 2** Find Discrete Fourier Transforms of  $g(y_k)$  and  $h_k$ , do term-by-term multiplication and get the Inverse Discrete Fourier Transform of the multiplied result,  $IDFT\{DFT(g(y_k)) \cdot * DFT(h_k)\}$

**Step 3** Find

$$y_{k+1} = y_k + y_0 - \alpha IDFT\{DFT(g(y_k)) \cdot * DFT(h_k)\}$$

The algorithm basically consists of an algebraic loop that uses the filtered signal as its initial value. As iterations in the algebraic loop are progressed, amplitudes at frequencies other than that of the original signal gradually diminish provided the convergence requirements are met.

## 2. Special Case: Negative Gradients

It was shown that the original signal could be recovered from the filtered signal if the gradients of the sensor function are not zero. While deriving the recovery procedure, it was assumed that the gradients are positive. This may not be true always and the derived procedure will not converge if the gradient of the sensor function at any point is negative. This could be easily proven by checking the spectral radius of the matrix  $I - \alpha FG$ .

Suppose that  $i^{th}$  segment of the linear piecewise function shown in Fig. 20 has a negative gradient,  $K_i$ . Let  $K = -K_i$  where  $K > 0$ . Let us now examine the matrix  $I - \alpha FG$  of Equation (4.48) for this case.

$$I - \alpha FG \approx \begin{pmatrix} 1 - \alpha h_0 K_1 & 0 & 0 & 0 & \dots \\ -h_1 K_1 & 1 - \alpha h_0 K_2 & 0 & 0 & \dots \\ \vdots & \vdots & \ddots & \vdots & \vdots \\ -h_2 K_1 & -h_1 K_2 & \dots & 1 + \alpha h_0 K_i & \dots \\ \vdots & \vdots & \vdots & \vdots & \ddots \end{pmatrix} \quad (4.50)$$

It is clear that the spectral radius is greater than one and therefore the convergence requirement is violated. This proves that the solution technique derived earlier cannot be used to recover the signals in this case. However, by suitably modifying the algorithm, a recovery procedure can be obtained. Let us see next how this can be done.

Recall that in order to write (4.43) in standard format as in (4.44), a scalar  $\alpha$



was brought into the picture. In fact,  $\alpha$  is not necessarily a scalar. It could also be a matrix, for example  $\alpha = \alpha_0 I$ . where  $I$  is an identity matrix of appropriate dimension and  $\alpha_0$  is a scalar. To derive the recovery procedure, the matrix  $\alpha$  is modified as

$$\alpha = \begin{pmatrix} \alpha_0 & 0 & \dots & 0 & \dots & 0 \\ 0 & \alpha_0 & \dots & 0 & \dots & 0 \\ \vdots & \vdots & \ddots & \vdots & \ddots & \vdots \\ 0 & 0 & \dots & -\alpha_i & \dots & 0 \\ \vdots & \vdots & \vdots & \vdots & \ddots & \vdots \end{pmatrix} \quad (4.51)$$

where  $\alpha_0$  and  $\alpha_i$  are positive scalars. Note that  $i^{\text{th}}$  diagonal element of the matrix  $\alpha$  is chosen to be negative and the matrix  $I - \alpha FG$  will have the following form:

$$I - \alpha FG \approx \begin{pmatrix} 1 - \alpha_0 h_0 K_1 & 0 & 0 & 0 & \dots \\ -h_1 K_1 & 1 - \alpha_0 h_0 K_2 & 0 & 0 & \dots \\ \vdots & \vdots & \ddots & \vdots & \vdots \\ -h_2 K_1 & -h_1 K_2 & \dots & 1 - \alpha_i h_0 K_i & \dots \\ \vdots & \vdots & \vdots & \vdots & \ddots \end{pmatrix} \quad (4.52)$$

It is noted that the spectral radius can now be less than one if  $0 < \alpha_0, \alpha_i < \frac{2}{h_0 K_p}$  and therefore, the algorithm will converge.

This modification needs to be done whenever the gradient is negative in order to guarantee successful signal recovery. It can be easily shown that unique signal recovery may not be possible if the sensor function has negative gradients. To ensure unique signal recovery, extreme care should be exercised in determining the correct gradient matrix,  $G$ .

### I. Signal Recovery with Non-monotonic Sensor Function

The iterative algorithm developed in the previous sections may not be used to recover signals that are distorted by non-monotonic nonlinear sensor functions of the type

shown in Fig. 21.

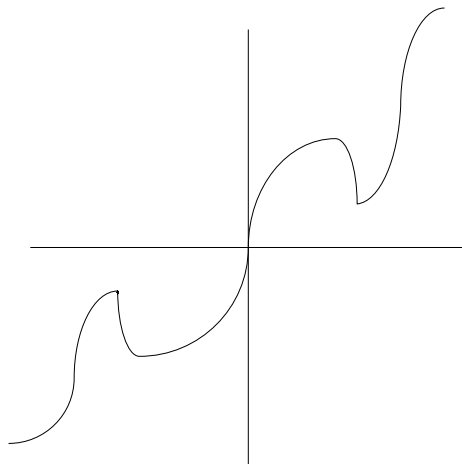


Figure 21: Non-monotonic Nonlinear Sensor Function

Other techniques should be sought in this case and we propose an optimization based signal recovery procedure in this section. Assuming that the original signal data is smooth with no sudden amplitude variation, which is the case with any bandlimited signal, the original data can be recovered by solving the following optimization problem:

$$\min_y J = \min_y \left\| z(k) - \sum_{i=-\infty}^{\infty} g(y(i))h(k-i) \right\|_2 \quad (4.53)$$

subject to

$$|y(k) - y(k-1)| < \epsilon \quad (4.54)$$

where  $\epsilon$  is the allowable amplitude variation. The inclusion of constraint (4.54) is very crucial here as the minimization of the objective function (4.53) alone will result in multiple optimal solutions. We present simulation data in Section 7 to validate this recovery procedure.

## J. Recovery of Signals Distorted by Non-invertible Sensor Nonlinearity

Methods developed in previous sections may not yield accurate results if the nonlinear sensor function dictates “ill-posed” input-output characteristic such as saturation and dead-band. Saturation nonlinearity is a common defect found in most real sensors and its effects are clearly apparent when the sensor is used to pick up high amplitude signals. The main issue with such sensors is that the accurate and unique reproduction of sensor input from the saturated sensor data may not be possible, in general.

### 1. Motivation

Bearing in mind that retrieving at least some of the original information and eliminating or reducing the distortion caused by saturation nonlinearity are useful contributions towards a “smart sensor technology”, we propose a new approach, which optimizes a non-quadratic performance index to recover the original data. The fact that the introduction of non-quadratic penalty in the cost function does not alter the optimal solution as much as the quadratic penalty does, makes it a better candidate for the problem posed. The nature of solutions generated by non-quadratic optimization suggests its unique ability to solve several practical problems. For example, non-quadratic optimization is applied to decentralize multi-variable model predictive control structures in [106].

We further elaborate the idea of using non-quadratic optimization to solve ill-conditioned equation by considering a simple numerical example.

Consider an optimization problem, which requires that the following performance index be minimized:

$$J_o = (x - a)^2 \tag{4.55}$$

where  $a$  is a constant and  $x$  is the variable to be optimized.

Suppose that certain specifications require that a penalty on the variable,  $x$ , be enforced. To investigate the effects of different penalty functions on the optimal solutions, let us add both the quadratic and non-quadratic penalty terms to the original cost function given in Equation (4.55) and compare the results. We first derive the quadratic cost function.

$$J_q = (x - a)^2 + \lambda_q x^2 \quad (4.56)$$

whose gradient is given by,

$$\nabla J_q = 2(x - a) + 2\lambda_q x \quad (4.57)$$

where  $\lambda_q$  is the weight on the quadratic penalty.

The non-quadratic cost function and its gradient are derived as follows.

$$J_n = (x - a)^2 + \lambda_n x^{0.5} \quad (4.58)$$

$$\nabla J_n = 2(x - a) + \frac{\lambda_n}{2\sqrt{x}} \quad (4.59)$$

We assume that the weight,  $\lambda_n$ , on the non-quadratic penalty term,  $\lambda_n x^{0.5}$ , is reasonably low so that the global minimum does not occur at the origin. Further discussion on the choice of the weights and their effects on the optimal solutions is given in Section 3.

Referring to Equation (4.57), the gradient of the quadratic cost function is linear and the optimal solution is the point where the terms  $2(x - a)$  and  $2\lambda_q x$  are equal but of opposite sign. As schematically shown in Fig. 22, the proximity of the optimal solution of the quadratic cost function,  $J_q$ , to the actual solution ( $a$  in this case) is determined by weight,  $\lambda_q$ .

Unlike the gradient in the quadratic case, the gradient of the non-quadratic

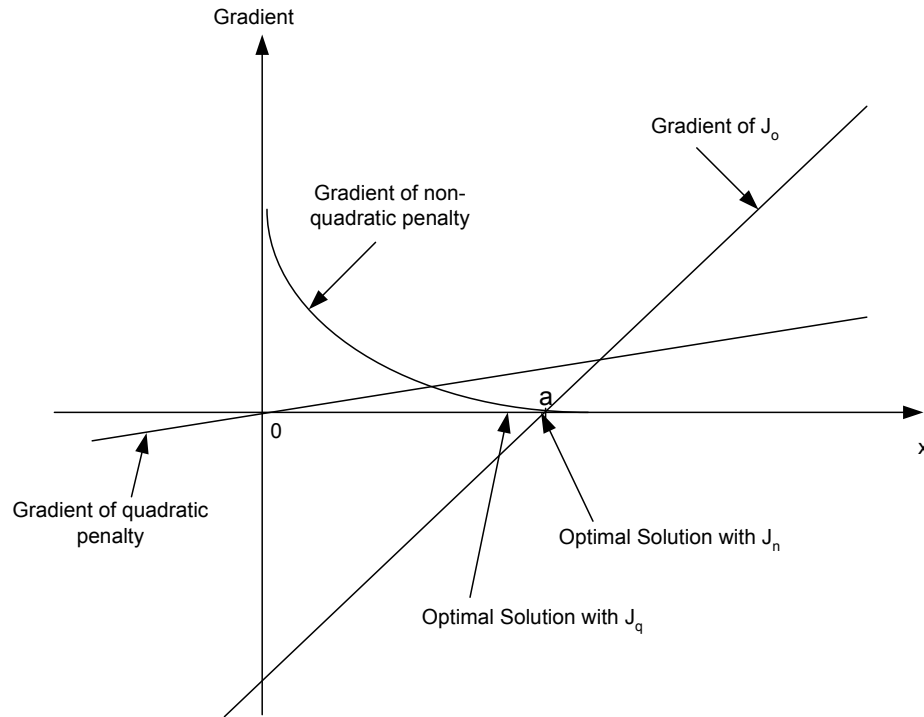


Figure 22: Comparison of Optimal Solutions Obtained with Quadratic and Non-quadratic Cost Functions

function given in Equation (4.59) has a different shape as shown in Fig. 22. Depending on the value of weight,  $\lambda_n$ , the gradient of the non-quadratic term,  $\frac{\lambda_n}{2\sqrt{x}}$ , has a very high value near zero and dies out as the value of the variable,  $x$ , increases. We point out that this feature of the non-quadratic function makes it a better candidate than the quadratic function. With a suitable choice of weight,  $\lambda_n$ , the non-quadratic penalty can be shaped such that it dies out very soon and consequently has a very small value at the actual solution,  $a$ , which will lead to an optimal solution very near  $a$ . Fig. 22 further illustrates this point. It is worth mentioning that the quadratic penalty does not possess this ability as its gradient is linear.

Another important point is that in order to drive the optimal solution closer

to the actual value, the weight on the quadratic penalty must be chosen as low as possible since the accuracy of the solution is simply determined by the weight. This may not be true in the case of non-quadratic penalty. This is because the gradient of the non-quadratic penalty will decrease as  $x$  increases and a reasonably low weight may be sufficient to guarantee a small gradient value near the actual solution. It is also pointed out that the shape of the gradient of the non-quadratic penalty is such that it would possibly have optimal solutions only in two neighborhoods: one is in the vicinity of the actual solution when the weight is low and the other is at the origin when the weight on the non-quadratic penalty is high. Fig. 23 further supports this point. This fact further encourages the use of non-quadratic cost function as the availability of wide range of suitable weights makes the tuning process very easy and the solution reliable.

Motivated by the above example, we tested this idea to solve the ill-posed signal recovery problem. The results, which are detailed in this section, have been promising and the optimization of non-quadratic cost function stands out from other available tools to generate accurate results. The class of non-quadratic functions considered in this section are those that exhibit infinite gradient at the origin,  $\{x^k | 0 < k < 1\}$ .

## 2. Non-quadratic Regularization

The method described in the previous section will fail if the nonlinear operation is singular. To solve “ill-conditioned” problems of this kind, the standard regularization techniques are applied in general. Tikhonov regularization [107, 108] is probably the most commonly used regularization method. This technique augments the least-squares performance index given in Equation (5.4) with an additional term, generally known as penalty, which incorporates prior information about signal,  $y$ , given by,

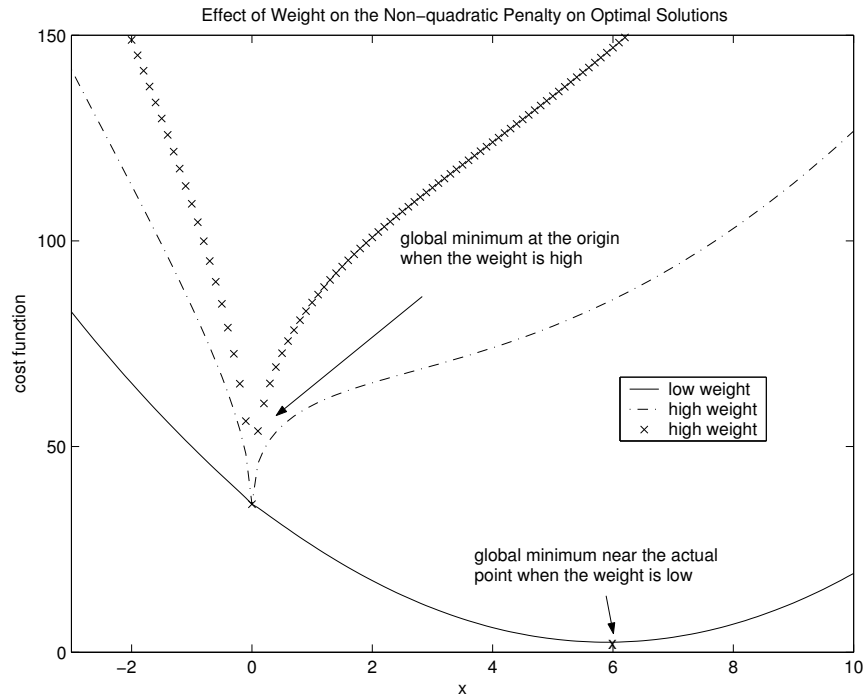


Figure 23: Effect of Weight on Non-quadratic Penalty on Optimal Solutions

$$\min_y J = \|z - \mathcal{F}^{-1}\{\mathcal{HF}\{g(y)\}\}\|^2 + \lambda_q \|y - y_o\|^2 \quad (4.60)$$

where  $\lambda$  is a weight on the penalty term and  $y_o$  is an estimate based on prior knowledge. The accuracy of the optimal solution is dependent on how close the initial estimate is to the actual solution. The effect of the penalty function on the optimal solution as well as on the shape of the resultant cost function is graphically shown in Fig. 24. For convenience, the variation of the cost function in only one direction is shown in the plot and the initial estimate,  $y_o$ , is assumed to be zero.

It is noted that the constraint enforced by means of a penalty moves the solution away from its actual value. To maintain the accuracy of the solution, the weight on the penalty,  $\lambda$ , must be kept at a low value. When the value of  $\lambda$  is increased

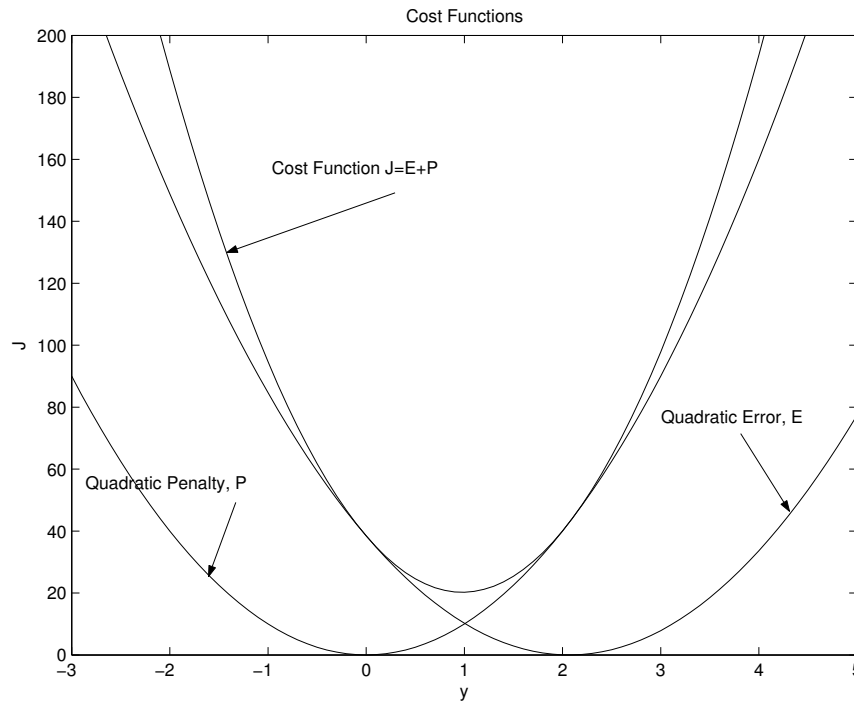


Figure 24: Effect of Adding a Quadratic Penalty Function

gradually, the error term on the expression becomes insignificant and the optimal solution moves towards  $y_o$ , which is zero in this case. However, it can be shown that the optimal solution will never be exactly zero for a finite value of  $\lambda$ . This fact is clear from Fig. 25.

We have shown that adding a quadratic penalty may not improve the accuracy of the solution, in general. If the accuracy of sensor data is of paramount importance, other approaches should be sought. In this section, we propose an approach, which replaces the quadratic penalty in the cost function (4.60) by a non-quadratic penalty as shown in the following equation:

$$\min_y J = \|z - \mathcal{F}^{-1}\{\mathcal{HF}\{g(y)\}\}\|^2 + \lambda_n \sum_{i=1}^N |y_i|^k \quad (4.61)$$



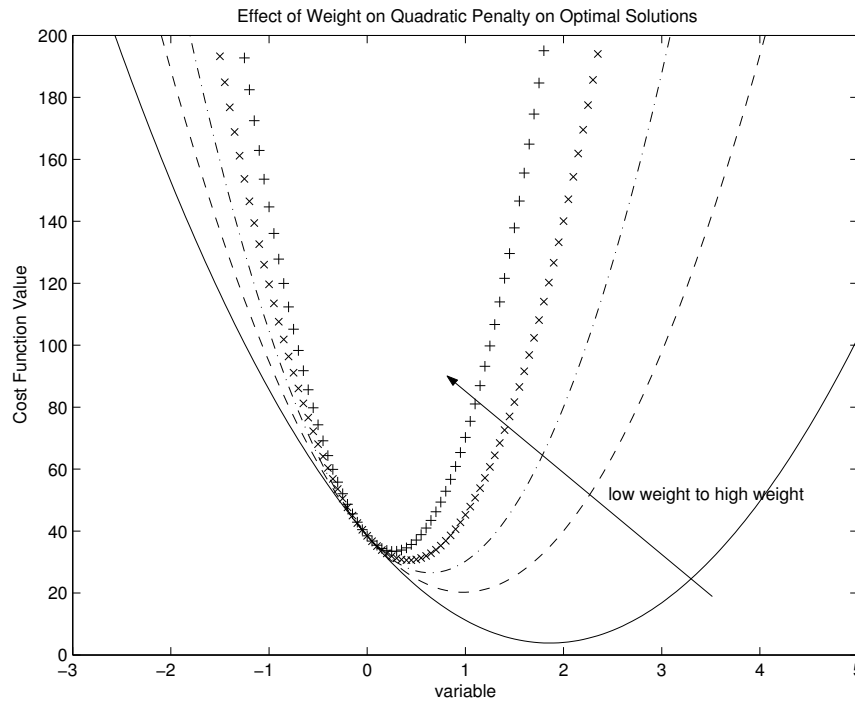


Figure 25: Effect of Penalty Function Weight on the Optimal Solution-Quadratic Penalty Case

where  $\{k|0 < k < 1\}$  is a non-quadratic index and  $N$  is the number of samples. In the above the discrete version of the process is considered and the signals are assumed to be sampled sufficiently fast.

The rationale behind the choice of the non-quadratic penalty has already been explained in Section 1. We will provide additional insights by showing how a non-quadratic penalty alters the shape of the cost function, which is otherwise quadratic. Fig. 26 shows how this alteration is done. Again, the variation of the cost function only in one direction is shown in the plot.

Referring to Fig. 27 and Fig. 28, with a low weight on the penalty, the cost function has two local minimum. One is at zero and the other, which is the global

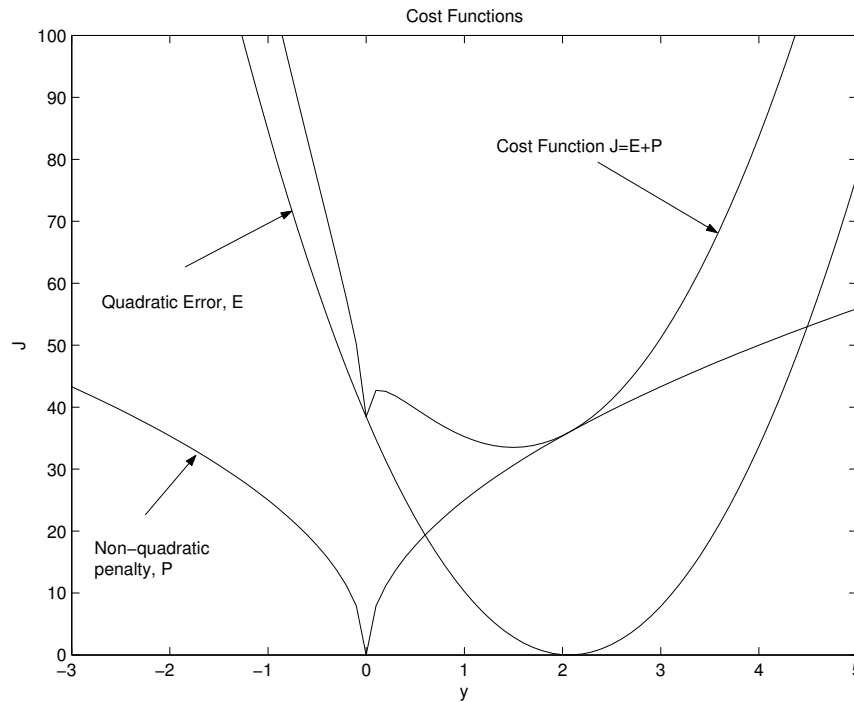


Figure 26: Effect of Adding a Non-Quadratic Penalty

minimum is very near the actual or expected solution. The local minimum at zero is caused by the very high gradient value of the non-quadratic penalty near zero. The fact is, with low or moderate weight on the non-quadratic penalty, a very low value of the gradient of the non-quadratic penalty when added to the gradient of the error will drive the global minimum of cost function (4.61) very near the actual value. This feature makes the proposed approach different from other traditional approaches. As shown in Fig. 27 and Fig. 28, with a high weight on the penalty, the cost function has only one local minimum, which is subsequently the global minimum.

To get further insight about the role of different penalties, we will study the effects of quadratic and non-quadratic penalties with the aid of Fig. 29. In Equations (4.60) and (4.61), the cost functions being minimized have the following general form:

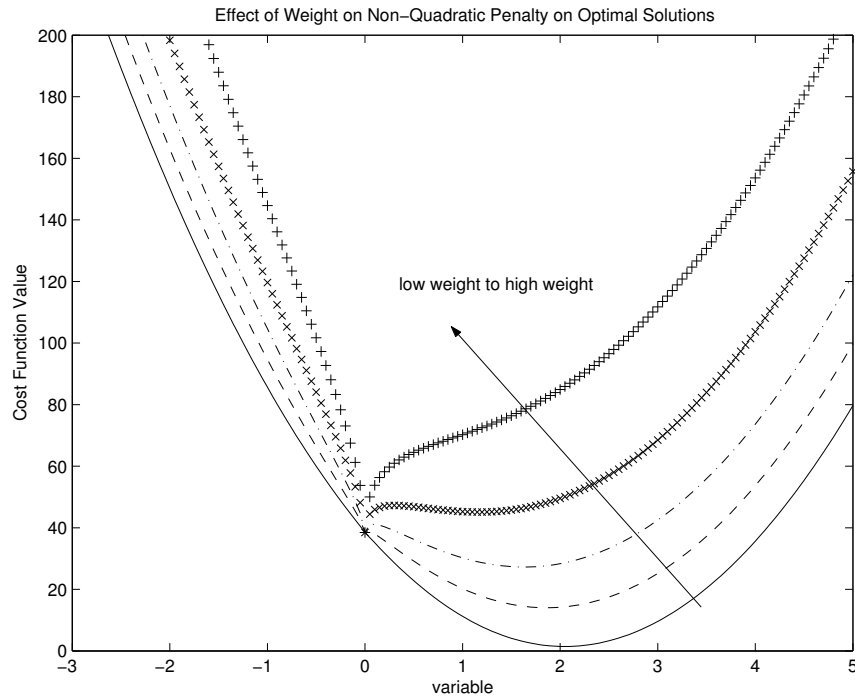


Figure 27: Effect of Penalty Function Weight on the Optimal Solution-Non-Quadratic Penalty Case

$$J = E + P \quad (4.62)$$

where  $E$  is the error function and  $P$  is the penalty on  $y$ .

Referring to Fig. 29, we deduce that when the value of  $y$  is high, the penalty on  $y$  is higher in the quadratic case than that in the non-quadratic case. The higher penalty on  $y$  may result in less accurate solution since the cost function being minimized is  $J$  not  $E$  and the optimizer “will choose” the solution that minimizes  $J$ , which may not necessarily minimize  $E$ . In order to accurately recover signals that exhibit large fluctuations in strength, it is desired that penalties on the variable  $y$  must be restricted in the working range. This requirement further encourages the use of non-quadratic

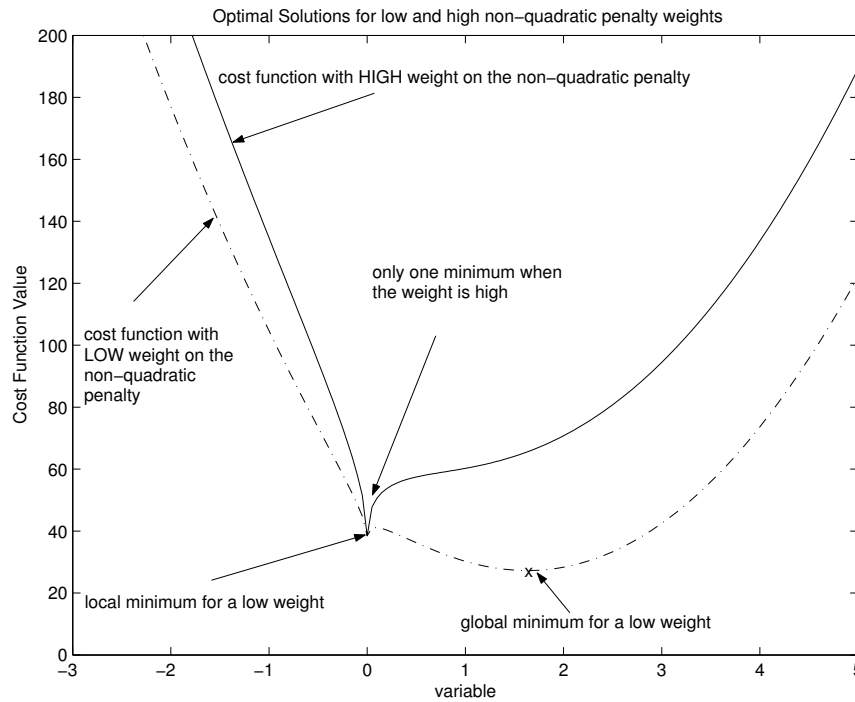


Figure 28: Optimal Solutions for High and Low Weights on Non-Quadratic Penalty penalty instead of quadratic penalty. Simulation examples presented in Section 5 supports this claim.

### 3. Optimization of Non-quadratic Cost Functions

The main issue with the proposed scheme is that it involves the optimization of non-quadratic cost functions, which may not be convex. Non-convexity does not guarantee a unique minimum and may lead to the existence of multiple local minima. An efficient search algorithm is an absolute necessity to locate the correct global minimum. In order to simplify the tasks involving the derivation of difficult algorithms to solve this optimization problem, we use a procedure in which penalty functions,  $|y|^k$  are approximated by piecewise linear functions. This approach will be acceptable only

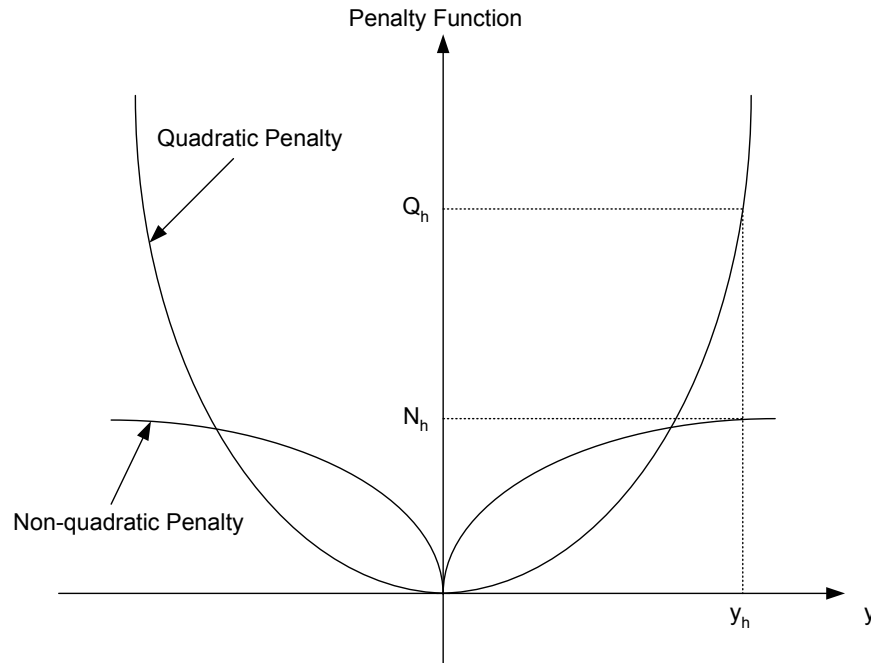


Figure 29: Comparison of Penalty Function Values When the Variable Is of High Value

if the accuracy of the function is less important and the approximation does not lead to any undesirable effects. It gives us a relatively simple solution method and could be applied to solve the non-quadratic optimization problems using standard optimization algorithms. The process of approximating convex and non-convex functions by linear piece-wise functions are illustrated in Fig. 30 and Fig. 31 respectively.

#### 4. Illustrative Example

We will present a numerical example to explain the proposed methodology. Consider the following sensor model:

$$z = \mathcal{F}^{-1}\{\mathcal{HF}\{g(y)\}\} \quad (4.63)$$

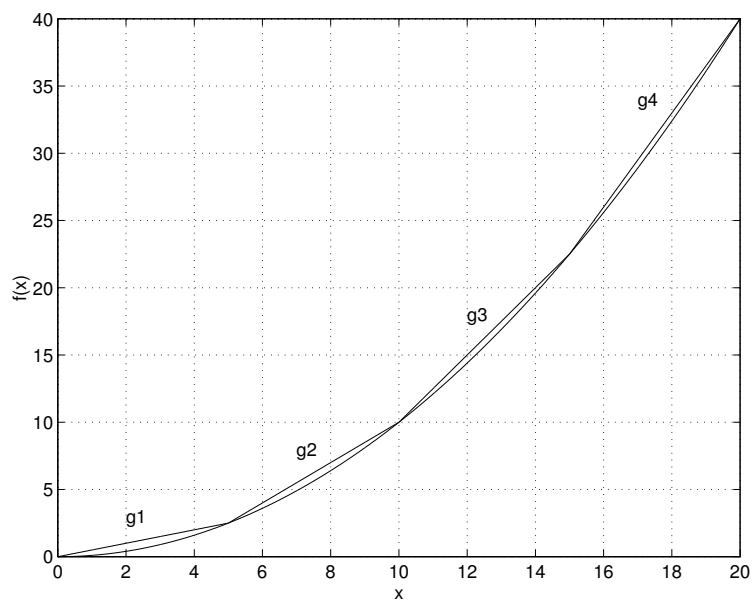


Figure 30: Approximating a Convex Function by a Linear Piece-wise Function

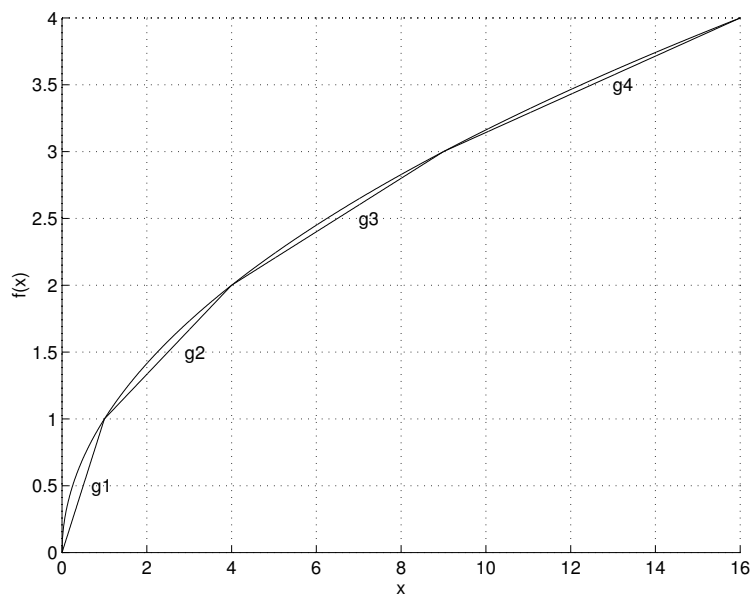


Figure 31: Approximating a Non-convex Function by a Linear Piece-wise Function

The discrete version of the above equation can be written in the following matrix equation form [96]:

$$z = FGy \quad (4.64)$$

where  $G$  corresponds to nonlinear operation,  $g$ , and  $F$  denotes the low pass filtering operation,  $\mathcal{H}$ .

Taking only the first two time samples, we will use the following ill-conditioned process to explain the algorithm.

$$z = \begin{pmatrix} 2 & 1 \\ 2 & 1.1 \end{pmatrix} y + n \quad (4.65)$$

that gives

$$\begin{aligned} z_1 &= 2y_1 + y_2 + 0.1 \\ z_2 &= 2y_2 + 1.1y_2 + 0.2 \end{aligned} \quad (4.66)$$

Suppose that the actual samples of the signals are given by

$$y = \begin{bmatrix} y_1 \\ y_2 \end{bmatrix} = \begin{bmatrix} 10 \\ 8 \end{bmatrix} \quad (4.67)$$

The samples of the sensor output for this case are given by,

$$z = \begin{bmatrix} z_1 \\ z_2 \end{bmatrix} = \begin{bmatrix} 28.1 \\ 29.0 \end{bmatrix} \quad (4.68)$$

To solve the above optimization problems, the following initial values are used to begin the solution search in all three problems.

$$y_o = \begin{bmatrix} -100 \\ -1000 \end{bmatrix} \quad (4.69)$$

Case 1: Minimization of Quadratic Error Function

$$\begin{aligned} \min_{y_1, y_2} J &= \left\| \begin{bmatrix} z_1 \\ z_2 \end{bmatrix} - \begin{pmatrix} 2 & 1 \\ 2 & 1.1 \end{pmatrix} \begin{bmatrix} y_1 \\ y_2 \end{bmatrix} \right\|^2 \\ &= \left\| \begin{bmatrix} 28.1 \\ 29.0 \end{bmatrix} - \begin{pmatrix} 2 & 1 \\ 2 & 1.1 \end{pmatrix} \begin{bmatrix} y_1 \\ y_2 \end{bmatrix} \right\|^2 \\ &= (28.1 - 2y_1 - y_2)^2 + (29.0 - 2y_1 - 1.1y_2)^2 \end{aligned} \quad (4.70)$$

The optimal solution is,

$$y^* = \begin{bmatrix} 9.55 \\ 9.00 \end{bmatrix} \quad (4.71)$$

Case 2: Minimization of Quadratic Error Function with Quadratic Penalty

$$\begin{aligned} \min_{y_1, y_2} J_q &= \left\| \begin{bmatrix} z_1 \\ z_2 \end{bmatrix} - \begin{pmatrix} 2 & 1 \\ 2 & 1.1 \end{pmatrix} \begin{bmatrix} y_1 \\ y_2 \end{bmatrix} \right\|^2 + 0.1 (y_1^2 + y_2^2) \\ &= \left\| \begin{bmatrix} 28.1 \\ 29.0 \end{bmatrix} - \begin{pmatrix} 2 & 1 \\ 2 & 1.1 \end{pmatrix} \begin{bmatrix} y_1 \\ y_2 \end{bmatrix} \right\|^2 + 0.1 (y_1^2 + y_2^2) \\ &= (28.1 - 2y_1 - y_2)^2 + (29.0 - 2y_1 - 1.1y_2)^2 + 0.1 (y_1^2 + y_2^2) \end{aligned} \quad (4.72)$$



The optimal solution is,

$$y^* = \begin{bmatrix} 11.0196 \\ 5.9384 \end{bmatrix} \quad (4.73)$$

Case 3: Minimization of Quadratic Error Function with Non-quadratic Penalty

$$\begin{aligned} \min_{y_1, y_2} J_s &= \left\| \begin{bmatrix} z_1 \\ z_2 \end{bmatrix} - \begin{pmatrix} 2 & 1 \\ 2 & 1.1 \end{pmatrix} \begin{bmatrix} y_1 \\ y_2 \end{bmatrix} \right\|^2 + 0.1 (|y_1|^{0.5} + |y_2|^{0.5}) \\ &= \left\| \begin{bmatrix} z_1 \\ z_2 \end{bmatrix} - \begin{pmatrix} 2 & 1 \\ 2 & 1.1 \end{pmatrix} \begin{bmatrix} y_1 \\ y_2 \end{bmatrix} \right\|^2 + 0.1 (|y_1|^{0.5} + |y_2|^{0.5}) \\ &= (28.1 - 2y_1 - y_2)^2 + (29.0 - 2y_1 - 1.1y_2)^2 + 0.1 (|y_1|^{0.5} + |y_2|^{0.5}) \end{aligned} \quad (4.74)$$

The optimal solution is,

$$y^* = \begin{bmatrix} 10.0379 \\ 8.0687 \end{bmatrix} \quad (4.75)$$

Clearly, with non-quadratic cost function, more accurate results are attained.

Tables I and II compare the effect of penalty function weights on the optimal solution.

Table I: Effects of Penalty Weights on Optimal Solution: Quadratic Cost Case

Cost Function	Weights, $[\lambda_1, \lambda_2]$	Optimal Solution, $[y_1, y_2]$
$J_q$	[0.001, 0.001]	[9.8823, 8.3647]
$J_q$	[0.01, 0.01]	[10.7173, 6.7511]
$J_q$	[0.1, 0.1]	[11.0196, 5.9384]
$J_q$	[1, 1]	[10.1851, 5.3653]
$J_q$	[10, 10]	[5.6514, 2.9700]
$J_q$	[100, 100]	[1.0362, 0.5444]

Table II: Effects of Penalty Weights on Optimal Solution: Non-quadratic Cost Case

Cost Function	Weights, $[\lambda_1, \lambda_2]$	Optimal Solution, $[y_1, y_2]$
$J_s$	[0.001, 0.001]	[9.5543, 8.9918]
$J_s$	[0.01, 0.01]	[9.5933, 8.9173]
$J_s$	[0.1, 0.1]	[10.0379, 8.0687]
$J_s$	[1, 1]	[14.2667, 0]
$J_s$	[10, 10]	[14.1916, 0]
$J_s$	[100, 100]	[19.2775, 0]

## CHAPTER V

## FUSION OF DISTORTED MULTI-SENSOR MEASUREMENTS

This chapter is concerned with the fusion of distorted multiple nonlinear sensor data. The optimization based algorithms presented are intended to identify the faulty or inaccurate measurements and to optimize the number of sensors used in a process. A shorter version of this work also appears in [109], [110], [111], [112]. A sensor scheduling procedure to identify the faulty sensor measurements using *Branch and Bound* technique is developed in section A. Having pointed out the difficulties in dealing with the combinatorial behavior of solution search procedures required by the *Branch and Bound* method, a multi-sensor fusion procedure using continuous optimization of the error function is developed in section B. Another fusion method that uses confidence measure of each sensor reading to pick the most accurate sensor measurement is developed in section (C).

## A. Fusion of Distorted Multi-sensor Data by Sensor Scheduling

The multi-sensor fusion problem considered in this chapter is schematically shown in Fig. 32. Nonlinear sensor functions  $g_i$  are essentially different. Without loss of generality, it is assumed that same low pass filters are used in all sensor channels. Let  $z_i$  and  $v_i$  be the corresponding filtered signals and the recovered signals respectively.  $z_i$  and  $y$  are related by,

$$z_i = FG_i y \quad (5.1)$$

Consider the following fusion equation:

$$y_r = \Phi_1 v_1 + \Phi_2 v_2 + \dots + \Phi_n v_n \quad (5.2)$$

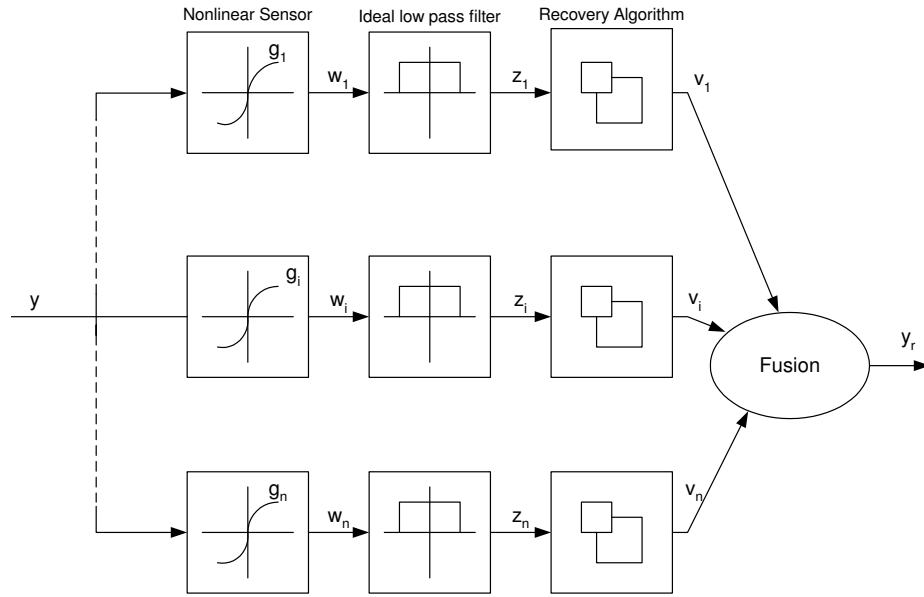


Figure 32: Multi-Sensor Data Fusion Setup

where  $\Phi_1, \Phi_2, \dots, \Phi_n$  are diagonal matrices whose entries are either 0 or 1. Let  $\phi_{ij}|_{j=1}^N$  be entries of matrix  $\Phi_i \forall i$ . The dimension of signal,  $v_i$  is  $N \times 1$ , and matrices  $\Phi_i$ 's are of size  $N \times N$ .

Suppose that fusion of signals can be done such that at a particular time instant only one measurement from the available  $n$  measurements can be used and a partial blending of signals is not possible. This assumption imposes additional constraints on the problem, which can be written as:

$$\sum_{i=1}^n \phi_{ij} = 1, \quad j = 1, 2, \dots, N \quad (5.3)$$

The problem is now simplified to find sensor schedule matrices,  $\Phi_i$ 's such that  $y_r$  is the best possible blend of all  $v_i$ 's and thus the best approximation to the original signal,  $y$ . It should be noted that  $y$  is unknown and the only available measurements are  $z_i$ 's and  $v_i$ 's.

**Claim:** The optimal sensor scheduling,  $\Phi_i^*$ 's can be obtained by minimizing the objective function,

$$\begin{aligned} J &= \|z_i - FG_i y_r\|^2 \\ &= \|z_i - FG_i(\Phi_1 v_1 + \Phi_2 v_2 + \dots + \Phi_n v_n)\|^2 \end{aligned} \quad (5.4)$$

subject to,

$$\{\phi_{ij} | \phi_{ij} \in \mathbb{R}\} \quad \forall i, j \quad (5.5)$$

and

$$\sum_{i=1}^n \phi_{ij} = 1 \quad \forall j \quad (5.6)$$

**Proof of Claim:** Ideally, the best way to solve this problem is to obtain  $\Phi^*$  that minimizes the error function

$$e = \|y - y_r\|_2$$

subject to constraints (5.5) and (5.6).

It is obvious that this is impossible as  $y$  is unknown. However, a close inspection of Equation (5.1) suggests that a weighted error measure can be evaluated by appropriately adjusting available measurements. This fact is illustrated in the following formulation:

$$\begin{aligned} z_i - FG_i y_r &= FG_i y - FG_i y_r \\ &= FG_i (y - y_r) \\ &= FG_i e \end{aligned}$$

Therefore, when  $FG_i \neq 0$ , the optimal sensor schedule matrices,  $\Phi_i^*$ 's obtained by solving the optimization problem described by Equations (5.4),(5.5) and (5.6) in fact, minimizes the weighted error function  $e$ . It is worth noting here that  $FG_i$  may not be zero in general. And if it is, then  $z_i$  will also be zero. This means that all the signals measured through that particular sensor,  $S_i$  will be zeroed out. In this case, data from sensor  $S_i$  should be discarded.  $\diamond$

Before deriving the algorithm for the optimization problem specified, we will validate the proposed idea by solving a simple numerical problem:

### 1. Example 1

Consider a two-sensor fusion setup shown in Fig. 33. It is noted that a problem with two sensors is considered in this example in order to simplify the computations involved but the proposed fusion scheme works with any finite number of sensors.

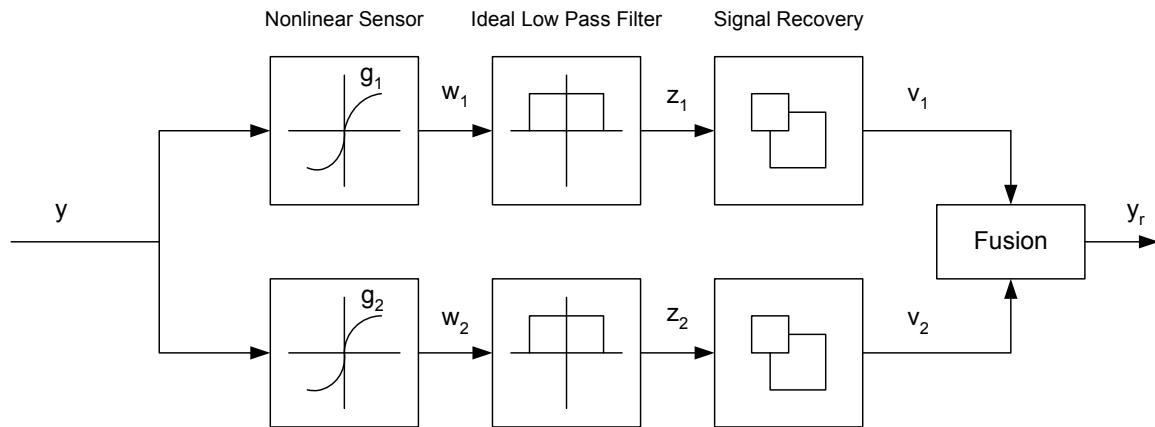


Figure 33: Two-Sensor Data Fusion Setup

It was shown in Section H of Chapter IV that the filtered signal vector  $z$ , and the original signal vector  $y$ , are related by  $z = FGy$ . Assume that the corresponding relationship for one of the sensors shown in Fig. 33 has the following form:

$$\begin{pmatrix} z_1 \\ z_2 \end{pmatrix} = \begin{pmatrix} 2 & 1 \\ 3 & 4 \end{pmatrix} \begin{pmatrix} y_1 \\ y_2 \end{pmatrix} \quad (5.7)$$

Let the original signal  $y$  at a particular time instance be:

$$\begin{pmatrix} y_1 \\ y_2 \end{pmatrix} = \begin{pmatrix} 1 \\ 2 \end{pmatrix} \quad (5.8)$$

and the corresponding  $z$  be:

$$\begin{pmatrix} z_1 \\ z_2 \end{pmatrix} = \begin{pmatrix} 4 \\ 11 \end{pmatrix} \quad (5.9)$$

Assume that the signal  $y$ , is measured by two sensors and the sensor outputs are recovered using the signal recovery algorithm described in Section 2. The original signal recovery may not always be possible and in order to obtain a good approximation to the original signal, recovered signals  $v_1$  and  $v_2$  should be blended. As partial blending of  $v_1$  and  $v_2$  is not possible, the fusion problem reduces to finding an optimal sensor schedule that extracts the original information from signals  $v_1$  and  $v_2$ .

Let the recovered signals be:

$$v_1 = \begin{pmatrix} v_{11} \\ v_{12} \end{pmatrix} = \begin{pmatrix} 2 \\ 2 \end{pmatrix} \quad (5.10)$$

$$v_2 = \begin{pmatrix} v_{21} \\ v_{22} \end{pmatrix} = \begin{pmatrix} 1 \\ 3 \end{pmatrix} \quad (5.11)$$

The above signals are artificially formed so that the original information is split and distributed between two signals. As can be seen, the first sample of signal  $v_2$  and the second sample of  $v_1$  contain the original information. It will be shown next that

the proposed fusion procedure is capable of extracting the original information while discarding the incorrect information.

The idea is to fuse  $v_1$  and  $v_2$  so that the error between the original signal and the fused signal is minimal. As described earlier, the first step involves the fusion of recovered signals using the equation,

$$y_r = \Phi_1 v_1 + \Phi_2 v_2 \quad (5.12)$$

As there are only two sensors, constraints (5.6) can be written as follows.

$$\Phi_1 + \Phi_2 = I \quad (5.13)$$

Let  $\Phi_1 = \Phi$  and  $\Phi_2 = (I - \Phi)$ . where

$$\Phi = \begin{pmatrix} \phi_1 & 0 \\ 0 & \phi_2 \end{pmatrix}$$

and  $I$  is an identity matrix of dimension 2.

The second step is to minimize the cost function as in (5.4):

$$\begin{aligned} \min_{\Phi} J &= \min_{\Phi} \|z - FGv_2 - FG\Phi(v_1 - v_2)\|^2 \\ &= \min_{\Phi} \left\| \begin{pmatrix} 4 \\ 11 \end{pmatrix} - \begin{pmatrix} 2 & 1 \\ 3 & 4 \end{pmatrix} \begin{pmatrix} 1 \\ 3 \end{pmatrix} - \begin{pmatrix} 2 & 1 \\ 3 & 4 \end{pmatrix} \begin{pmatrix} \phi_1 & 0 \\ 0 & \phi_2 \end{pmatrix} \begin{pmatrix} 1 \\ -1 \end{pmatrix} \right\|^2 \\ &= \min_{\Phi} \left\| \begin{pmatrix} 2\phi_1 - \phi_2 + 1 \\ 3\phi_1 - 4\phi_2 + 4 \end{pmatrix} \right\|^2 \\ &= \min_{\Phi} \{(2\phi_1 - \phi_2 + 1)^2 + (3\phi_1 - 4\phi_2 + 4)^2\} \end{aligned} \quad (5.14)$$



The optimal solution is clearly

$$\Phi = \begin{pmatrix} 0 & 0 \\ 0 & 1 \end{pmatrix}$$

The corresponding fused signal  $y_r$  would be

$$\begin{aligned} y_r &= \begin{pmatrix} 0 & 0 \\ 0 & 1 \end{pmatrix} \begin{pmatrix} 2 \\ 2 \end{pmatrix} + \begin{pmatrix} 1 & 0 \\ 0 & 0 \end{pmatrix} \begin{pmatrix} 1 \\ 3 \end{pmatrix} \\ &= \begin{pmatrix} 1 \\ 2 \end{pmatrix} \end{aligned}$$

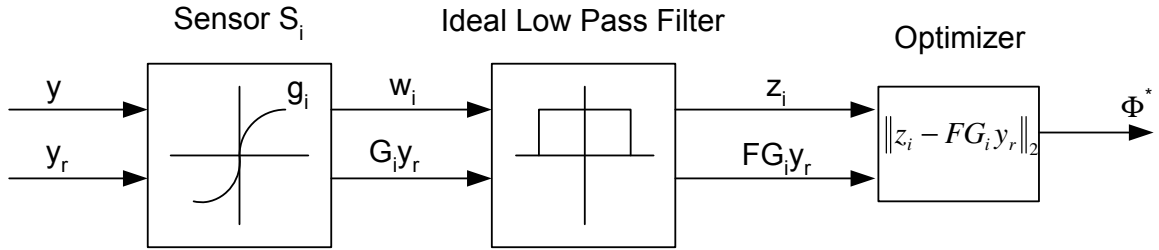
which agrees with the original signal.

It is noted that the cost function value at optimal conditions is zero and the original signal is reproduced because the exact original information is available. When the exact information is not available, the fusion algorithm will generate a signal that is the best possible approximation to the original signal and obviously the cost function value may not be exactly zero in this case. Development of the implementation scheme and Example 2 given in the next section provide further evidence of this point.

## 2. Implementation Scheme

In this section, we will show how an implementation scheme for the multi-sensor fusion procedure proposed in the previous section could be devised. The process of evaluating the optimal sensor scheduling matrices,  $\Phi_i^*$ 's is schematically illustrated in Fig. 34.

Let us first formulate the optimization problem stated above in standard form. To do so, we define a vector  $\theta$  that is formed by stacking all  $\phi_{ij}$ 's in one column as follows:

Figure 34: Optimization Setup to Find  $\Phi^*$ 

$$\theta = \left( \phi_{11} \dots \phi_{1N} \phi_{21} \dots \phi_{2N} \dots \phi_{n1} \dots \phi_{nN} \right)^T \quad (5.15)$$

The objective function  $J$  in Equation (5.4) can now be easily written in terms of  $\theta$  as:

$$\begin{aligned} J &= \|z - FG(D_1^N(\theta)v_1 + D_{N+1}^{2N}(\theta)v_2 + \dots + D_{(n-1)N+1}^{nN}(\theta)v_n)\|^2 \\ &= \|z - FG(D_N(\theta)v_1 + D_{2N}(\theta)v_2 + \dots + D_{nN}(\theta)v_n)\|^2 \end{aligned} \quad (5.16)$$

where  $D_{(i-1)N+1}^{iN}(\theta) = D_{iN}(\theta)$  is an  $N \times N$  diagonal matrix, whose entries are elements of  $\theta$  from  $\{(i-1)N+1\}^{th}$  row to  $\{iN\}^{th}$  row. It is easy to verify that the following relationship is maintained.

$$D_{iN}(\theta)v_i = \Phi_i v_i \quad (5.17)$$

Similarly, the constraints given in Equation (5.6) should be written in terms of  $\theta$ . To do so, we will expand Equation (5.6) as follows:

$$\begin{aligned}
\phi_{11} + \phi_{21} + \dots + \phi_{n1} &= 1 \\
\phi_{12} + \phi_{22} + \dots + \phi_{n2} &= 1 \\
&\vdots \\
\phi_{1N} + \phi_{2N} + \dots + \phi_{nN} &= 1
\end{aligned} \tag{5.18}$$

It is noted that the left hand side of  $i^{th}$  constraints in Equation (5.18) is simply the sum of  $i^{th}$  diagonal elements of matrices  $\Phi_1, \Phi_2, \dots, \Phi_n$ . This interesting pattern enables us to write constraints (5.18) in a compact form in terms of  $\theta$  as follows:

$$\begin{pmatrix} I_n & I_n & \dots & I_n \end{pmatrix} \theta = \begin{pmatrix} 1 \\ 1 \\ \vdots \\ 1 \end{pmatrix} \tag{5.19}$$

where  $I_n$  is an  $n \times n$  identity matrix and the matrix

$$\begin{pmatrix} I_n & I_n & \dots & I_n \end{pmatrix}$$

is formed by inserting  $N$  number of  $I_n$  matrices as shown in order to match the dimension of  $\theta$ .

Now that all variables to be optimized are included in vector  $\theta$  and objective function is in terms of  $\theta$ , this completes the problem formulation. It is noted that the variables to be optimized are zero-one variables and therefore it is required that an integer programming technique be used on top of any standard optimizer in order to solve this problem. In this section, we will use a popular integer programming technique, *Branch and Bound* to derive an optimization procedure [113], [114].

Define an integer programming problem  $P_I$  as:

Problem **P<sub>I</sub>**

Minimize

$$J = \|z - FG(D_N(\theta)v_1 + D_{2N}(\theta)v_2 + \dots + D_{nN}(\theta)v_n)\|^2 \quad (5.20)$$

subject to

$$\begin{pmatrix} I_n & I_n & \dots & I_n \end{pmatrix} \theta = \begin{pmatrix} 1 \\ 1 \\ \vdots \\ 1 \end{pmatrix} \quad (5.21)$$

and

$$\{\theta_i | \theta_i \in \mathbb{R}\}, \quad \theta_i \text{ is } 0 \text{ or } 1 \quad \forall i \in \mathbb{I}$$

where  $\mathbb{I}$  is the set of integer variables and  $\mathbb{R}$  is the (closed) feasible region of the continuous problem.

Next, define a continuous time problem as follows.

Problem **P<sub>C</sub>**

Minimize

$$J = \|z - FG(D_N(\theta)v_1 + D_{2N}(\theta)v_2 + \dots + D_{nN}(\theta)v_n)\|^2 \quad (5.22)$$

subject to

$$\begin{pmatrix} I_n & I_n & \dots & I_n \end{pmatrix} \theta = \begin{pmatrix} 1 \\ 1 \\ \vdots \\ 1 \end{pmatrix} \quad (5.23)$$

and

$$\{\theta_i | \theta_i \in \mathbb{R}\}$$

If the optimal solution to the problem  $P_C$ ,  $\theta^o$  is feasible in  $P_I$ , then it solves the integer programming problem,  $P_I$ . If not, the following two continuous sub problems should be created by branching on  $\theta^o$ .

Problem  $\mathbf{P}^-$

Minimize

$$J = \|z - FG(D_N(\theta)v_1 + D_{2N}(\theta)v_2 + \dots + D_{nN}(\theta)v_n)\|^2 \quad (5.24)$$

subject to

$$\begin{pmatrix} I_n & I_n & \dots & I_n \end{pmatrix} \theta = \begin{pmatrix} 1 \\ 1 \\ \vdots \\ 1 \end{pmatrix} \quad (5.25)$$

and

$$\{\theta_i | \theta_i \in \mathbb{R}\}, \quad \theta_i \leq [\theta_i^o] \quad \forall i \in \mathbb{I}$$

and

Problem  $\mathbf{P}^+$

Minimize

$$J = \|z - FG(D_N(\theta)v_1 + D_{2N}(\theta)v_2 + \dots + D_{nN}(\theta)v_n)\|^2 \quad (5.26)$$

subject to

$$\begin{pmatrix} I_n & I_n & \dots & I_n \end{pmatrix} \theta = \begin{pmatrix} 1 \\ 1 \\ \vdots \\ 1 \end{pmatrix} \quad (5.27)$$

and

$$\{\theta_i | \theta_i \in \mathbb{R}\}, \quad \theta_i \geq [\theta_i^o] + 1 \quad \forall i \in \mathbb{I}$$

where  $[\theta_i]$  is the largest integer not greater than  $\theta_i$ .

The branching process should be repeated until no further branching is possible. The optimal solutions to all feasible subproblems are compared and the one that corresponds to the least cost function value is chosen as the optimal solution to problem  $P_I$ . This process is described in detail in the following algorithm:

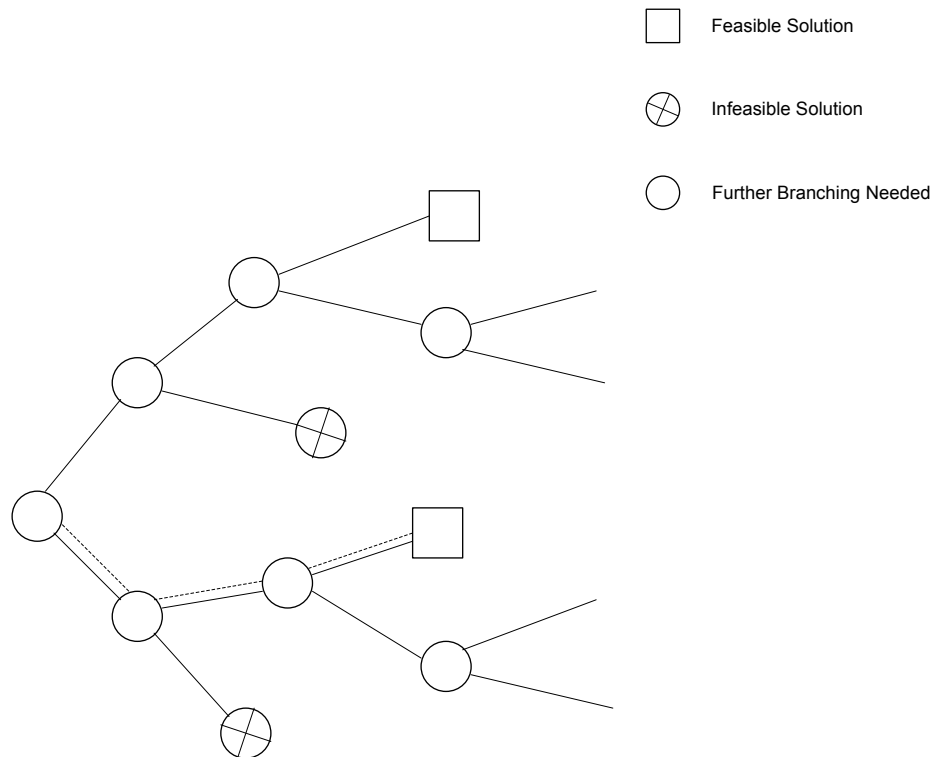


Figure 35: Branch and Bound Tree Structure

**Algorithm 3** *Discrete Zero-One Optimization Procedure*

**Step 1** [*Solving the Continuous Problem*]. Solve the continuous problem ( $P_C$ ) assuming no constraints. If the optimal solution  $\Phi^o$  of  $P_C$  exists, go to next step.

Otherwise, the solution found is not feasible.

**Step 2** [Checking the necessity of Branch and Bound Technique]. If  $\Phi^o$  is feasible in the integer programming problem ( $P_I$ ), then  $\Phi^* = \Phi^o$ . If not, go to next step.

**Step 3** [Applying the Branch and Bound Technique]. Define two problems,  $P^-$  and  $P^+$  by branching on variable  $\Phi^o$  in Problem  $P_C$ . Solve problems  $P^-$  and  $P^+$  and let  $\Phi^-$  and  $\Phi^+$  be the corresponding optimal solutions.

**Step 4** [Identifying the parent problem and special cases]. The special cases and the parent problems can be identified by following the instructions given below:

1. If any problem has no feasible point, it corresponds to one special case ( $\otimes$  in Fig. 35).
2. If any solution is feasible in  $P_I$  (i.e. satisfies all constraints and is integer feasible), then it is the other special case ( $\square$  in Fig. 35). This case also corresponds to one of the feasible solutions.
3. If any problem does not fall in any one of the above-mentioned categories, then it is a parent problem. Go to Step 3.

**Step 5** [Choosing the optimal solution]. Expand the problem tree till no further branching is possible and compute all feasible solutions. The required solution  $\Phi^*$  is the one which has the least feasible cost function value.

Having derived the solution method for the optimization problem, we formally state the sensor fusion procedure in the following algorithm:

**Algorithm 4** *Sensor Scheduling Procedure*

**Step 1** [Measuring Filtered Signals] Pass the sensor outputs through the ideal low pass filters as shown in Fig. 32 and measure the filtered signals.

**Step 2** [*Recovering the original signal*] Recover the original from filtered signals using the signal recovery procedure derived in [96] and given in the previous chapter

**Step 3** [*Obtaining the optimal sensor schedule*] Solve the optimization problem described by the objective function (5.4) and constraints (5.5) and (5.6) using Algorithm 3 and obtain the optimal sensor schedule matrix,  $\Phi_i^*$ 's.

**Step 4** [*Fusing recovered signals*] Fuse recovered signals by (5.2) and  $\Phi_i^*$ 's.

To demonstrate the efficiency of the above fusion procedure, we will present another example:

### 3. Example 2

Consider again the two-fusion setup discussed in Example 1. As before, assume that  $z = FGy$  relationship for one of the sensors has the following form:

$$\begin{pmatrix} z_1 \\ z_2 \end{pmatrix} = \begin{pmatrix} 2 & 1 \\ 3 & 4 \end{pmatrix} \begin{pmatrix} y_1 \\ y_2 \end{pmatrix} \quad (5.28)$$

Let original signal  $y$  be:

$$\begin{pmatrix} y_1 \\ y_2 \end{pmatrix} = \begin{pmatrix} 1 \\ 2 \end{pmatrix} \quad (5.29)$$

and the corresponding  $z$  be:

$$\begin{pmatrix} z_1 \\ z_2 \end{pmatrix} = \begin{pmatrix} 4 \\ 11 \end{pmatrix} \quad (5.30)$$

Recall that in Example 1, the fusion procedure was able to reproduce the original signal because recovered signals  $v_1$  and  $v_2$  were formed such that the exact original information was distributed between  $v_1$  and  $v_2$ . This may not be the case always. That is, the exact original information may not be available in recovered signals. In



this case, the original signal may not be exactly reproduced and the problem reduces to finding a signal that is the best possible approximation to the original signal. To illustrate that the developed fusion scheme is capable of generating such a signal, it is assumed that recovered signals do not contain the exact original information between them.

Let recovered signals be:

$$v_1 = \begin{pmatrix} v_{11} \\ v_{12} \end{pmatrix} = \begin{pmatrix} 2 \\ 1.6 \end{pmatrix} \quad (5.31)$$

$$v_2 = \begin{pmatrix} v_{21} \\ v_{22} \end{pmatrix} = \begin{pmatrix} 1.2 \\ 3 \end{pmatrix} \quad (5.32)$$

As before, signals  $v_1$  and  $v_2$  are fused by:

$$y_r = \Phi v_1 + (I - \Phi)v_2 \quad (5.33)$$

Now, consider the following optimization problem:

$$\begin{aligned} \min_{\Phi} J &= \|z - FGv_2 - FG\Phi(v_1 - v_2)\|^2 \\ &= \left\| \begin{pmatrix} 4 \\ 11 \end{pmatrix} - \begin{pmatrix} 2 & 1 \\ 3 & 4 \end{pmatrix} \begin{pmatrix} 1.2 \\ 3 \end{pmatrix} - \begin{pmatrix} 2 & 1 \\ 3 & 4 \end{pmatrix} \begin{pmatrix} \phi_1 & 0 \\ 0 & \phi_2 \end{pmatrix} \begin{pmatrix} 0.8 \\ -1.4 \end{pmatrix} \right\|^2 \\ &= \left\| \begin{pmatrix} 1.6\phi_1 - 1.4\phi_2 + 1.4 \\ 2.4\phi_1 - 5.6\phi_2 + 4.6 \end{pmatrix} \right\|^2 \\ &= \{(1.6\phi_1 - 1.4\phi_2 + 1.4)^2 + (2.4\phi_1 - 5.6\phi_2 + 4.6)^2\} \end{aligned} \quad (5.34)$$

subject to

$$\{\Phi | \Phi \in \mathbb{R}\}, \text{ and } \phi(i) \text{ is } 0 \text{ or } 1 \forall i \in \mathbb{I}.$$

This optimization problem is not straightforward and therefore an integer programming technique such as Branch and Bound should be applied in conjunction with any standard optimizers. Let us now demonstrate how branch and bound method could be used to obtain a solution.

The first step is to solve the unconstrained optimization problem. The solution to this problem is,

$$\Phi^o = \begin{pmatrix} \phi_1^o \\ \phi_2^o \end{pmatrix} = \begin{pmatrix} 0 \\ 0.8319 \end{pmatrix} \quad (5.35)$$

The cost function value is  $J^o = 0.0588$ .

As  $\phi_2$  is not an integer, this solution is not feasible. We want  $\phi_2$  to be either 0 or 1. To do so, we branch on  $\phi_2$ , creating two subproblems.

Problem  $\mathbf{P}^-$

$$\min_{\Phi} J^- = \{(1.6\phi_1 - 1.4\phi_2 + 1.4)^2 + (2.4\phi_1 - 5.6\phi_2 + 4.6)^2\} \quad (5.36)$$

subject to,

$$0 \leq \phi(1) \leq 1$$

$$0 \leq \phi(2) \leq 0$$

and  $\phi(i)$  is 0 or 1  $\forall i \in \mathbb{I}$ .

The solution to this problem is

$$\Phi^- = \begin{pmatrix} \phi_1^- \\ \phi_2^- \end{pmatrix} = \begin{pmatrix} 0 \\ 0 \end{pmatrix} \quad (5.37)$$

The objective function value is  $J^- = 23.12$ .

The solution obtained is feasible and therefore no further branching is necessary.

Let us now consider the other subproblem.

Problem  $\mathbf{P}^+$

$$\min_{\phi} J^+ = \{(1.6\phi_1 - 1.4\phi_2 + 1.4)^2 + (2.4\phi_1 - 5.6\phi_2 + 4.6)^2\} \quad (5.38)$$

subject to

$$0 \leq \phi(1) \leq 1$$

$$1 \leq \phi(2) \leq 1$$

and  $\phi(i)$  is 0 or 1  $\forall i \in \mathbb{I}$ .

The solution to this problem is

$$\Phi^+ = \begin{pmatrix} \phi_1^+ \\ \phi_2^+ \end{pmatrix} = \begin{pmatrix} 0.2885 \\ 1 \end{pmatrix} \quad (5.39)$$

The objective function value is  $J^+ = 0.3077$ .

This solution is not feasible and therefore further branching is necessary. Let us create two more subproblems by branching on  $\phi_1$ .

Problem  $\mathbf{P}^{+-}$

$$\min_{\Phi} J^{+-} = \{(1.6\phi_1 - 1.4\phi_2 + 1.4)^2 + (2.4\phi_1 - 5.6\phi_2 + 4.6)^2\} \quad (5.40)$$

subject to

$$0 \leq \phi(1) \leq 0$$

$$1 \leq \phi(2) \leq 1$$

and  $\phi(i)$  is 0 or 1  $\forall i \in \mathbb{I}$

The solution to this problem is

$$\Phi^{+-} = \begin{pmatrix} \phi_1^{+-} \\ \phi_2^{+-} \end{pmatrix} = \begin{pmatrix} 0 \\ 1 \end{pmatrix} \quad (5.41)$$

The objective function value is  $J^{+-} = 1$ . This solution is feasible and therefore no further branching is necessary.

Let us consider other subproblem.

Problem  $\mathbf{P}^{++}$

$$\min_{\Phi} J^{++} = \{(1.6\phi_1 - 1.4\phi_2 + 1.4)^2 + (2.4\phi_1 - 5.6\phi_2 + 4.6)^2\} \quad (5.42)$$

subject to

$$1 \leq \phi(1) \leq 1$$

$$1 \leq \phi(2) \leq 1$$

and  $\phi(i)$  is 0 or 1  $\forall i \in \mathbb{I}$ .

The solution to this problem is

$$\Phi^{++} = \begin{pmatrix} \phi_1^{++} \\ \phi_2^{++} \end{pmatrix} = \begin{pmatrix} 1 \\ 1 \end{pmatrix} \quad (5.43)$$

The objective function value is  $J^{++} = 4.52$ . As the solution is feasible, no further branching on this path is possible. As there are no further active subproblems, the optimal solution to this problem is then the one that gives the least cost function value. The optimal solution is therefore,

$$\Phi^* = \begin{pmatrix} 0 & 0 \\ 0 & 1 \end{pmatrix}$$

The fused signal is

$$\begin{aligned} y_r &= \begin{pmatrix} 0 & 0 \\ 0 & 1 \end{pmatrix} \begin{pmatrix} 2 \\ 1.6 \end{pmatrix} + \begin{pmatrix} 1 & 0 \\ 0 & 0 \end{pmatrix} \begin{pmatrix} 1.2 \\ 3 \end{pmatrix} \\ &= \begin{pmatrix} 1.2 \\ 1.6 \end{pmatrix} \end{aligned}$$

which is obviously the best possible approximation to the original signal. Note that the optimal cost function value is not exactly zero. This is because the original signal is not exactly reproduced.

Simulation results are presented in chapter VII to validate the multi-sensor fusion scheme developed.

## B. Fusion of Distorted Data by Continuous Optimization

The examples presented in the previous section clearly demonstrate performance of the fusion scheme. The main drawback of the proposed procedure is the increased

computational load due to the combinatorial nature of solutions generated by the Branch and Bound Method. Implementing this scheme in real time may require faster computational resources be used. In order to resolve this issue, we make necessary modifications to the above algorithm and show that efficiency of the algorithm can be improved.

It is assumed that at least one of the sensor models ( $S_p$ ) is exactly known. It will be shown later that the proposed framework is robust to model uncertainty or modelling errors. Consider the following fusion equation:

$$y_r = \Lambda_1 v_1 + \Lambda_2 v_2 + \dots + \Lambda_n v_n \quad (5.44)$$

where  $\Lambda_1, \Lambda_2, \dots, \Lambda_n$  are weighting matrices. Let  $\lambda_{ij}|_{j=1}^N$  be entries of matrix  $\Lambda_i \forall i$ . The dimension of signal,  $v_i$  is  $N \times 1$ , and matrices  $\Lambda_i$ 's are of size  $N \times N$ .

The first step is to find the weighting matrices such that the error between the fused signal  $y_r$  and  $y$  is minimal. We claim that the optimal weighting matrices can be generated by solving the following optimization problem.

$$\begin{aligned} \min_{\Lambda_i} J &= \|z_p - FG_p y_r\|^2 \\ &= \|z_p - FG_p(\Lambda_1 v_1 + \Lambda_2 v_2 + \dots + \Lambda_n v_n)\|^2 \end{aligned} \quad (5.45)$$

subject to,

$$\{\lambda_{ij} | \lambda_{ij} \in \mathbb{R}\} \quad \forall i, j \quad (5.46)$$

where  $\mathbb{R}$  is set of real variables.

Therefore, when  $FG_p \neq 0$ , the optimal sensor schedule matrices,  $\Lambda_i^*$ 's obtained by solving the optimization problem described by Equations (5.45) and (5.46) in fact, minimizes the weighted error function  $e$ . It is worth noting here that  $FG_p$  may not

be zero in general. And if it is, then  $z_p$  will also be zero. This means that all the signals measured through that sensor,  $S_p$  will be zeroed out. In this case, data from sensor  $S_p$  should be discarded.  $\diamond$

### 1. Implementation Scheme

In this section, we will show how an implementation scheme for the multi-sensor fusion procedure proposed in the previous section could be devised. The process of evaluating the optimal sensor scheduling matrices,  $\Lambda_i^*$ 's is schematically illustrated in Fig. 36.

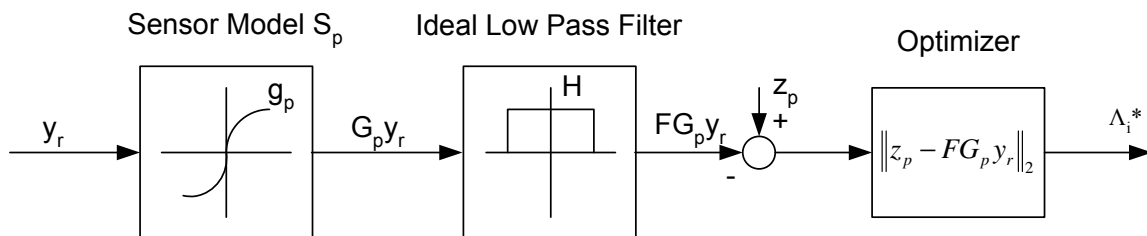


Figure 36: Optimization Setup to Find  $\Lambda_i^*$

Let us first formulate the optimization problem stated above in standard form. To do so, we define a vector  $X$  that is formed by stacking all  $\lambda_{ij}$ 's in one column as follows:

$$X = \left( \lambda_{11} \dots \lambda_{1N} \lambda_{21} \dots \lambda_{2N} \dots \lambda_{n1} \dots \lambda_{nN} \right)^T \quad (5.47)$$

The objective function  $J$  in Equation (5.45) can now be easily written in terms of  $X$  as:

$$\begin{aligned} J &= \|z_p - FG_p(D_1^N(X)v_1 + D_{N+1}^{2N}(X)v_2 + \dots + D_{(n-1)N+1}^{nN}(X)v_n)\|^2 \\ &= \|z_p - FG_p(D_N(X)v_1 + D_{2N}(X)v_2 + \dots + D_{nN}(X)v_n)\|^2 \end{aligned} \quad (5.48)$$

where  $D_{(i-1)N+1}^{iN}(X) = D_{iN}(X)$  is an  $N \times N$  diagonal matrix, whose entries are elements of  $X$  from  $\{(i-1)N+1\}^{th}$  row to  $\{iN\}^{th}$  row. It is easy to verify that the following relationship is maintained:

$$D_{iN}(X)v_i = \Lambda_i v_i$$

Solving the unconstrained optimization problem formulated above will yield the optimal weighting matrices. These values should then be used to obtain  $y_r$  as in Equation (5.44), which is the best possible blend of multi-source data. It is often the case that fusion of signals can be done such that at a particular time instant only one measurement from the available  $n$  measurements can be used and a partial blending of signals is not possible. The situations like this can be best tackled by scheduling the available multi-sensor data so as to obtain the best possible combination. Having found the best estimation of  $y$ , the sensor scheduling problem becomes straightforward. At each time instant, all available data  $v_i$  should be compared with the corresponding entry of  $y_r$  and the sensor data that is closest to this entry  $y_r$  should be the best candidate to fill the spot in the sensor schedule. This process can be automated by formulating the problem as an optimization problem.

Let  $v_f$  be the fused signal. Relate  $v_f$  and the multi-sensor data by

$$v_f = \Gamma_1 v_1 + \Gamma_2 v_2 + \dots + \Gamma_n v_n \quad (5.49)$$

where  $\Gamma_1, \Gamma_2, \dots, \Gamma_n$  are diagonal matrices whose entries are either 0 or 1. Let  $\gamma_{ij}|_{j=1}^N$  be entries of matrix  $\gamma_i \forall i$ . The matrices  $\Gamma_i$ 's are of size  $N \times N$ .

The optimal sensor scheduling matrices,  $\Gamma_i^*$ 's can be obtained by minimizing the objective function



$$J = \|y_r - v_f\|^2 \quad (5.50)$$

subject to,

$$\{\gamma_{ij} | \gamma_{ij} \in \mathbb{I}\} \quad \forall i, j \quad (5.51)$$

and

$$\sum_{i=1}^n \gamma_{ij} = 1 \quad \forall j \quad (5.52)$$

where  $\mathbb{I}$  is the set of positive integer variables.

The constraint set (5.52) is necessary to generate discrete zero-one output. Any integer programming technique such as Branch and Bound can be used on top of any standard optimizer to solve the above zero-one discrete optimization problem [114], [113].

The multi-sensor fusion scheme given above is summarized in the following algorithm.

**Algorithm 5** *Sensor Scheduling Procedure*

**Step 1** [*Measuring Filtered Signals*] Pass the sensor outputs through the ideal low pass filters as shown in Fig. 32 and measure the filtered signals.

**Step 2** [*Recovering the original signal*] Recover the original from filtered signals using the signal recovery procedure derived in [96] and given in the previous chapter.

**Step 3** [*Obtaining the best blend*] Solve the unconstrained optimization problem described by the objective function (5.45) to obtain the optimal weighting matrices,  $\Lambda_i^*$ . Plug in these values in Equation (5.44) to obtain the best possible blend  $y_r$ .

**Step 4** [*Scheduling of the multi-sensor data*] Minimize the objective function (5.50) subject to constraints (5.51) and (5.52) to obtain the sensor schedule matrices  $\Gamma_i$ . The best possible combination of the multi-sensor data (without partial

Table III: Signal Data for Examples 1 &amp; 2

Time	$y$	$v_1$	$v_2$	$v_3$	$z$
1	2.2	4.6	2.2	-2	7.45
2	-3.4	-3.4	4.3	1.1	-12.98
3	4.1	-2.4	10.1	4.1	13.5

*blend*) can be obtained by plugging in  $\Gamma_i$  in Equation (5.49).

## 2. Example 1

We present a numerical example to illustrate the proposed fusion scheme. Consider a fusion problem with three sensors. Suppose that the original signal has three samples and one of the sensor models is known and is given by (according to Equation (58)),

$$FG_1 = \begin{pmatrix} 4 & 1 & 0.5 \\ 3 & 6 & 0.2 \\ 3 & 4 & 5 \end{pmatrix} \quad (5.53)$$

The original signal,  $y$ , three sensor measurements(recovered signals)  $v_1$ ,  $v_2$  and  $v_3$  and the filtered output of the sensor whose model is given above,  $z$  are tabulated in Table III.

Applying Algorithm 5, the optimal weighting matrices are calculated and the signal  $y_r$  of Equation (5.44) is formed as:

$$y_r = \begin{pmatrix} 2.2 \\ -3.4 \\ 4.1 \end{pmatrix} \quad (5.54)$$

Table IV: Sensor Schedule (Example 1)

<i>Time</i>	$S_1$	$S_2$	$S_3$
1	x	√	x
2	√	x	x
3	x	x	√

which agrees with the original data,  $y$ . The next task is to schedule the sensor data. The automated sensor scheduling procedure proposed earlier can be used to solve this problem. The result is tabulated in Table IV, where  $x$  and  $\sqrt{\phantom{x}}$  are the off and on positions of sensors respectively. For example, at time instant 1, data from sensor #2 should be used and the other two values should be discarded.

### 3. Example 2

Let us now investigate the problem of not having the exact sensor model or the model available is inaccurate. Considering the same data given in Table III, we will use the following model to obtain the sensor schedule:

$$FG_1 = \begin{pmatrix} 4.2 & 1 & 0.5 \\ 3 & 6.4 & 0.2 \\ 3 & 4 & 5.5 \end{pmatrix} \quad (5.55)$$

As was done in the previous example, the signal  $y_r$  is obtained as follows.

$$y_r = \begin{pmatrix} 2.09 \\ -3.12 \\ 3.58 \end{pmatrix} \quad (5.56)$$

Table V: Sensor Schedule (Example 2)

<i>Time</i>	$S_1$	$S_2$	$S_3$
1	x	✓	x
2	✓	x	x
3	x	x	✓

The sensor schedule is tabulated in Table V.

The sensor schedule is same as before even though the correct sensor model was not used.

If the model uncertainty or modelling errors are modelled by,

$$\Delta = \begin{pmatrix} \delta_1 & 0 & 0 \\ 0 & \delta_2 & 0 \\ 0 & 0 & \delta_3 \end{pmatrix} \quad (5.57)$$

it can then be shown that there exists  $l_1, l_2, l_3, u_1, u_2, u_3 \in \mathbb{R}$  such that

$$\begin{aligned} l_1 &\leq \delta_1 \leq u_1 \\ l_2 &\leq \delta_2 \leq u_2 \\ l_3 &\leq \delta_3 \leq u_3 \end{aligned} \quad (5.58)$$

for which the algorithm generates the correct sensor schedule.

It can be concluded from this example that the algorithm is robust to small modelling errors or model uncertainty.

Table VI: Signal Data for Example 3

Time	$y$	$v_1$	$v_2$	$v_3$	$z$
1	2.2	4.6	1.9	-2	7.45
2	-3.4	-3.0	4.3	1.1	-12.98
3	4.1	-2.4	10.1	3.8	13.5

#### 4. Example 3

In the above examples, it was shown that the proposed algorithm is capable of extracting the original information, which is randomly distributed in the multi-sensor data. In general, the original information may not be exactly available in the sensed data. Consider the signal data given in Table VI.

The sensor measurements  $v_1, v_2$  and  $v_3$  do not contain the actual signal data. The fused signal  $y_r$  is found to be,

$$y_r = \begin{pmatrix} 2.3 \\ -3.4 \\ 4.1 \end{pmatrix} \quad (5.59)$$

The original information is reproduced even though the multi-sensor data do not contain it. As discussed earlier, the partial blending of data may not be possible always and the process may require that one of the available measurements be used. The sensor scheduling is necessary in this case and the automated scheduling algorithm could be used to obtain the best possible measurements. Table VII summarizes the result.

Table VII: Sensor Schedule (Example 3)

<i>Time</i>	$S_1$	$S_2$	$S_3$
1	x	✓	x
2	✓	x	x
3	x	x	✓

### C. Effective Sensor Fusion by Confidence Measures

In this section, we propose another sensor fusion scheme in which sensor data fusion is done by assigning a “confident measure” to all available sensor data and picking the ones that lead the list of confidence measures. The result is then used to solve the sensor scheduling problem.

#### 1. Characterization of Sensor Measurements

The characterization of sensor measurements is the first step of the proposed multi-sensor fusion procedure. Assuming that sensor measurements are given as time samples, we characterize each sample of the sensed data by assigning a “confidence measure”. The confidence measure, which is estimated by solving an optimization problem is used to understand how close a particular sensor measurement is to its actual value. For example, a confidence measure of 1 means that the sensor measurement is 100% accurate whereas a measure that is not close to 1 denotes that the corresponding sensor measurement is the least desirable. The idea of assigning confidence measures to sensor data is illustrated in Fig. 37. The processor uses the algorithm proposed in this section to calculate confidence measures. Each sensor data  $v_i$  is replaced by  $(v_i, \alpha_i)$  while being passed through the processor, where  $\alpha_i$  is its confidence measure.

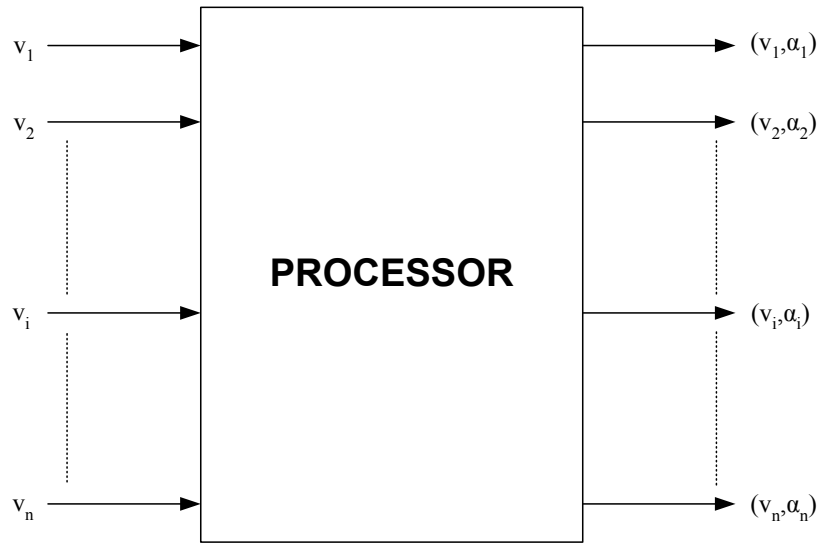


Figure 37: Assigning “Confidence Measure” to Sensor Data

**Claim:**

It is claimed that such confidence measures can be calculated by solving the following optimization problem:

$$\min_{\alpha_{ij}} \|z_i - F_i G_i \alpha_i v_i\| \quad (5.60)$$

$$\text{subject to } \alpha_{ij} \in \mathbb{R} \quad (5.61)$$

where  $v_i$  is the recovered signal/sensor measurements,  $z_i$  is the corresponding filtered signal, and  $F_i$  and  $G_i$  are the low pass filter and nonlinear sensor matrices respectively as defined in the previous sections. The confidence measure matrix  $\alpha_i$  is defined as

follows.

$$\alpha_i = \begin{pmatrix} \alpha_{i1} & 0 & \dots & 0 \\ 0 & \alpha_{i2} & \dots & 0 \\ \vdots & \vdots & \ddots & \vdots \\ 0 & 0 & \dots & \alpha_{iN} \end{pmatrix} \quad (5.62)$$

**Proof of Claim:** As the optimization problem formulated above is unconstrained, the optimal cost function value must be zero. This implies that the optimal  $\alpha_i^*$  should satisfy the following equation:

$$z_i = F_i G_i \alpha_i^* v_i \quad (5.63)$$

Recalling that the actual signal  $y_i$  and  $z_i$  are related by,

$$z_i = F_i G_i y_i \quad (5.64)$$

Comparing Equations (5.63) and (5.64), the following equation is obtained.

$$\alpha_i^* v_i = y \quad (5.65)$$

Expanding Equation (5.65),

$$\begin{pmatrix} \alpha_{i1}^* & 0 & \dots & 0 \\ 0 & \alpha_{i2}^* & \dots & 0 \\ \vdots & \vdots & \ddots & \vdots \\ 0 & 0 & \dots & \alpha_{iN}^* \end{pmatrix} \begin{pmatrix} v_{i1} \\ v_{i2} \\ \vdots \\ v_{iN} \end{pmatrix} = \begin{pmatrix} y_1 \\ y_2 \\ \vdots \\ y_N \end{pmatrix} \quad (5.66)$$

That is

$$\alpha_{ij}^* = \frac{y_i}{v_{ij}} \quad (5.67)$$

As the confidence measure  $\alpha_{ij}^*$  is the ratio of the actual value and the sensor measurement, any measurement whose confidence measure is closest to 1 is most



desirable. This completes the proof.  $\diamond$

## 2. Multi-sensor Fusion

Consider the fusion problem that is schematically shown in Fig. 32. Nonlinear sensor functions  $g_i$  are essentially different. Let  $v_1, v_2, \dots, v_n$  be recovered signals,  $z_1, z_2, \dots, z_n$  be filtered signals,  $n_1, n_2, \dots, n_n$  be sensor noise and  $w_1, w_2, \dots, w_n$  be output signals of sensors  $S_1, S_2, \dots, S_n$  respectively. Define  $v_i$  as follows:

$$v_i = \begin{pmatrix} v_{i1} \\ v_{i2} \\ \vdots \\ v_{iN} \end{pmatrix} \quad (5.68)$$

where  $i = 1, 2, \dots, n$  and  $N$  is the number of samples.

As explained in Section 2, the filtered ( $z_i$ ) and original ( $y$ ) signals are related by,

$$\begin{aligned} z_1 &= F_1 G_1 y \\ z_2 &= F_2 G_2 y \\ &\vdots \\ z_n &= F_n G_n y \end{aligned}$$

Define the  $n$  diagonal matrices namely  $A_1, A_2, \dots, A_n$  each of dimension  $N \times N$  as:

$$A_i = \begin{pmatrix} \alpha_{i1} & 0 & \dots & 0 \\ 0 & \alpha_{i2} & \dots & 0 \\ \vdots & \vdots & \ddots & \vdots \\ 0 & 0 & \dots & \alpha_{iN} \end{pmatrix} \quad (5.69)$$

where  $i = 1, 2, \dots, n$ .

As formulated in the previous section, the confidence measures  $\alpha_{ij}$  are calculated by solving  $n$  optimization problems. For instance, the  $i^{\text{th}}$  optimization problem is formulated as:

$$\min_{\alpha_{ij}} \|z_i - F_i G_i A_i v_i\| \quad (5.70)$$

$$\text{subject to } \alpha_{ij} \in \mathbb{R} \quad (5.71)$$

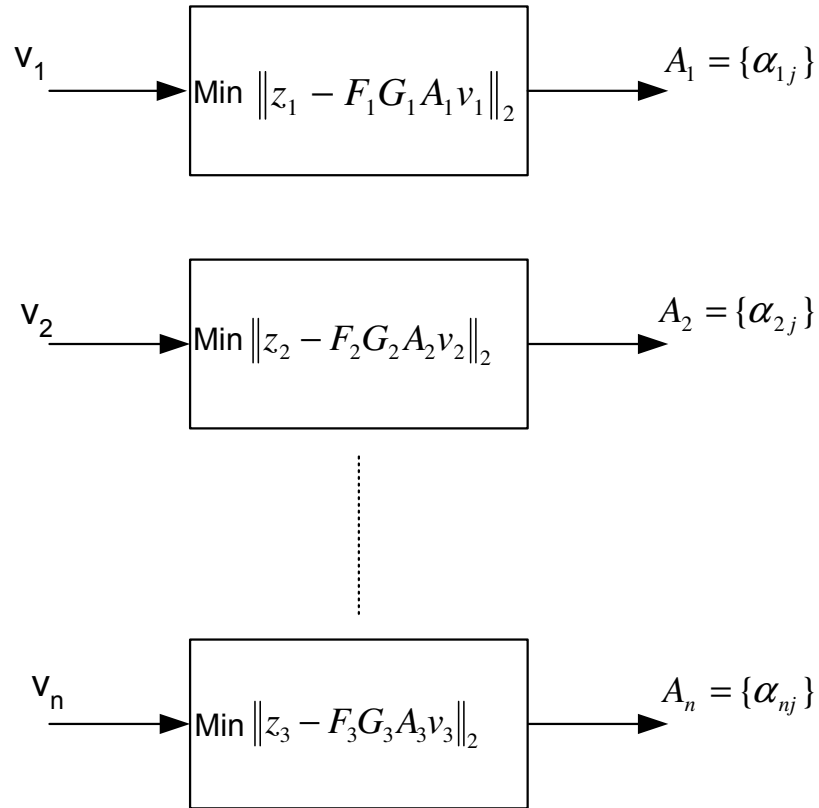
where  $i = 1, 2, \dots, n$ .

For  $i = 1, 2, \dots, n$ , we have  $n$  optimization problems, which should be formulated and solved to obtain  $\alpha_{ij}$ . For a problem with  $n$  sensors and a signal sample size of  $N$ , the number variables (confidence measures) to be optimized are  $nN$ . This process of evaluating confidence measures is illustrated in Fig. 38.

As all of the above optimization formulations are convex quadratic programming problems, the solutions can be easily obtained. Once all  $\alpha_{ij}$  are available, the fusion of signals at some time  $k$  should be done by comparing confidence measures of all samples at that particular instant and choosing the signal value whose confidence measure is closest to 1. The fusion rule is stated as follows.

### 3. Fusion Rule

At some time  $k$ , given  $n$  multi-sensor data  $v_{1k}, v_{2k}, \dots, v_{nk}$  and their corresponding confidence measures  $\alpha_{1k}, \alpha_{2k}, \dots, \alpha_{nk}$ , the best available sensor measurement at that particular time instant,  $k$  is  $v_{qk}$  that corresponds to the confidence measure obtained by the rule

Figure 38: Calculation of  $\alpha_{ij}$ 

$$\alpha_{qk} = \min_{i=1}^n |1 - \alpha_{ik}| \quad (5.72)$$

where  $q \in \{1, 2, \dots, n\}$

#### 4. Illustrative Example

We present a numerical example to illustrate the proposed fusion scheme. Consider a fusion problem with two sensors. Let the sensor models be given by

$$z_1 = \begin{pmatrix} 2 & 1 \\ 3 & 4 \end{pmatrix} y \quad (5.73)$$

$$z_2 = \begin{pmatrix} 4 & 0.5 \\ 1 & 2.5 \end{pmatrix} y \quad (5.74)$$

Let the original signal  $y$  be:

$$y = \begin{pmatrix} 1 \\ 2 \end{pmatrix} \quad (5.75)$$

The corresponding  $z_1$  and  $z_2$  are

$$z_1 = \begin{pmatrix} 4 \\ 11 \end{pmatrix} \quad (5.76)$$

$$z_2 = \begin{pmatrix} 5 \\ 6 \end{pmatrix} \quad (5.77)$$

Let recovered signals/sensor measurements be:

$$v_1 = \begin{pmatrix} v_{11} \\ v_{12} \end{pmatrix} = \begin{pmatrix} 2 \\ 2 \end{pmatrix} \quad (5.78)$$

$$v_2 = \begin{pmatrix} v_{21} \\ v_{22} \end{pmatrix} = \begin{pmatrix} 1 \\ 3 \end{pmatrix} \quad (5.79)$$

Define two diagonal matrices  $\alpha_1$  and  $\alpha_2$  as:

$$\alpha_1 = \begin{pmatrix} \alpha_{11} & 0 \\ 0 & \alpha_{12} \end{pmatrix} \quad (5.80)$$

$$\alpha_2 = \begin{pmatrix} \alpha_{21} & 0 \\ 0 & \alpha_{22} \end{pmatrix} \quad (5.81)$$

As explained in the previous section, the unconstrained optimization problems are formulated as follows.

Minimize

$$J_1 = \|z_1 - F_1 G_1 \alpha_1 v_1\|^2 \quad (5.82)$$

$$= \left\| \begin{pmatrix} 4 \\ 11 \end{pmatrix} - \begin{pmatrix} 2 & 1 \\ 3 & 4 \end{pmatrix} \begin{pmatrix} \alpha_{11} & 0 \\ 0 & \alpha_{12} \end{pmatrix} \begin{pmatrix} 2 \\ 2 \end{pmatrix} \right\|^2 \quad (5.83)$$

$$= (4 - 4\alpha_{11} - 2\alpha_{12})^2 + (11 - 6\alpha_{11} - 8\alpha_{12})^2 \quad (5.84)$$

The solution to the above optimization problem is

$$\begin{pmatrix} \alpha_{11}^* \\ \alpha_{12}^* \end{pmatrix} = \begin{pmatrix} 0.5 \\ 1 \end{pmatrix} \quad (5.85)$$

or written according to our notation,  $\{(2,0.5),(2,1)\}$ . That is, the second sample is 100% accurate.

Let us now solve the other optimization problem:

Minimize

$$J_2 = \|z_2 - F_2 G_2 \alpha_2 v_2\|^2 \quad (5.86)$$

$$= \left\| \begin{pmatrix} 5 \\ 6 \end{pmatrix} - \begin{pmatrix} 4 & 0.5 \\ 1 & 2.5 \end{pmatrix} \begin{pmatrix} \alpha_{21} & 0 \\ 0 & \alpha_{22} \end{pmatrix} \begin{pmatrix} 1 \\ 3 \end{pmatrix} \right\|^2 \quad (5.87)$$

$$= (5 - 4\alpha_{21} - 1.5\alpha_{22})^2 + (6 - \alpha_{21} - 7.5\alpha_{22})^2 \quad (5.88)$$

The solution to the above optimization problem is

$$\begin{pmatrix} \alpha_{11}^* \\ \alpha_{12}^* \end{pmatrix} = \begin{pmatrix} 1 \\ 0.6667 \end{pmatrix} \quad (5.89)$$

Or written according to our notation,  $\{(1,1),(3,0.6667)\}$ . That is, the first sample is 100% accurate.

From Equations (5.85) and (5.89), it can be concluded that the second sample of sensor #1 and first sample of sensor #2 are 100% accurate and therefore should be chosen.

Or applying the fusion rule,

$$\alpha_{qk} = \min_{i=1}^2 |1 - \alpha_{ik}| \quad (5.90)$$

where  $q \in \{1, 2\}$  and choosing the corresponding sensor outputs, the following estimate of the original signal is obtained:

$$v = \begin{pmatrix} 1 \\ 2 \end{pmatrix} \quad (5.91)$$

It is noted that the original signal is detected accurately, which validates the proposed scheme. Simulation data is presented in Chapter VII to further validate the proposed scheme.

## CHAPTER VI

## ATTAINING HIGH OPERATING BANDWIDTH BY SENSOR ARRAYS

This chapter is devoted to the development of sensor arrays to attain a high operating bandwidth. Three approaches are presented to implement the sensor array framework introduced in chapter I. Simulation results are presented in chapter VII to validate the schemes developed. The material presented in this chapter also appears in [115], [116].

## A. Implementation of Sensor Arrays

To implement the sensor array framework proposed in chapter I, it is required that a suitable multi-sensor data fusion scheme be developed first. As discussed, the proposed sensor array should have several frequency segments that are characterized by frequency responses of low pass-band sensors. Transition from one operating region to the other may not be sharp. This would result in several overlapping regions where data from more than one sensor is available. The individual measurements must be combined to yield a single inference. An effective data fusion plays a crucial role in improving the accuracy of sensor array measurements.

In this section, we develop a data fusion scheme using Frequency Response Methods. The sensor array design problem is formulated as a feedforward problem and Quantitative Feedback Theory (QFT) loopshaping techniques are adopted to solve the problem posed. QFT is a controller design methodology that is well suited for the design of controllers or compensators for systems with large parameter uncertainty for which it is required to meet point-wise, closed loop frequency domain performance tolerances [117, 118]. Sensors used in the proposed sensor arrays may have complex and time varying dynamics and analytic models may be difficult to obtain. This

would make the data fusion and the design process, in general, very difficult and challenging. To simplify this task and utilize the features of the QFT methodology, the sensor array design is done in a QFT environment. The QFT methodology fits a wide range of applications of this kind. In particular, Bentley [119] uses the QFT method to combine the inertial-angle-sensor data with the less perfect information in the command signal to achieve maximum jitter reduction. Though data fusion is done primarily using frequency domain techniques in this setup, other techniques are also explored and their applicability is tested. For example, the design of a multi-sensor system for a high speed land vehicle navigation and control system using the continuous time Kalman Filter and classical frequency response techniques is given in [68]. A detailed discussion on other fusion techniques and their limitations are presented in Section C. Furthermore, a new optimization based sensor fusion technique is developed in Section 38.

## B. Sensor Arrays

In general, the term ‘sensor array’ is used to denote a collection of multiple sensors arranged in a specific pattern. The way sensors are arranged may differ from one application to another. In the literature, there are several general and many more application specific definitions given for sensor arrays [120], [121], [122], [123], [124]. The Oxford English Dictionary definition of an array is: *A series of things exhibited or displayed in line or order.* Using this definition, in this context, a sensor array is defined as *a multi-sensor arrangement in which each sensor is assigned to cover only a specific segment of the overall operating bandwidth and the required bandwidth is covered by the union of all the pass-bands of the sensors in the collection.*

The proposed sensor array configuration is schematically shown in Fig. 39, where



$y$  is a signal whose frequency spectrum spans over a wide range,  $S_1, S_2, \dots, S_n$  are sensor transfer functions,  $y_1, y_2, \dots, y_n$  are their respective outputs and  $y_r$  is the fused signal. Frequency responses of sensor dynamics are shown in Fig. 40, where the idea of proposed sensor array is illustrated. It is noted that sensor bandwidth of  $\sum_{i=1}^n \omega_i$  can be achieved with low cost, low pass-band sensors, where  $\omega_i$  are bandwidths of sensors used in a sensor array shown in Fig. 40.

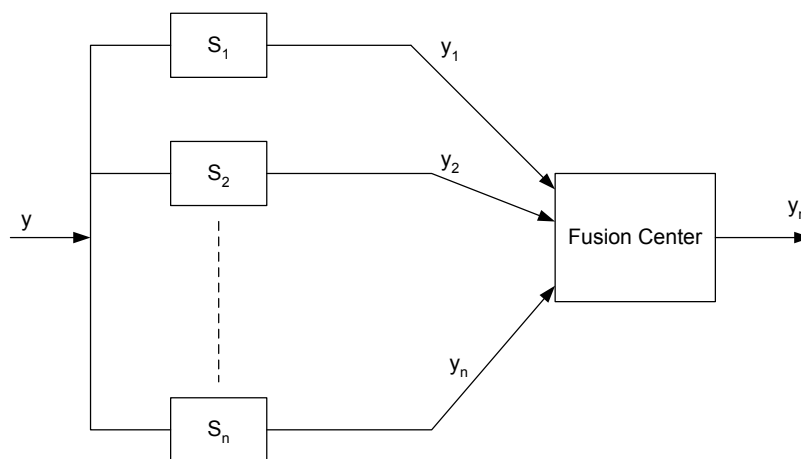


Figure 39: Sensor Array Configuration

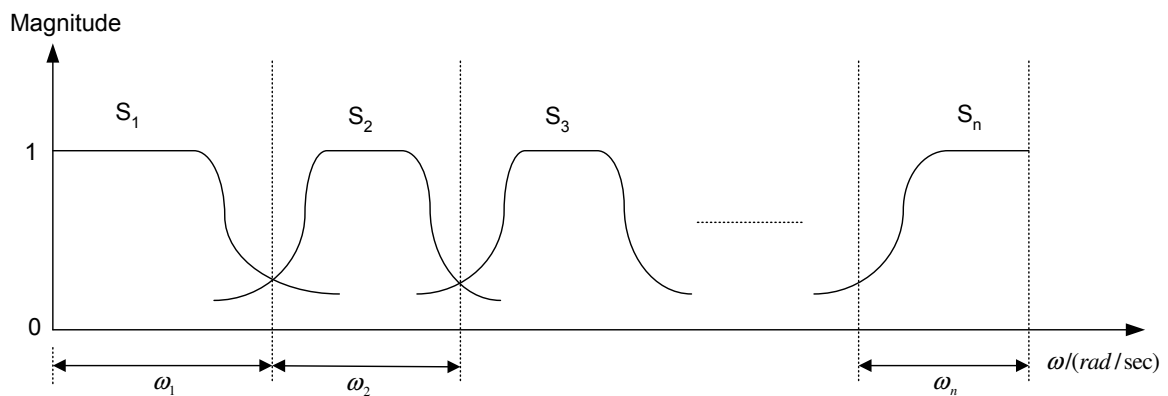


Figure 40: Sensor Array with Low Pass-band Sensors

A part of the frequency response shown in Fig. 40 is zoomed in and shown in Fig. 41. With a region where data from more than one sensor is available, it is evident that the implementation of the sensor array is not straightforward and an efficient sensor fusion scheme is necessary.

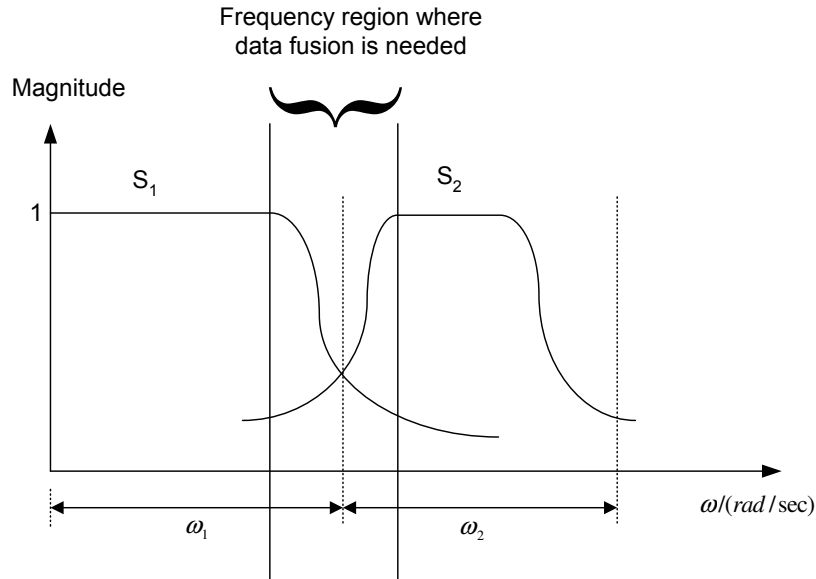


Figure 41: Sensor Array with Two Sensors

Ideally, the proposed scheme would work best with sensors whose frequency responses have sharp cutoffs as shown in Fig. 42. It is well known that these ideal sensors are not physically realizable and this would mean that the difficult task of data fusion is unavoidable. It is noted that sensor arrays whose frequency responses form another ideal sensor array as shown in Fig. 43 are not considered here. This would require that a large number of sensors be used in a sensor array, however, an effective trade off between performance and system complexity may not be made. Furthermore, uncertainties associated with sensors might place the sensory system in a vulnerable condition. We argue that good system performance can be achieved with

just enough sensors (optimum number of sensors if it is possible to obtain this number) and a suitable sensor fusion scheme. As will be discussed later, a sensor fusion scheme integrated in a sensory system improves system reliability and robustness.

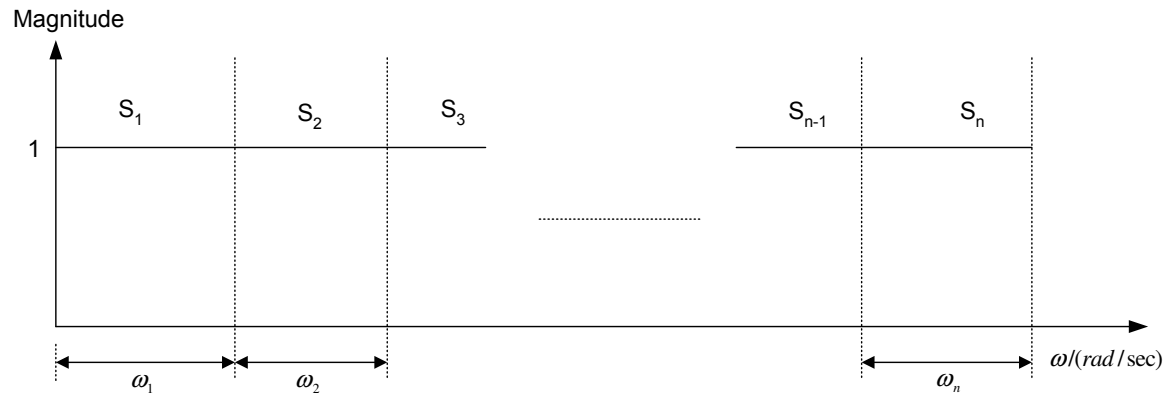


Figure 42: Ideal Sensor Array

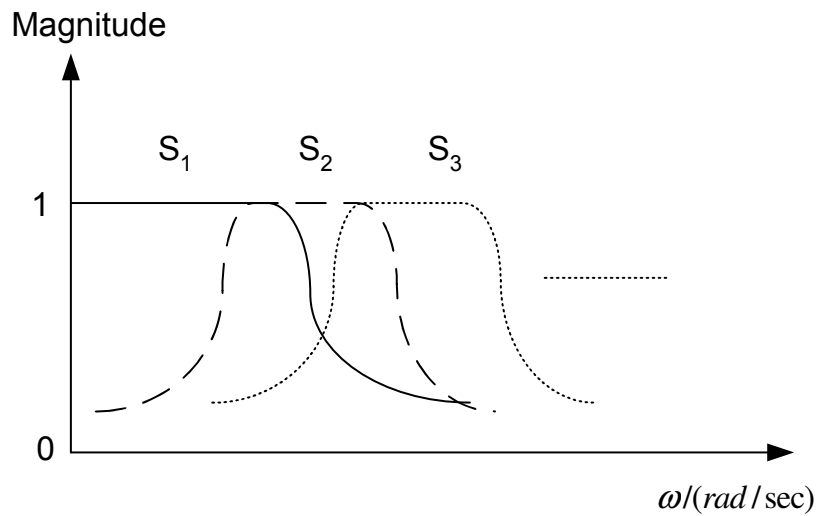


Figure 43: Another Ideal Sensor Array

### C. Multi-sensor Fusion in Sensor Arrays

As discussed in the previous sections, effective fusion of multi-sensor data is essential for the successful implementation of sensor arrays. Multi-sensor data fusion is the process of integrating information from different sensors. Several specific advantages obtained by using more than one source of data in seeking some typical conclusions are the following: improved system reliability and robustness, increased confidence, reduced ambiguity, shorter response time, improved resolution, extended coverage and in some cases, reduced cost of operation [30]. The fusion of redundant information can reduce overall uncertainty and thus serves to increase the accuracy of the process measurements. Complementary measurements from multiple sensors allow certain features of the environment to be perceived that may not be possible or feasible with a single sensor. As discussed earlier, the idea of sensor arrays evolved from the difficulty that a single sensor cannot accurately measure low as well as high frequency measurements.

A common data fusion approach is to take the weighted average of the various sensor data to arrive at a composite fused value. Kalman Filtering provides another fusion method, which generates the estimates of the required data. The estimates are optimal in a statistical sense. The Kalman Filtering technique is a linear systems technique that works well for reconstructing the environment, when the data is corrupted by measurement noise only. This approach is useful when the state vector can be identified and related to its previous values through a state transition matrix. Cluster analysis provides a powerful tool to classify multi-sensor data [82]. In the clustering methods, the distance between two clusters are optimized or adjusted to reach the final decision. The Bayesian inference fusion methods allow the multi-sources to be united according to the rules of probability theory [84]. The artificial

intelligence methods use *a priori* set of training data to establish an inference system and the applicable rules are identified by searching the complete set of rules [86, 31].

Even though the above techniques have been proven to conduct sensor fusion at different levels, there is still a need for a generic, efficient multi-sensor fusion tool. Taking weighted-average of the multi-source information may not always yield a reliable measurement, especially when one or more of the sensors are faulty. Kalman filtering cannot be used if the model of the process is not available. Furthermore, such an approach is very sensitive to outliers in the data; they can completely throw off the estimate of the system state vector [95]. The artificial intelligence methods require that an extensive training of the system be performed prior to the actual experiment.

Though sensors are, in general, used to measure signals that come from plants or processes, it would be advantageous to consider the sensor and the data fusion setup as an integrated system, which does not interact with the process/plant. Such a setup would allow the integrated sensory system to be used as a stand-alone process. When used in feedback control systems, this would simplify the controller design as no additional consideration for the feedback loop needs to be given. This fact is illustrated in Fig. 44. To facilitate the above implementation, we will consider the data fusion setup schematically shown in Fig. 45. In the above setup, the data fusion is done by suitable compensators  $P_1, P_2, \dots, P_n$ . The compensators  $P_1, P_2, \dots, P_n$  must be designed such that the magnitude and the phase of the frequency response of the integrated setup of sensors and compensators are 1 and 0 respectively and remain the same over the entire frequency range or the required bandwidth as shown in Fig. 46 .

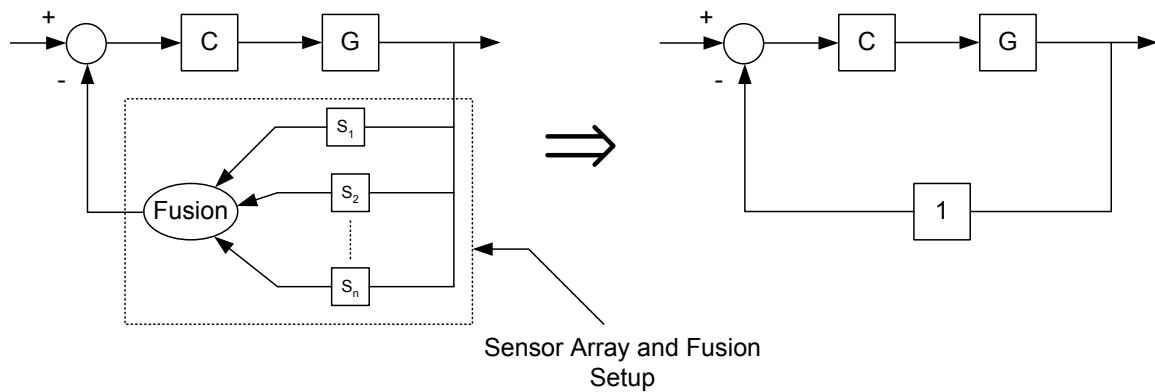


Figure 44: Sensor Array as a Stand-alone Process

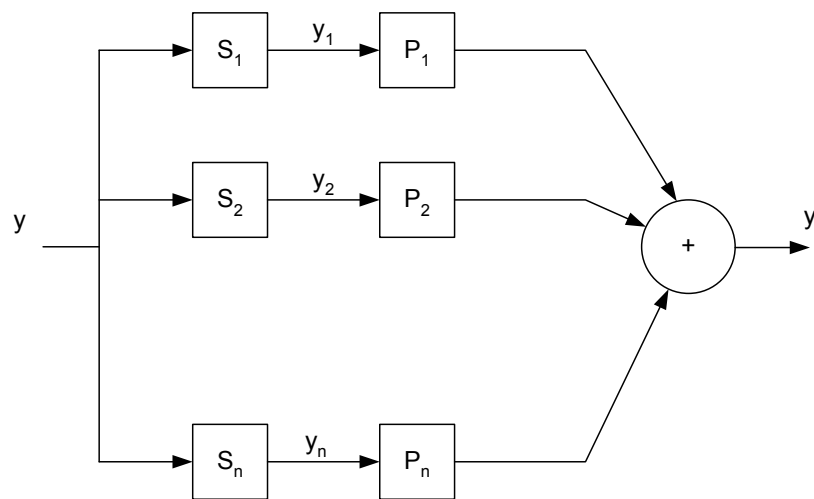


Figure 45: Multi-sensor Data Fusion Setup in Sensor Arrays

#### D. Design of Compensators by Frequency Domain Methods

We will now discuss how the compensators can be designed to meet the above requirements. As the objective is to shape the frequency response of the integrated system in Fig. 45, the design of compensators can be done using frequency response models of sensors only and the analytical models may not be needed. This assumption would

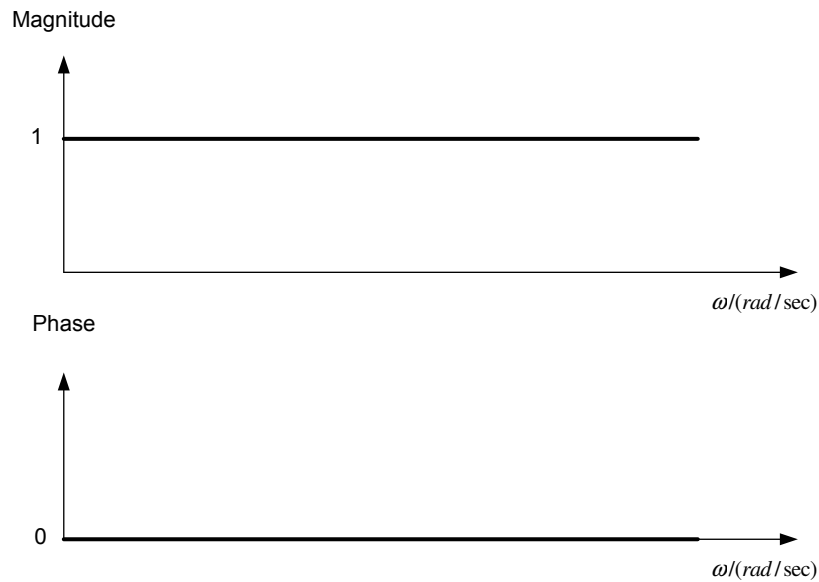


Figure 46: Ideal Frequency Response of the Sensors and Compensators Integrated Setup

remove the burden of tedious modelling processes. The approach may also yield a more accurate design than that may be possible with analytical models of sensors as modelling errors are inevitable due to certain assumptions and/or approximations that are needed in deriving such models.

Like any other control system design, uncertainty associated with sensor models must be taken into account in order to obtain a robust design. This is a critical issue with sensors as they are sensitive to environmental factors, for example, temperature. Therefore, compensators must cope with the sensor uncertainty to satisfy the goals expressed in terms of the frequency response shown in Fig. 46 of the integrated system.

Sensor uncertainties may not be truly characterized. However, it is reasonable to assume that they have some bounds. Multi-sensor fusion setup shown in Fig. 45

is modified to include sensor uncertainties and is shown in Fig. 47.

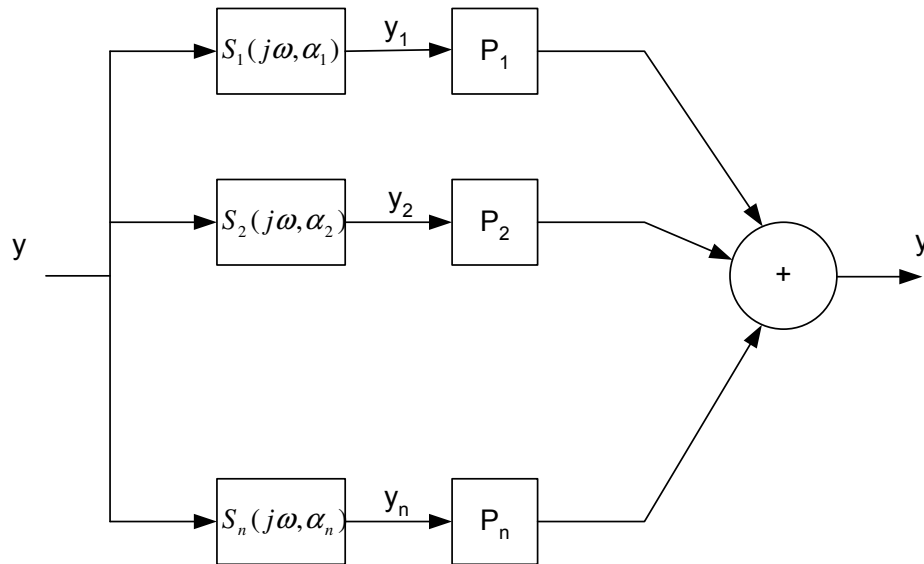


Figure 47: Multi-sensor Data Fusion Setup in Sensor Arrays with Uncertain Sensor Models

$S_1(j\omega, \alpha_1), S_2(j\omega, \alpha_2), \dots, S_n(j\omega, \alpha_n)$  are uncertain sensor models, where uncertainties are characterized by variables,  $\alpha_1, \alpha_2, \dots, \alpha_n$ .  $\omega$  is frequency in rad/sec. It is assumed that these variables vary within known bounds. The inclusion of sensor uncertainties into the design problem requires families of sensor functions, namely,  $\mathbb{S}_1, \mathbb{S}_2, \dots, \mathbb{S}_n$  be considered rather than single sensor functions.

$$\begin{aligned} \mathbb{S}_1 &= \{S_1(j\omega, \alpha_1)\} \forall \alpha_1 \\ \mathbb{S}_2 &= \{S_2(j\omega, \alpha_2)\} \forall \alpha_2 \\ &\vdots \\ \mathbb{S}_n &= \{S_n(j\omega, \alpha_n)\} \forall \alpha_n \end{aligned}$$

With uncertain sensor models, the ideal frequency response of Fig. 46 may not be



achieved by any robust design technique. To obtain a practically feasible design, the expected frequency response of the integrated system is modified as shown in Fig. 48.

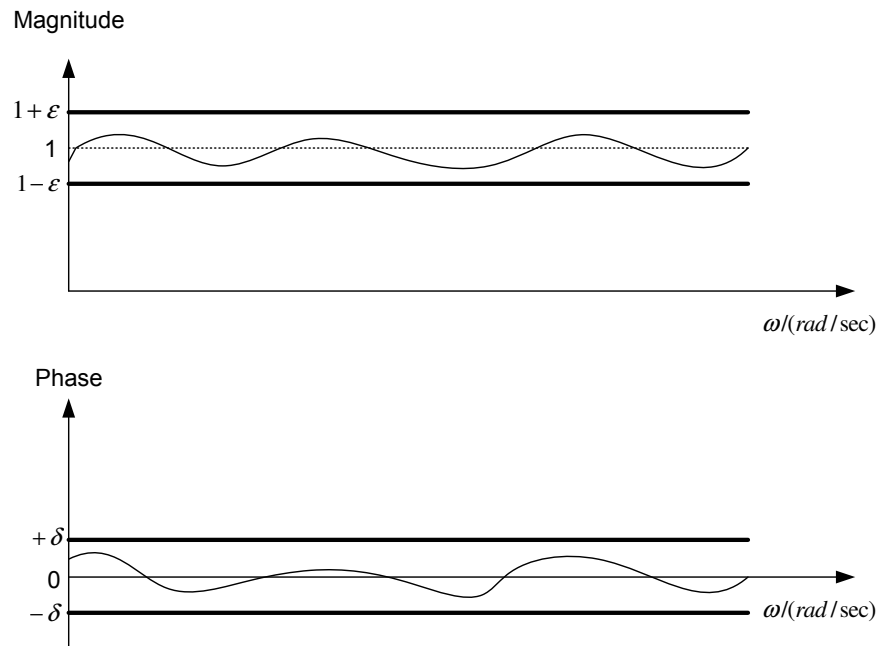


Figure 48: Expected Frequency Response of the Sensors and Compensators Integrated Setup

The robust design process involves obtaining compensators  $P_1, P_2, \dots, P_n$  to satisfy the following  $\forall \omega$ :

$$1 - \epsilon \leq |I(j\omega)| \leq 1 + \epsilon \quad (6.1)$$

$$-\delta \leq \angle I(j\omega) \leq +\delta \quad (6.2)$$

where

$$\begin{aligned}
 I(j\omega) &= \mathbb{S}_1(j\omega)P_1(j\omega) + \mathbb{S}_2(j\omega)P_2(j\omega) + \cdots + \mathbb{S}_n(j\omega)P_n(j\omega) \\
 &= \sum_{i=1}^n \mathbb{S}_i(j\omega)P_i(j\omega).
 \end{aligned} \tag{6.3}$$

$\omega$  – frequency in rad/sec.

$\epsilon$  – maximum allowable deviation of  $\|I(j\omega)\|$  from 1.

$\delta$  – maximum allowable deviation of  $\angle I(j\omega)$  from 0.

$S_i$  – Sensor assigned to cover frequency segment  $(\omega_i, \omega_{i+1})$ .

$\mathbb{S}_i$  – Family of Sensors  $\{S_i(j\omega, \alpha_i)\} \forall \alpha_i$

$P_i$  – Compensator associated with sensor  $S_i$ .

This is a feedforward control problem and techniques used in Quantitative Feedback Theory can be adopted to solve the robust design problem formulated above. The QFT loop-shaping is generally done in the Nichols Chart. As shown in Fig. 49, constraints (6.1) and (6.2) restrict the feasible region of  $I(j\omega)$  to a rectangle in the Nichols Chart. Using the QFT loopshaping techniques, compensators  $P_1, P_2, \dots, P_n$  can be designed so that  $I(j\omega)$  stays within this region for all frequencies within the required bandwidth.

#### E. Design of Compensators by Optimization

If there is no uncertainty associated with sensors, then compensators can also be designed using optimization based approaches. One way to obtain compensators by optimization is to minimize the error function,  $e = 1 - I(j\omega)$  as formulated in

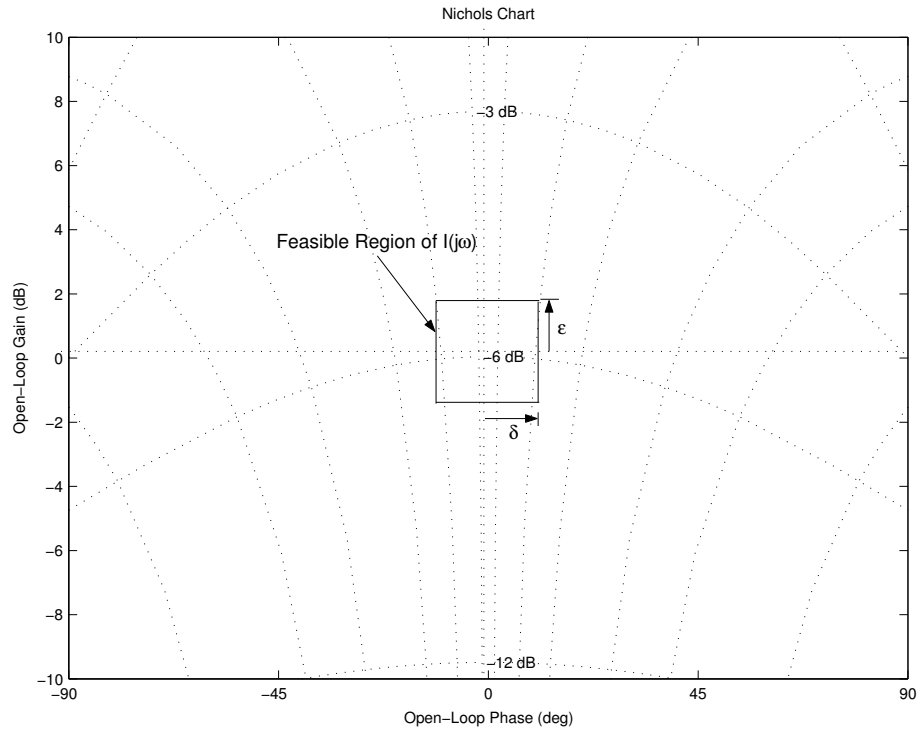


Figure 49: Feasible Region of  $I(j\omega)$  in Nichols Chart

Equation (6.4).

$$\min_{P_1(j\omega), P_2(j\omega), \dots, P_n(j\omega)} J = \left\| 1 - \sum_{i=1}^n S_i(j\omega) P_i(j\omega) \right\| \quad (6.4)$$

As the optimization problem is unconstrained, the optimal cost function value should be zero. Therefore, compensators generated by minimizing the objective function,  $J$ , will satisfy conditions (6.1) and (6.2). However, the optimal design may not address some important practical concerns. Referring to Fig. 50, in frequency region  $R_1$ , the measurement obtained by sensor,  $S_1$  is more reliable than any other measurement available. Similarly, in frequency region,  $R_3$ , sensor,  $S_2$  is expected to have the most reliable data. Any design that chooses data from a sensor other than the specialized one should not be considered good and if this happens, the whole idea

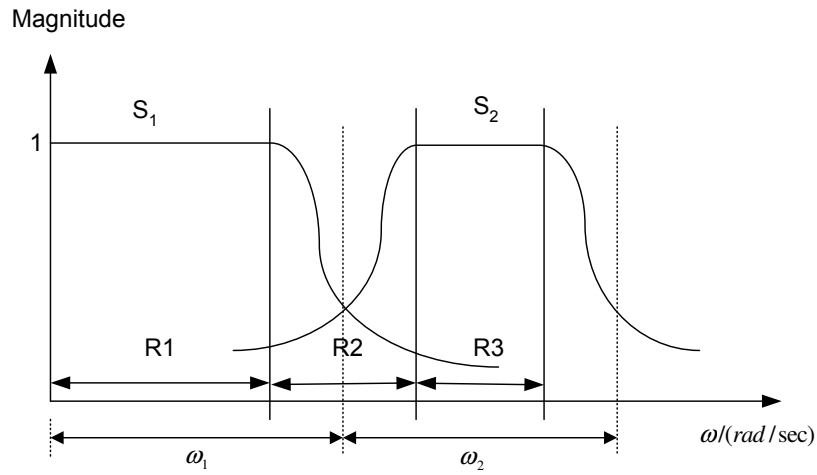


Figure 50: Identifying Different Confidence Regions in a Sensor Array

of the proposed sensor array would be lost. One way to prevent this from happening is to add more constraints to the optimization problem.

Referring to Fig. 51, such constraints may be formulated as:

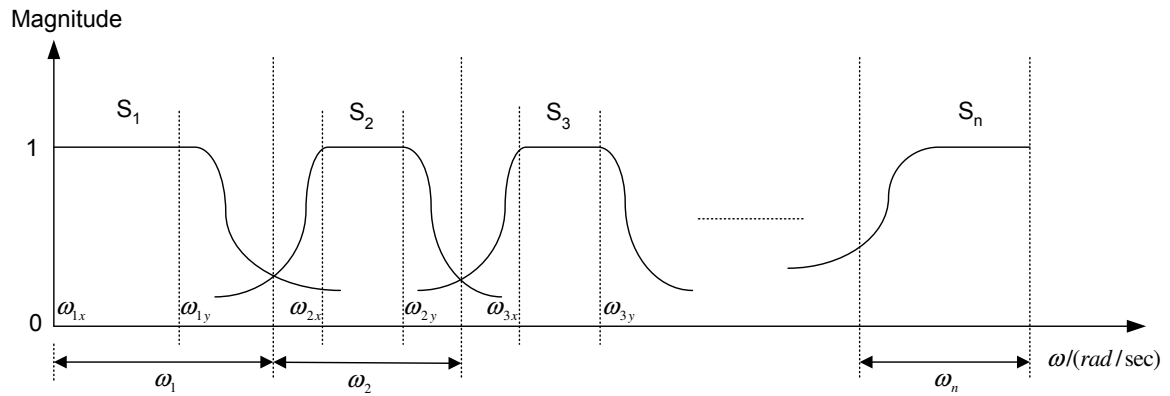


Figure 51: Sensor Array with Different Confidence Regions

$$\text{Constraint Set 1}$$

$$\text{If } \omega_{ix} \leq \omega \leq \omega_{iy} \implies P_k(j\omega) = \begin{cases} P_i(j\omega) & \text{when } k=i \\ 0 & \text{otherwise.} \end{cases} \quad \forall i, k = 1, 2, \dots, n$$

or

Constraint Set 2

$$\text{If } |S_i(j\omega)| > |S_k(j\omega)| \implies |P_i(j\omega)| > |P_k(j\omega)| \quad \forall k \neq i \quad \forall i = 1, 2, \dots, n$$

Constraint Set 1 may generate compensators with discontinuous frequency responses. If continuous compensator responses are preferred, Constraint Set 2 may be chosen. It is noted that phase angle condition (6.2) will automatically be satisfied if only magnitude response data is used in the optimization process and optimal value of  $I(j\omega)$  is 1.

The optimization problem proposed above is not very difficult and it can be easily shown that a unique solution always exists. In fact, this problem can also be solved by a rule-based solution technique. A close look at the problem will reveal that the optimizer is employed to do two tasks at any given frequency: 1) choose the sensor whose data is more reliable, 2) shape the frequency response so that the magnitude of the compensator plus sensor setup is unity. Though many techniques can be utilized to do these two tasks, the main advantage of the optimization framework is that specifications can be easily translated into objectives and constraints.

#### F. Implementation of Sensors Array by Feedback Mechanisms

In the previous sections, two methods are developed to implement an array of several low bandwidth pass-band sensors. Sensor models are assumed to be known in both cases. However, in practice, obtaining sensor models may not be easy and may be

an additional burden to an already challenging and tedious problem. To address this issue, a novel multi-sensor data fusion approach that does not require the sensor models is presented in this section. The cut-off frequencies of the pass-band sensors must be known to make use of this approach.

To explain how this method works, a sensor array with three pass-band sensors is considered and is shown in Fig. 52.

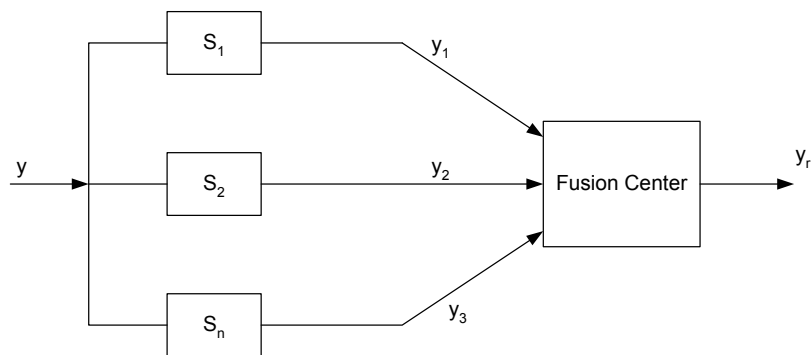


Figure 52: Sensor Arrays

The frequency responses of sensors  $S_1$ ,  $S_2$  and  $S_3$  used in the setup (Fig. 52) are shown in Fig. 53. It will be shown that only the cut-off frequency information is necessary to implement this sensor array.

It is proposed that the fusion of multi-sensor data of sensors  $S_1$ ,  $S_2$  and  $S_3$  can be effectively done by a two-stage process depicted in Fig. 54. The methods described in the previous two sections shape the frequency responses of the sensor functions by means of compensators in order to get a flat frequency response over the working range. In this method, we manipulate the multi-sensor data and combine them smoothly by means of low and high filters whose cut off frequencies are chosen to be consistent with the frequency responses of sensors. For example, the cut off frequency of the low pass filter,  $F_1$  must be the same as that of sensor  $S_1$ . Similarly,

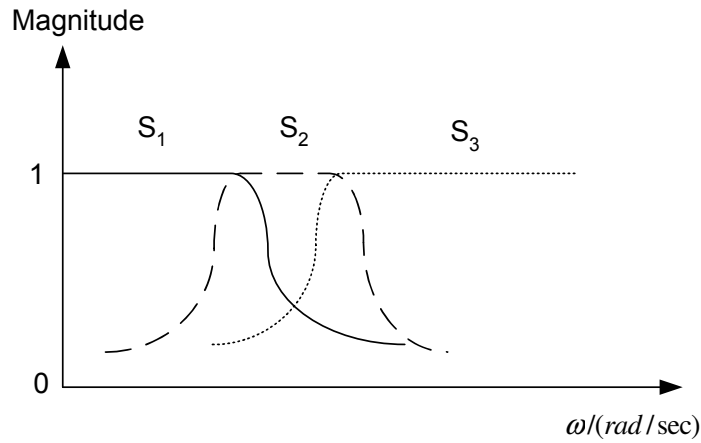


Figure 53: Frequency Responses of Sensors

the cut off frequencies of the high pass filter  $F_h$  and sensor  $S_3$  should match.

The output of the closed loop control system of stage 1  $y_{2c}$  is related to the inputs that are the output of sensor  $S_1$ ,  $y_1$  and the output of sensor  $S_2$ ,  $y_2$  by the following equation:

$$\begin{aligned} y_{2c} &= \frac{F_l C_l}{1 + F_l C_l} y_1 + \frac{1}{1 + F_l C_l} y_2 \\ &= T_l y_1 + S_l y_2 \end{aligned} \quad (6.5)$$

where  $S_l$  is the Sensitivity Function and  $T_l$  is the Complementary Sensitivity Function of the closed loop control system of Stage 1.

The purpose of using the low pass filter  $F_l$  is to attenuate the frequency data that lie above the cut off frequency of sensor  $S_1$ . The low pass filter must be chosen so that its frequency response cuts off as sharply as possible to improve its high frequency amplitude attenuation capability. The controller  $C_l$  is employed to ensure the closed loop stability and consequently the smooth fusion of sensor data  $y_1$  and  $y_2$ .

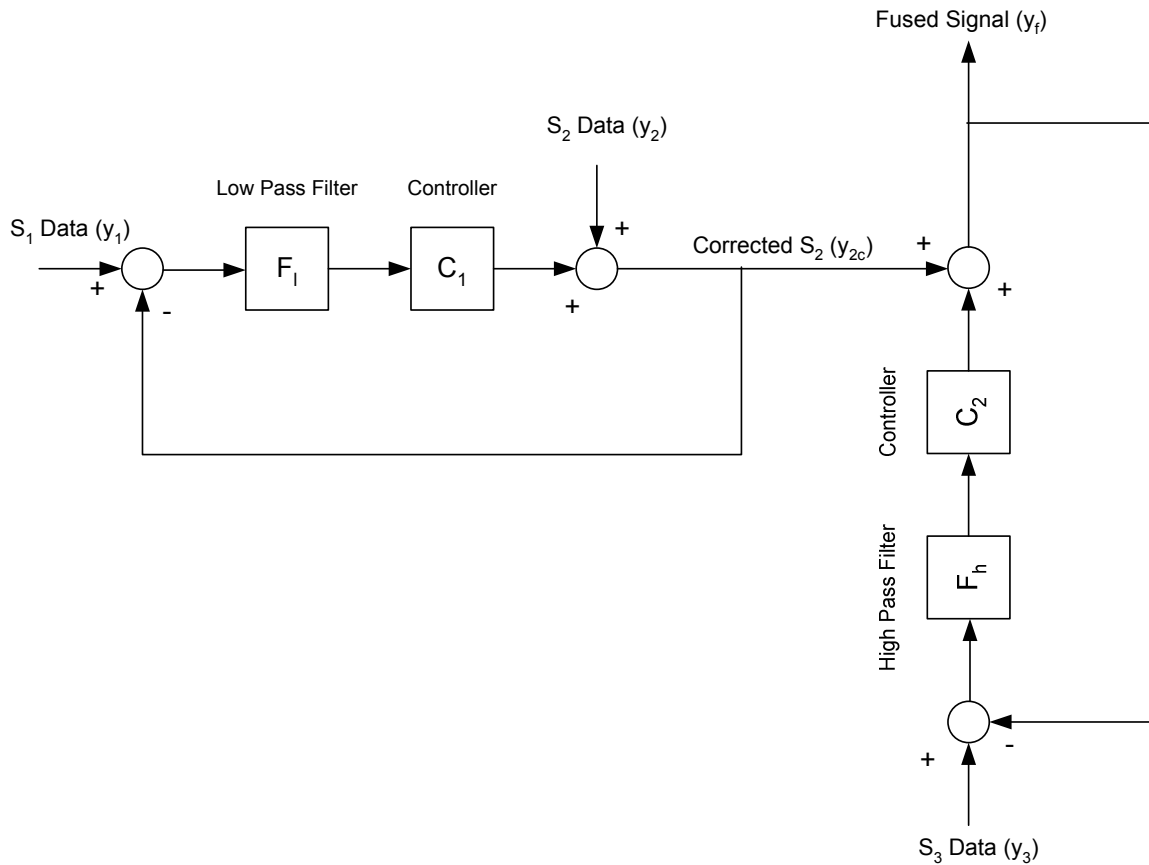


Figure 54: Multi-sensor Data Fusion by Feedback Mechanisms

The specifications that the closed loop control system of stage 1 should satisfy in order to guarantee a smooth fusion can be translated in terms of low pass function  $F_l$  and the controller  $C_l$  as follows. Referring to Equation (6.5), the controller  $C_l$  and the low pass filter must be chosen such that:

1. The frequency response of the sensitivity function  $S_l \left( \frac{1}{1+F_l C_l} \right)$  is equal to one within the band of sensor  $S_2$  and as small as possible within the band of sensor  $S_1$  (This condition will automatically satisfy the requirements on complementary sensitivity function  $T_l$  as  $S_l + T_l = 1$ , *i.e.* the frequency response of  $T_l$  is equal to one within the band of sensor  $S_1$  as small as possible beyond the cut off



frequency of sensor  $S_1$ ).

2. The closed control system is stable.
3. The cut off frequency of the low pass filter should be equal to that of sensor  $S_1$ .
4. The frequency response of the low pass filter  $F_1$  should cut off as sharply as possible.

When the above specifications are closely met, the output of stage 1  $y_{2c}$  will contain the fused information of data  $y_1$  and  $y_2$ . Stage 2 of this process will undergo similar actions. The feedback control system of stage 2 has two inputs that are the fused signal from stage 1  $y_{2c}$  and the data from sensor  $S_3$ . The output of stage 2 control system  $y_f$  is the final outcome of this process and contain the data from all three sensors. The following equation relates the output with the inputs:

$$\begin{aligned} y_f &= \frac{F_h C_h}{1 + F_h C_h} y_3 + \frac{1}{1 + F_h C_h} y_{2c} \\ &= T_h y_3 + S_h y_{2c} \end{aligned} \quad (6.6)$$

where  $S_h$  and  $T_h$  are the Sensitivity and Complementary Sensitivity Functions of the closed loop control system of Stage 2 respectively.

The filter  $F_h$  and the controller  $C_h$  are designed in a similar fashion as was done in Stage 1. In summary, the specifications on  $F_h$  and  $C_h$  are:

1. The frequency response of the sensitivity function  $S_h \left( \frac{1}{1 + F_h C_h} \right)$  is equal to one below the cut off frequency of sensor  $S_3$  and as small as possible elsewhere (This condition will automatically satisfy the requirements on complementary sensitivity function, *i.e.* the frequency response of  $T_h$  is equal to one within the band of sensor  $S_3$  as small as possible below the cut off frequency of sensor  $S_3$ ).
2. The closed control system is stable.

3. The cut off frequency of the high pass filter should be equal to that of sensor  $S_3$ .
4. The frequency response of the high pass filter  $F_h$  should cut off as sharply as possible.

Simulation results are presented in chapter VII to validate this method. The above approach can be easily extended to a general problem that consists of  $n$  stages. The only difference is that one has to use to band-pass filters (where ever appropriate) in place of low and high filters. The underlying assumption behind this approach is that sensor measurements are accurate within their respective frequency bands. Excluding the possibility of the sensors being faulty, this assumption may be reasonable in real situations. This is because the corruption by sensor noise and other factors is generally a major problem whenever the amplification due to sensor is insufficient, which is inevitable outside the working band of a sensor. Within the band of a sensor, signal amplification may be guaranteed and it is possible to maintain a reasonably high signal-to-noise noise, which enables the designer to apply some commonly used techniques to remove sensor noise.

## CHAPTER VII

### RESULTS AND ANALYSIS

In this chapter, experimental and simulation results are presented to further explain the methods developed in this dissertation. The results are analyzed to validate the claims.

#### A. Signal Conditioning

This section is devoted to the analysis of the signal conditioning schemes developed in chapter IV.

##### 1. Nonlinear Filtering Example: A Computer Simulation

To demonstrate the validity and performance of Algorithm 2, a simulation example is presented in this section. Consider a sensor that has the nonlinear input-output characteristic depicted in Fig. 55.

This sensor characteristic is chosen because it satisfies the necessary and sufficient conditions of Theorem 5. It can be easily shown that any signal that is measured through this sensor will get distorted. Consider an input signal shown in Fig. 56 and its distorted version is shown Fig. 57. The high harmonics of the distorted signal are filtered out using an ideal low pass filter whose cutoff frequency is the bandwidth of the input signal. The filtered signal is depicted in Fig. 58. The procedure given in Algorithm 2 is then used to recover the original signal using the filtered signal. Fig. 59 shows the recovered signal, which is exactly the same as the original signal. This implementation scheme is illustrated in Fig. 60.

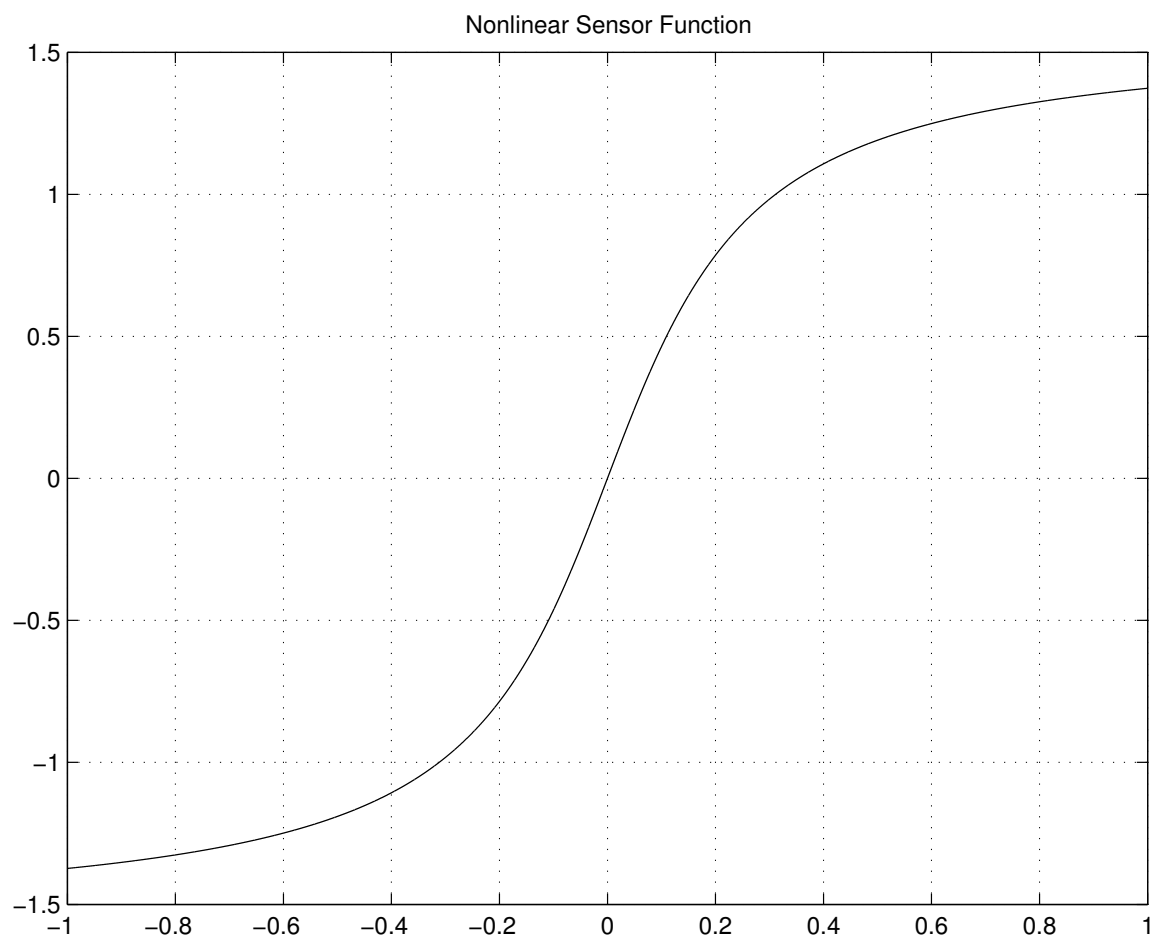


Figure 55: Sensor Function

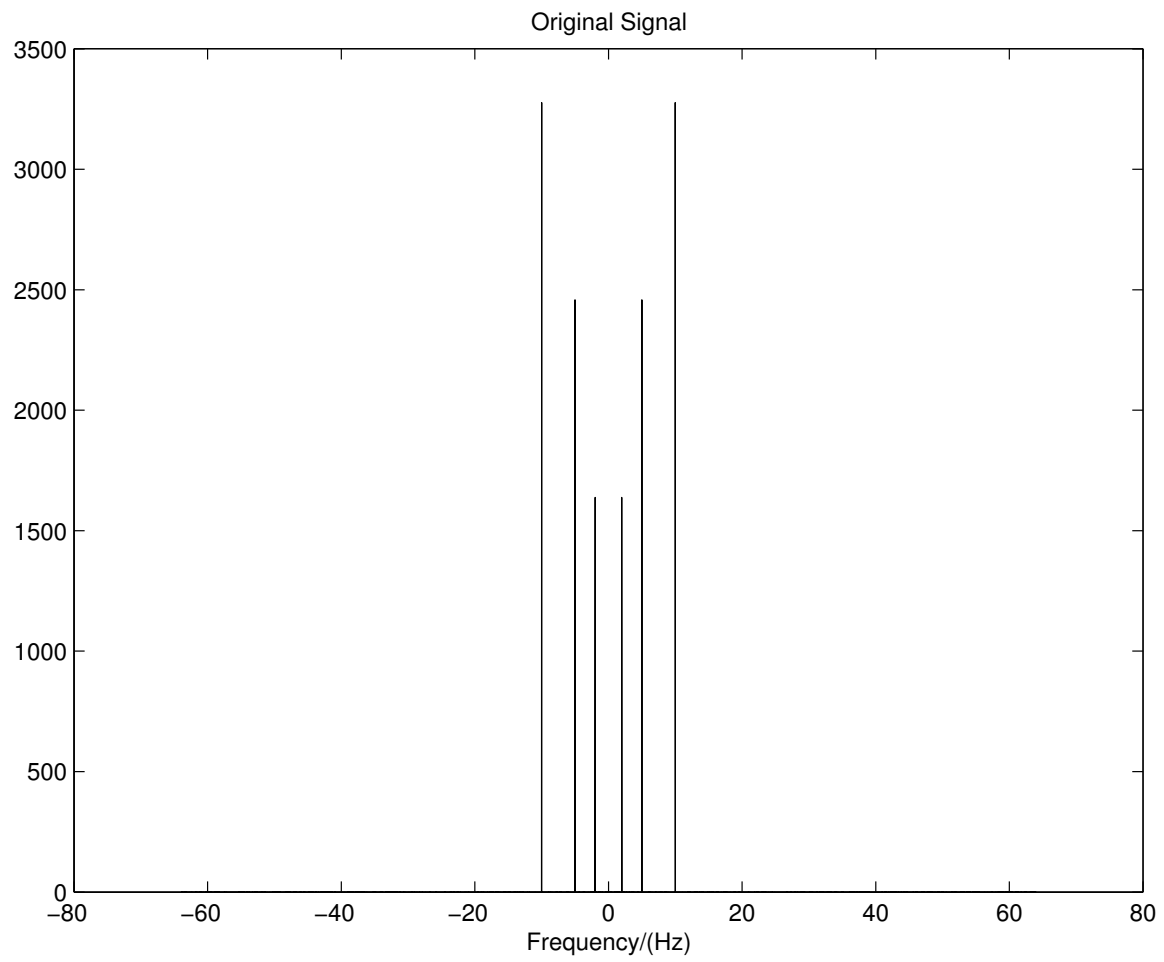


Figure 56: Original Signal Used for Computer Simulation

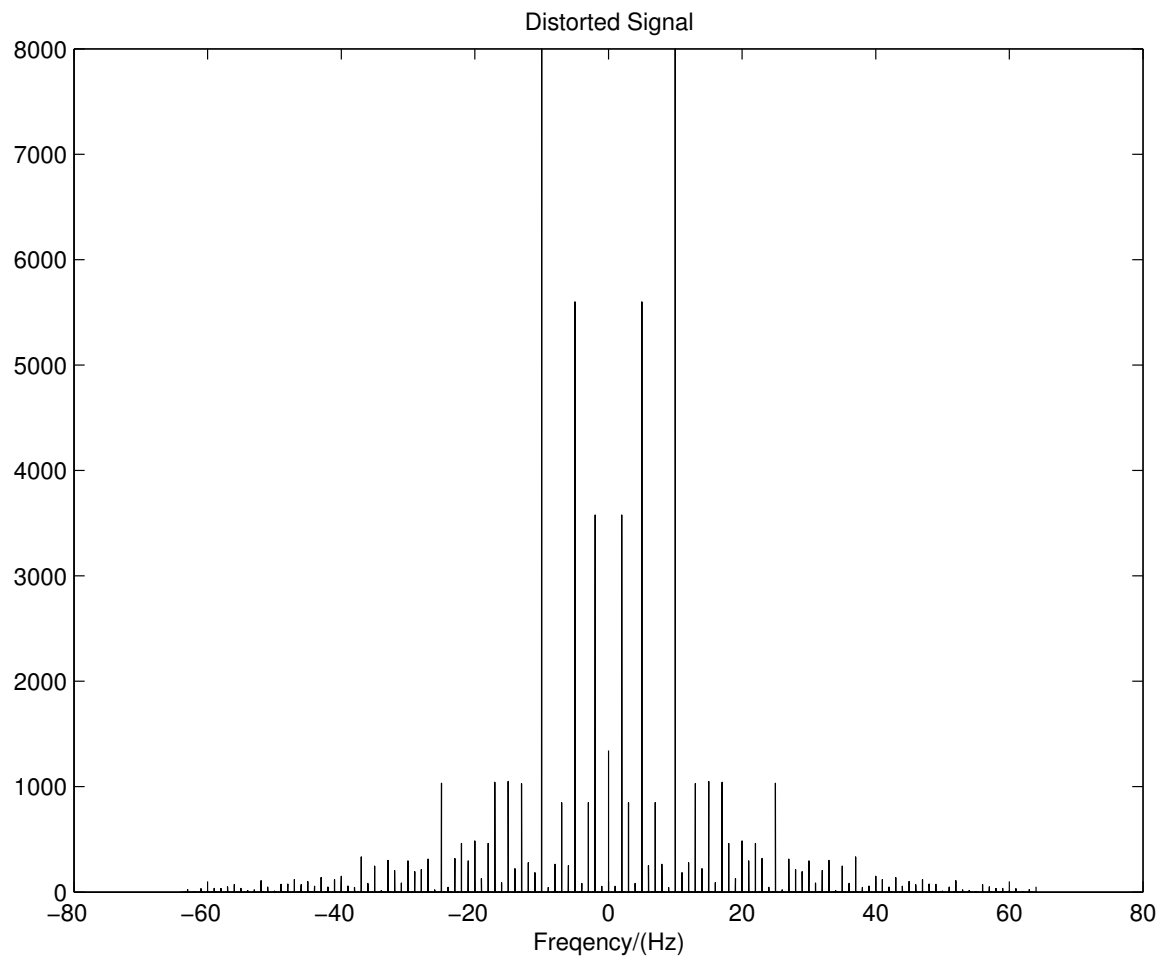


Figure 57: Distorted Version of Signal Shown in Fig. 56

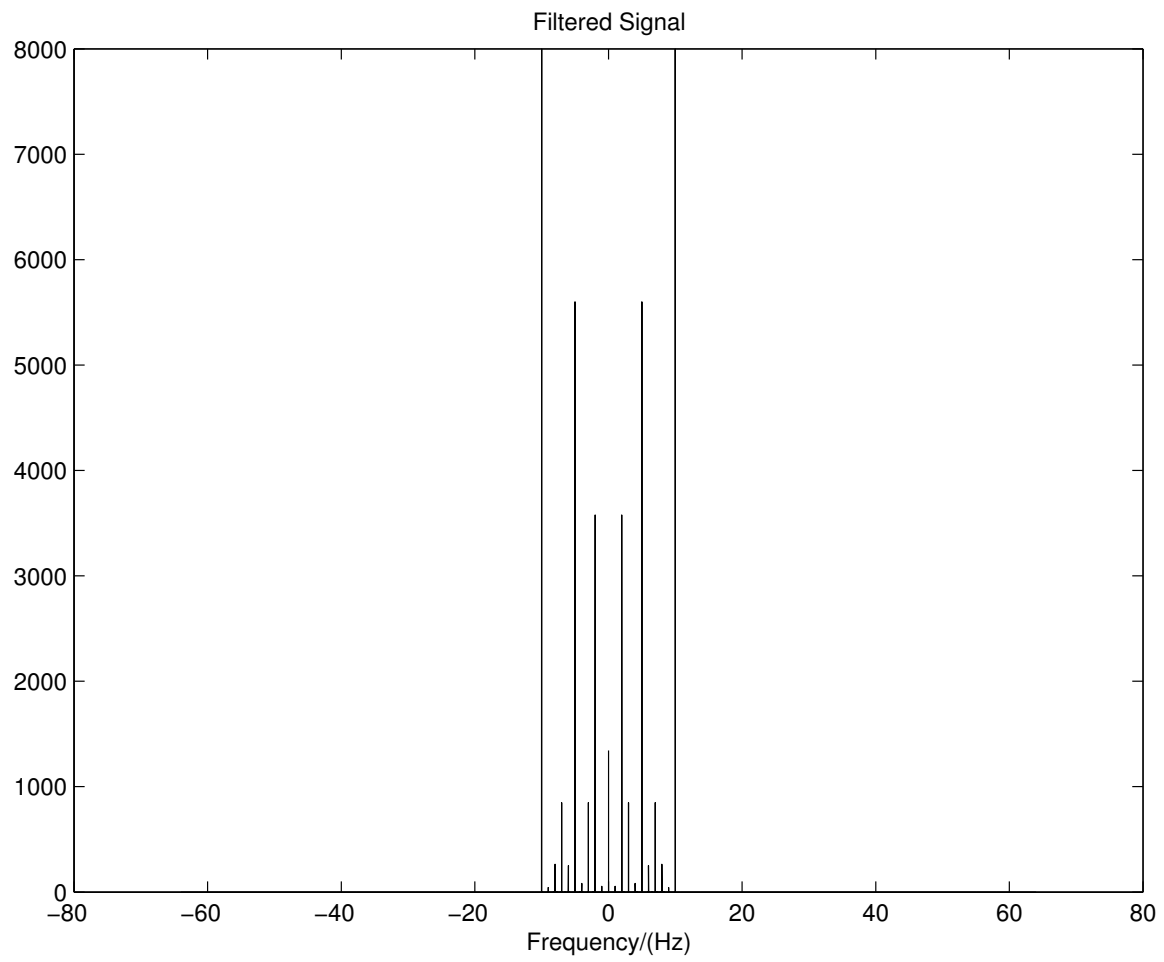


Figure 58: Filtered Signal Obtained Using the Ideal Low Pass Filter

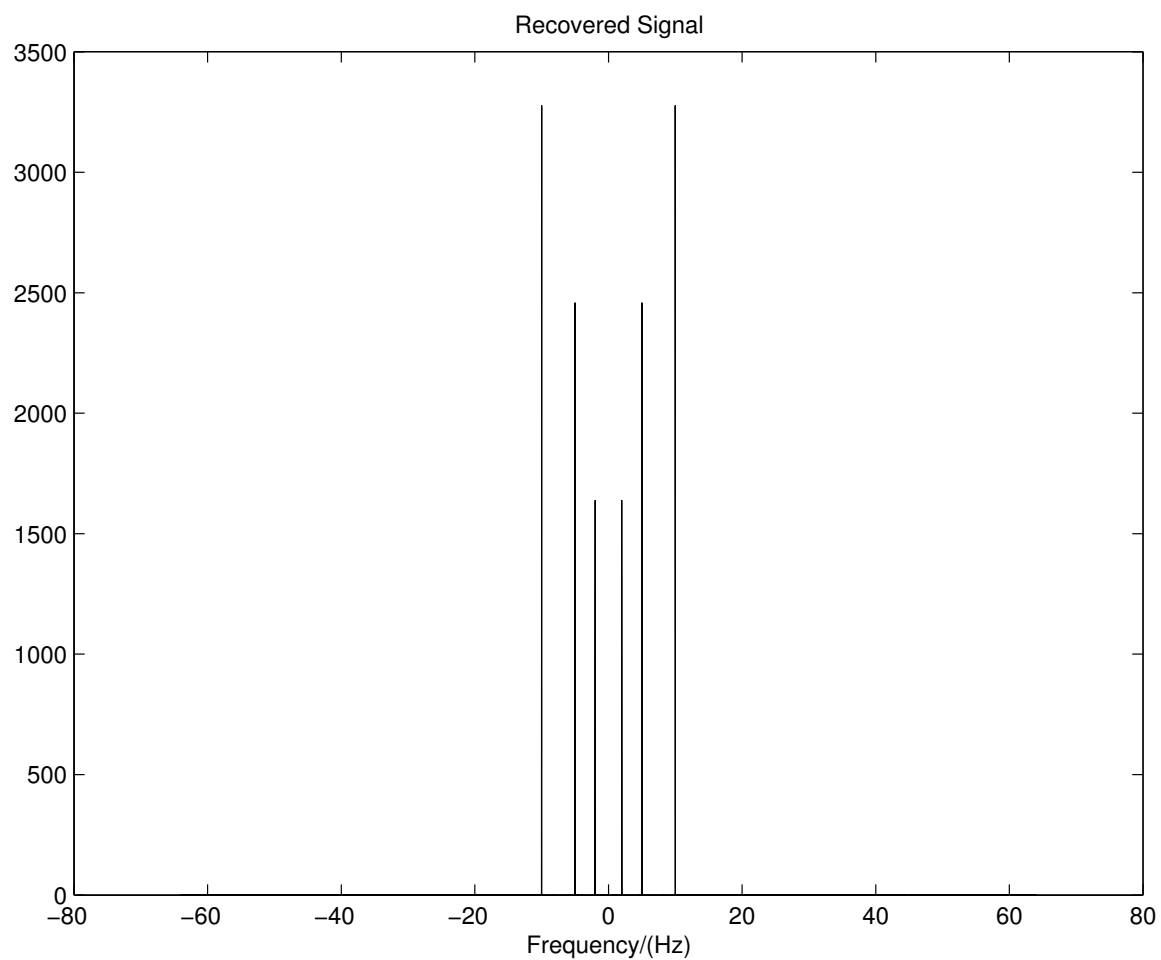


Figure 59: Frequency Spectrum of Recovered Signal

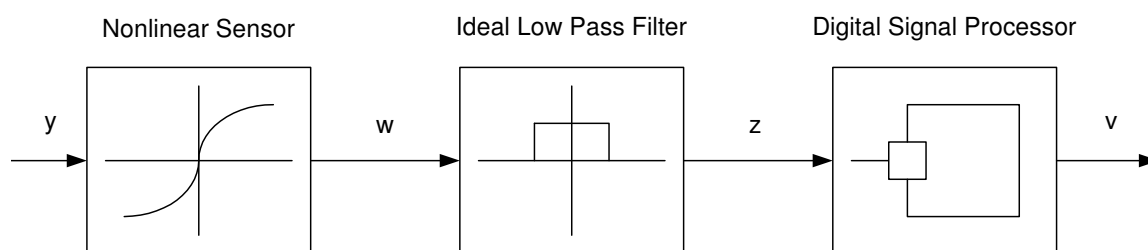


Figure 60: Implementing Signal Recovery Scheme



## 2. Experimental Demonstration of Performance of the Nonlinear Filtering Algorithm

In order to demonstrate how signal recovery algorithm described in Algorithm 2 could be used in practice, a nonlinear physical sensor shown in Fig. 61 is considered.  $V_{in}$  and  $V_{out}$  are the input and the output of the system respectively. As the actual model of this system is not available it is necessary to employ a model identification technique. It is noted that the incorporation of such an identification scheme extends the scope of the signal recovery procedure developed in this section. Among various model identification procedures found in the literature, the fuzzy clustering technique, which is proposed in [125] and applied to identify models in [126] is chosen because of its simplicity and practicality. The fuzzy rule based model is first derived using a known input signal and the corresponding output. The signal-processing scheme is then developed based on this model. The signal data is acquired using dSPACE Acquisition Real Time System. This process is illustrated in Fig. 62 and Fig. 63.

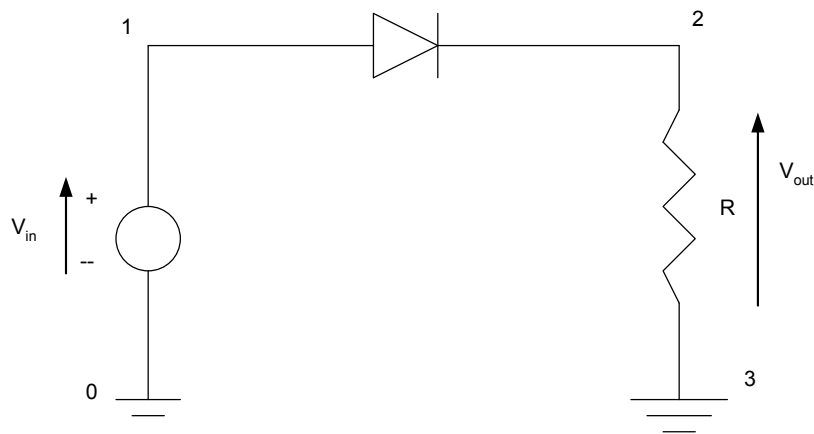


Figure 61: Nonlinear Diode Circuit

Having derived the model, an input signal shown in Fig. 64 is distorted by the

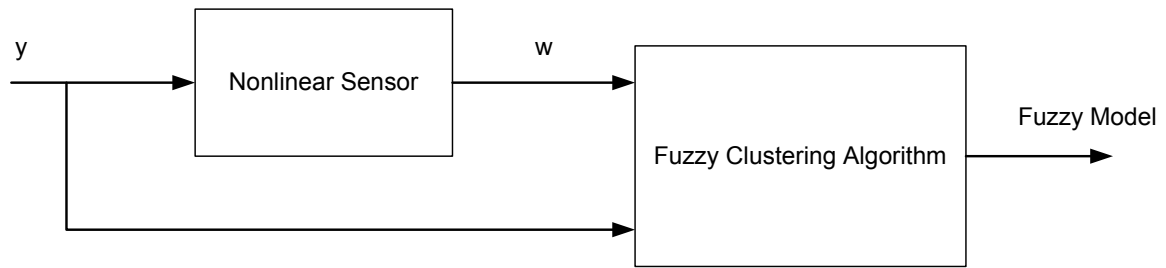


Figure 62: Model Identification Scheme

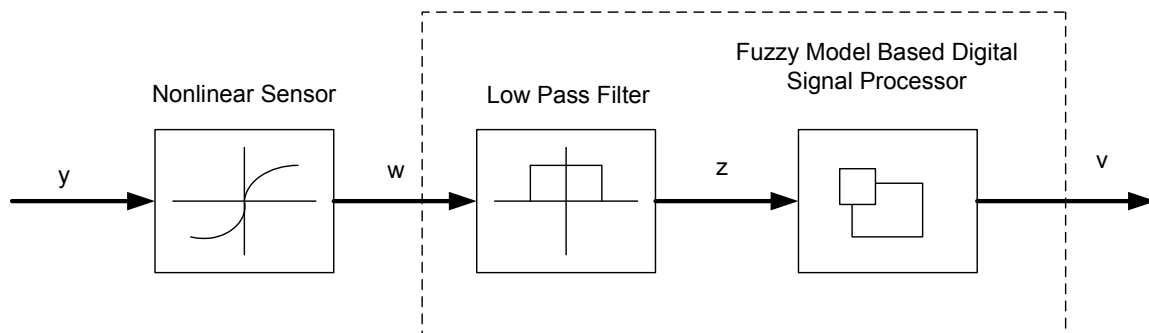


Figure 63: Signal Recovery Implementation Scheme Based on Fuzzy Model

nonlinear circuit and the distorted signal is then passed through the low pass filter. The distorted signal is shown in Fig. 65. The signal processing scheme developed in Algorithm 2 is applied to the filtered signal. The recovered signal and the error signal (difference between the recovered and the input signals) are shown in Fig. 66.

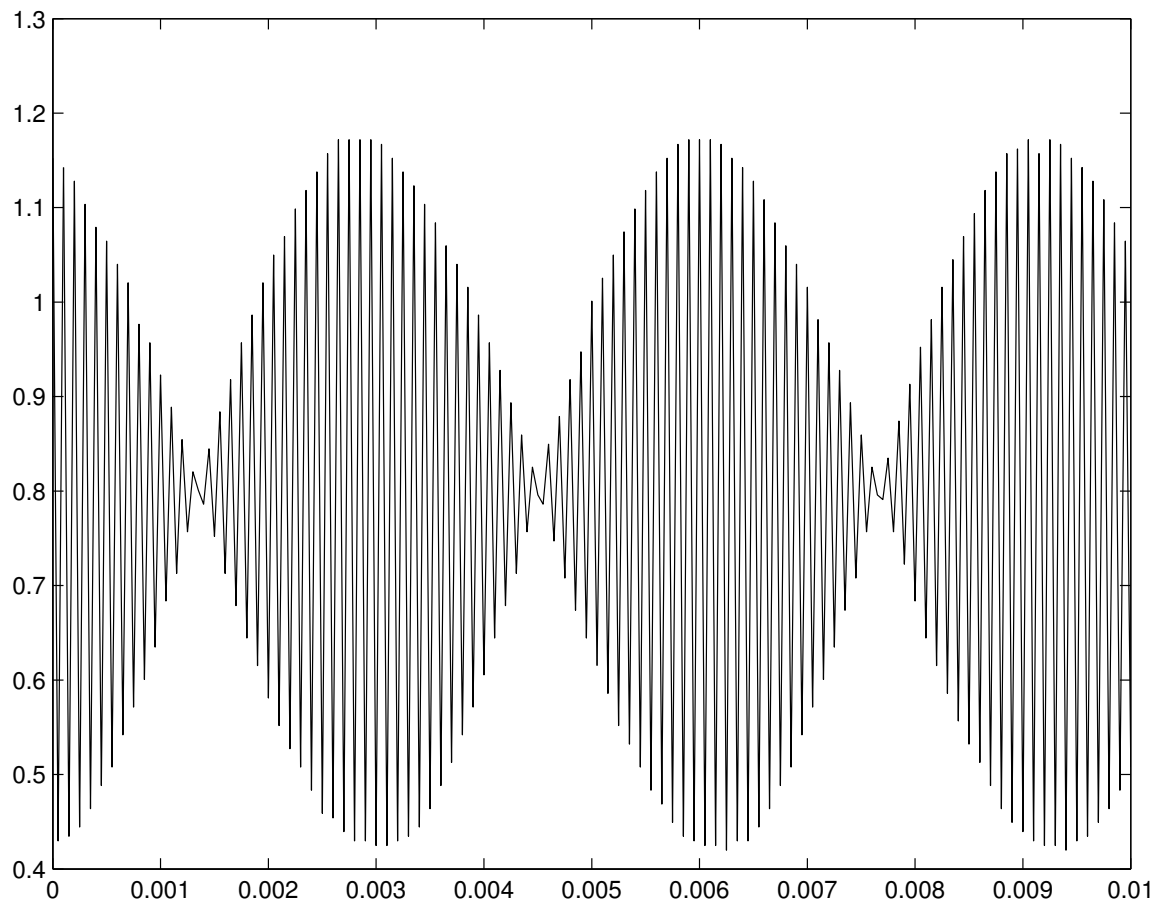


Figure 64: Input Voltage,  $v_{in}$

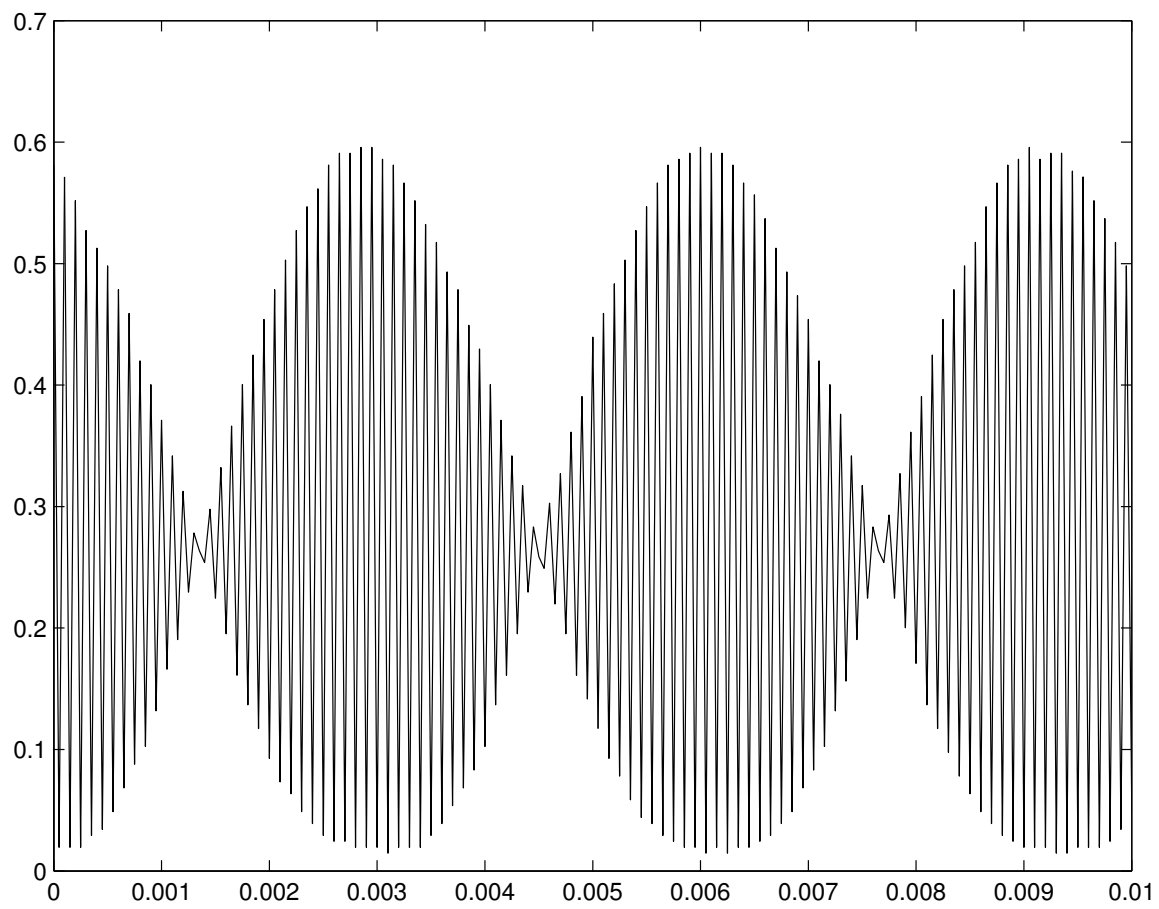


Figure 65: Distorted Voltage Output,  $v_{out}$

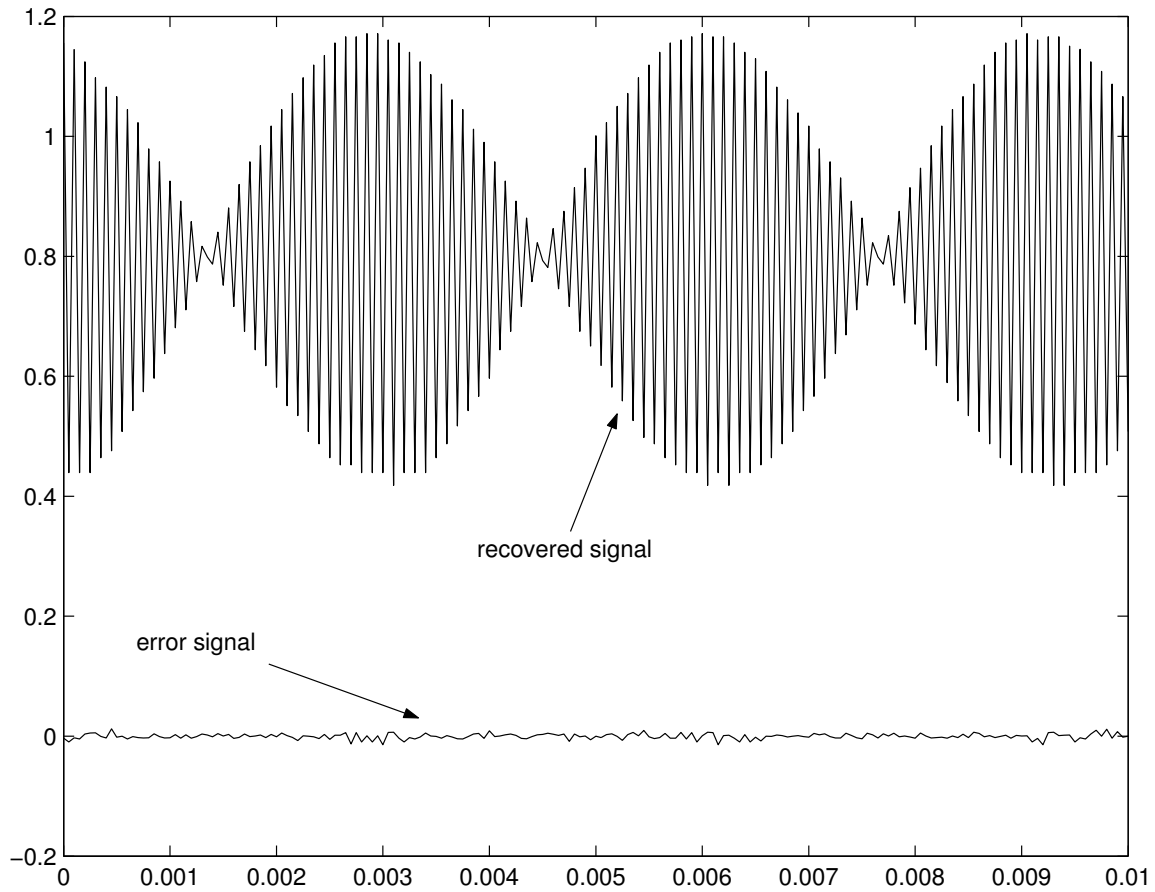


Figure 66: Recovered Signal and Error Values

### 3. Nonlinear Filtering Algorithm as a Distortion Compensation Technique

In [19], Frank uses a digital post processing technique to compensate the distortions caused by nonlinear sensors. Analyzed in the section is a nonlinear acceleration sensor, whose nonlinearity is described by the equation,  $y = 10^{-6} \tan^{-1}\left(\frac{a}{40}\right)$ , where  $a$  is the acceleration and  $y$  is the displacement. This nonlinear characteristic is depicted in Fig. 67.

Let us now show how the algorithm developed in this dissertation could be used to compensate the distortion caused by this nonlinear sensor. Suppose that a ban-

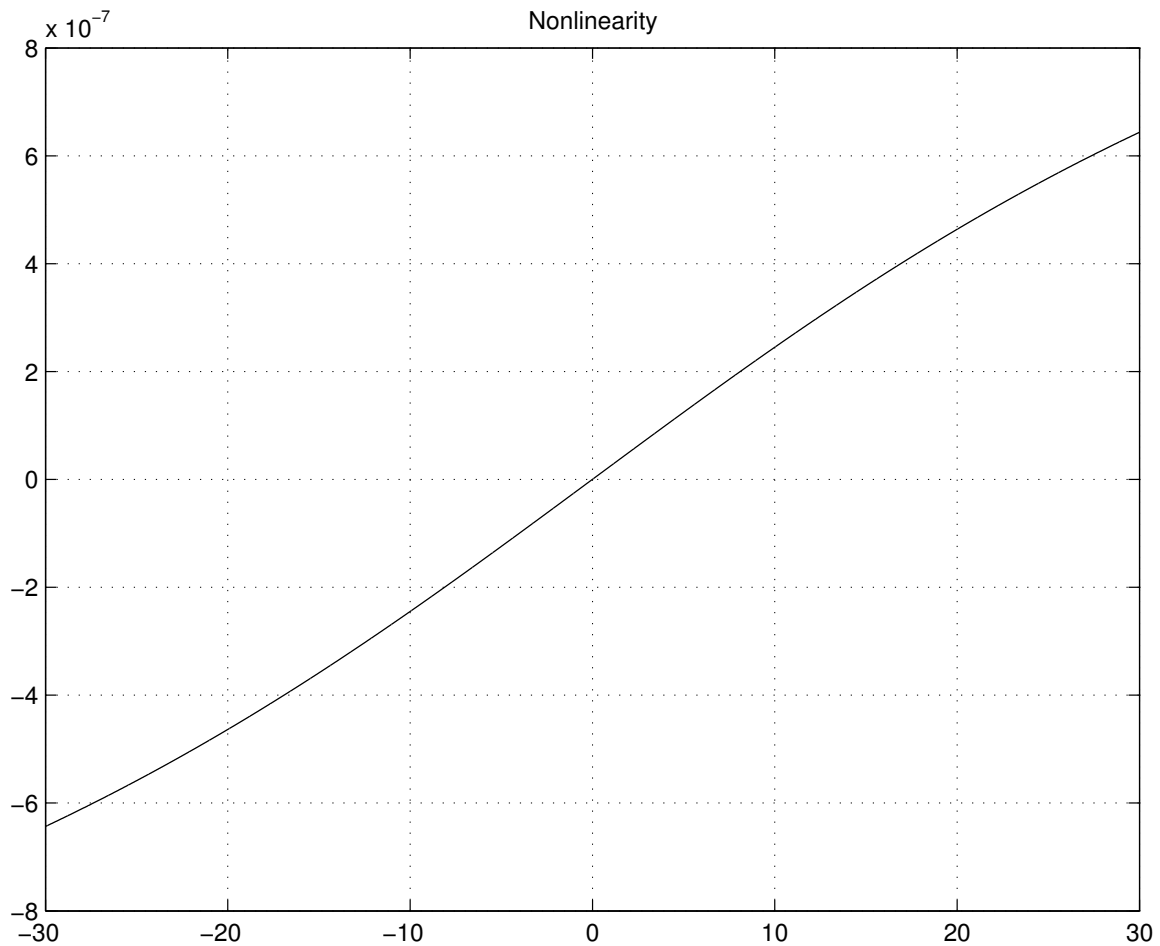


Figure 67: Nonlinear Sensor Used by Frank

limited input signal shown in Fig. 68 is deliberately distorted by this nonlinearity and the distorted signal is shown in Fig. 69. As the model of the sensor is available, Algorithm 2 is used to see whether the distortions could be compensated. As was done earlier, high harmonics of the distorted signal are filtered out by an ideal low pass filter and the procedure given in Algorithm 2 is used to recover the original signal or compensate the distorted signal.

As the nonlinear characteristic depicted in Fig. 67 satisfies all the conditions of

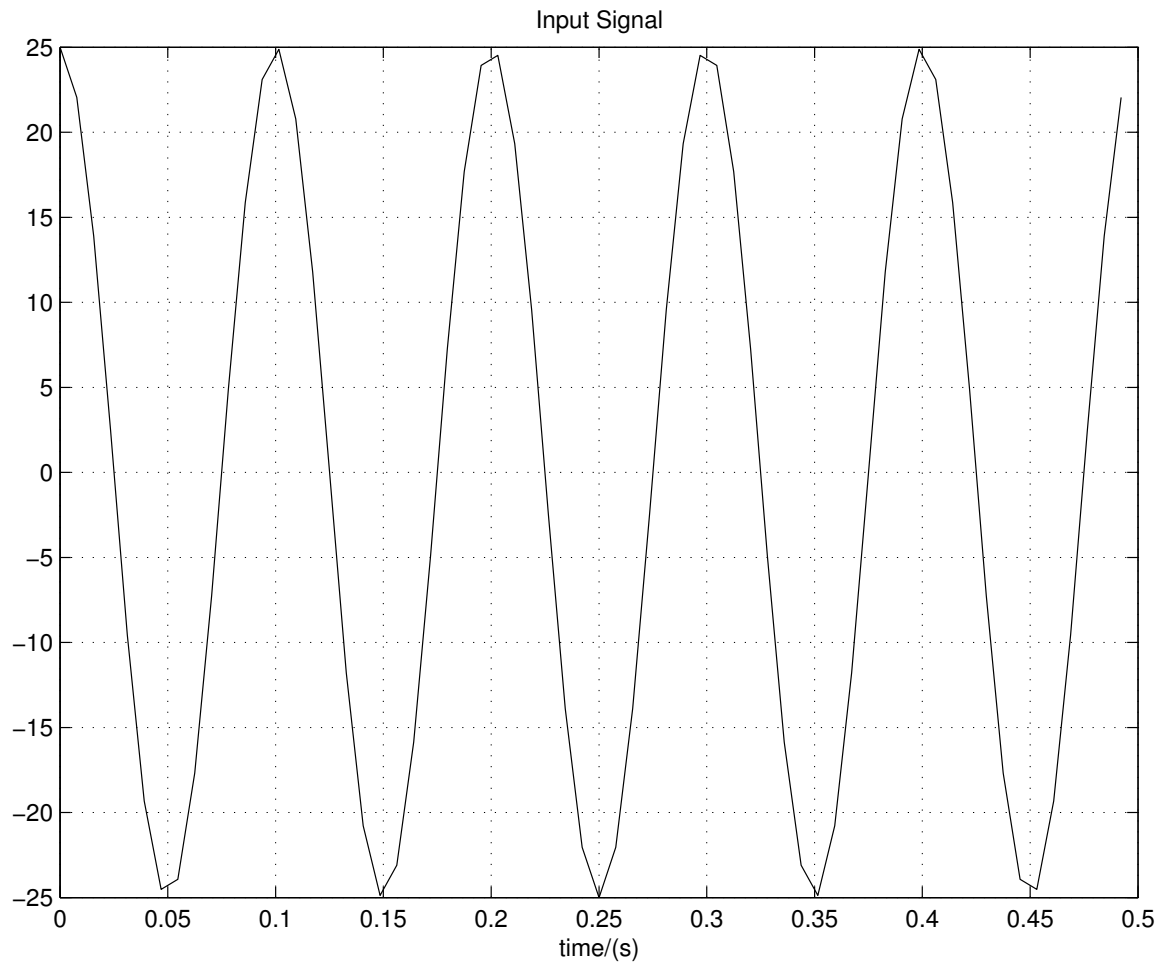


Figure 68: Bandlimited Input Signal

Theorems 4 and 5, it is expected that the original signal could be uniquely recovered. The recovered signal is depicted in Fig. 70 and it is evident that the distortions caused by the nonlinear sensor are completely compensated and the compensated signal is exactly the same as the original signal. Comparison with the results shown in [19] clearly demonstrates the fact that the results produced by the nonlinear filtering algorithm is better than that of [19]. This study shows that Algorithm 2 can also be used to compensate the distortions caused by linear and nonlinear sensors.

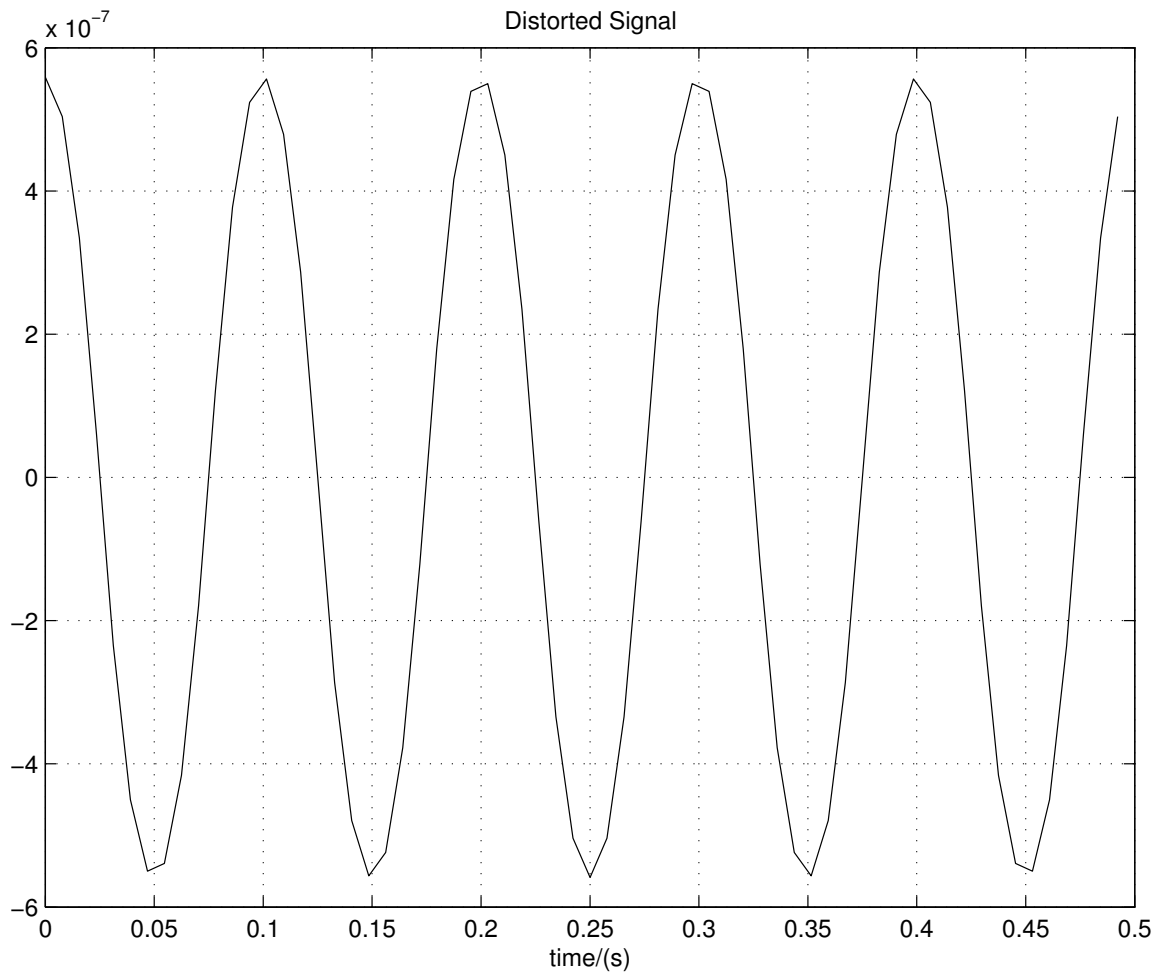


Figure 69: Distorted Signal

#### 4. Recovery with Monotonic Nonlinear Sensor Function

In this section, the simulation results are presented to further support the proposed nonlinear sensor design scheme and the signal recovery algorithm. Consider a signal detection problem where a band-limited signal shown in Fig. 72 is to be measured. Band-limitedness of this signal is guaranteed by its spectrum with frequency band  $[-41,41]$  Hz as shown in Fig. 73. To show how the characteristics of a nonlinear sensor function can be utilized to remove sensor noise, to increase the input dynamic range



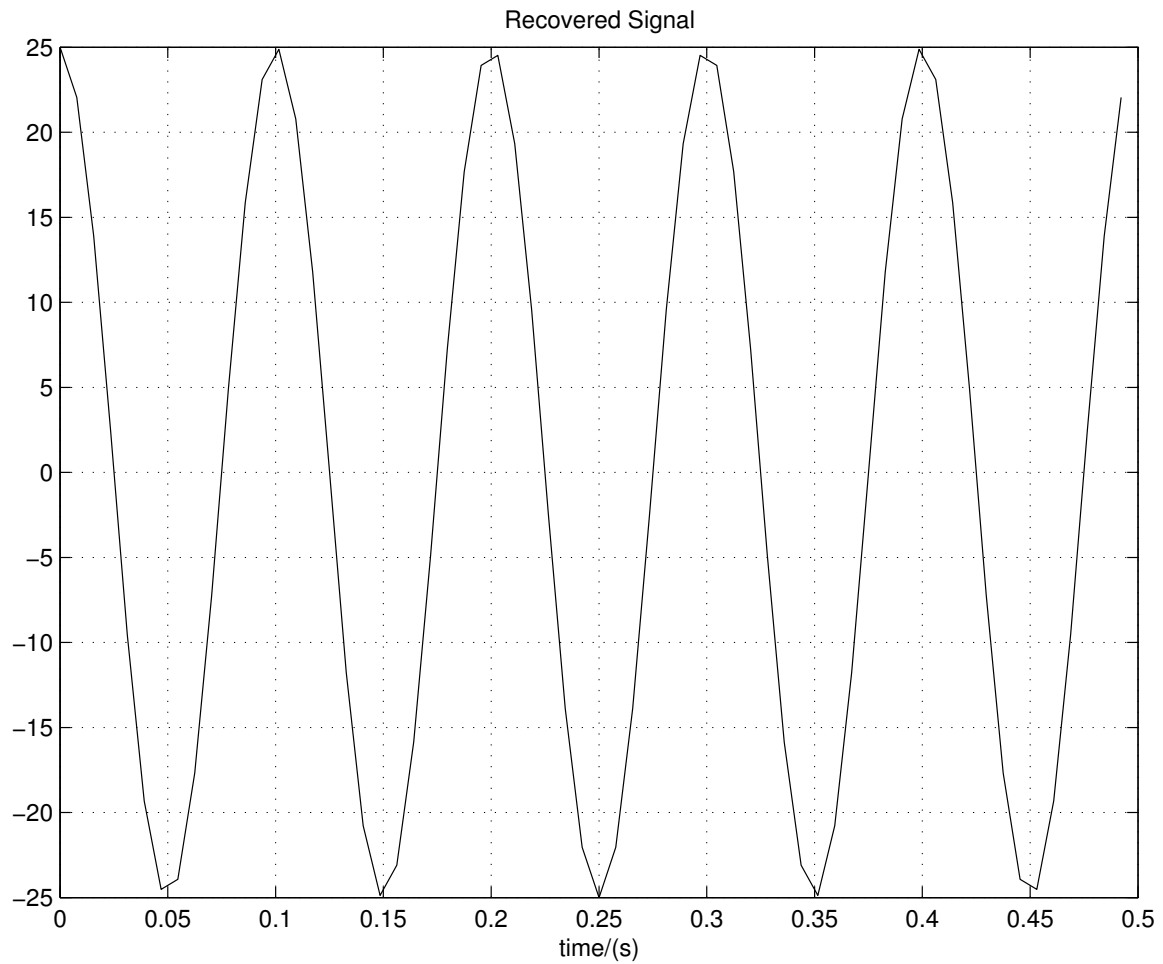


Figure 70: Compensated Signal

and to compare the results with that of a linear sensor, the input signal is measured through the linear and nonlinear sensors that are characterized by the functions shown in Fig. 71 and the results are analyzed.

The first conclusion is that the nonlinear sensor is capable of covering a wider input dynamic range for a given sensor output (voltage, in general) limit. Fig. 71 provides evidence to this conclusion. The next issue is the noise removal. Assuming that sensor noise is stationary, it is modelled as a random signal as shown in Fig. 74.

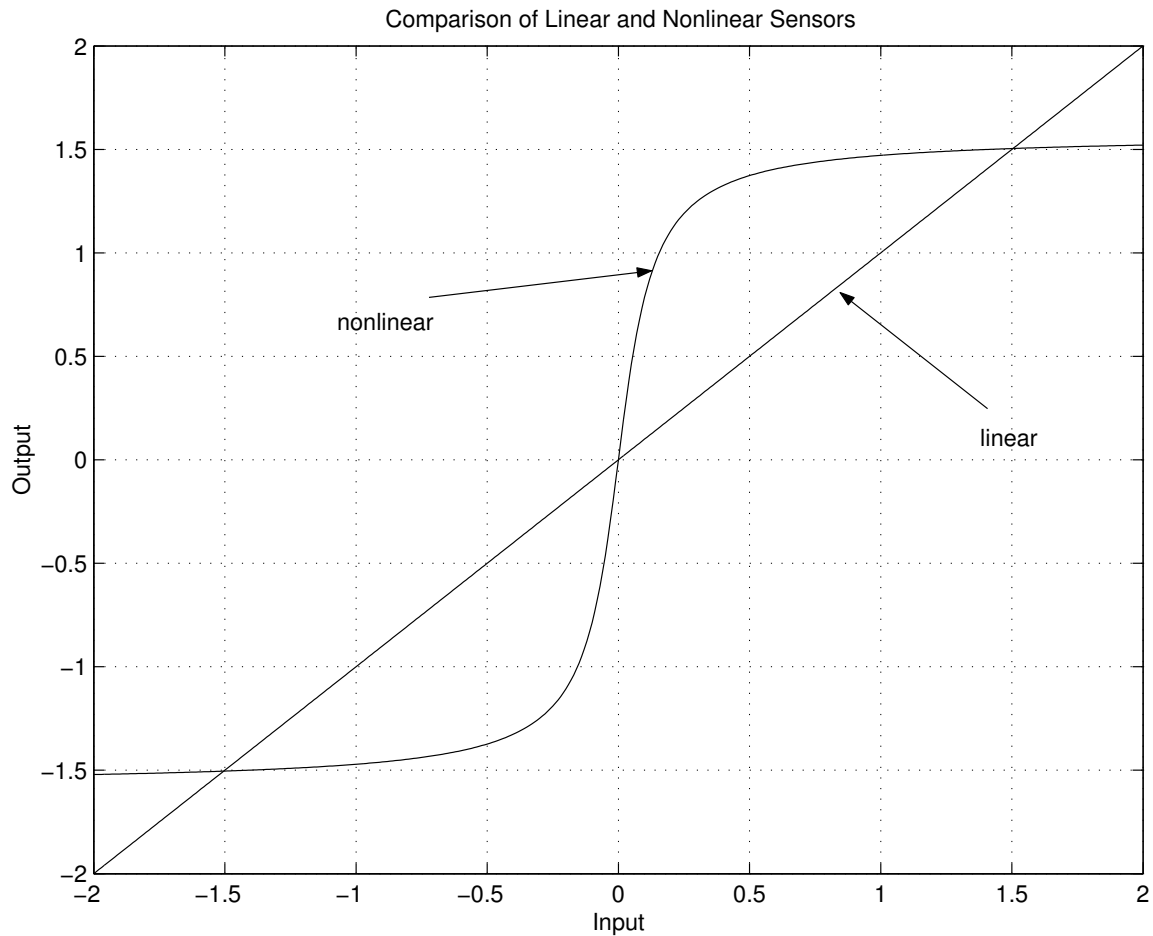


Figure 71: Comparison of Linear and Nonlinear Sensor Functions

The frequency spectrum of this noise signal is shown in Fig. 75. It is worth pointing out that the spectrum of sensor noise spans over a wide frequency range and a low pass filter alone cannot remove this noise.

Fig. 76 and Fig. 77 show the corrupted linear and nonlinear sensor measurements respectively. As nonlinear sensor function has a high slope near zero, it amplifies low strength original data. This signal amplification helps distinguish the original data from measurement noise. Fig. 77 supports this fact. As the linear sensor does not share this advantage, its measurement shown in Fig. 76 has relatively equal strength

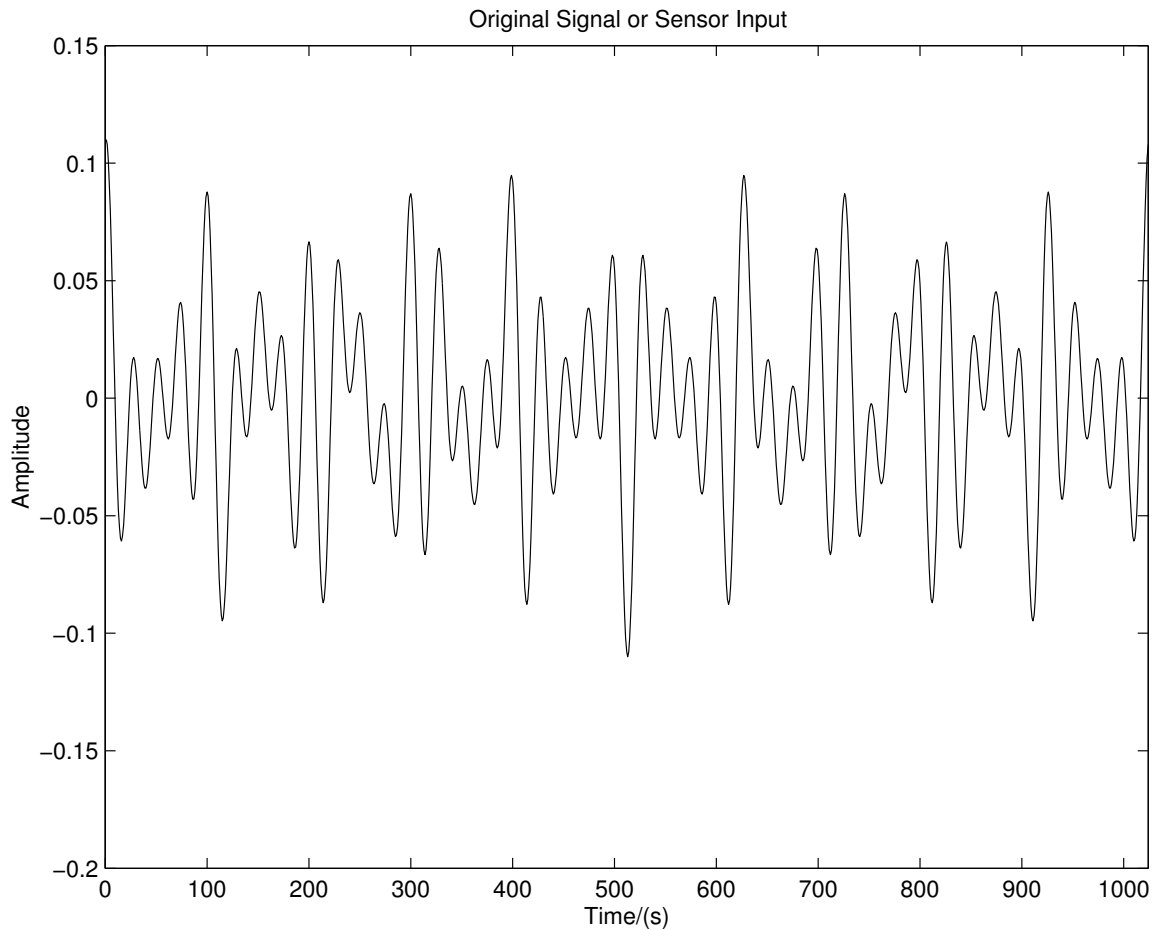


Figure 72: Input Signal Used in Subsection 4

frequency spikes and noise and the original data are not easily distinguishable.

As discussed earlier, sensor noise is removed by a simple threshold filter. High harmonics are removed by an ideal low pass filter, which is primarily used to preserve band-limitedness of signals. The filtered signal is shown in Fig. 78. The iterative scheme given in Algorithm 1 is then used to recover the original signal from the filtered signal. The recovered signal and its spectrum are given in Fig. 79 and Fig. 80 respectively. Comparison with the sensor input data reveals that the original signal is reproduced.

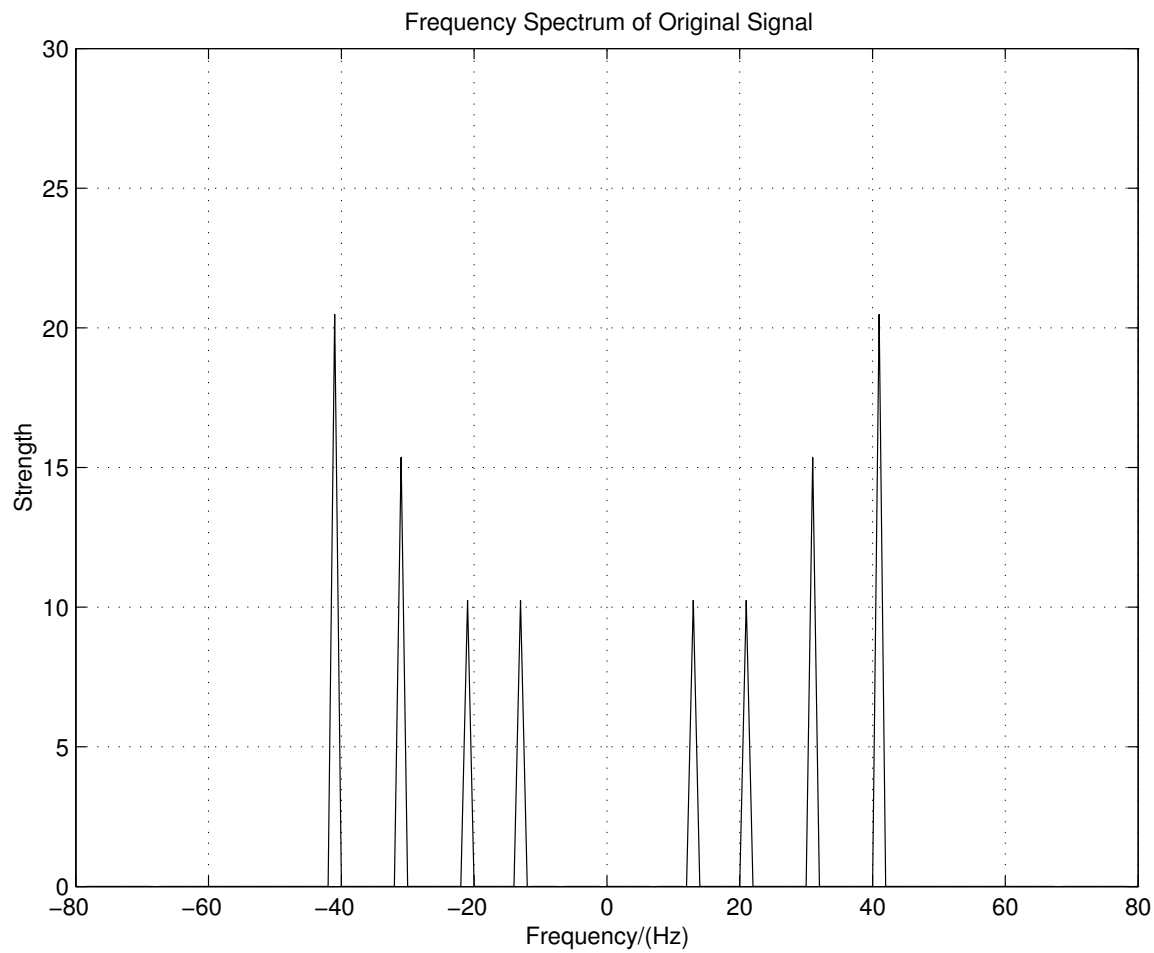


Figure 73: Spectrum of Input Signal Shown in Fig. 72

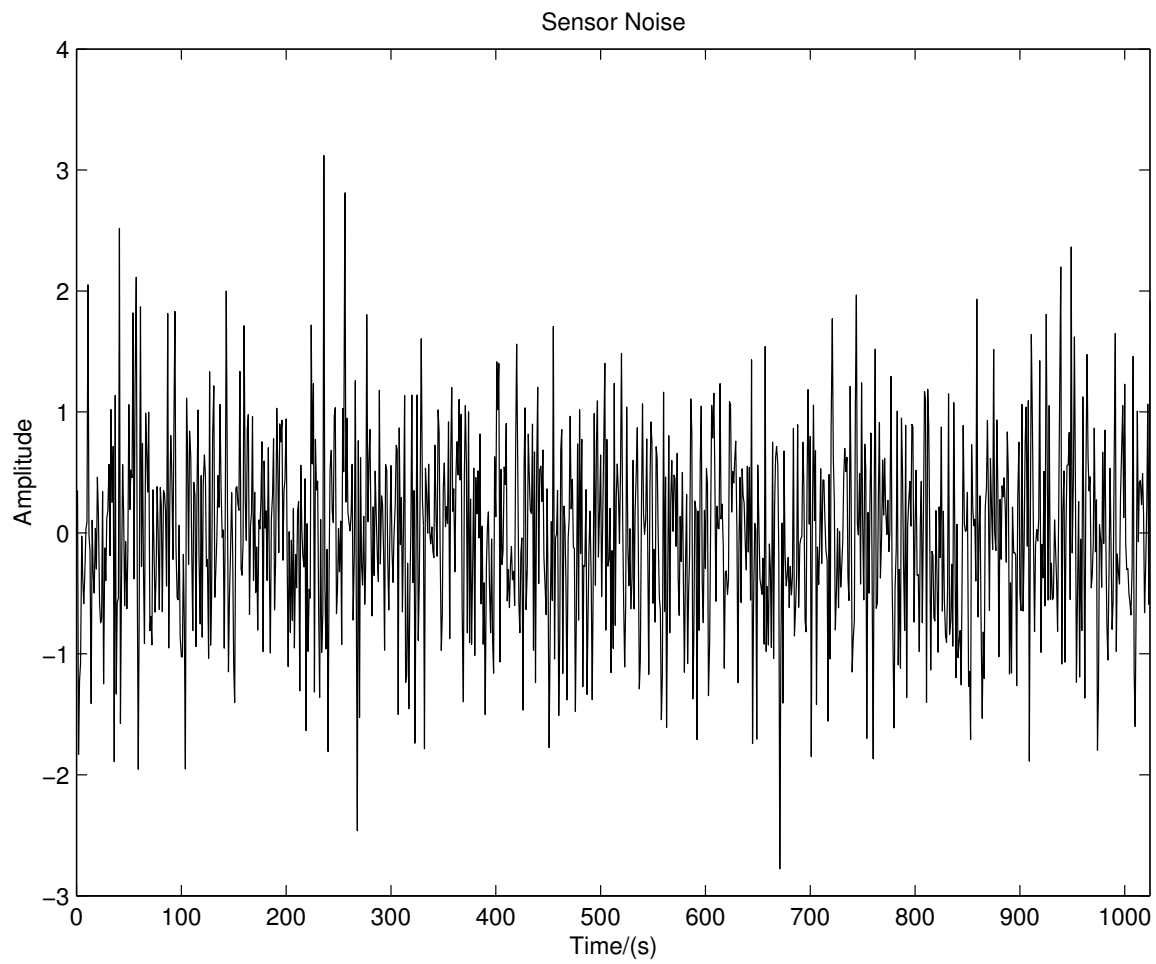


Figure 74: Sensor Noise

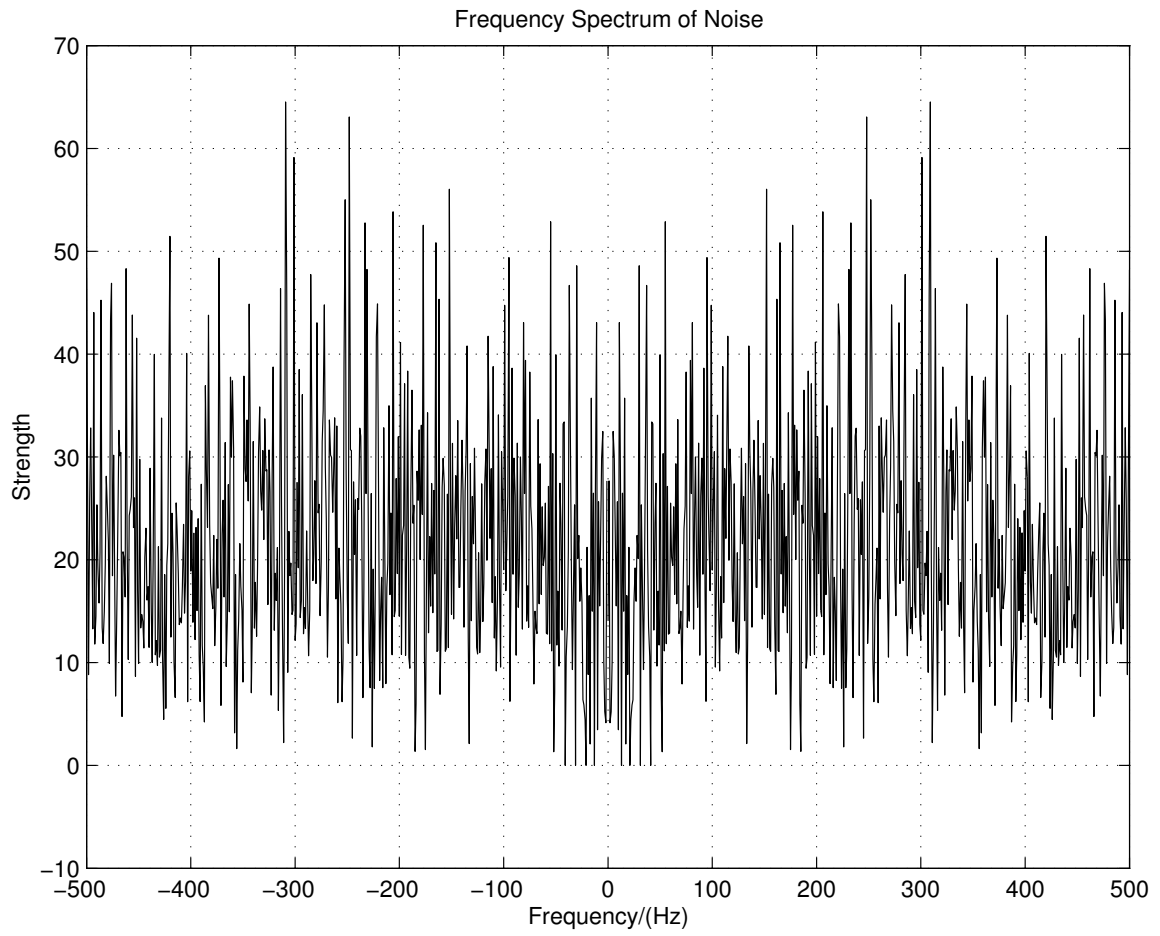


Figure 75: Spectrum of Sensor Noise Shown in Fig. 74

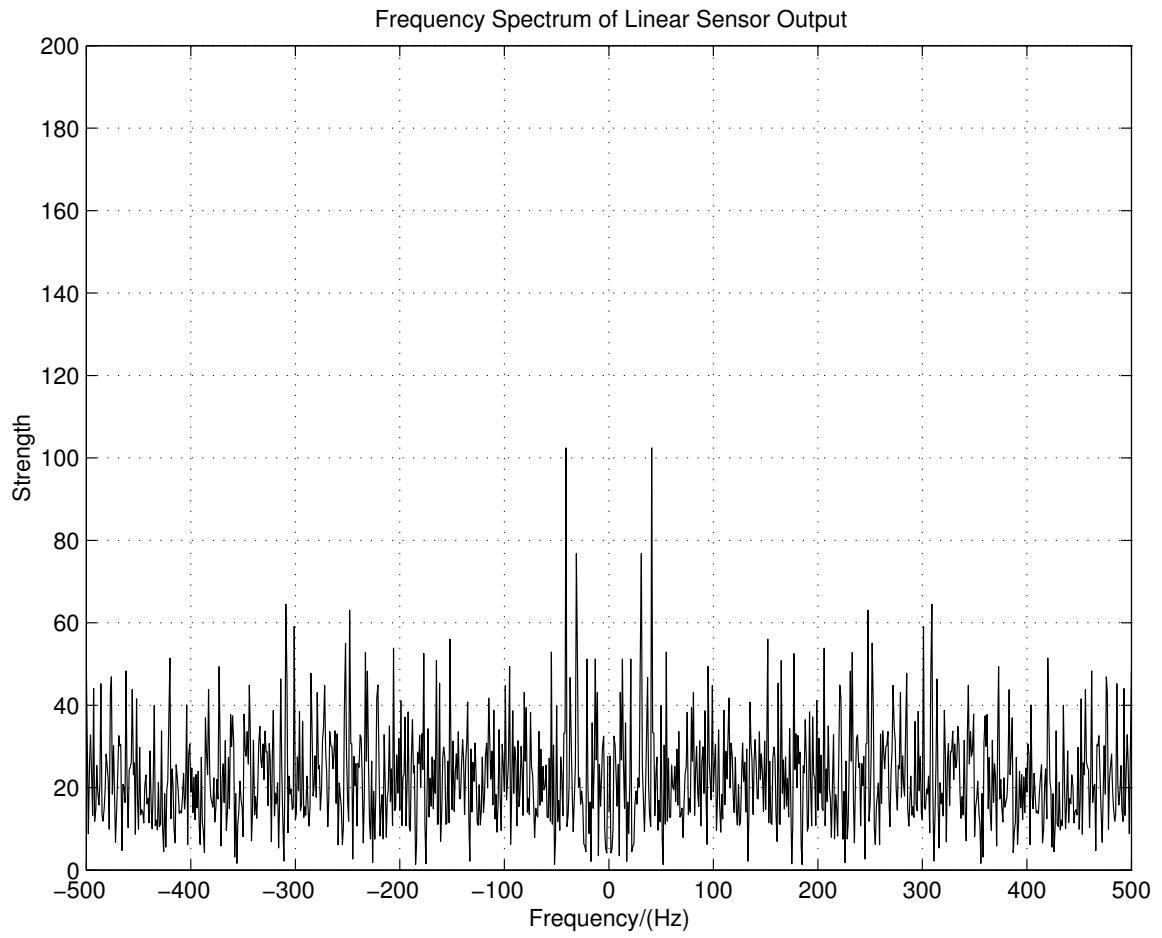


Figure 76: Spectrum of the Linear Sensor Output

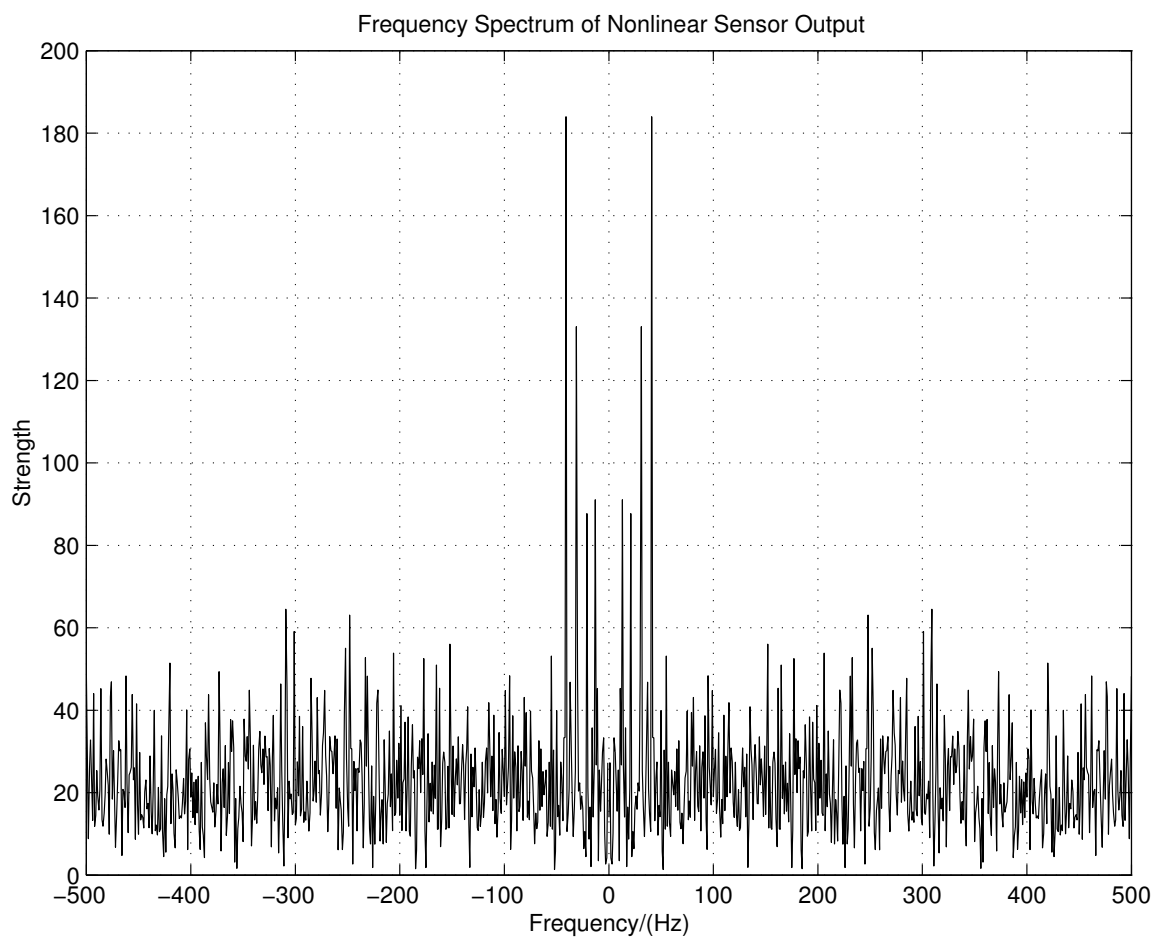


Figure 77: Spectrum of the Nonlinear Sensor Output



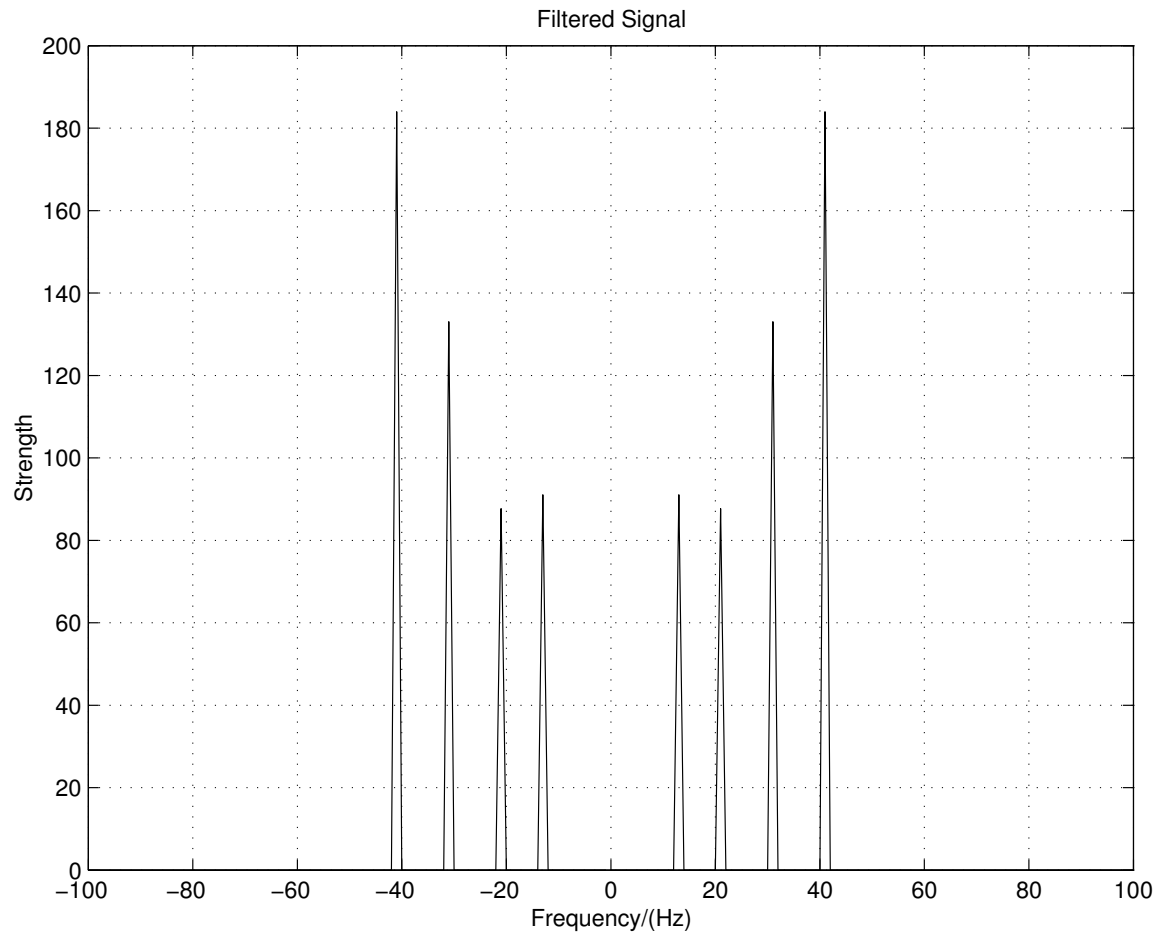


Figure 78: Filtered Sensor Output Obtained by Removing High Harmonics

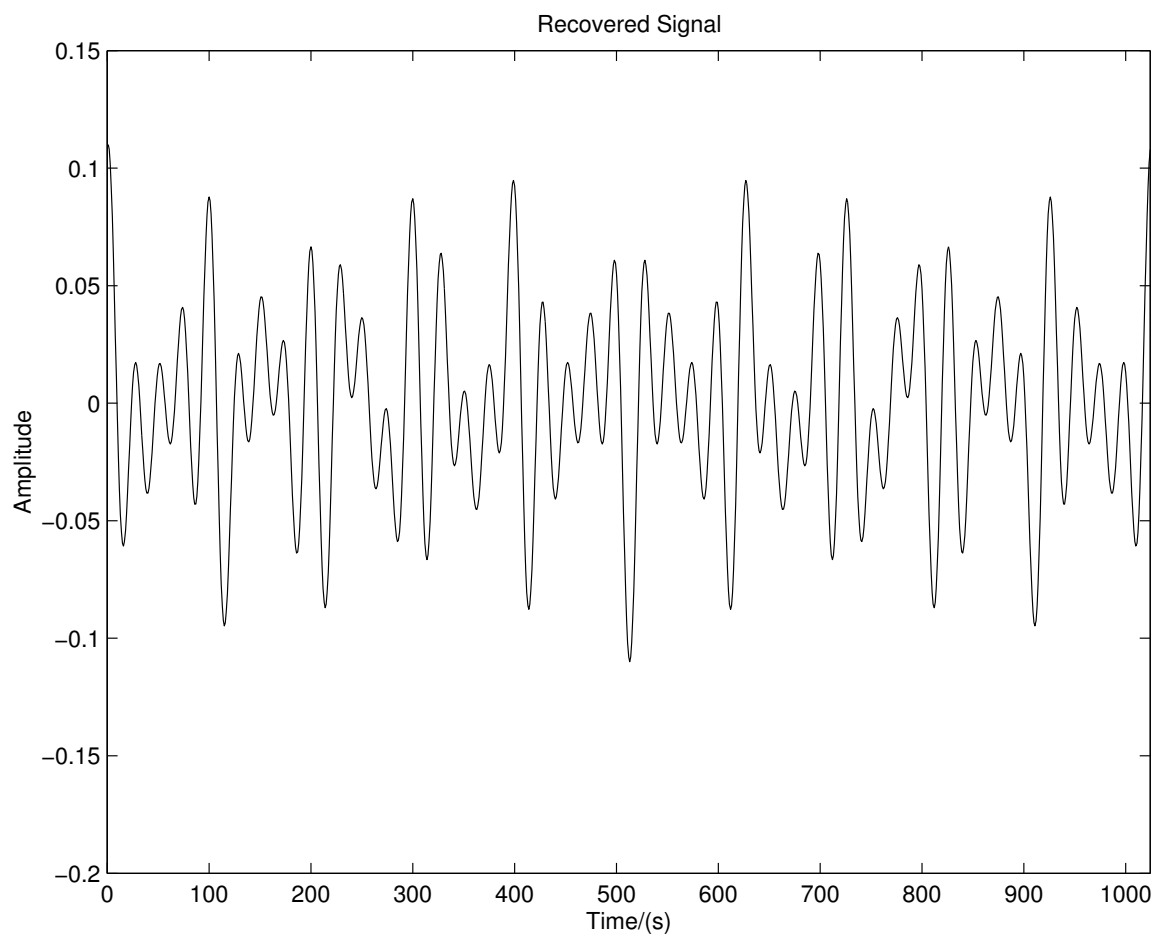


Figure 79: Reconstructed Signal

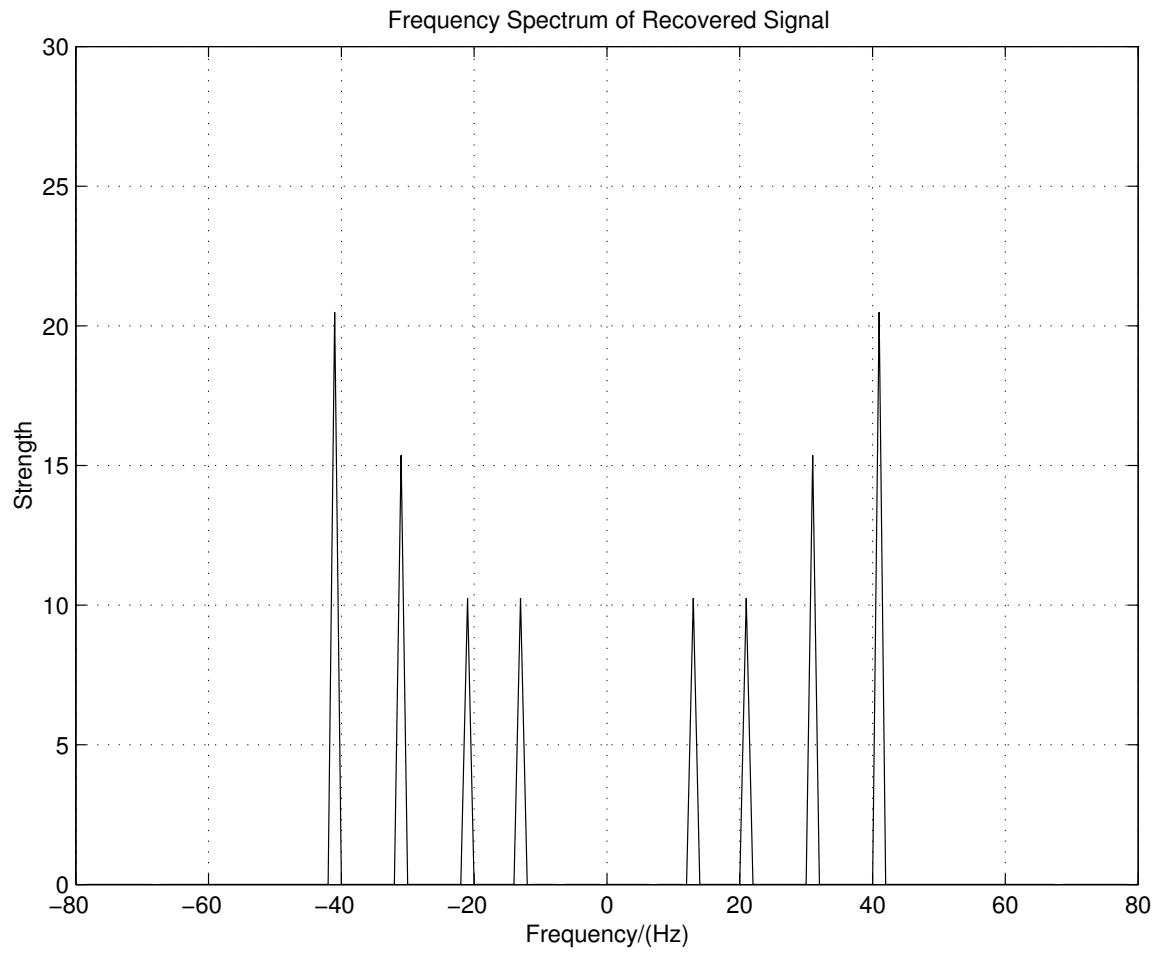


Figure 80: Spectrum of Recovered Signal Shown in Fig. 79

#### 5. Recovery of Distorted Signals in Non-stationary Noisy Environments

In this section, experimental and simulation results are presented to support the method developed in section E of chapter IV.

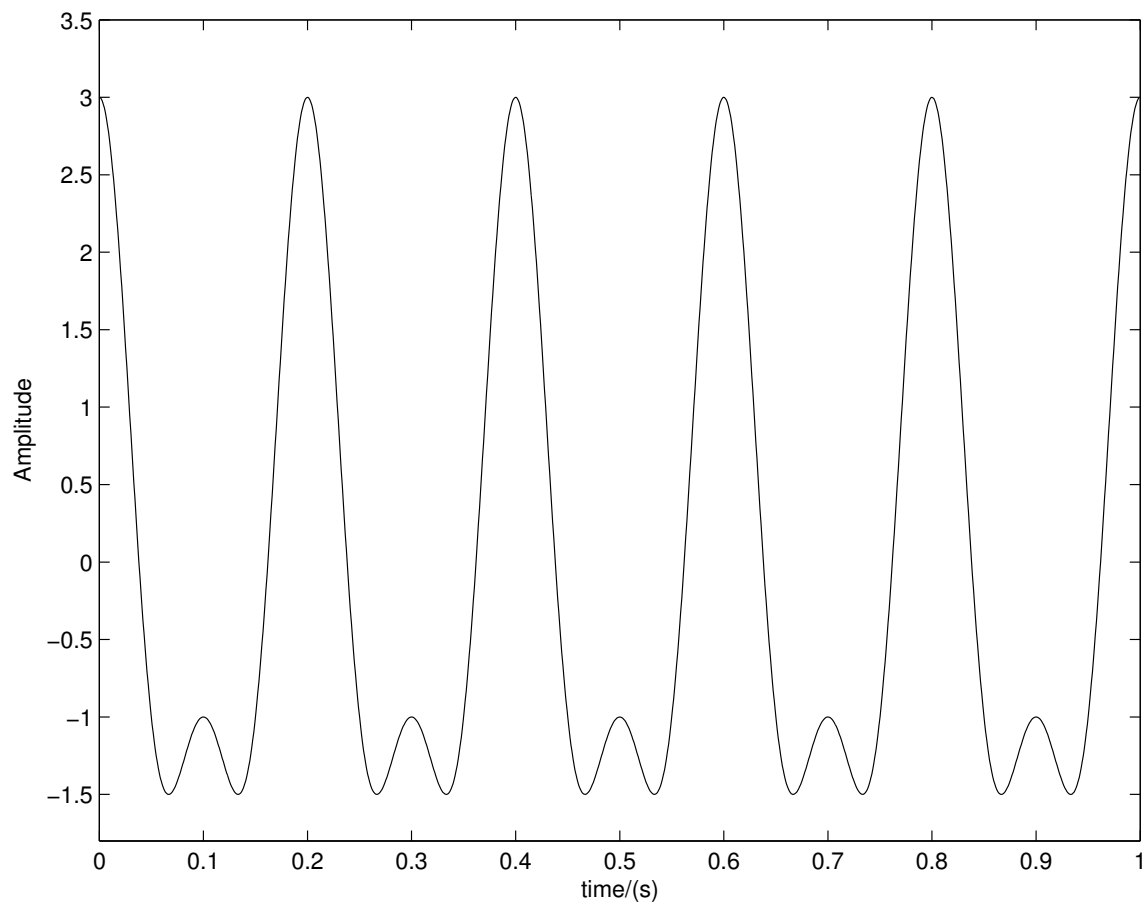
### a. Simulation Results

We will use a bandlimited signal,  $y$ , shown in Figure 81 to demonstrate the performance of the proposed method. Signal,  $y$ , is measured through a nonlinear sensor,  $g(\cdot)$ , whose input-output characteristic is shown in Figure 82.

The distorted sensor output,  $g(y)$ , is corrupted by adding a non-stationary noise and the resultant output signal,  $w$ , is shown in Figure 83. Signal,  $w$ , is then passed through an ideal low pass filter to obtain signal,  $z$ . The Discrete Wavelet Transform discussed in the previous section is implemented through the Filter Bank setup shown in Figure 84. The low pass filter output,  $z$ , is decomposed into details and approximations using the DWT, which is evaluated using the Daubechies (db15) wavelets [127]. The decomposition process is carried out with a Filter Bank that has three sub-bands as illustrated in Figure 84 and signals obtained through this process are shown in Figure 85.

The insignificant details are processed using hard threshold filters and the denoised estimate ( $v$ ) of the low pass filter output,  $z$ , is reconstructed using the IDWT as shown in Figure 84. The intermediate signals of this reconstruction process and the final denoised estimate,  $v$ , are shown in Figure 86.

The denoised estimate is then used to solve the iterative recovery scheme described by Equation (4.33) to recover the original sensor input and the recovered signal is shown in Figure 87. A comparison of this recovered signal with the actual signal shown in Figure 81 clearly demonstrates that the signal is recovered with a reasonable accuracy.

Figure 81: Input Signal,  $y$

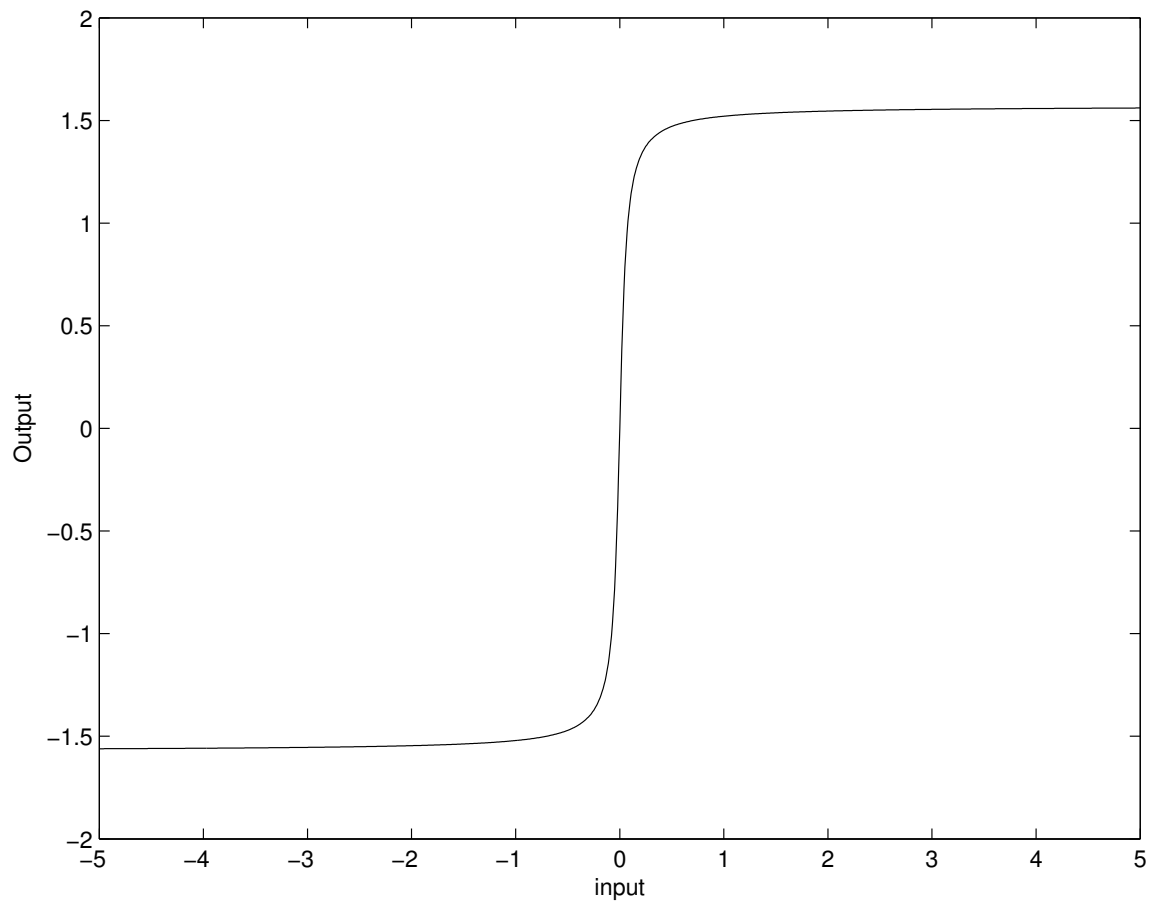


Figure 82: Nonlinear Sensor,  $g$

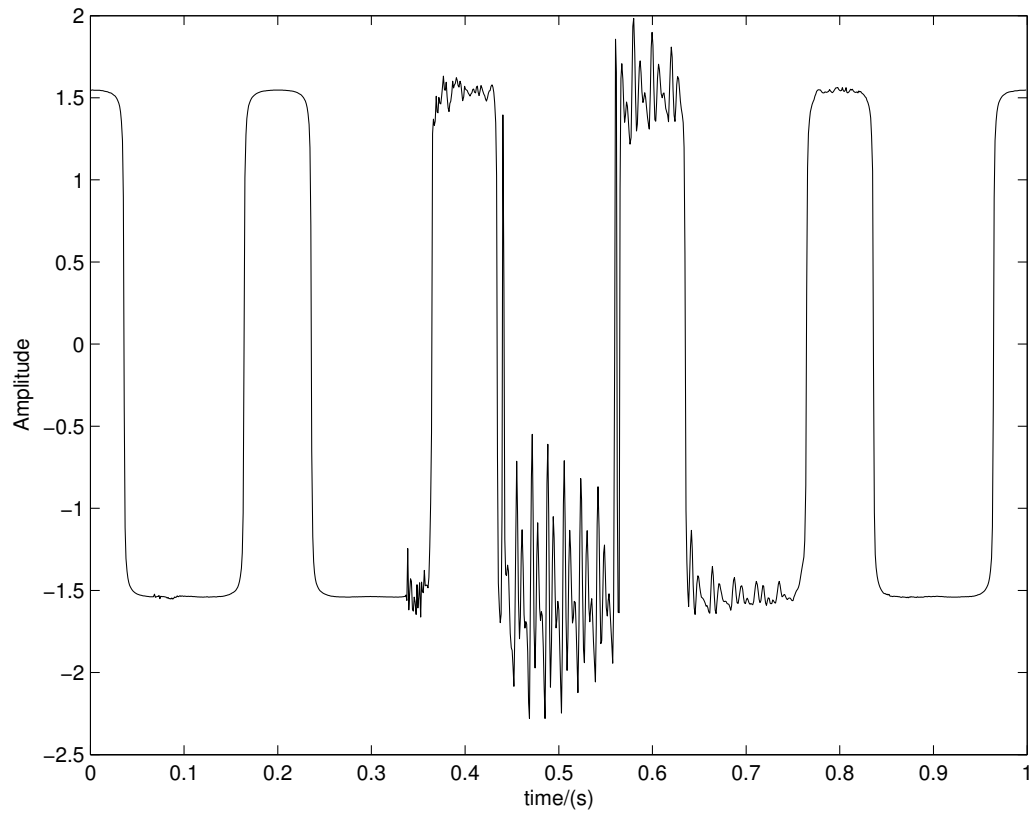
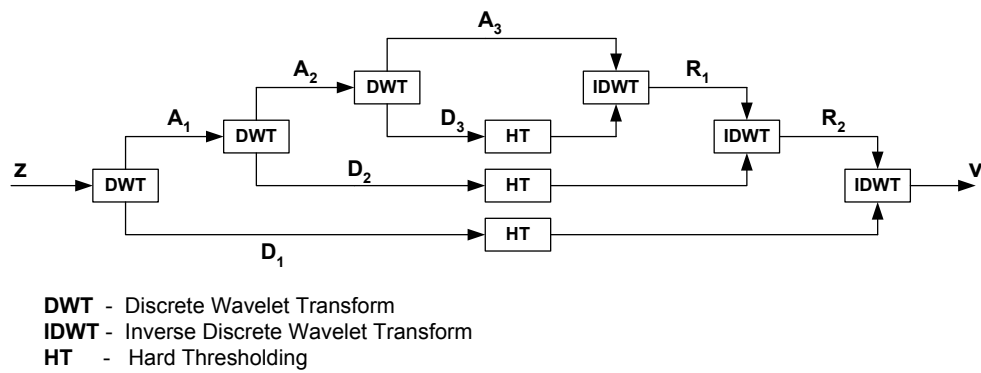
Figure 83: Sensor Output,  $w$ 

Figure 84: Filter Bank Setup

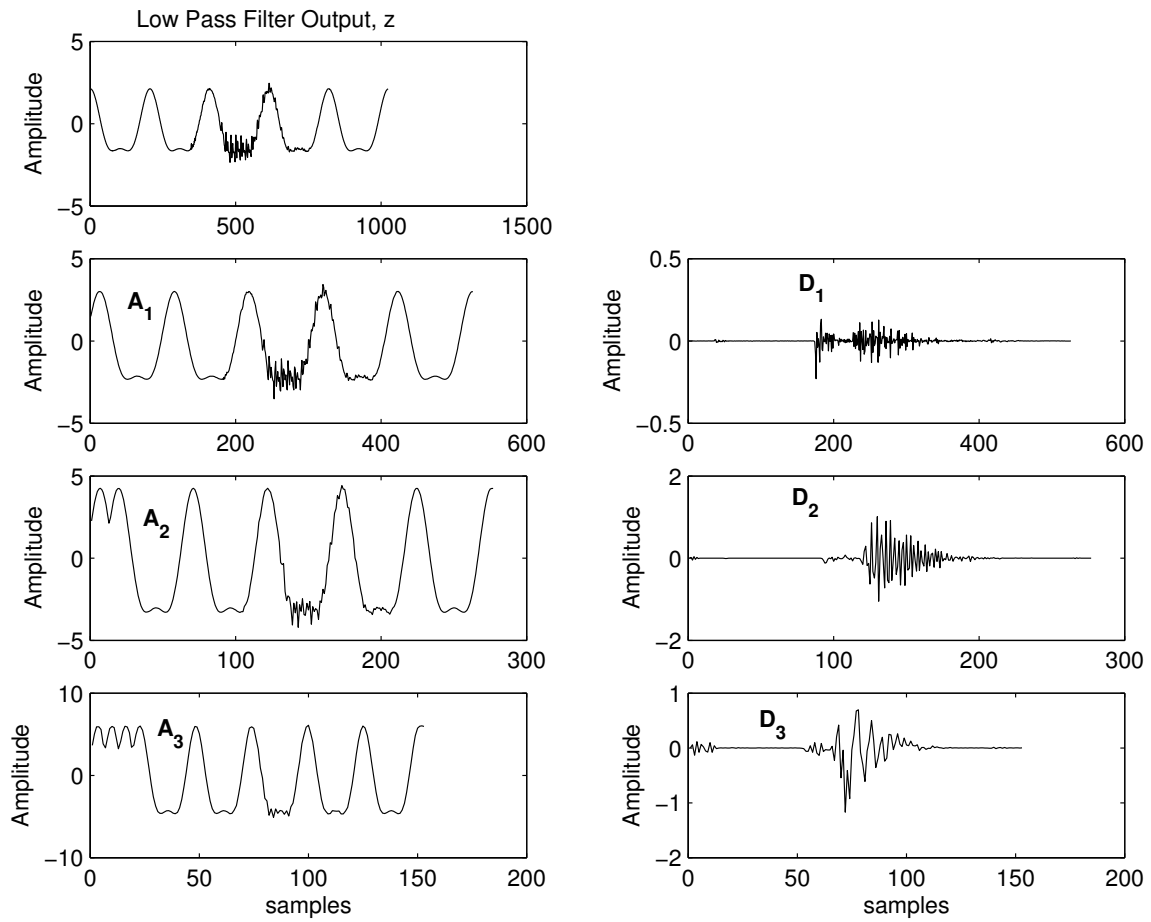


Figure 85: Decompositions of Low Pass Filter Output



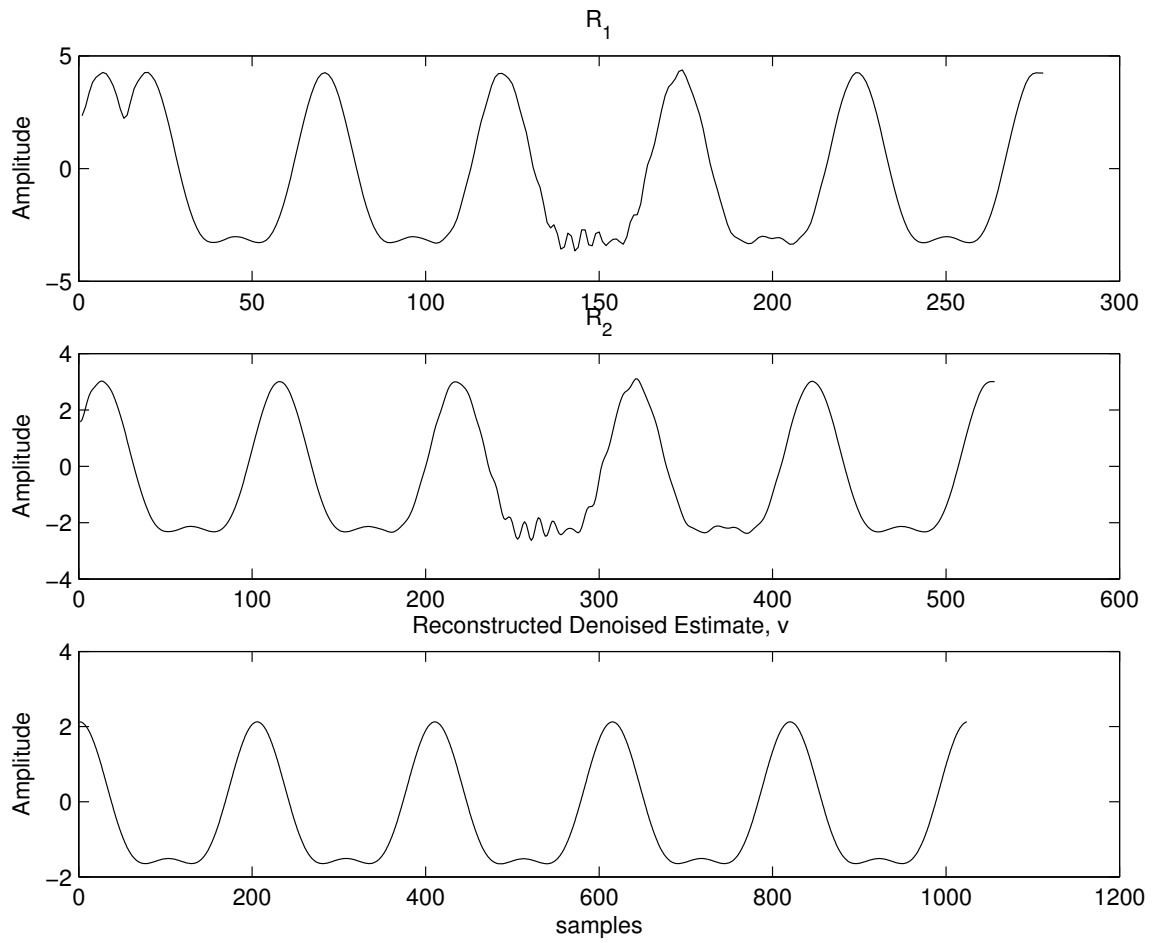


Figure 86: Reconstruction to Obtain Denoised Estimate

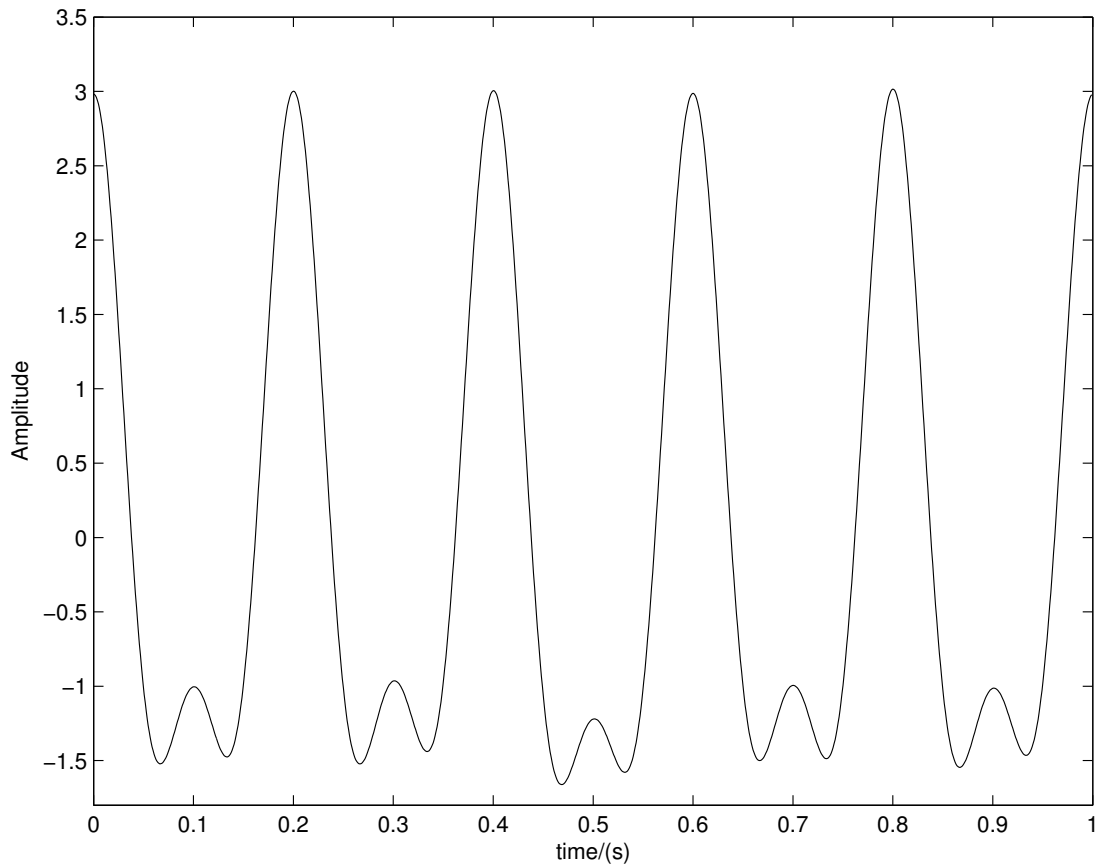


Figure 87: Signal Recovered Using the Iterative Algorithm

#### b. Experimental Results

This section documents the experimental results, which support the proposed methodology. A simple nonlinear diode circuit shown in Figure 61 was built and the output voltage,  $v_{out}$ , shown in Figure 89 was acquired using the dSpace Real Time Data Acquisition System and the data were processed in Matlab platform to recover the unknown voltage signal,  $v_{in}$ , shown in Figure 88. The output signal,  $v_{out}$ , was further corrupted by adding a non-stationary noise signal to it and the noisy output signal,  $v_n$ , is shown in Figure 90. A filter bank with four sub-bands as shown in Figure

91 was used to decompose the signal,  $v_n$ , and the details and approximations of  $v_n$  obtained at each sub-band of the filter bank using the DWT are shown in Figure 92. The insignificant details were removed using hard threshold filters and the denoised estimate,  $v$ , (of signal  $v_n$ ) shown in Figure 93 was obtained by reconstructing the processed details and approximations using the IDWT. The Daubechies [127] (db15) wavelets were used for the implementation of the DWT and the IDWT. The recursive signal recovery scheme described by Equation (4.33) was then solved using the denoised estimate,  $v$ , and the signal recovered is shown in Figure 94. It is clear that the signal is recovered with a reasonable accuracy, which supports the proposed methods.

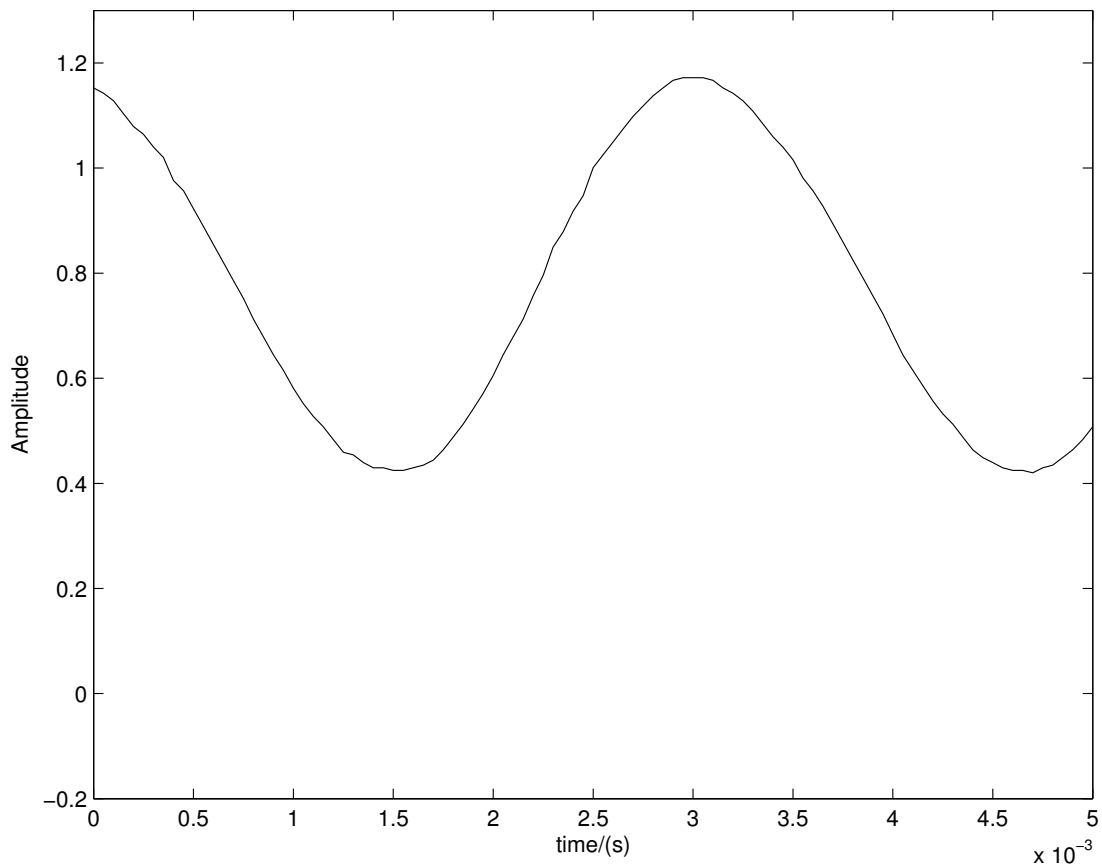
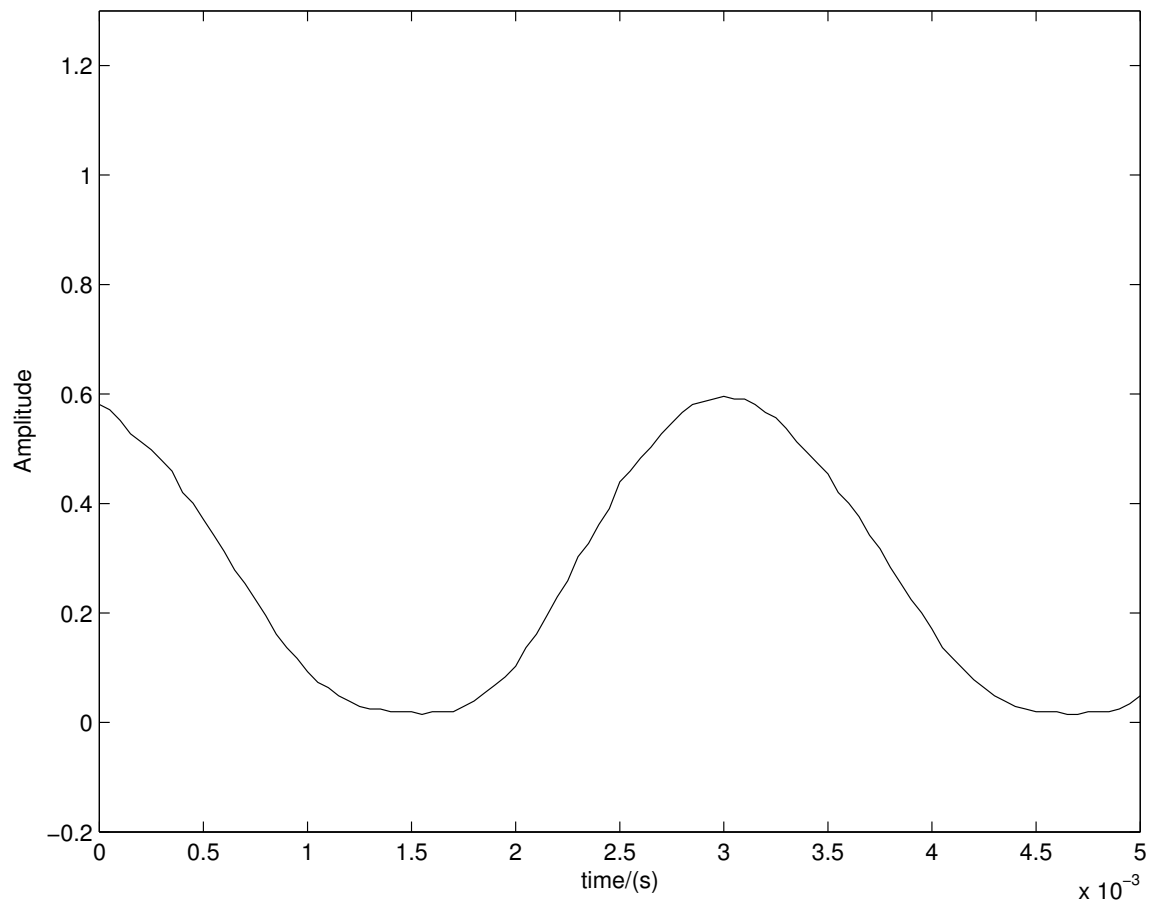


Figure 88: Actual Input Signal,  $v_{in}$

Figure 89: Acquired Output,  $v_{out}$

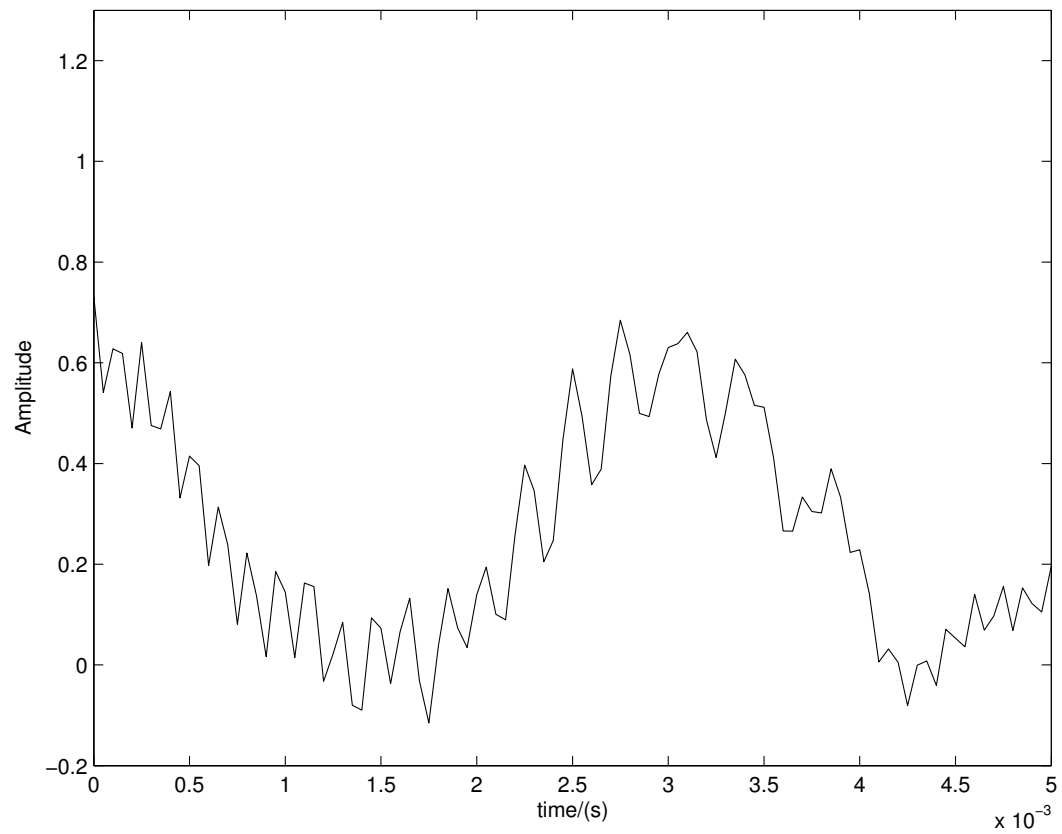
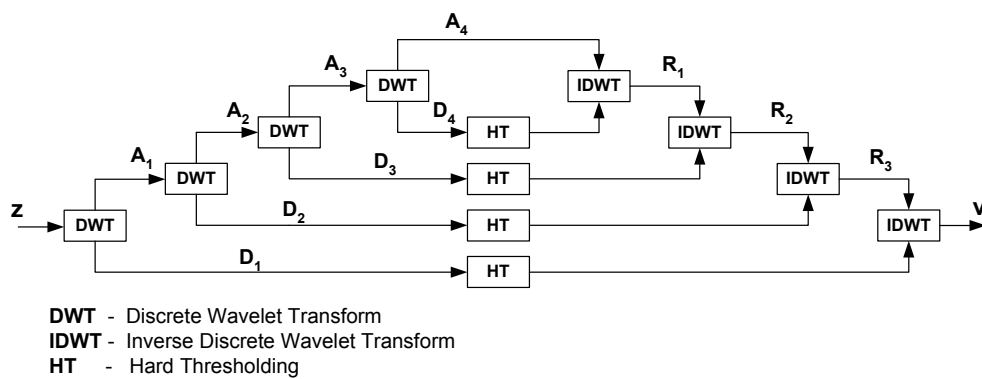
Figure 90: Corrupted Output,  $v_n$ 

Figure 91: Filter Bank Setup

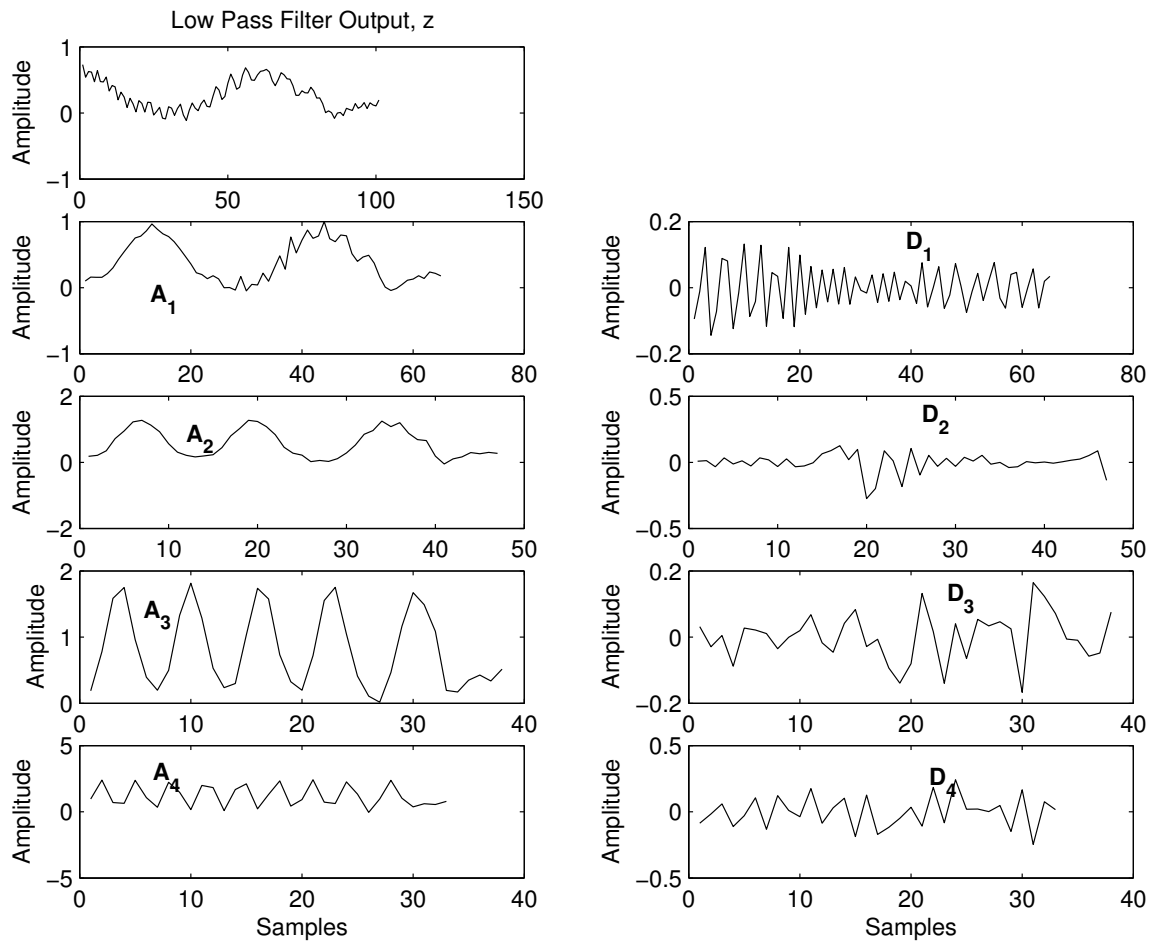


Figure 92: Decompositions of Low Pass Filter Output

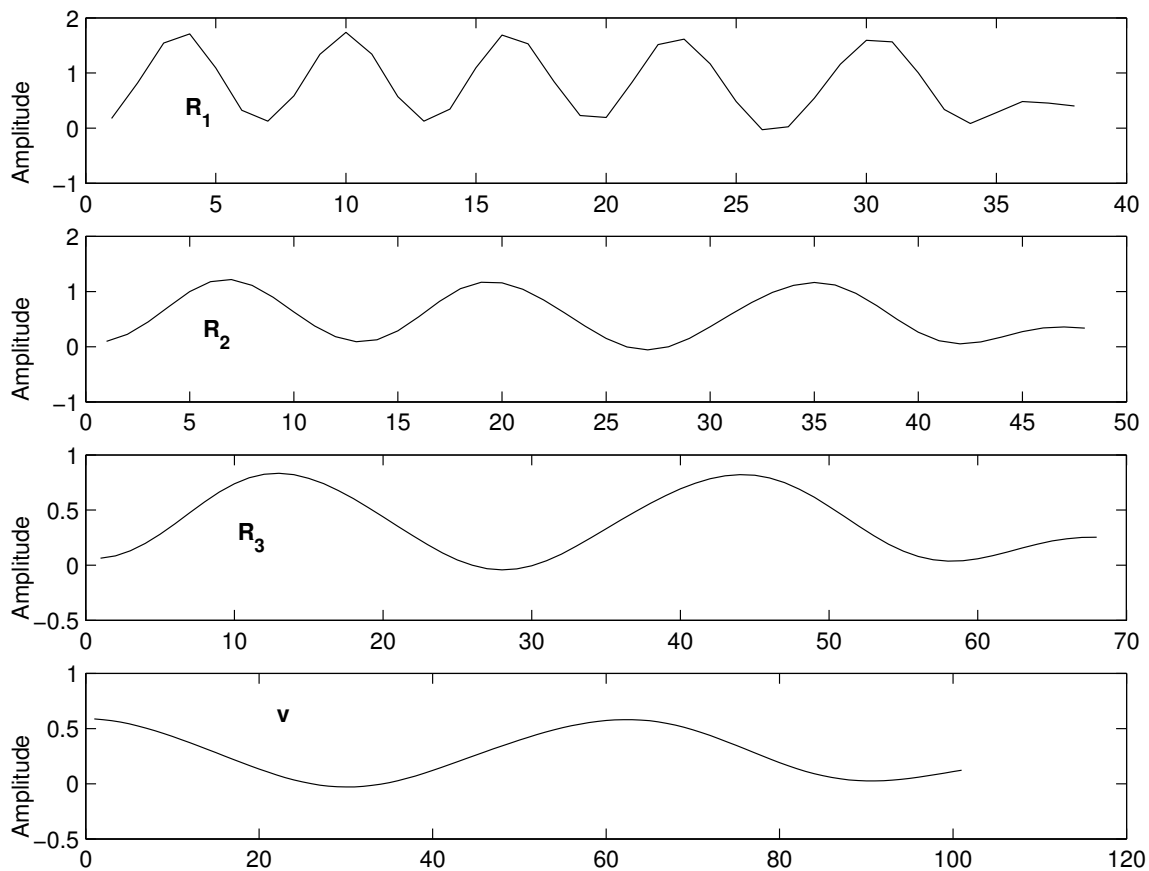


Figure 93: Reconstruction to Obtain Denoised Estimate

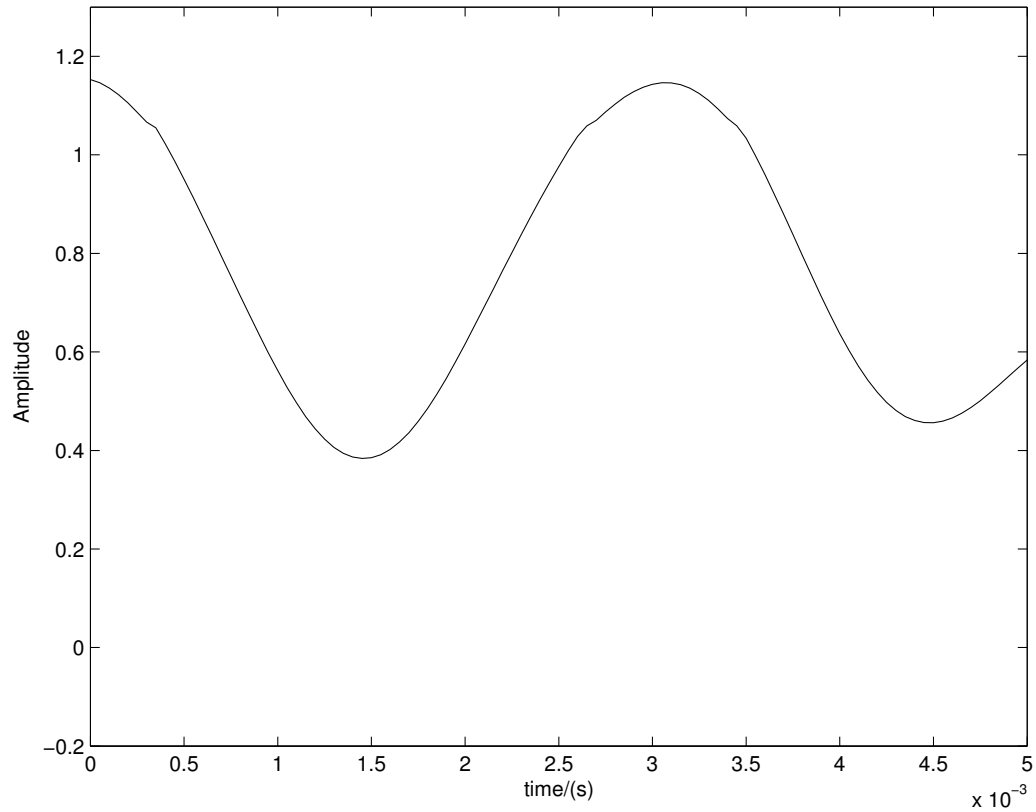


Figure 94: Unknown Signal Recovered by Solving the Iterative Algorithm

## 6. Signal Recovery Using Nominal Sensor Model

In this subsection, an example is presented to support the findings derived in section G of chapter IV. Consider a nonlinear sensor function, which is characterized by the following input-output relationship.

$$w = y + y^2 + 2y^3 \quad (7.1)$$

It is noted that the term  $y^2$  in the above expression will not preserve the original frequency information and therefore may not be needed to reproduce the original signal. We will show that the exact reproduction of original signal is possible using



the following nominal model.

$$\hat{w} = y + 2y^3 + 8 \quad (7.2)$$

The actual and nominal sensor models are shown in Fig. 95. We will measure the signal shown in Fig. 96 through the actual sensor. The sensed signal is shown in Fig. 97. The iterative signal recovery scheme given in Section 2 is then used to recover the signal. The important point is that the recovery process is carried out using the nominal model, not the actual. The recovered signal shown in Fig. 98 supports the fact that the actual sensor model may not always be needed to reproduce the original signal exactly.

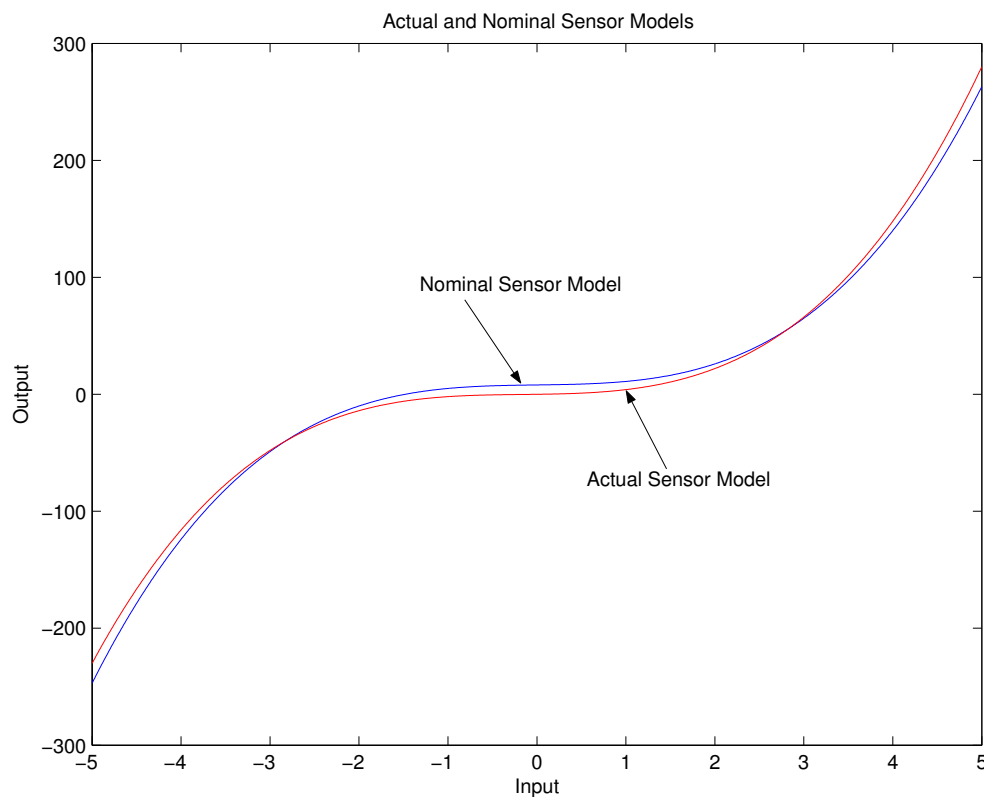


Figure 95: Actual and Nominal Sensor Models

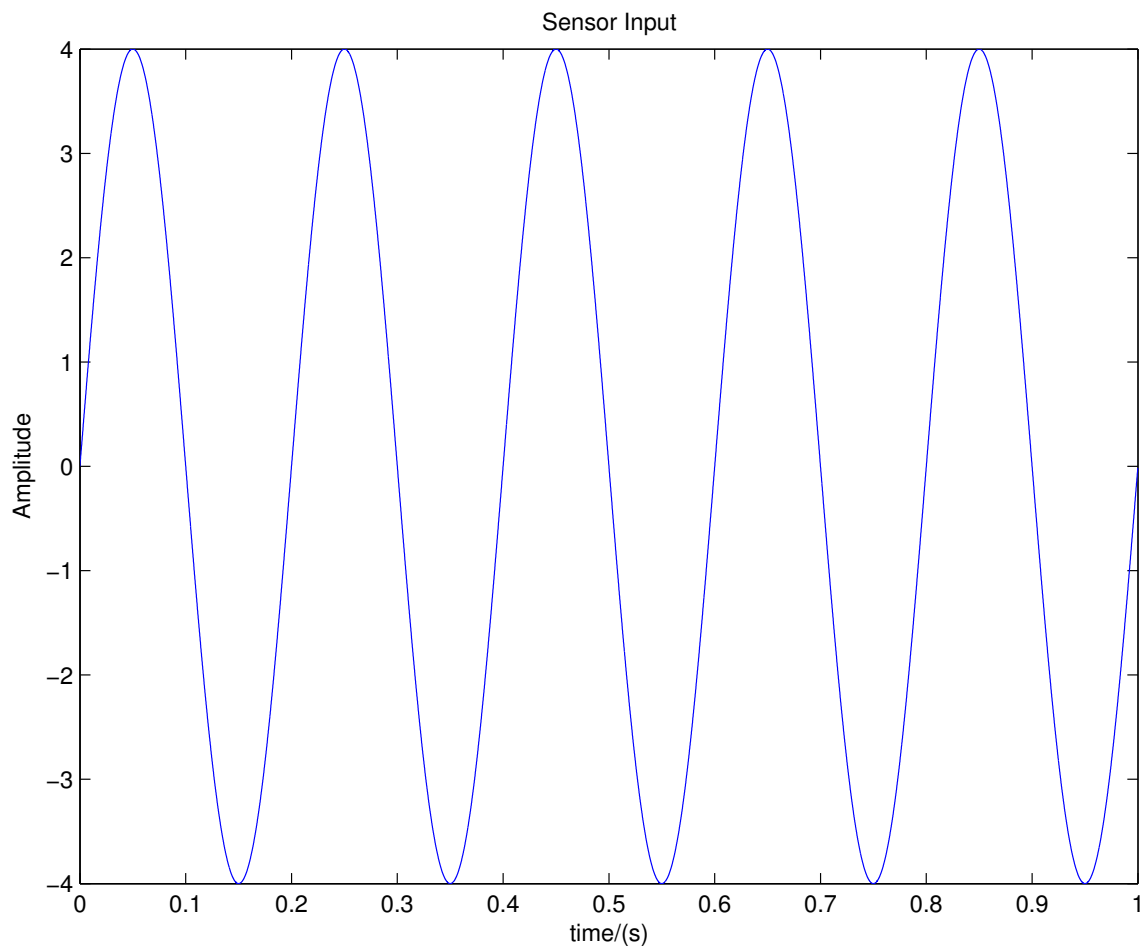


Figure 96: Sensor Input

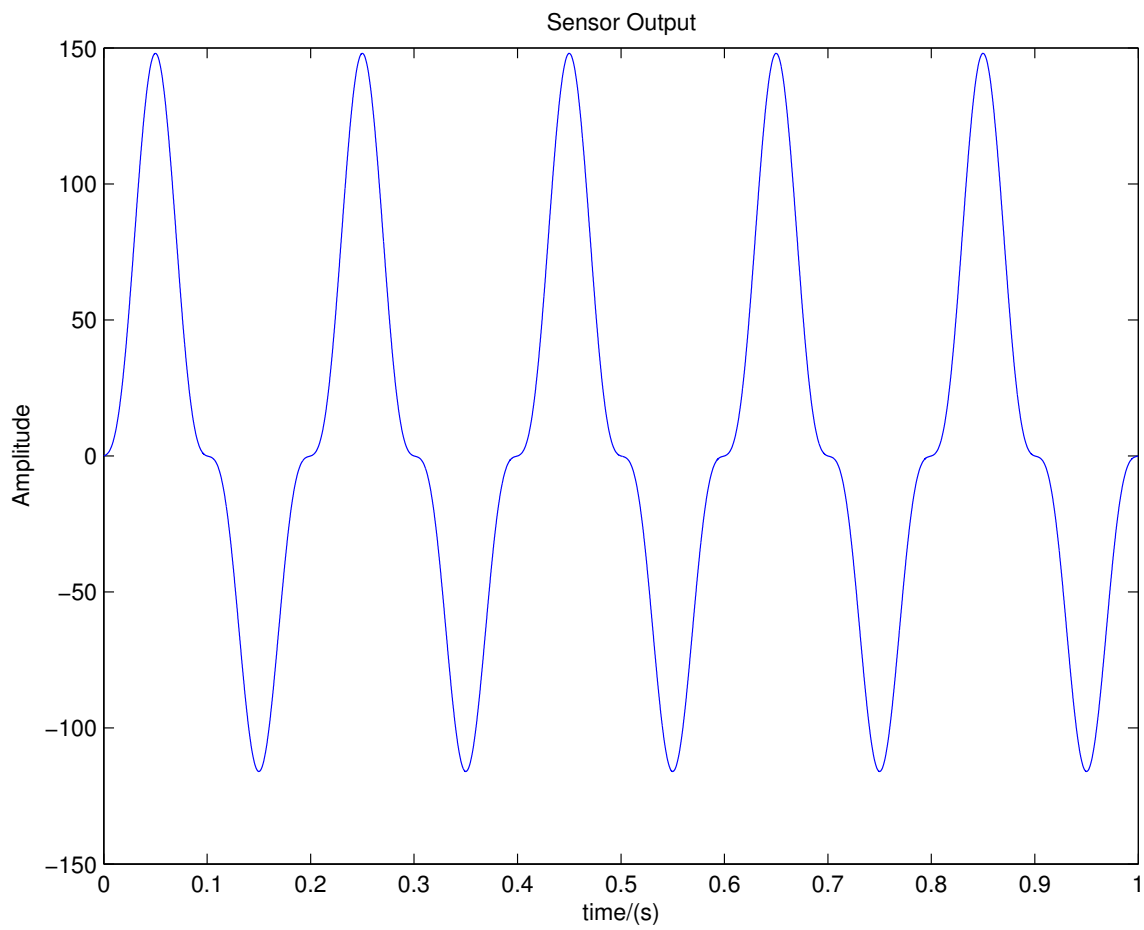


Figure 97: Sensor Output

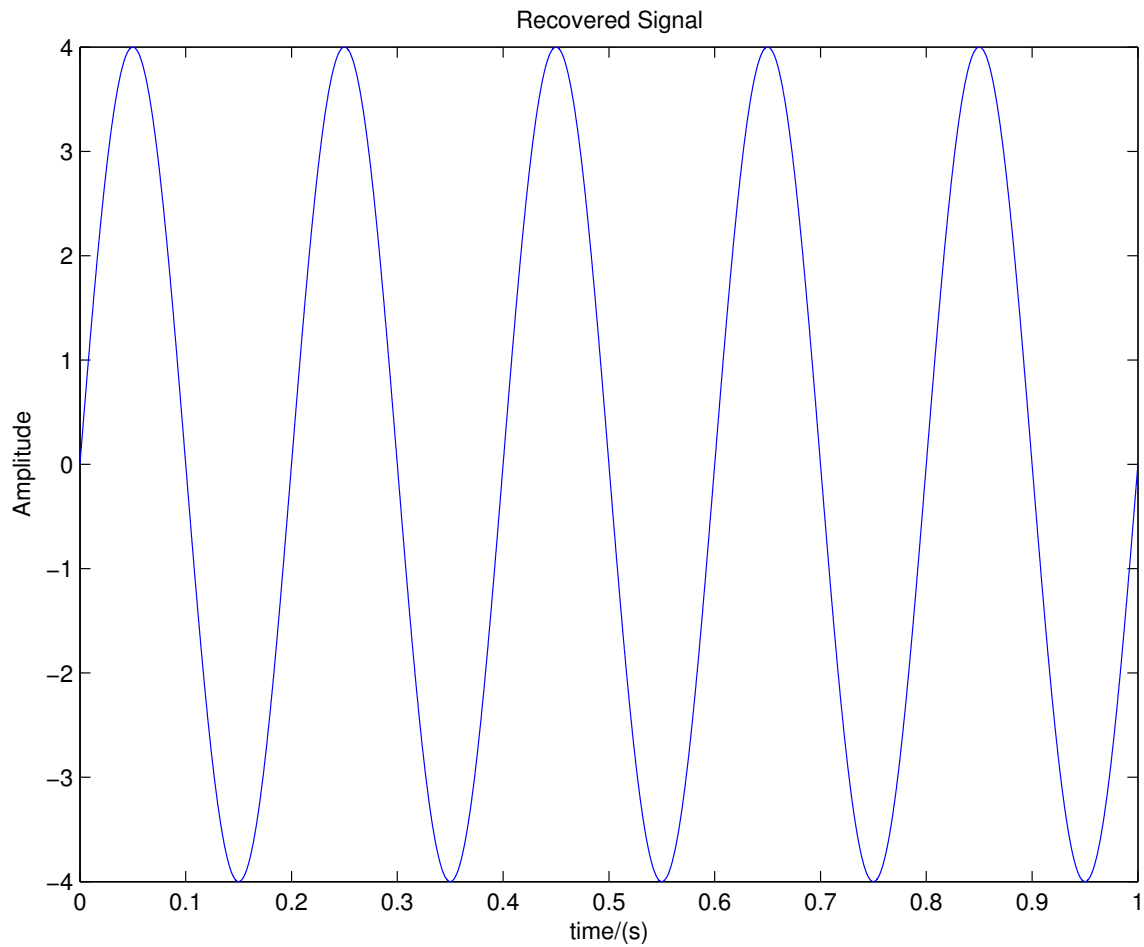


Figure 98: Recovered Signal Using Nominal Sensor Model

### 7. Recovery with Non-monotonic Nonlinear Sensor

To further illustrate the optimization-based recovery scheme developed in Section I of chapter IV, a simulation example is presented in this section. The signal shown in Fig. 99 is measured through the non-monotonic nonlinear sensor whose input-output characteristic is shown in Fig. 100. The distorted sensor output shown in Fig. 101 is passed through an ideal low pass filter and the optimization-based recovery scheme

proposed is then used to recover the input signal. The fact that the recovered signal shown in Fig. 102 agrees with the actual input signal validates the proposed recovery procedure.

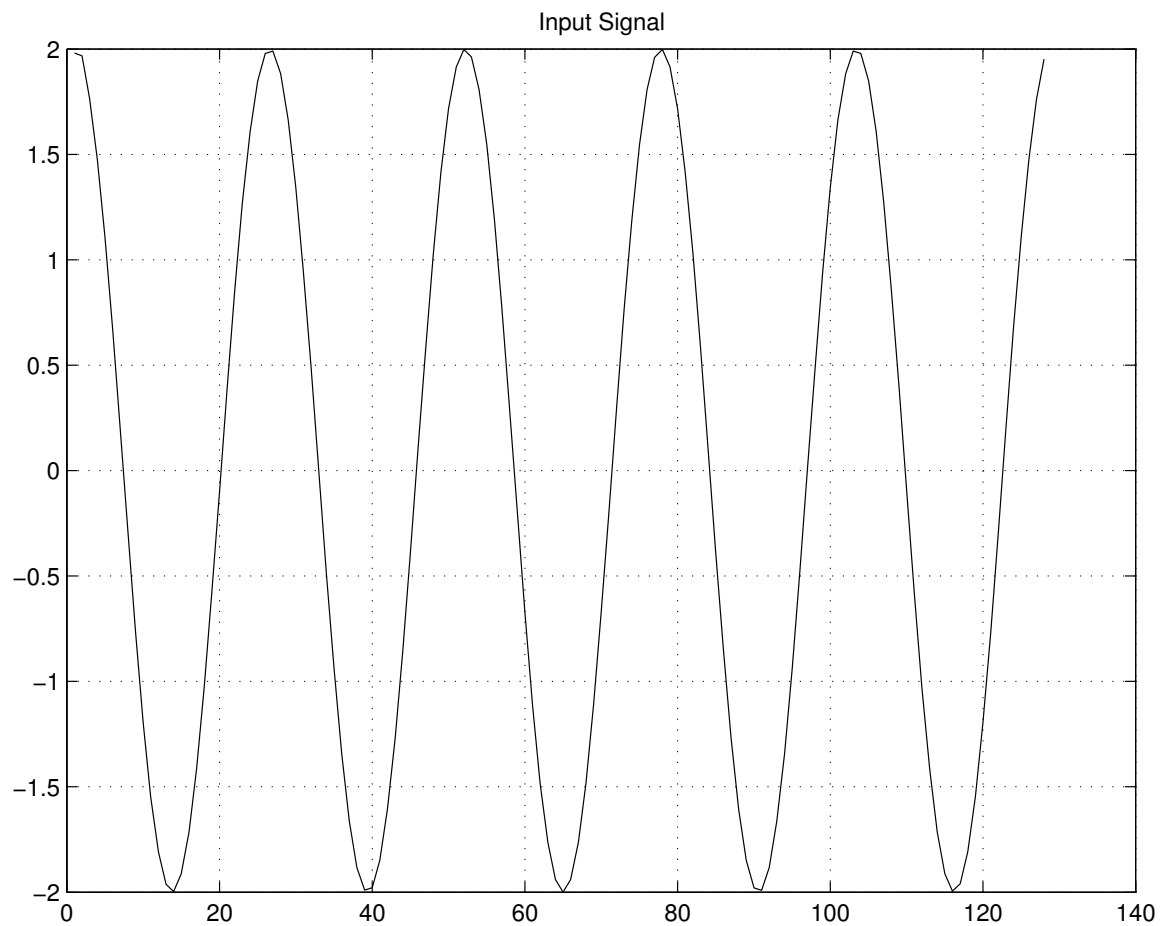


Figure 99: Input Signal Used in Subsection 7

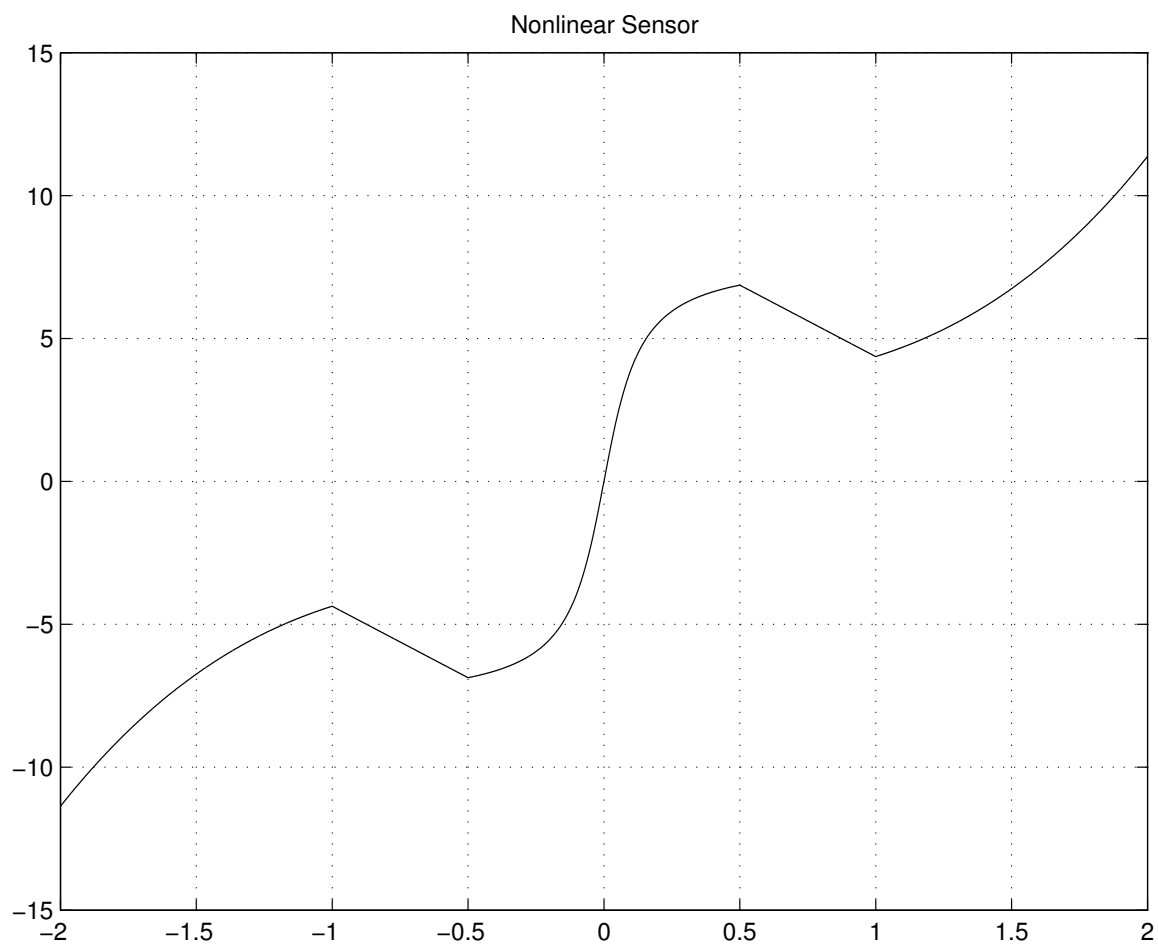


Figure 100: Non-monotonic Nonlinear Sensor

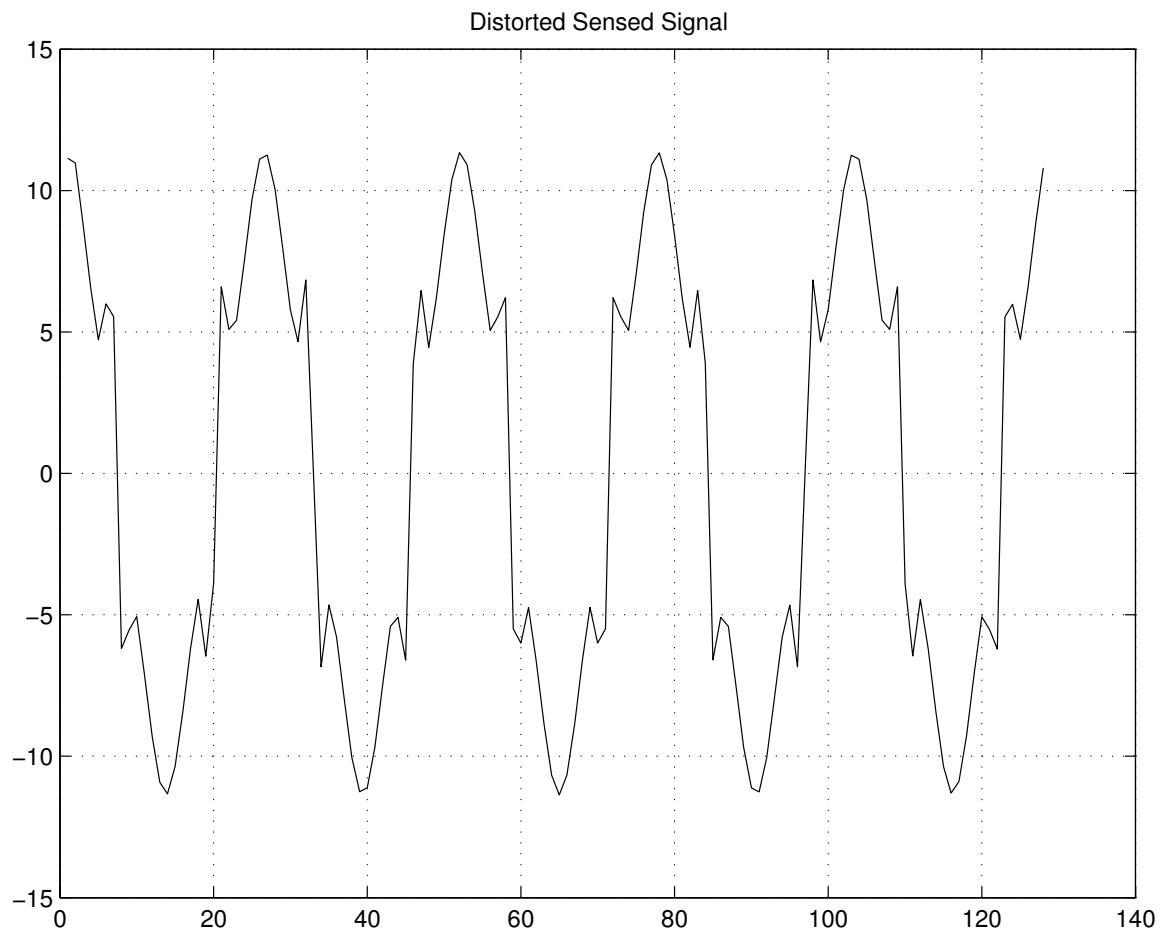


Figure 101: Distorted Sensed Signal

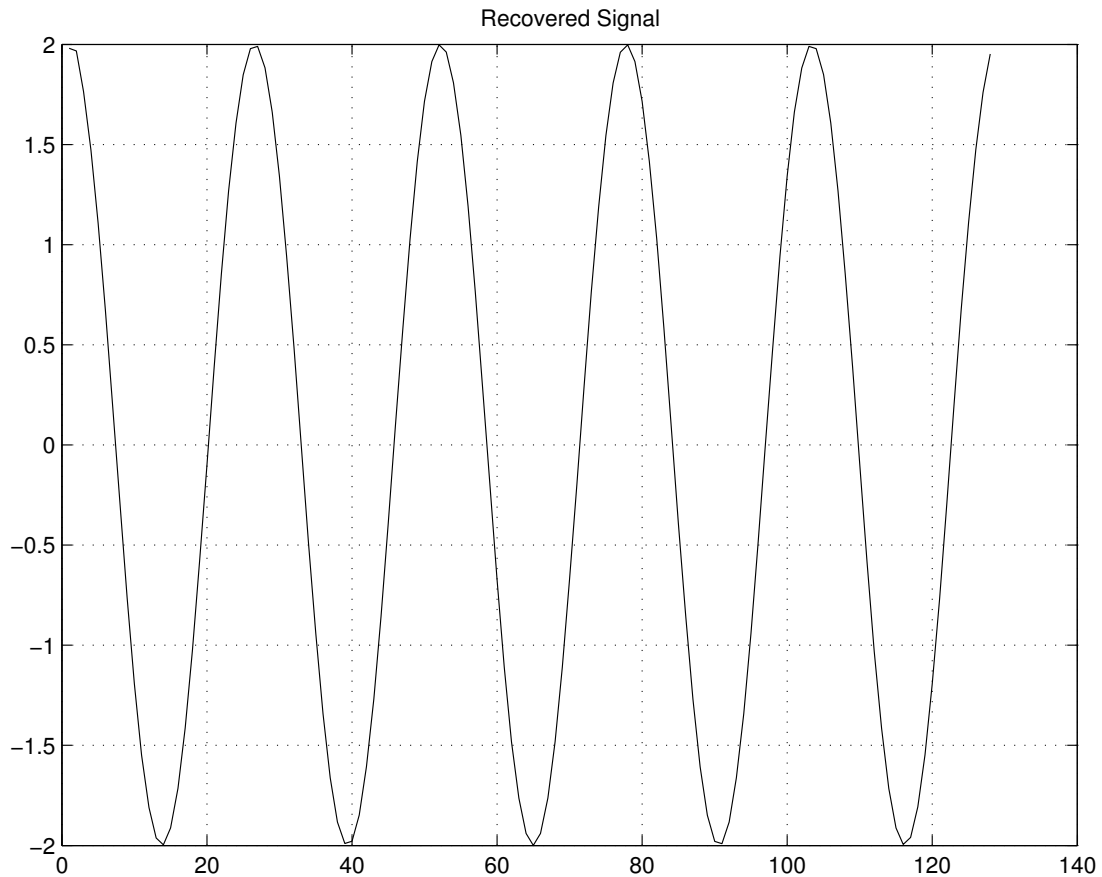


Figure 102: Recovered Signal from the Distorted Sensor Output

## 8. Recovery of Signals Distorted by Non-invertible Sensor Nonlinearity

In this subsection, the method presented in section J of chapter IV is further analyzed by illustrative examples.

### a. Simulation Example 1

To illustrate performance of the proposed non-quadratic optimization scheme, we will present a simulation example in this section. Consider the measurement of a signal shown in Fig. 103 through a nonlinear sensor whose input-output characteristics is



depicted in Fig. 105. The distorted sensor output is shown in Fig. 104. The different performance indices formulated in the previous section are optimized to obtain an estimate of the original signal.

$$J_{e_1} = \|z - \mathcal{F}^{-1}\{\mathcal{HF}\{g(y)\}\}\| \quad (7.3)$$

$$J_{q_1} = \|z - \mathcal{F}^{-1}\{\mathcal{HF}\{g(y)\}\}\| + \lambda_q \sum_{i=1}^N y_i^2 \quad (7.4)$$

$$J_{n_1} = \|z - \mathcal{F}^{-1}\{\mathcal{HF}\{g(y)\}\}\| + \lambda_n \sum_{i=1}^N |y_i|^{0.5} \quad (7.5)$$

where  $N$  is the number of samples of signal,  $y$ .

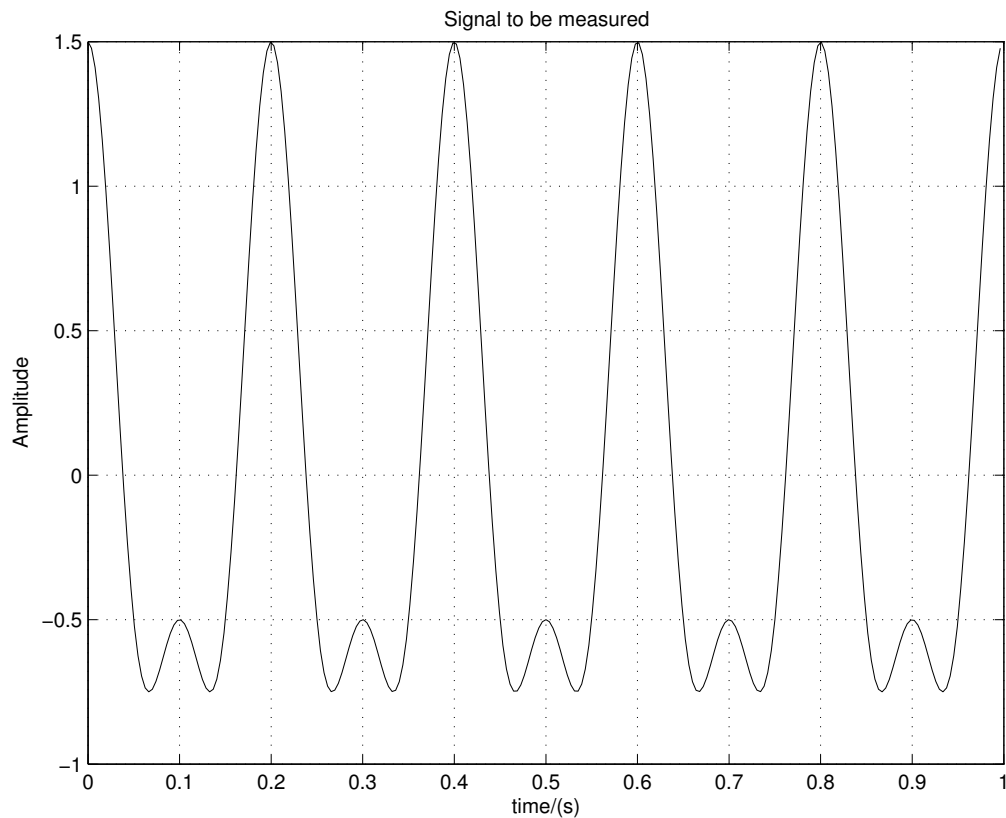


Figure 103: Signal to Be Estimated

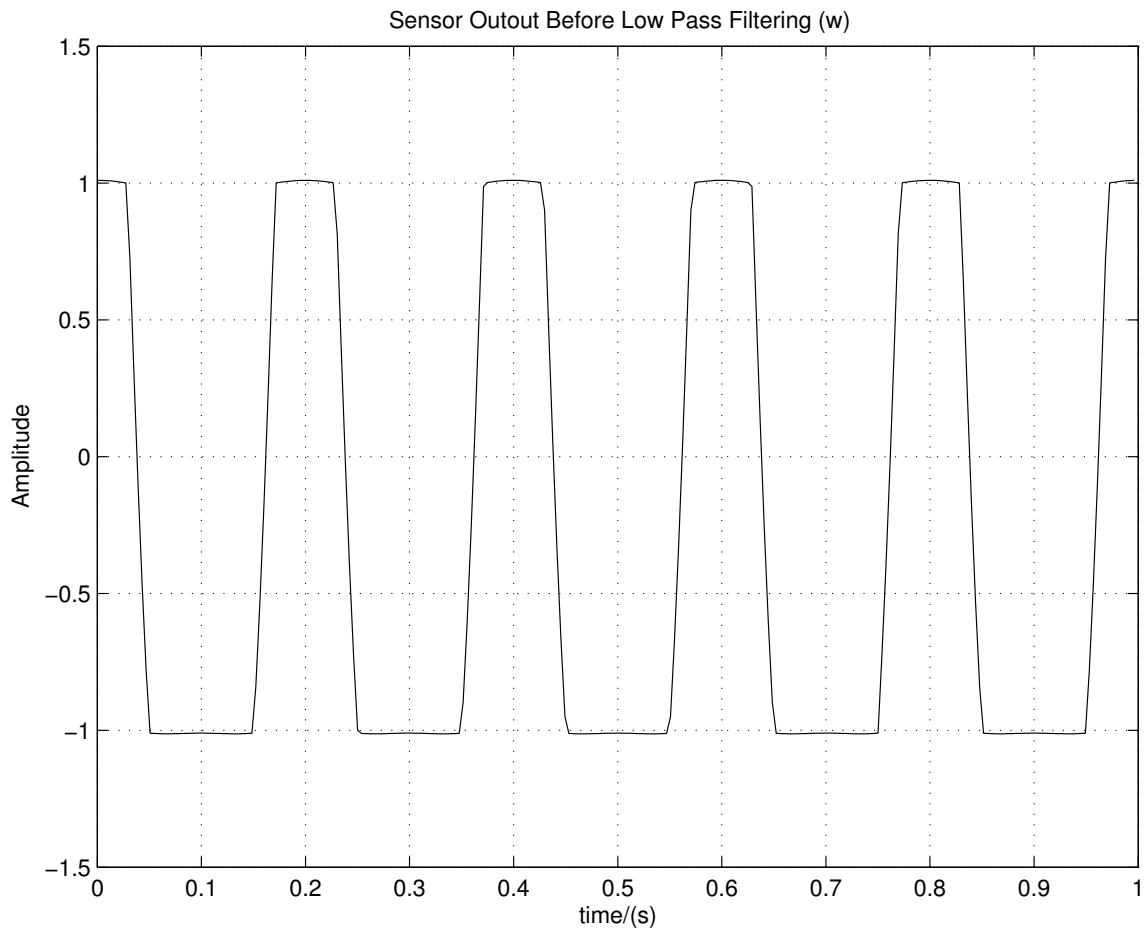


Figure 104: Sensor Output before Low Pass Filtering,  $w$

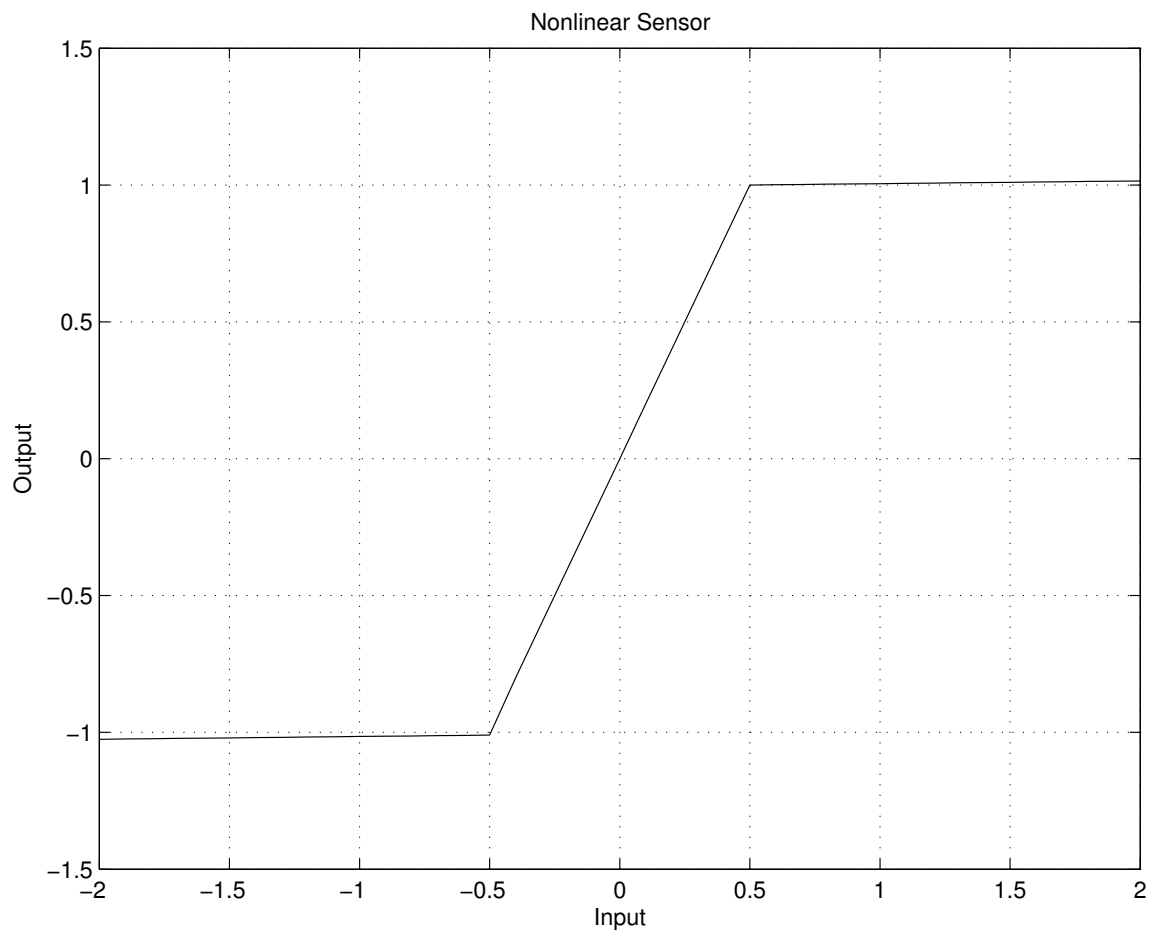


Figure 105: Non-invertible Nonlinear Sensor

Fig. 106, Fig. 107 and Fig. 108 show the signals recovered by optimizing the error function,  $J_{e1}$ , quadratic cost function,  $J_{q1}$  and non-quadratic cost function,  $J_{n1}$ , respectively. A simple comparison with the actual data clearly demonstrates that the signal obtained with non-quadratic criteria is the closest to the actual data.

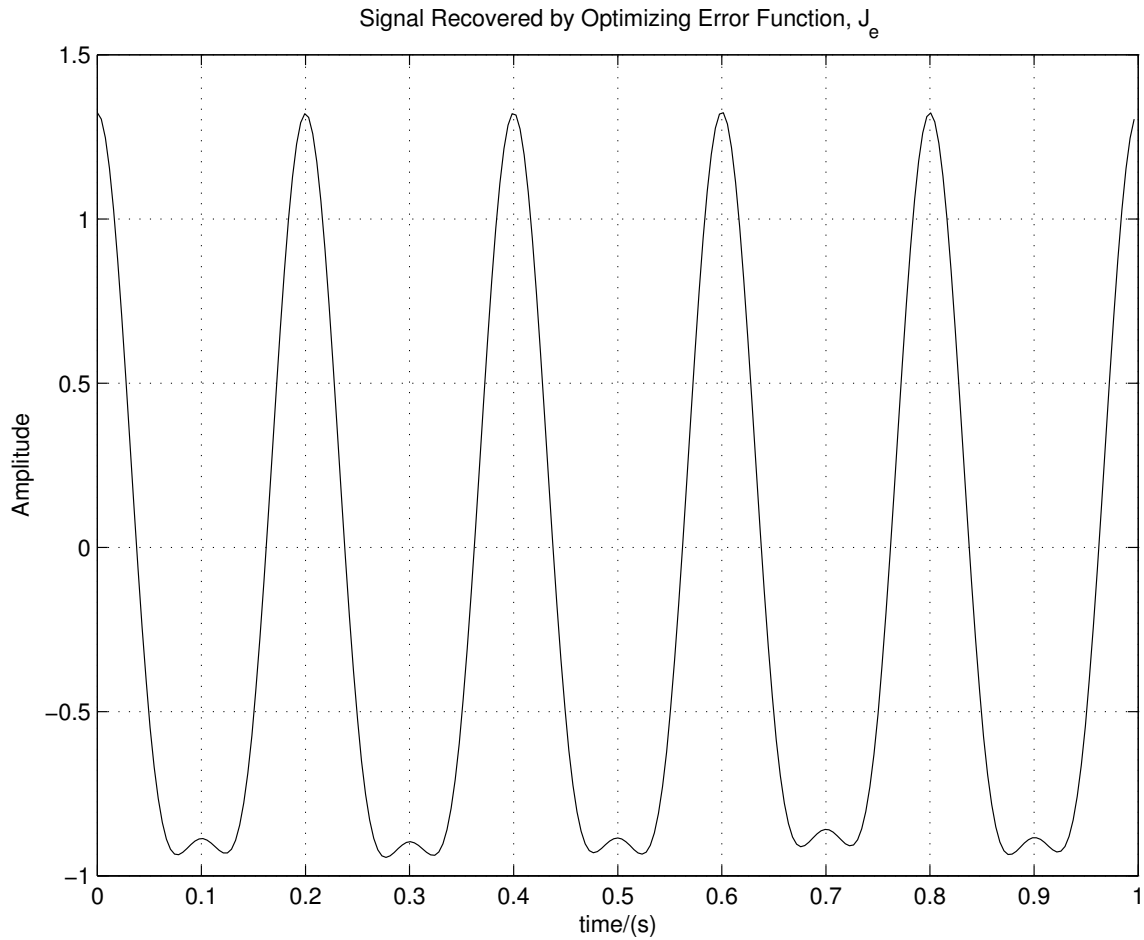


Figure 106: Signal Recovered by Optimizing Quadratic Error Function,  $J_{e1}$

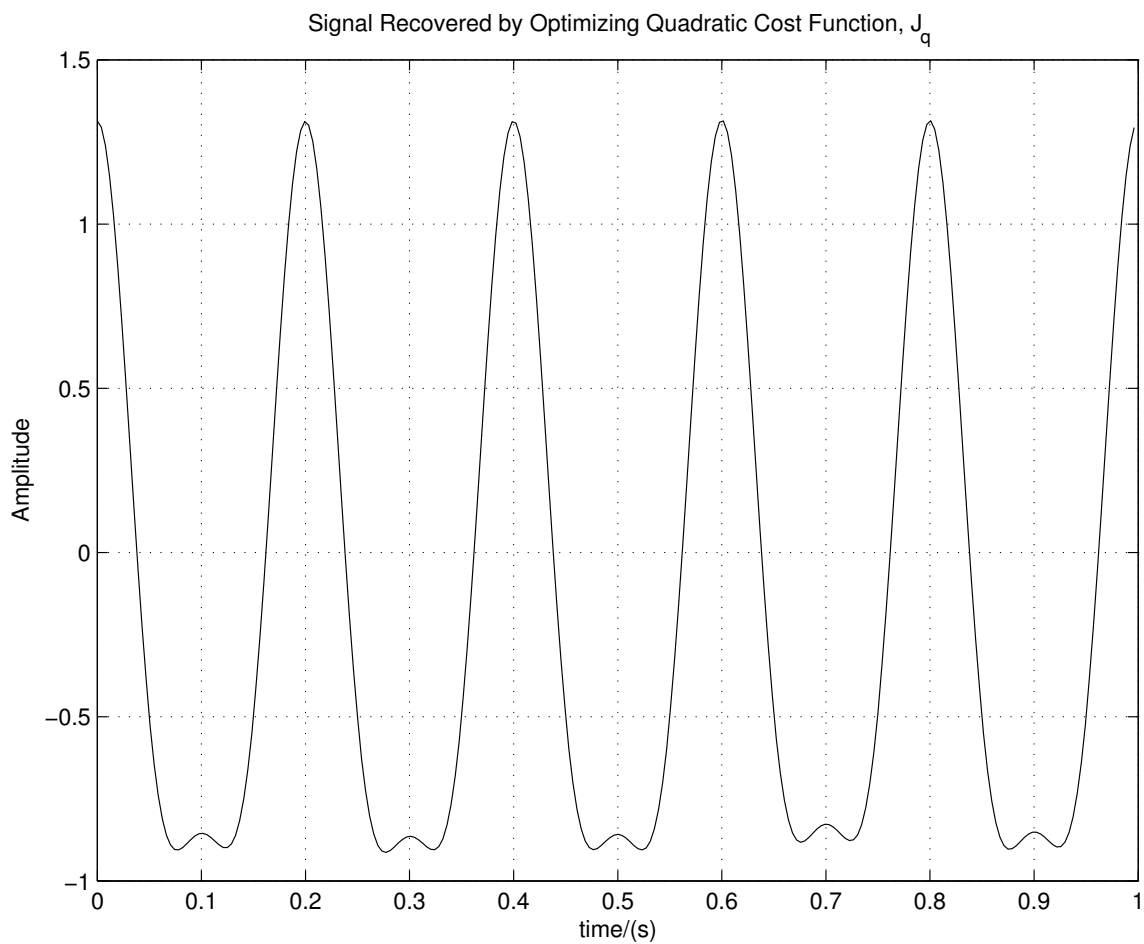


Figure 107: Signal Recovered by Optimizing Quadratic Cost Function,  $J_{q1}$

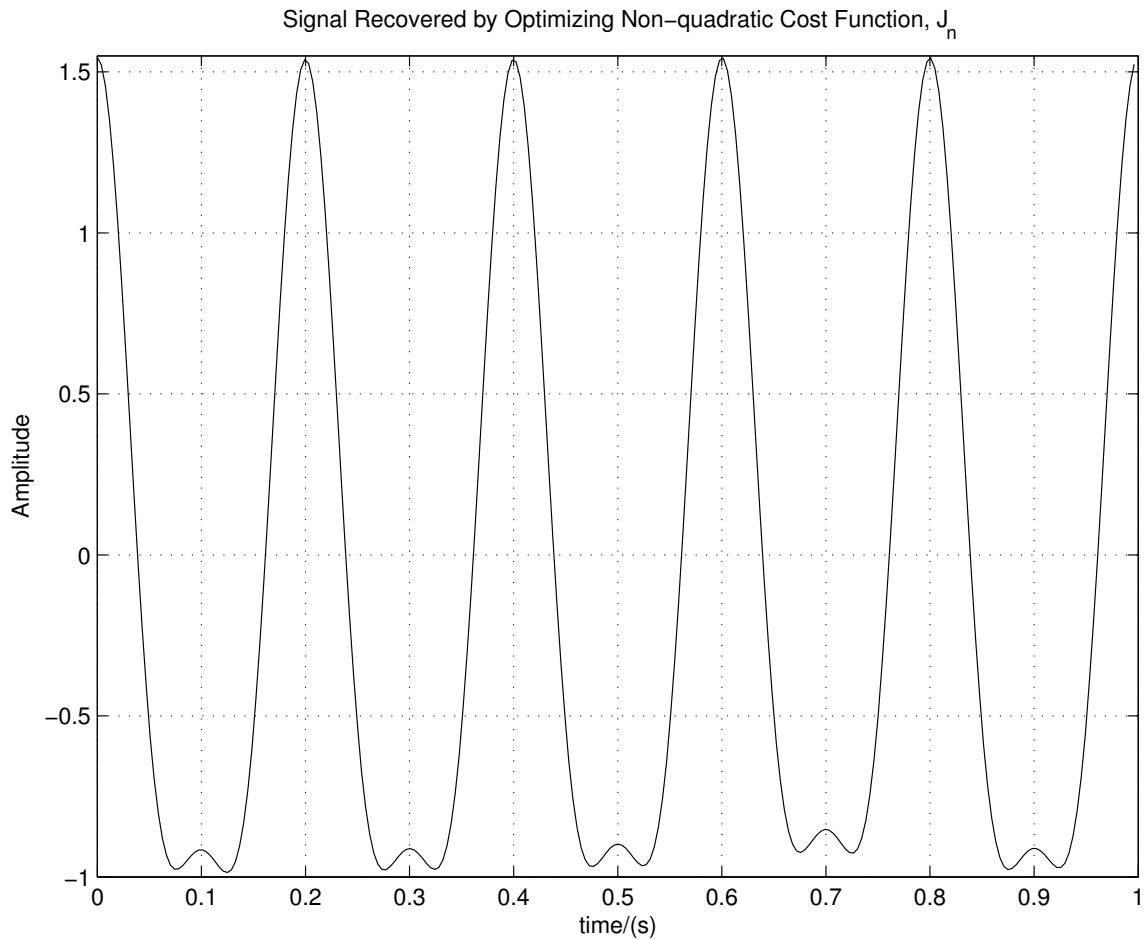


Figure 108: Signal Recovered by Optimizing Non-quadratic Cost Function,  $J_{n_1}$

b. Simulation Example 2

We will present another example to further demonstrate performance of the proposed scheme. The signal to be measured and its frequency spectrum are shown in Fig. 109 and Fig. 110 respectively. We will use the same nonlinear sensor, which is used in the previous example. The distorted sensor output and its frequency spectrum are shown in Fig. 111 and Fig. 112.

The following performance indices are derived to obtain the actual signal.

$$J_{q_2} = \|z - \mathcal{F}^{-1}\{\mathcal{HF}\{g(y)\}\}\| + \lambda_q \sum_{i=1}^N y_i^2 \quad (7.6)$$

$$J_{n_2} = \|z - \mathcal{F}^{-1}\{\mathcal{HF}\{g(y)\}\}\| + \lambda_n \sum_{i=1}^N |y_i|^{0.1} \quad (7.7)$$

where  $N$  is the number of samples of signal,  $y$  and  $\lambda_q$  and  $\lambda_n$  are weights on quadratic and non-quadratic penalties respectively.

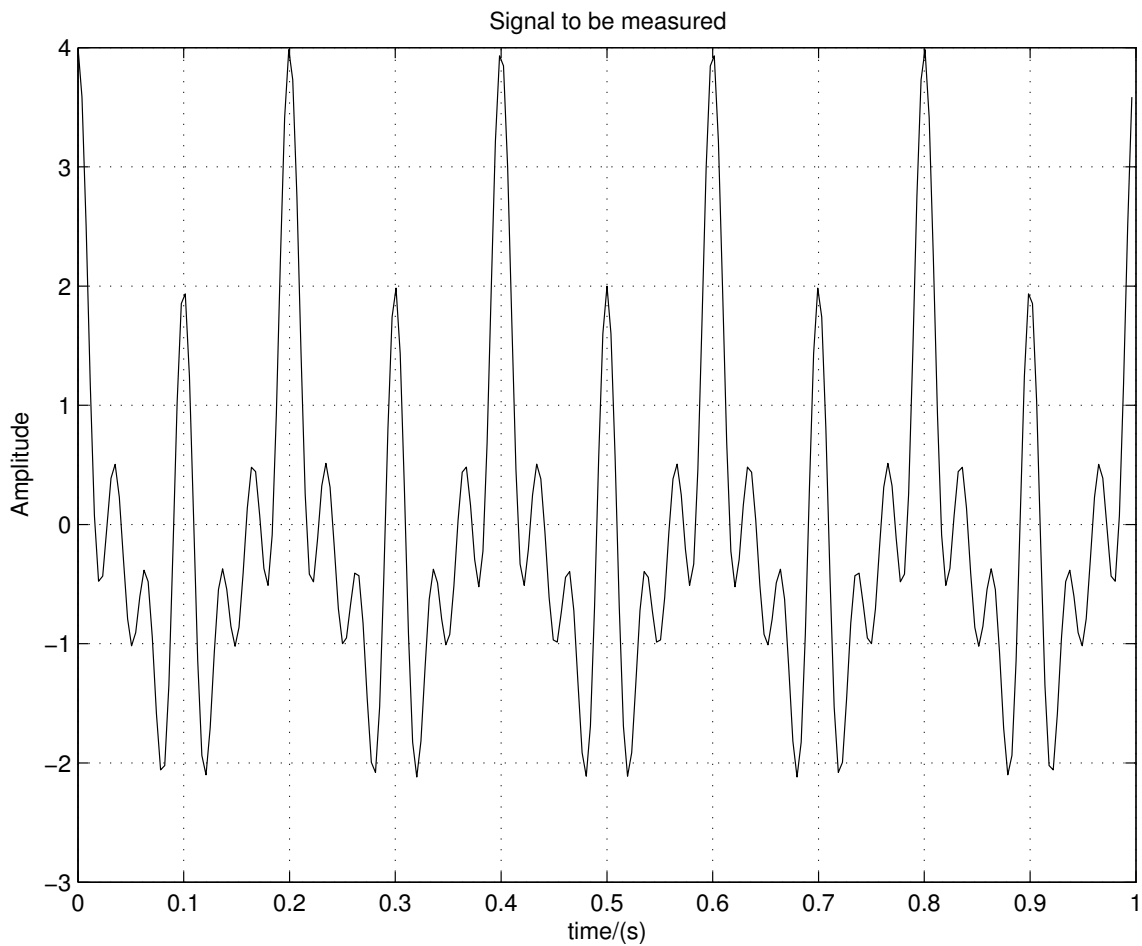


Figure 109: Signal to Be Measured

The signal recovered by minimizing the quadratic criteria,  $J_{q_2}$  and its frequency spectrum are shown in Fig. 113 and Fig. 115 respectively. Fig. 114 and Fig. 116 show the signal recovered by optimizing the non-quadratic criteria,  $J_{n_2}$  and its spectrum respectively. By filtering out the low strength or insignificant frequency components appearing in Fig. 115 and Fig. 116, we will obtain signals shown in Fig. 117 and Fig. 118, which are the solutions to the quadratic and non-quadratic criteria respectively. Clearly, the signal obtained using the non-quadratic criteria is more accurate than that of quadratic performance index.

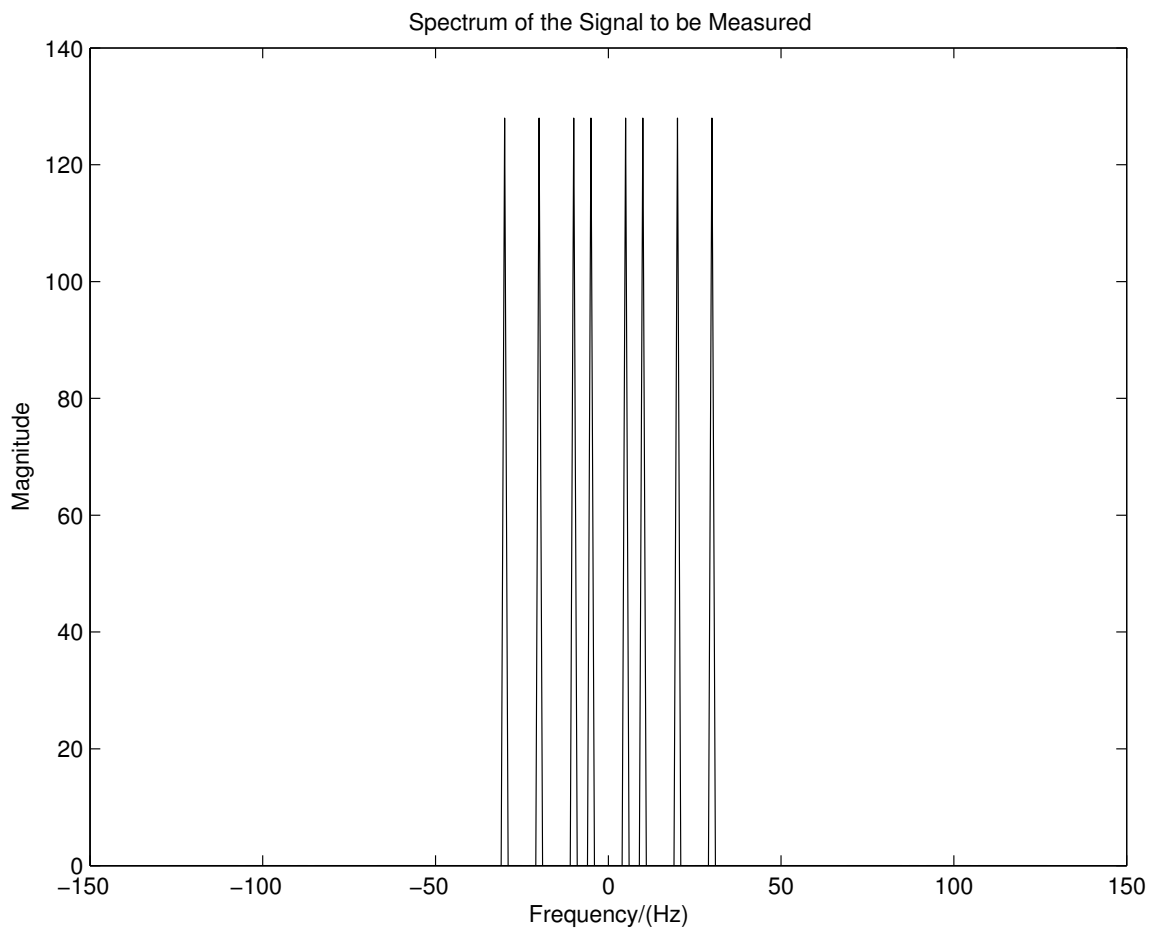


Figure 110: Spectrum of the Signal to Be Measured



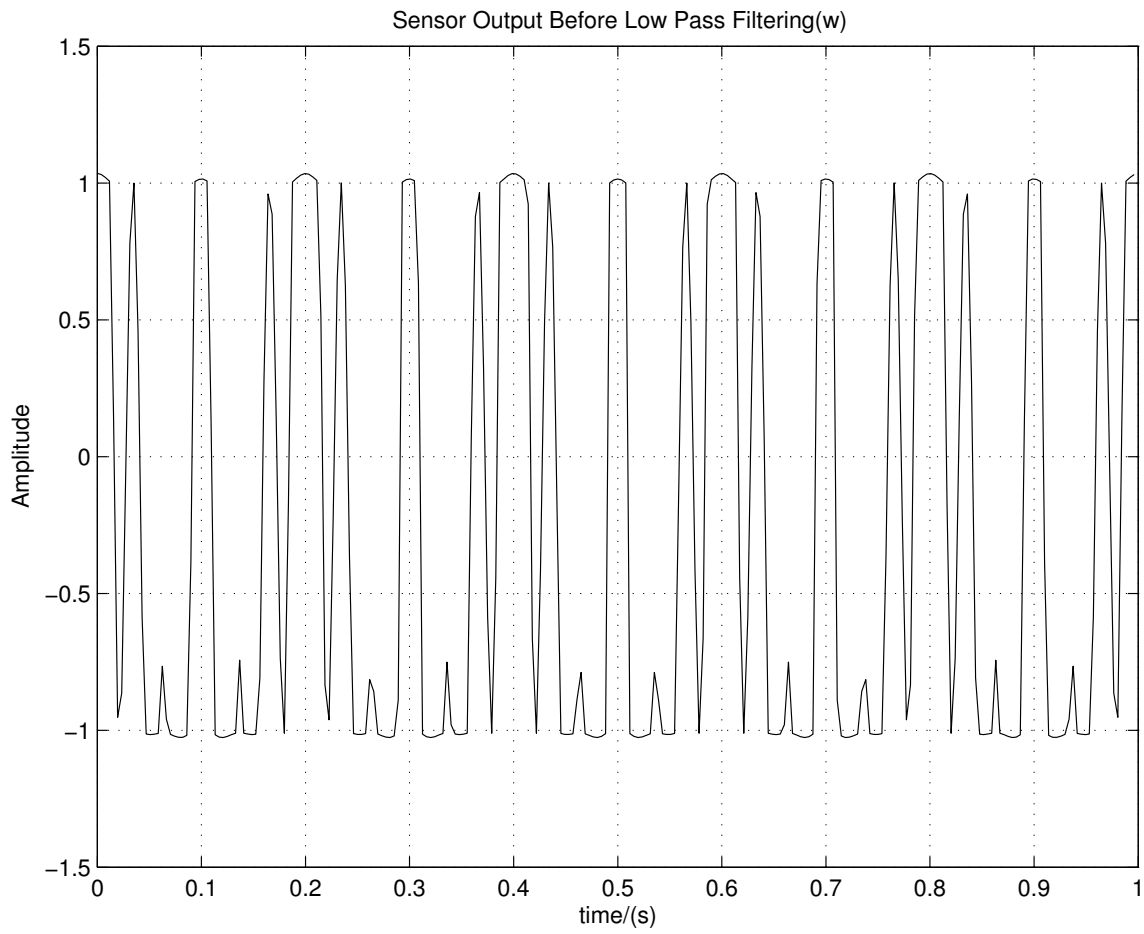


Figure 111: Signal Output Before Low Pass Filtering

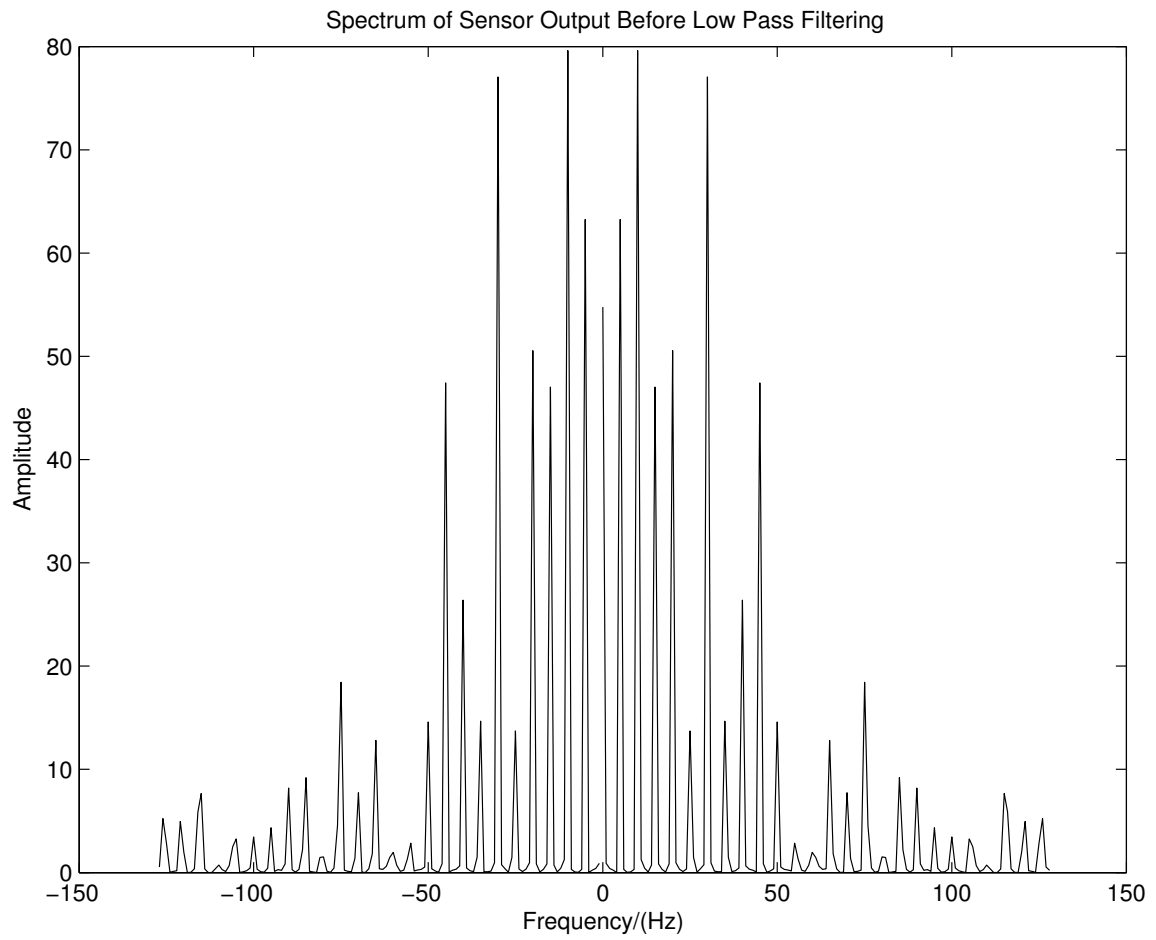


Figure 112: Spectrum of the Sensor Output before Low Pass Filtering

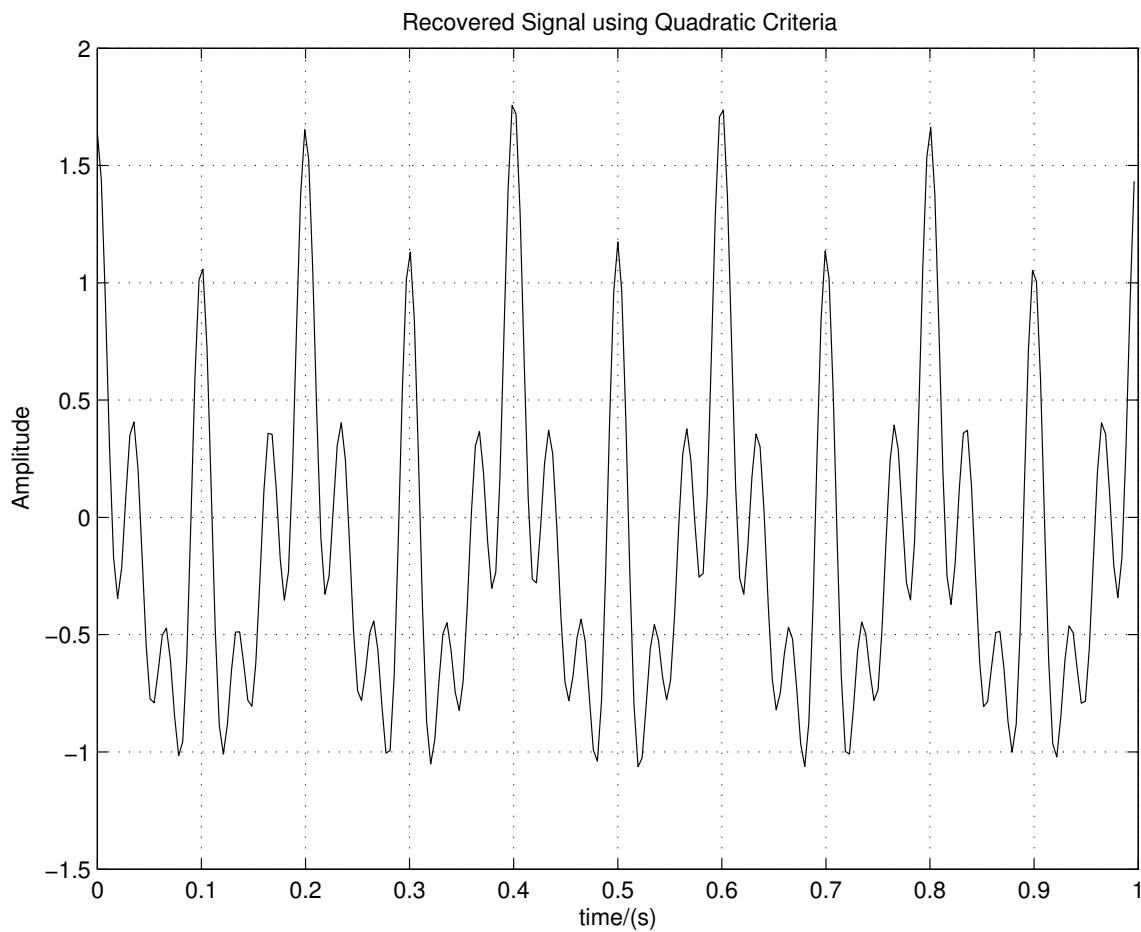


Figure 113: Signal Recovered by Optimizing Quadratic Cost Function,  $J_{q2}$

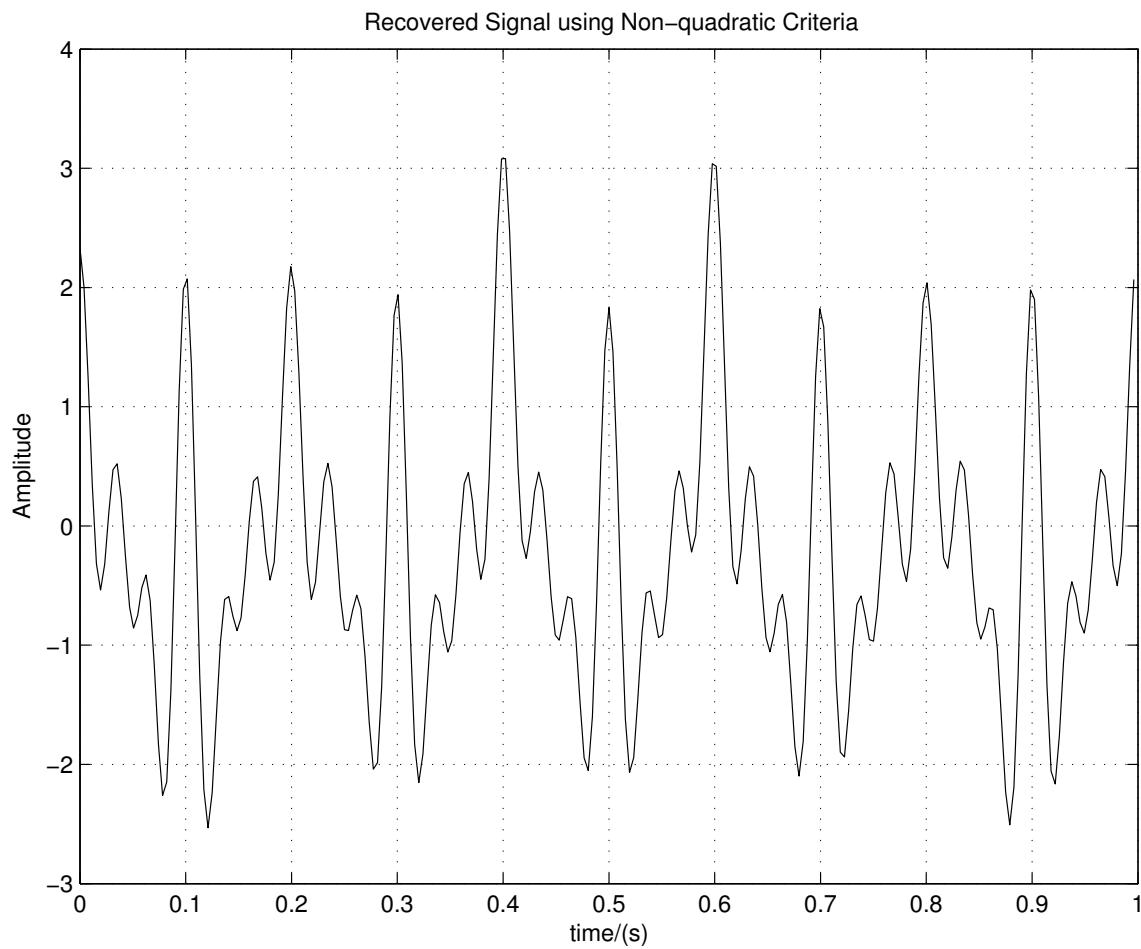


Figure 114: Signal Recovered by Optimizing Non-quadratic Cost Function,  $J_{n_2}$

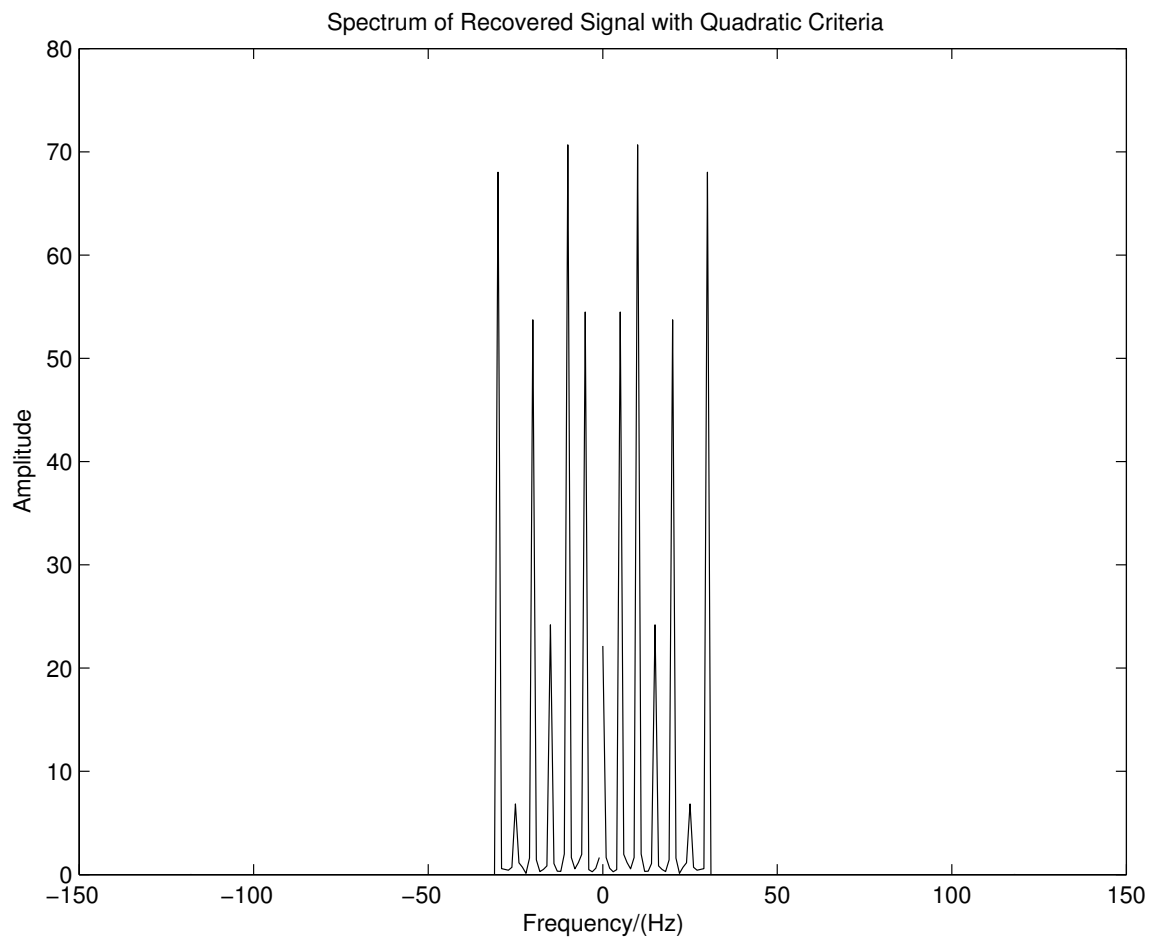


Figure 115: Spectrum of Signal Recovered by Optimizing Quadratic Cost Function,  $J_{q_2}$

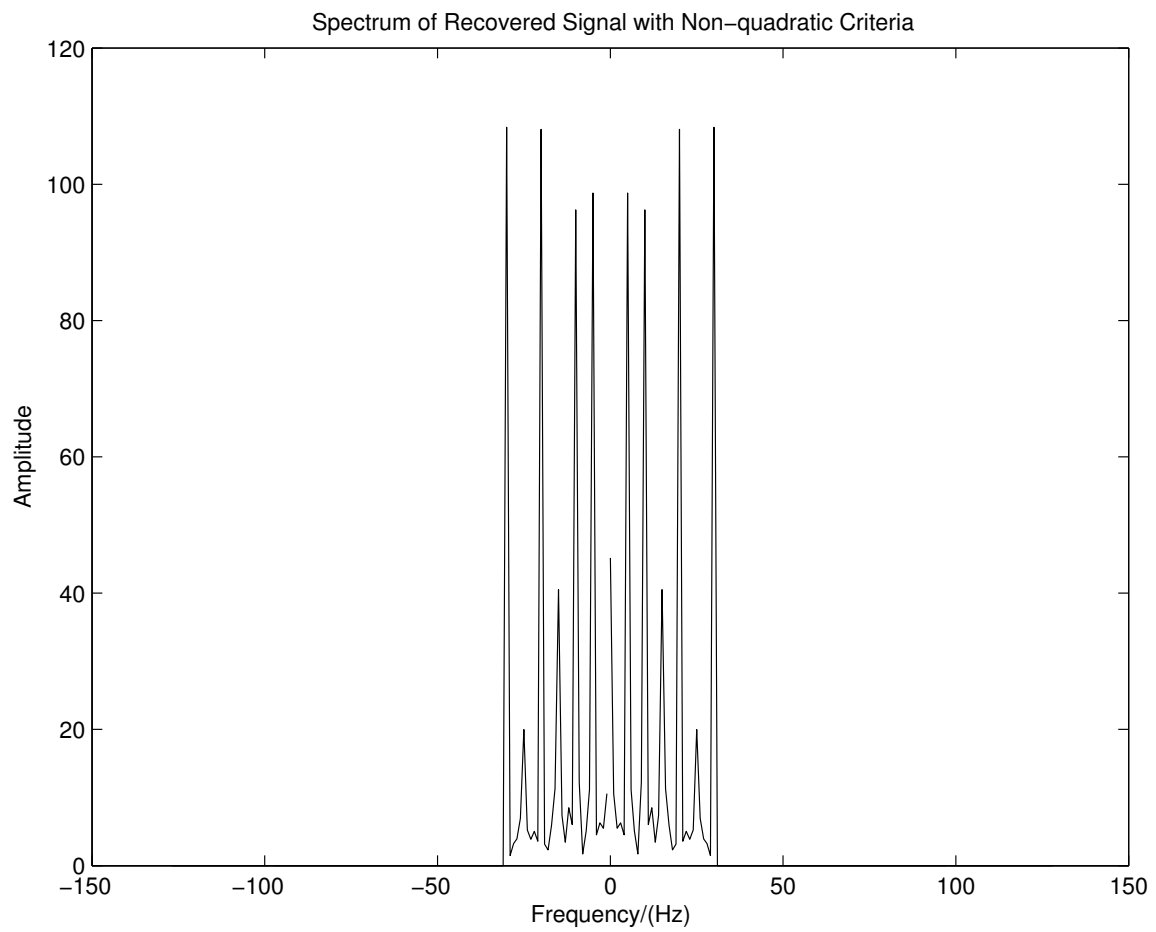


Figure 116: Spectrum of Signal Recovered by Optimizing Non-quadratic Cost Function,  $J_{n_2}$

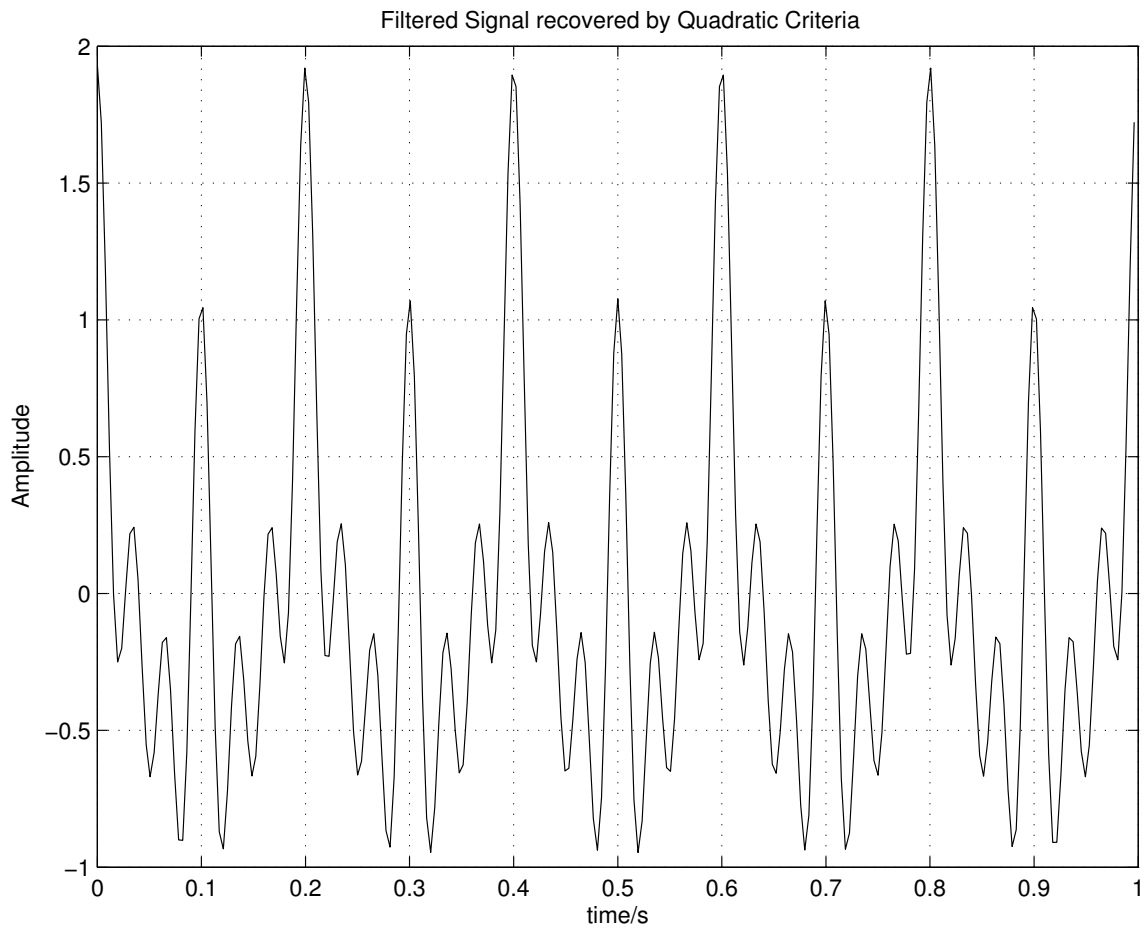


Figure 117: Signal Recovered by Quadratic Criteria ( $J_{q_2}$ )(after Filtering out Insignificant Frequency Components)

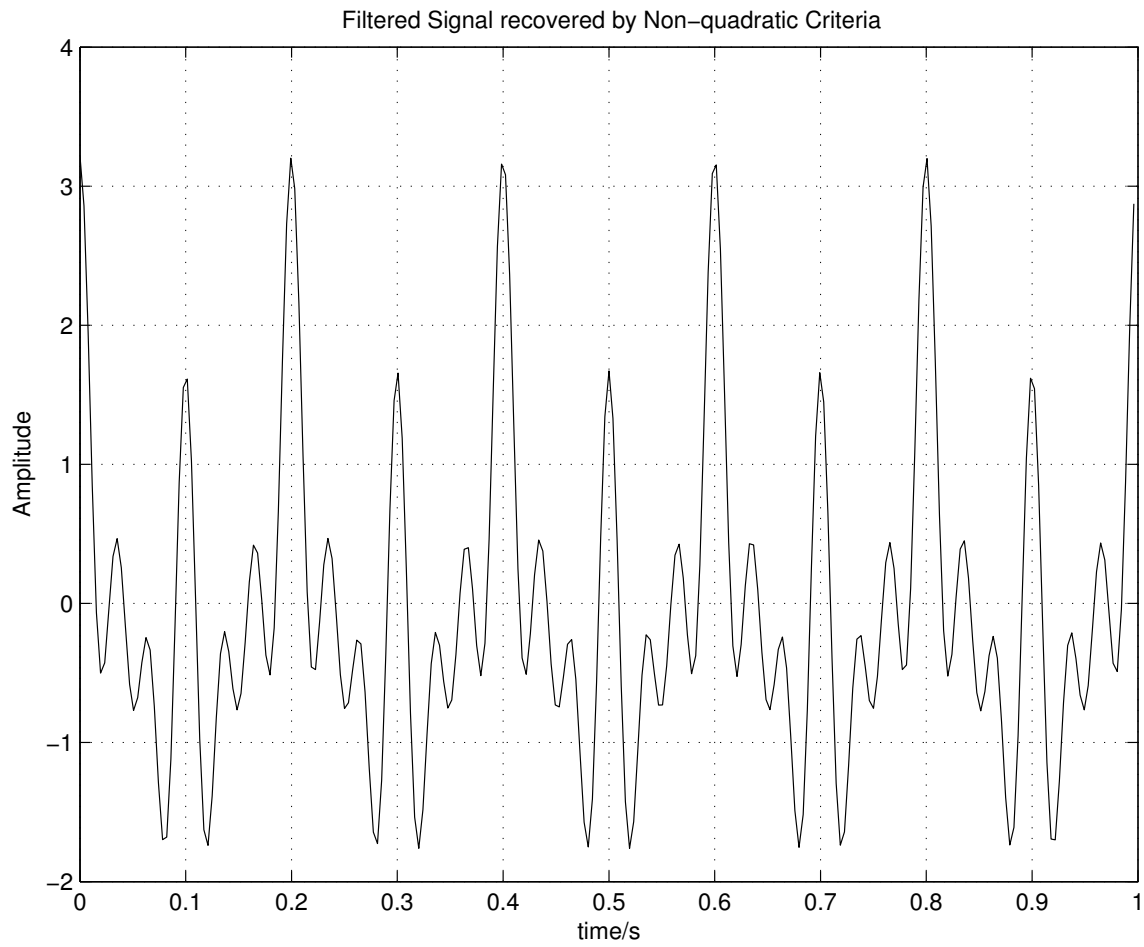


Figure 118: Signal Recovered by Non-quadratic Criteria, ( $J_{n_2}$ ) (after Filtering out Insignificant Frequency Components)

## B. Fusion of Distorted Multi-sensor Data

This section is concerned with the analysis of the sensor fusion schemes developed in chapter V.



### 1. Fusion of Distorted Data by Sensor Scheduling

This subsection further analyzes the sensor scheduling scheme presented in section A of chapter V. Consider a multi-sensor fusion problem with three sensors. A signal  $y$  shown in Fig. 119 is measured through three different nonlinear sensors and distorted sensor outputs are then filtered using ideal low pass filters. The filtered signals are used to recover the original signal using the sensor recovery procedure. The next task is to fuse three recovered signals to obtain the best approximation to the original signal. We will show how the derived fusion procedure could be used to do this.

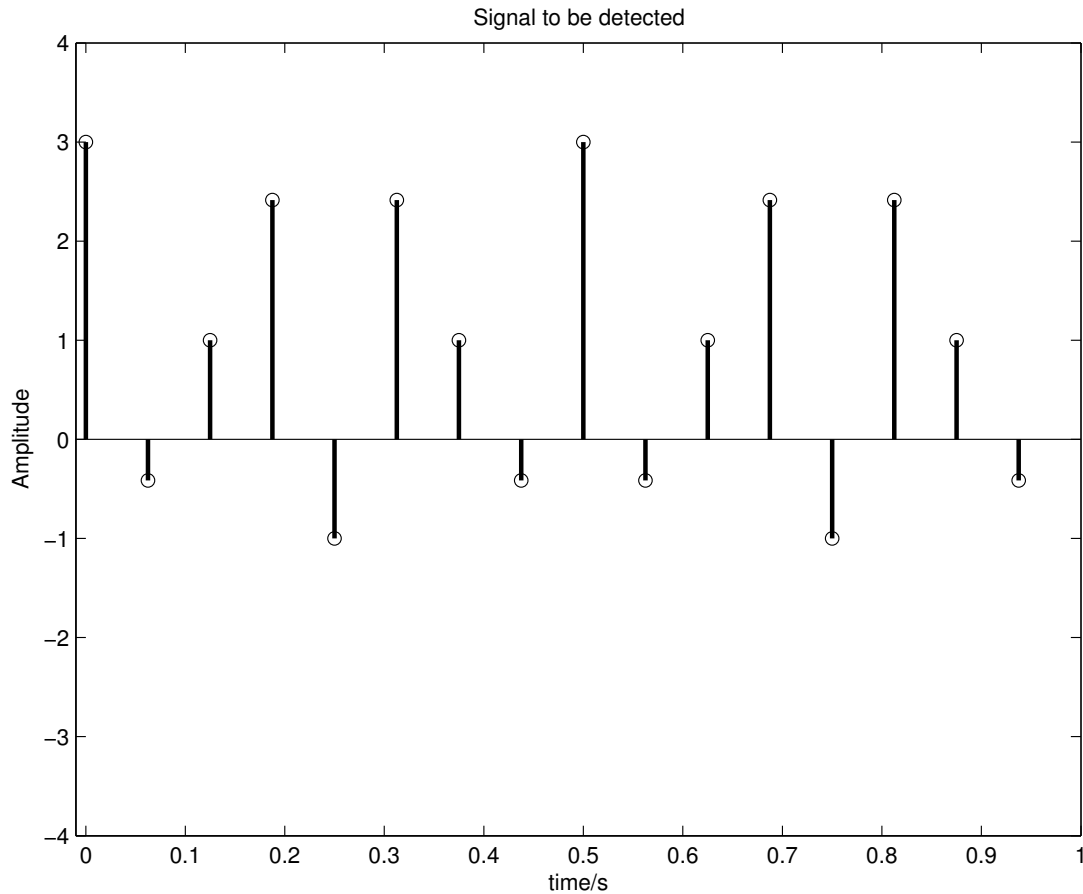


Figure 119: Original Signal  $y$  Used to Demonstrate the Sensor Scheduling Scheme

To demonstrate the performance of Algorithm 4 in providing the accurate sensor schedule, the original signal data is split into three and distributed among three data sets which are otherwise random sets as shown in Fig. 120, Fig. 121 and Fig. 122. The distribution of original information is done in such a way that it is hidden in three sets and could only be retrieved by any smart algorithm to reproduce the original signal. Let these data sets be recovered signals  $v_1$ ,  $v_2$  and  $v_3$ .

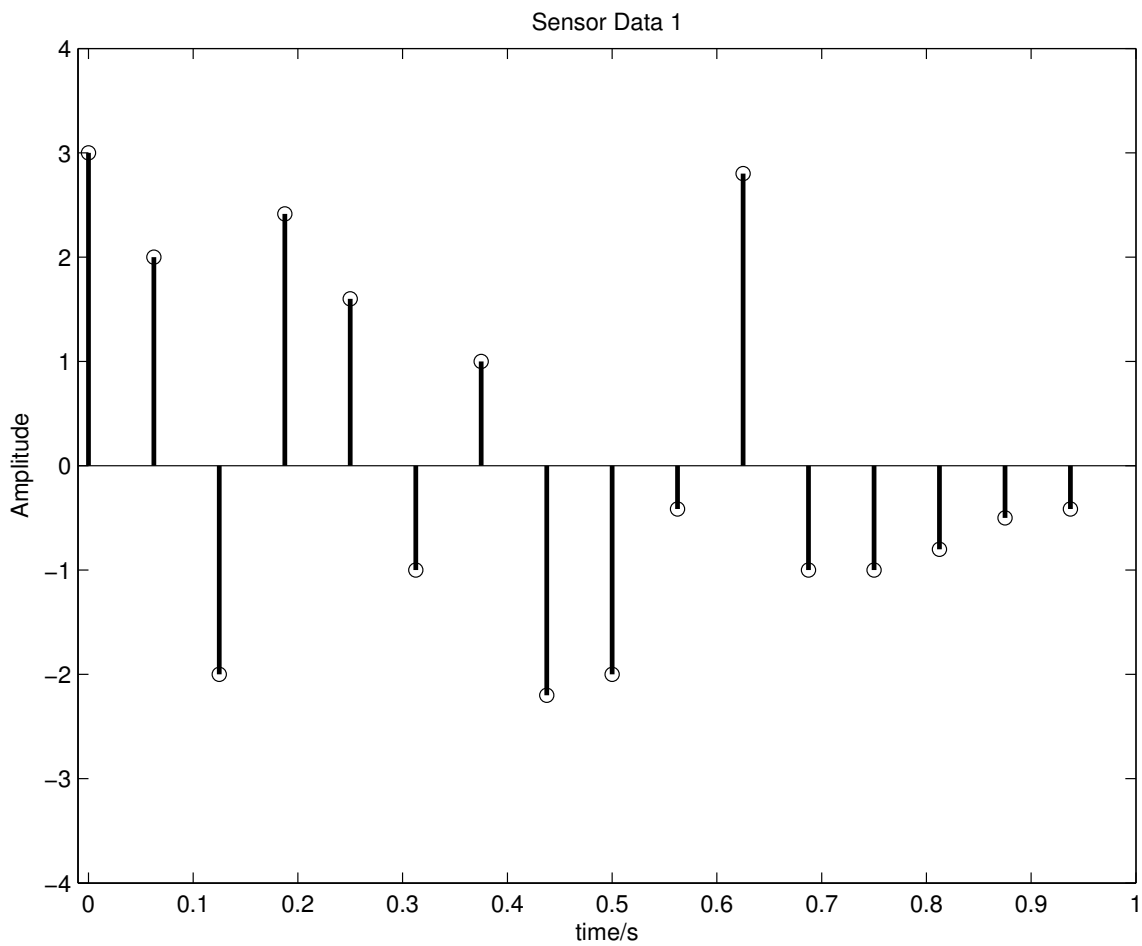


Figure 120: Sensor Data 1 Used to Demonstrate Sensor Scheduling Scheme

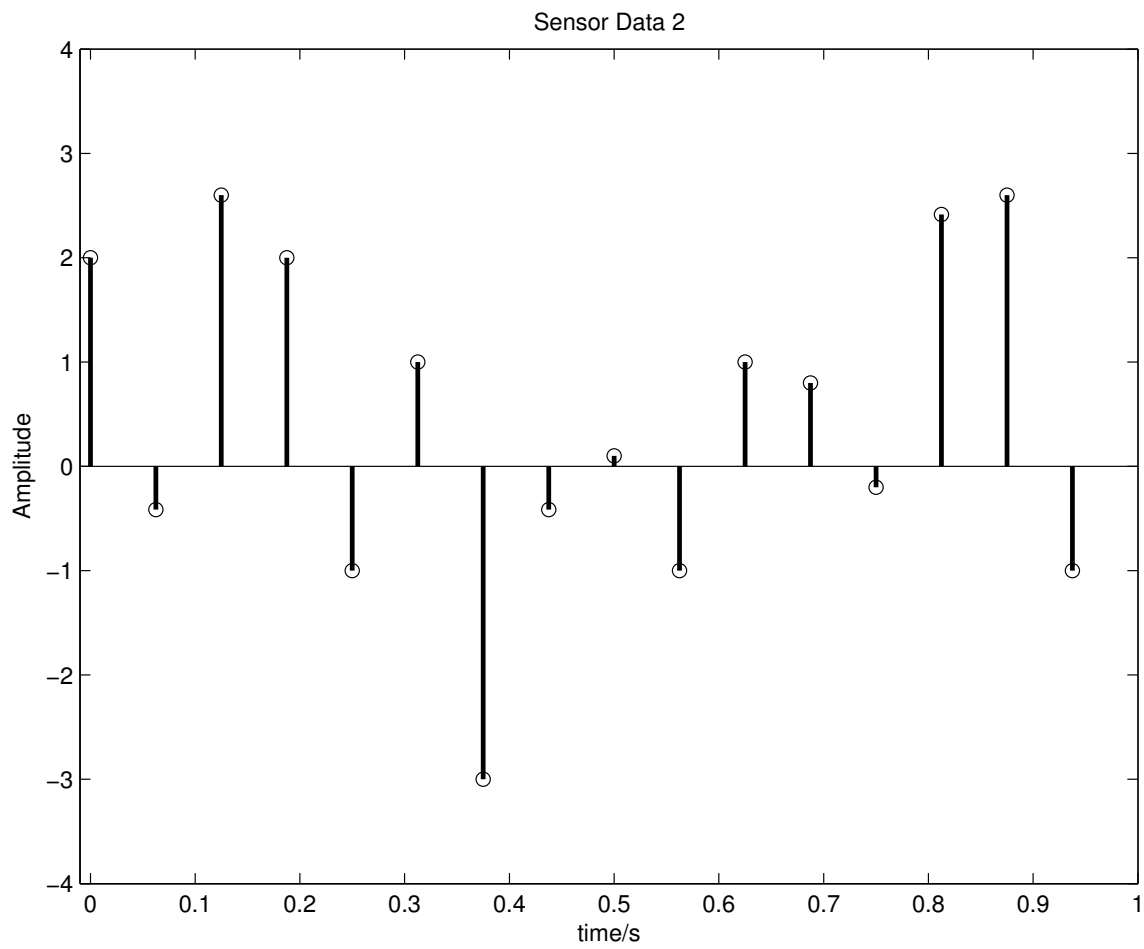


Figure 121: Sensor Data 2 Used to Demonstrate Sensor Scheduling Scheme

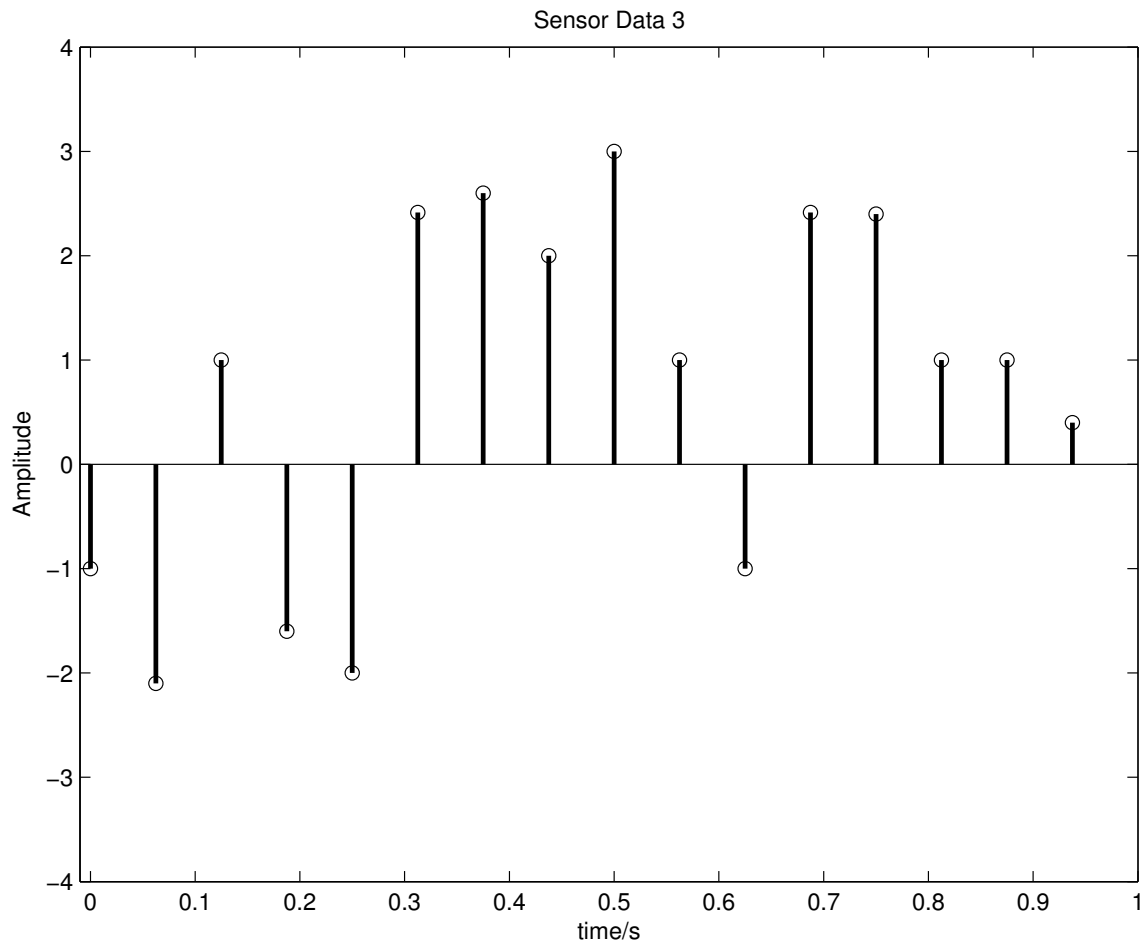


Figure 122: Sensor Data 3 Used to Demonstrate Sensor Scheduling Scheme

Let us use the sensor function shown in Fig. 123 to generate the filtered signal depicted in Fig. 124.

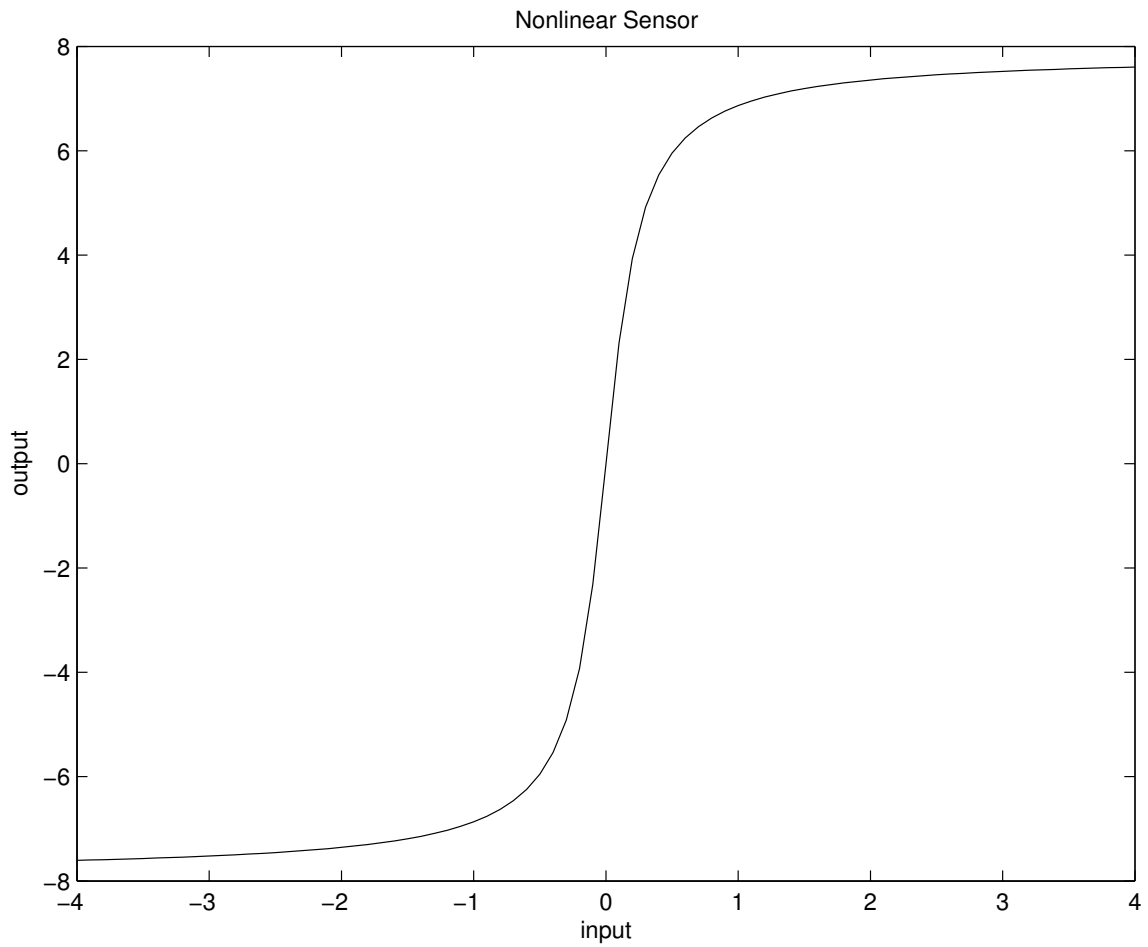


Figure 123: Nonlinear Sensor Function

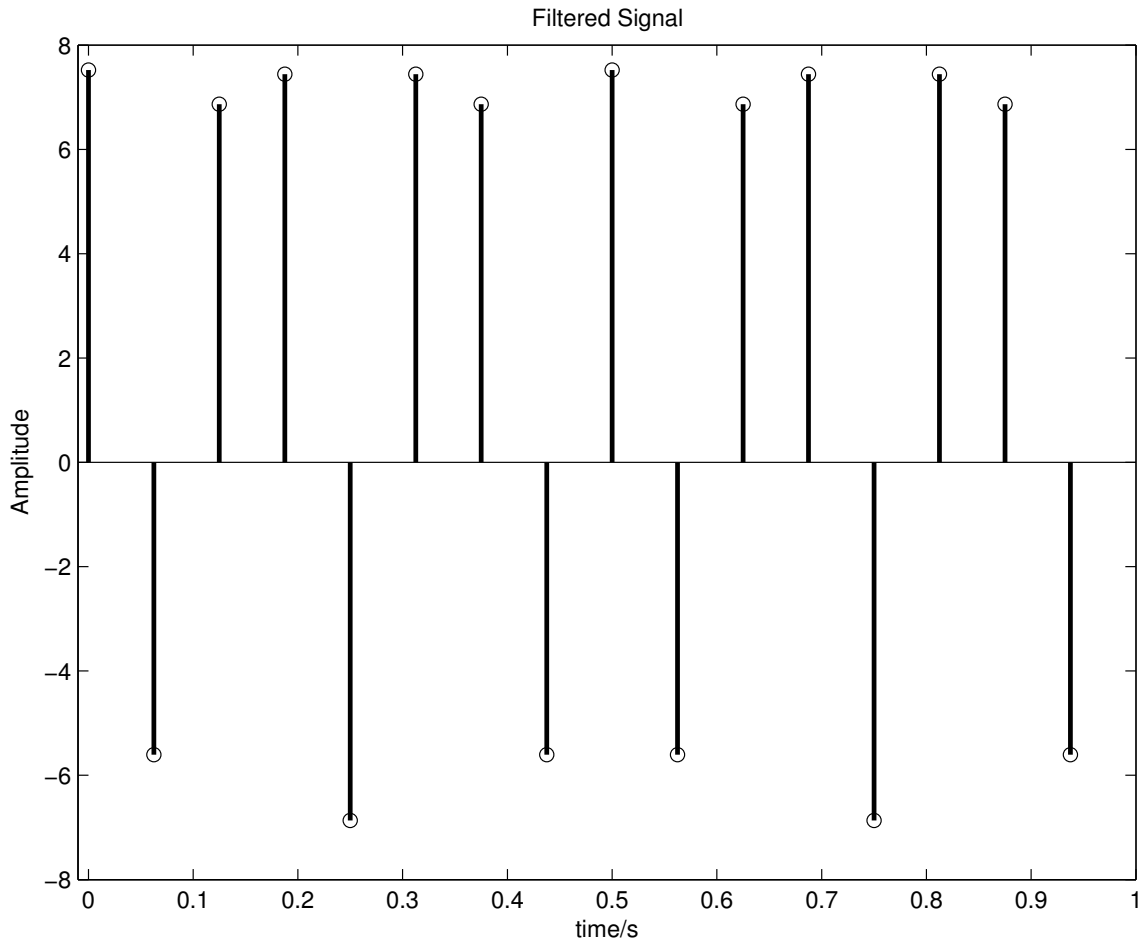


Figure 124: Filtered Signal  $z$  of Nonlinear Sensor Shown in Fig. 123

Let the fused signal be

$$y_r = \Phi_1 v_1 + \Phi_2 v_2 + \Phi_3 v_3 \quad (7.8)$$

We now apply Algorithm 4 to obtain the sensor schedule and the result is shown in Fig. 125. Using this schedule  $\theta$ , the fused signal  $y_r$  is constructed and shown in Fig. 126. It is noted that the original signal is reproduced, which demonstrates the fact that the switching between sensors is done as desired and thus the fused signal is

exactly same as the original. The exact original signal recovery is further guaranteed by the zero cost function value at optimal conditions.

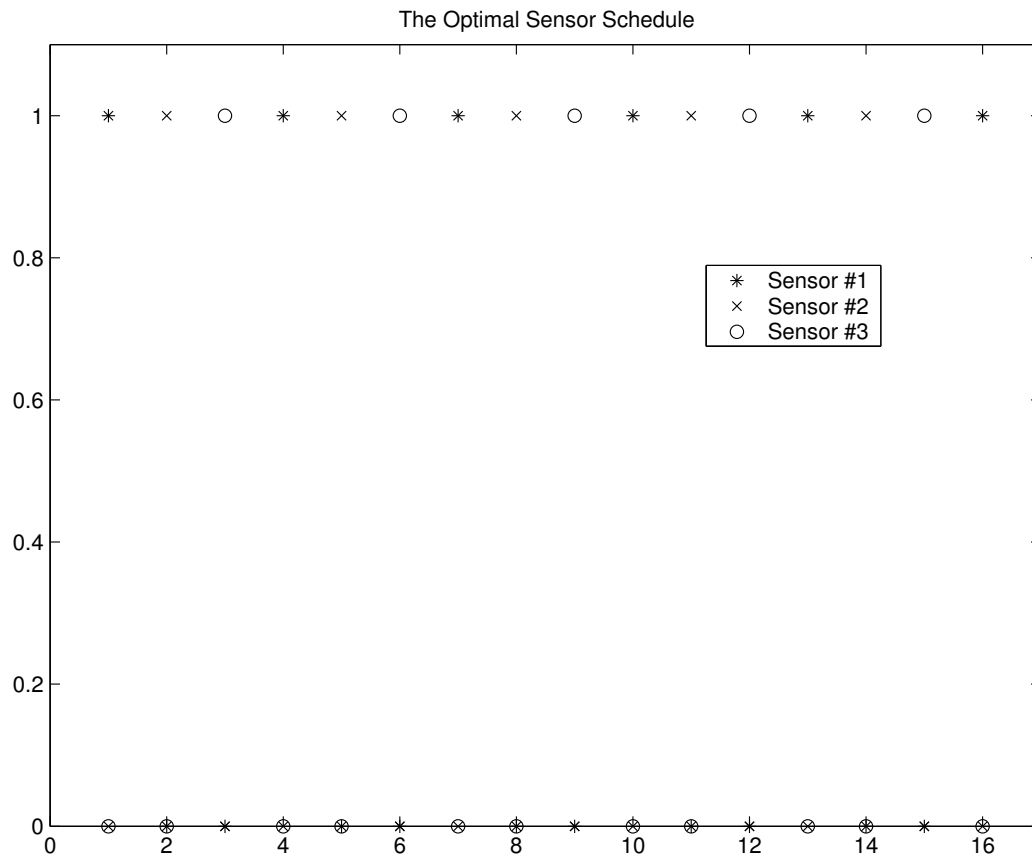
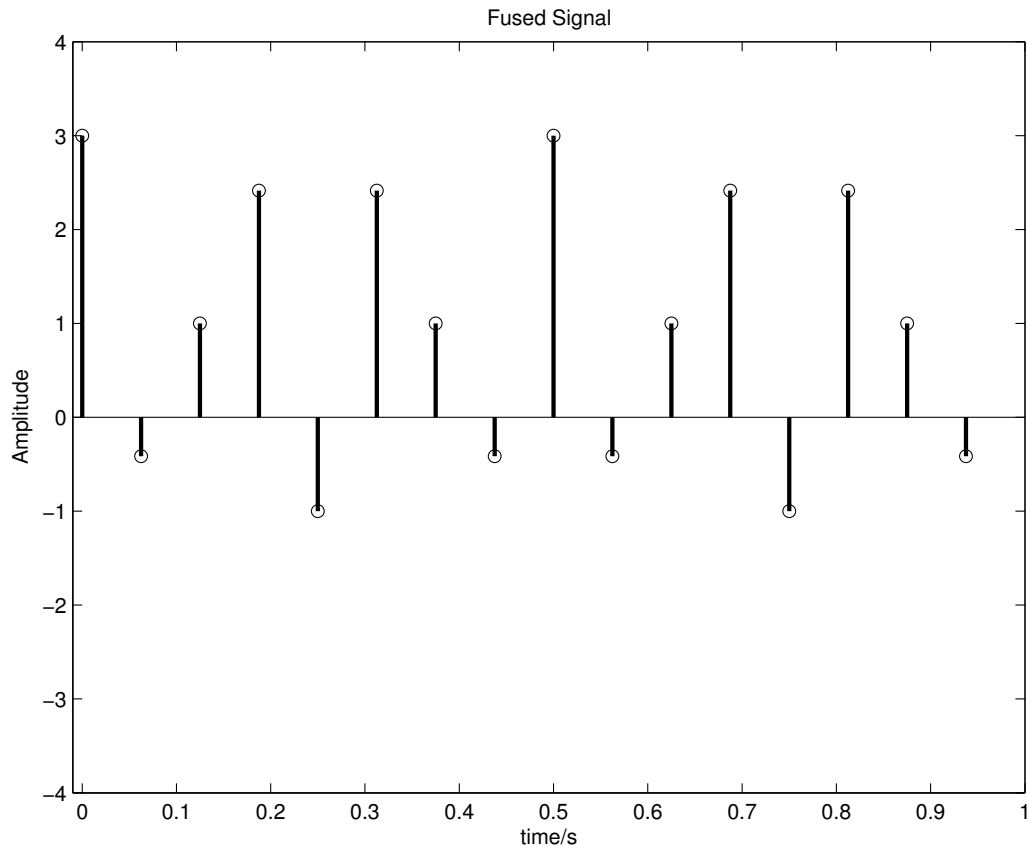


Figure 125: Optimal Sensor Schedule, 0 and 1 Are Used to Denote off and on Positions Respectively

Figure 126: Fused Signal  $y_r$ 

## 2. Fusion of Distorted Data by Continuous Optimization

This subsection presents evidence to validate the claim made in section B of chapter V. Consider a multi-sensor fusion problem with three sensors. A signal  $y$  shown in Fig. 127 is measured through three different nonlinear sensors and distorted sensor outputs are then filtered using ideal low pass filters. The filtered signals are used to recover the original signal using the sensor recovery procedure. The next task is to fuse three recovered signals to obtain the best approximation to the original signal. We will show how the derived fusion procedure could be used to do this.



To demonstrate performance of the Algorithm 5 in providing the accurate sensor schedule, the original signal data is split into three and distributed among three data sets which are otherwise random sets as shown in Fig. 128, Fig. 129 and Fig. 130. The distribution of original information is done in such a way that it is hidden in three sets and could only be retrieved by any smart algorithm to reproduce the original signal. Let these data sets be sensor measurements  $v_1$ ,  $v_2$  and  $v_3$ . Suppose that one of the sensor functions ( $S_p$ ) is known and is shown in Fig. 131. The filtered signal output of sensor  $S_p$  is depicted in Fig. 132.

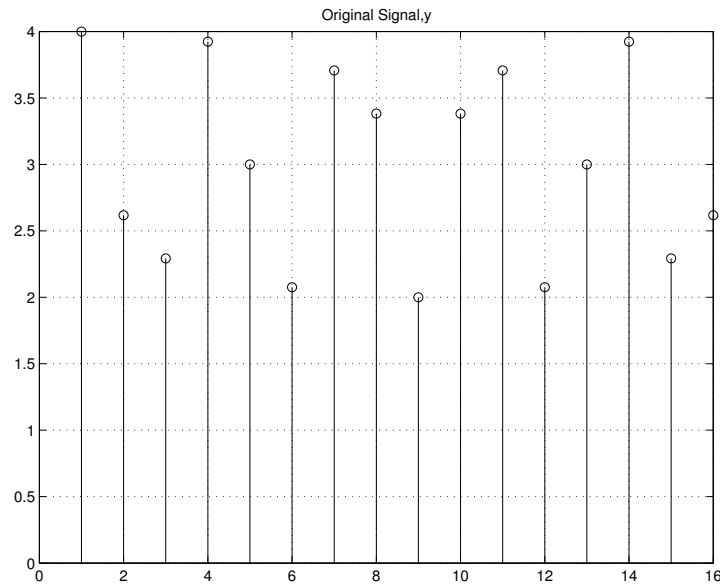


Figure 127: Original Signal  $y$

Let the fused signal be,

$$y_r = \Lambda_1 v_1 + \Lambda_2 v_2 + \Lambda_3 v_3 \quad (7.9)$$

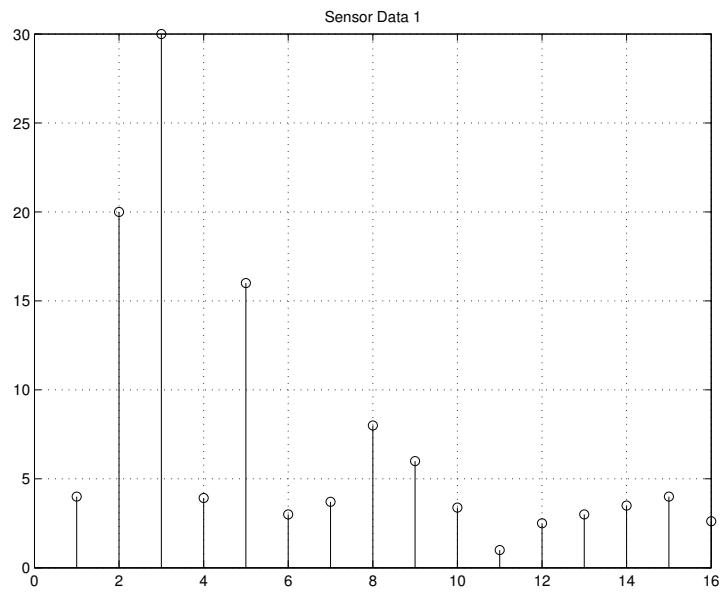


Figure 128: Sensor Data 1

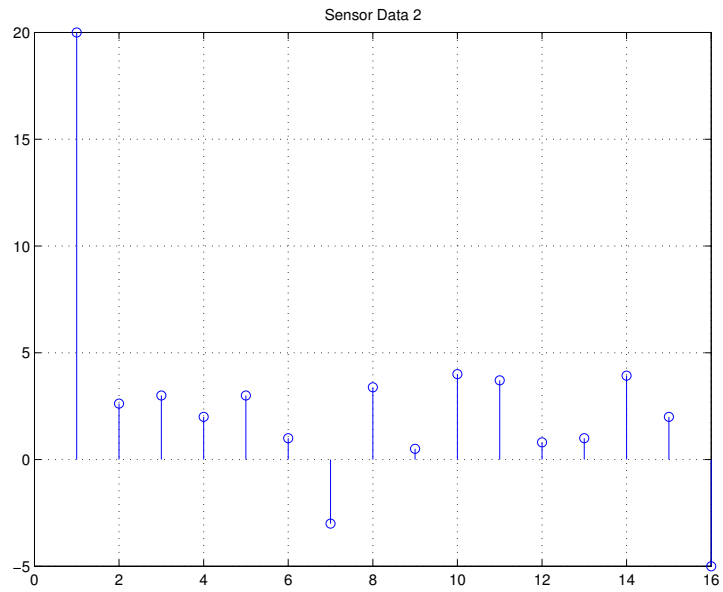


Figure 129: Sensor Data 2

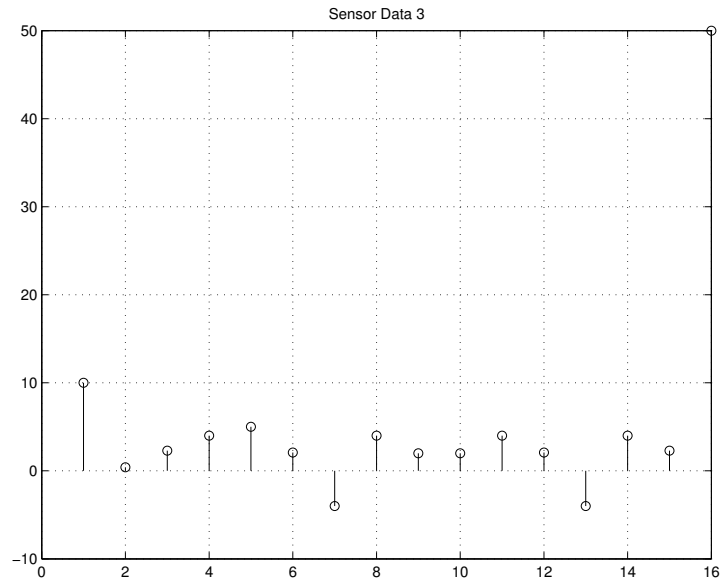


Figure 130: Sensor Data 3

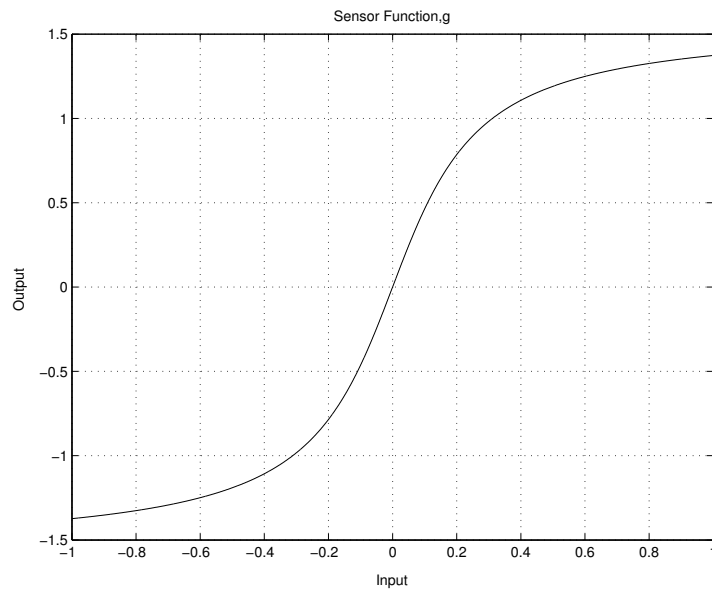


Figure 131: Known Nonlinear Sensor Function

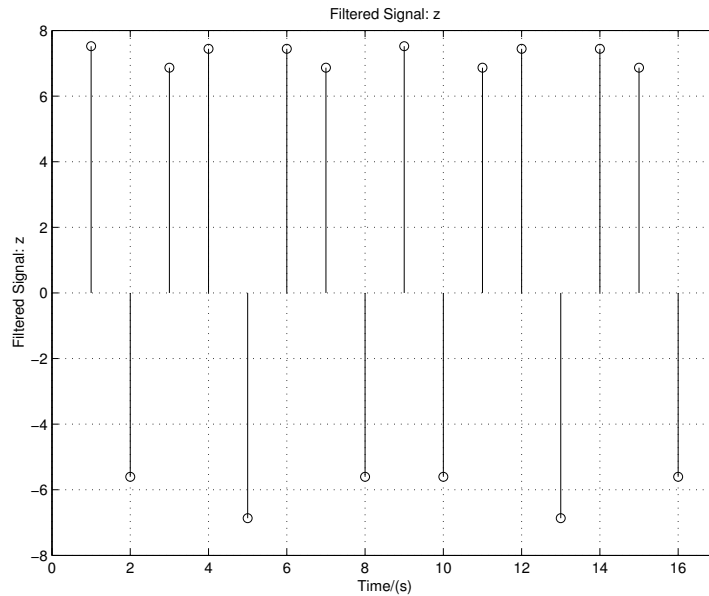


Figure 132: Filtered Signal  $z$  of Nonlinear Sensor Shown in Fig. 131

We now apply Algorithm 5 to obtain the best possible blend  $y_r$  and the sensor schedule. The optimal sensor schedule is shown in Fig. 133. Using this sensor schedule, the original signal is estimated and shown in Fig. 134. It is noted that  $v_f$  is exactly the same as the original signal, which demonstrates the fact that the switching between sensors is done as desired. The optimal solution is further guaranteed by its zero cost function value at optimal conditions.

### 3. Effective Sensor Fusion by Confidence Measures

The sensor fusion technique developed in section C of chapter V is further explained in this subsection by simulation results. Consider a multi-sensor fusion problem with two sensors. A signal  $y$  shown in Fig. 135 is measured through two different nonlinear sensors ( $S_1, S_2$ ) shown in Fig. 136 and Fig. 137 respectively. The sensor measurements are passed through low pass filter as explained in Section 2 and the filtered sensor

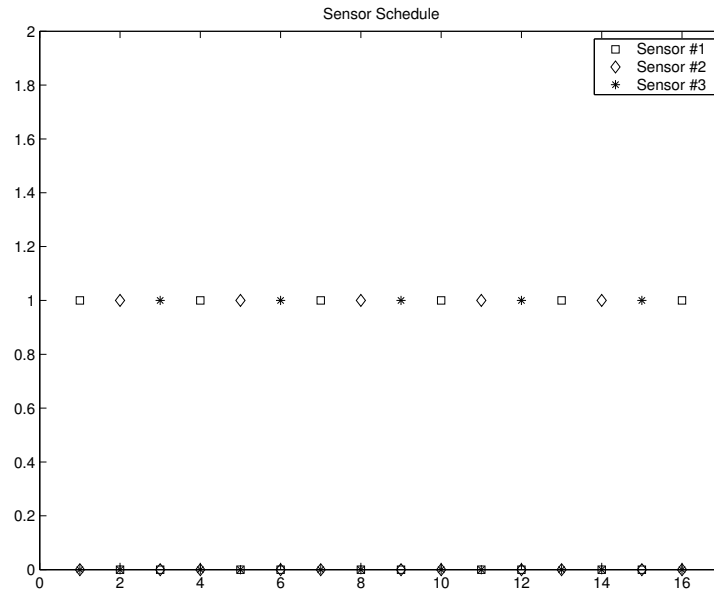


Figure 133: Optimal Sensor Schedule, 0 and 1 Are Used to Denote off and on Positions Respectively

outputs  $(z_1, z_2)$  are shown in Fig. 140 and Fig. 141. The goal is to fuse two sensor measurements to obtain the best approximation to the original signal. We will show how the derived fusion procedure could be used to do this.

To demonstrate performance of the fusion algorithm proposed, the original signal data is split into two signals and each of which is randomly distributed among two data sets  $(v_1, v_2)$  which are otherwise random sets. The signals  $v_1$  and  $v_2$  are shown in Fig. 138 and Fig. 139 respectively. The distribution of the original information is done in such a way that it is hidden in two sets and can only be retrieved by a smart algorithm to reproduce the original signal. The algorithm proposed in this dissertation is used to obtain the confidence measures, which are shown in Fig. 142 and Fig. 143. Applying the fusion rule (Equation (5.72)), inaccurate data found in the sensor measurements are identified and discarded. By replacing the inaccurate samples by zero and keeping

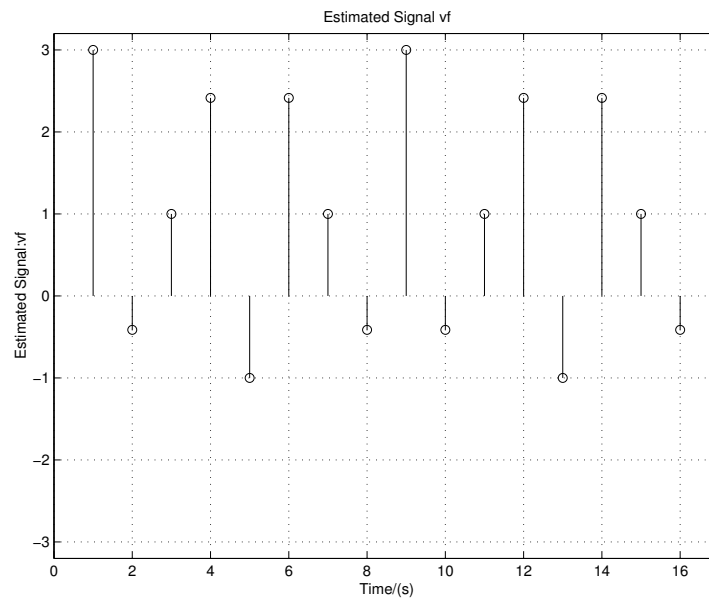


Figure 134: Estimated Signal  $v_f$

the accurate samples as is, sensor measurements obtained are shown in Fig. 144 and Fig. 145. Comparing the confidence measures of the overlapping data and the fusion rule (Equation (5.72)), the signals shown in Fig. 144 and Fig. 145 are fused and the fused signal is shown in Fig. 146. The fact that the fused signal is exactly the same as the signal to be measured demonstrates performance of the proposed fusion scheme.

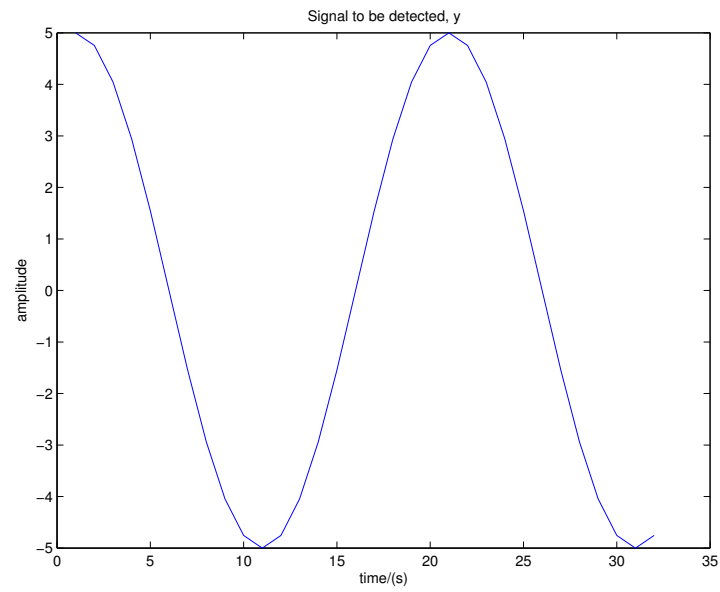


Figure 135: Original Signal  $y$  Used to Demonstrate Sensor Fusion Algorithm

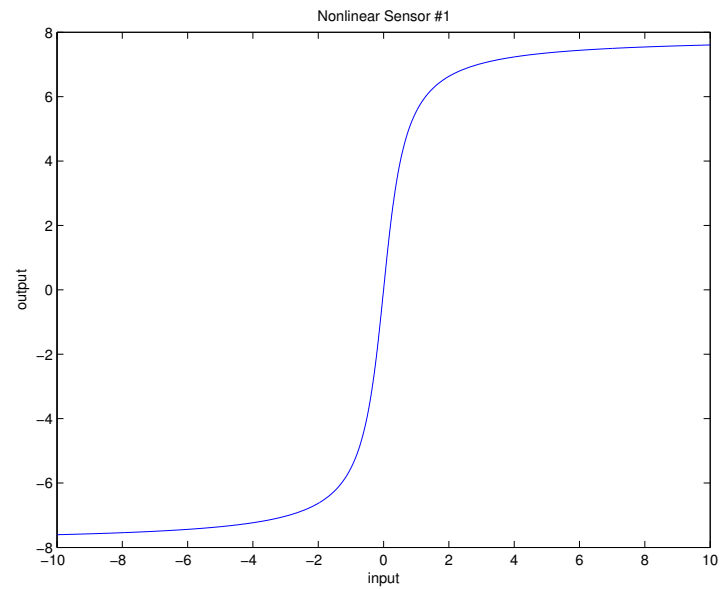
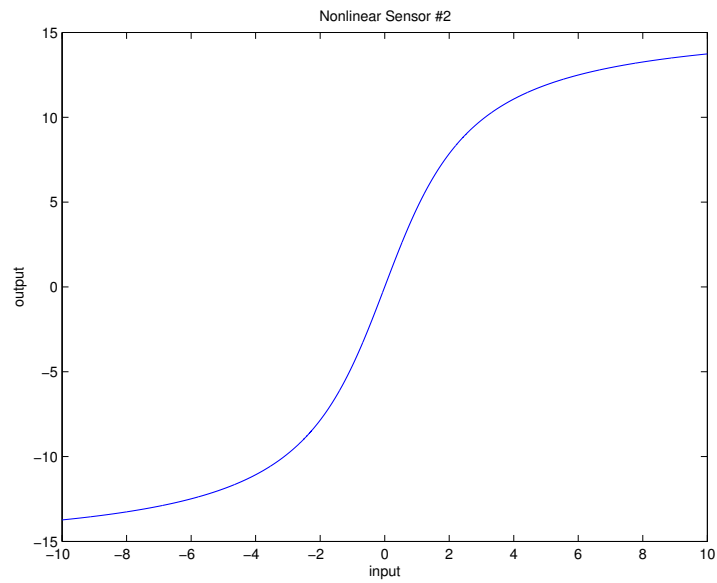
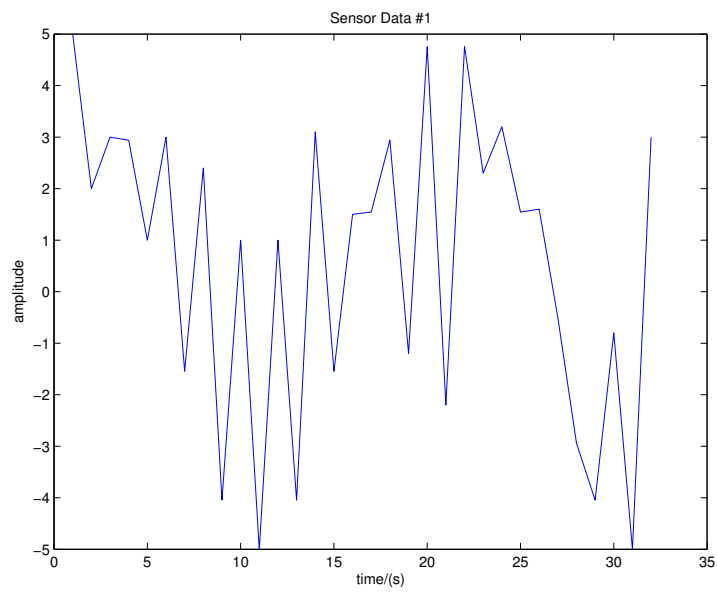
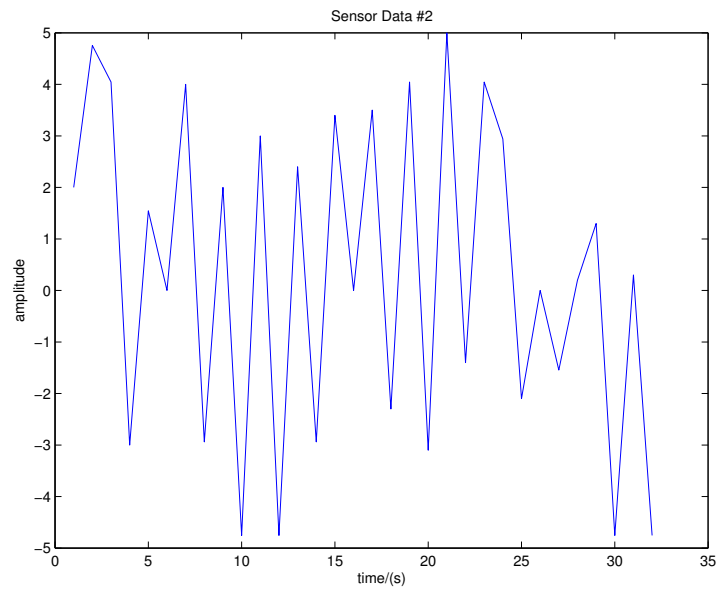
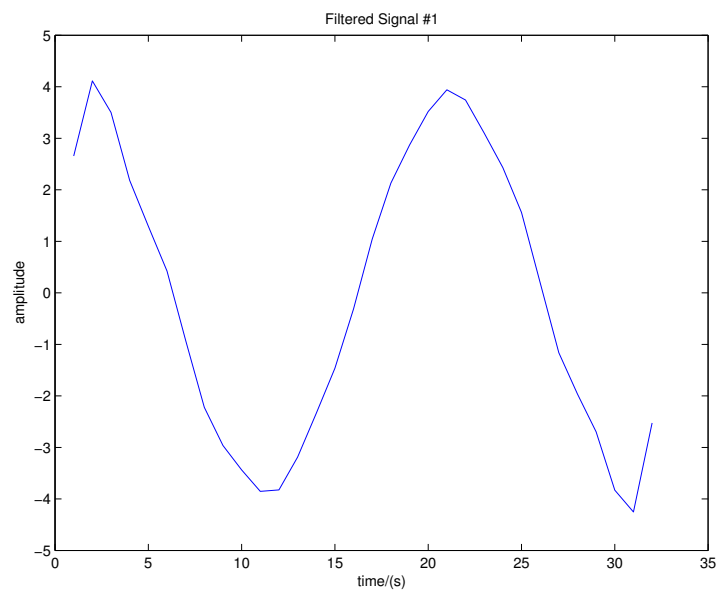


Figure 136: Nonlinear Sensor  $S_1$

Figure 137: Nonlinear Sensor  $S_2$ Figure 138: Sensor Data  $v_1$



Figure 139: Sensor Data  $v_2$ Figure 140: Filtered Signal  $z_1$

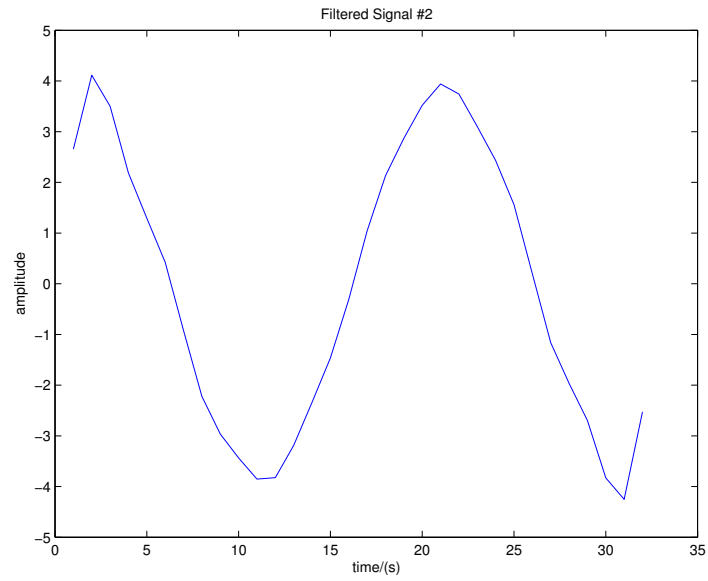
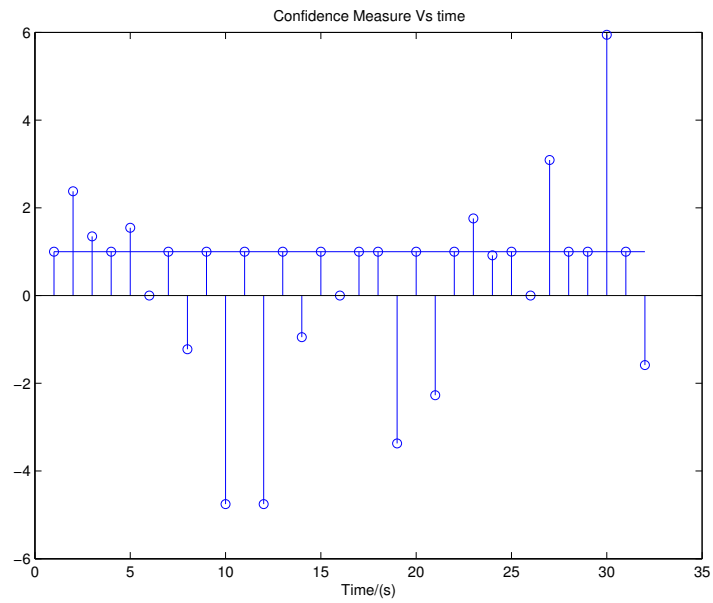
Figure 141: Filtered Signal  $z_2$ 

Figure 142: Confidence Measures for Sensor Data 1

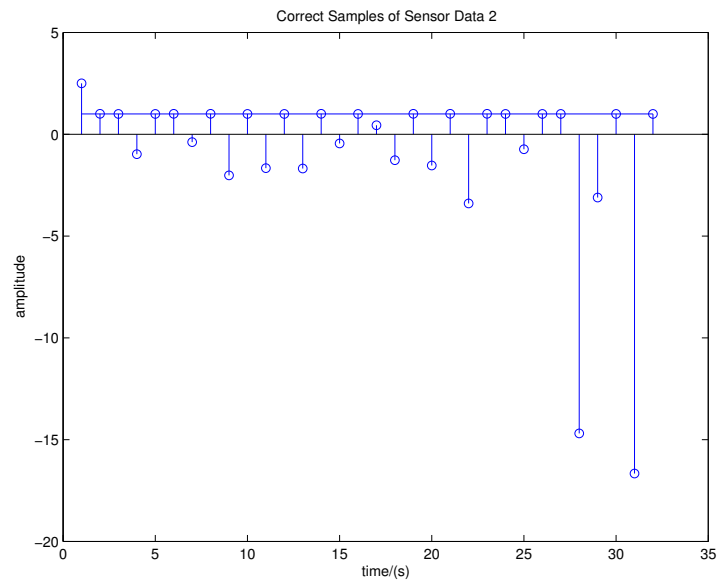


Figure 143: Confidence Measures for Sensor Data 2

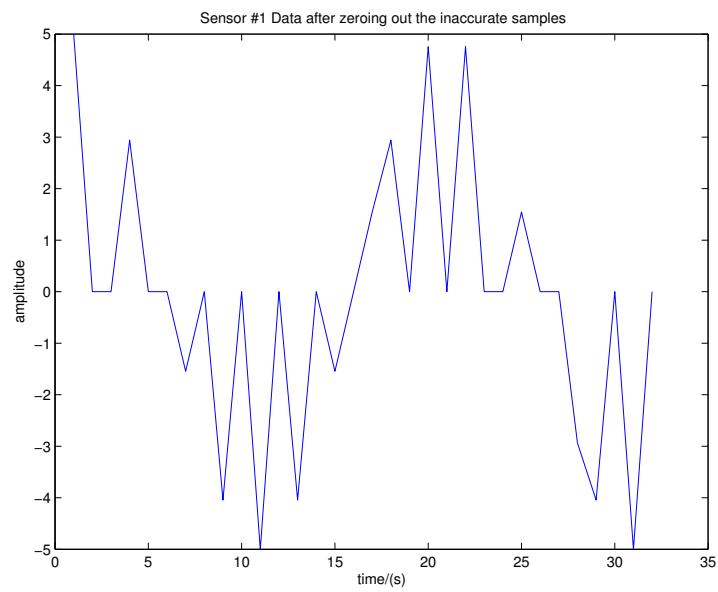


Figure 144: Correct Samples of Sensor Data 1

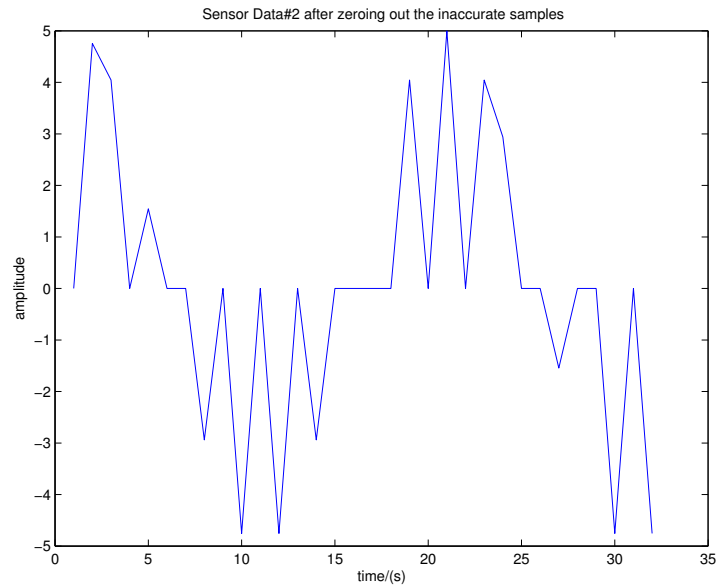


Figure 145: Correct Samples of Sensor Data 2

### C. Sensor Arrays: Illustrative Examples

Presented in this section are the simulation results to further analyze the sensor array implementation schemes developed in chapter VI.

#### 1. Design of Sensor Arrays by Frequency Domain Methods

We present a design example to validate the proposed frequency domain loop-shaping design procedure developed in section D of chapter VI. To extend the bandwidth to 10000 rad/sec, we will use a three-sensor array. Frequency responses of sensors  $S_1$ ,  $S_2$  and  $S_3$  are shown in Fig. 147 and Fig. 148.

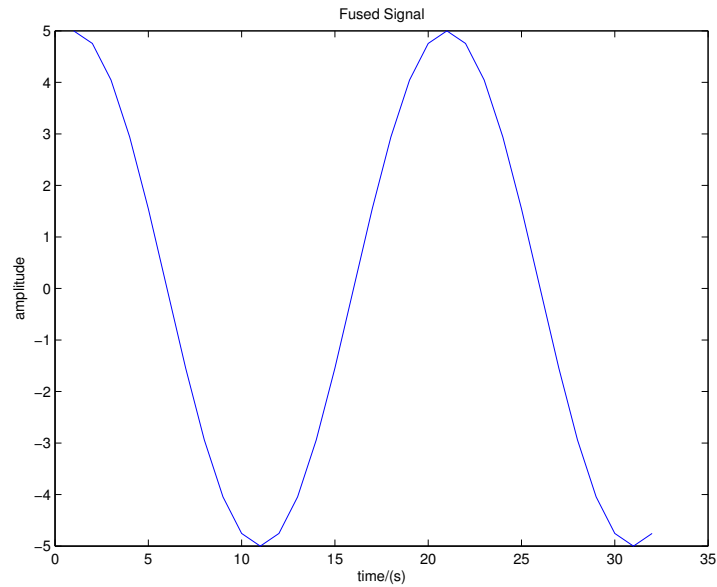


Figure 146: Fused Signal Obtained Using the Confidence Measure Based Sensor Fusion Algorithm

The transfer function of the integrated system,  $I(j\omega)$ , is formulated as follows.

$$I(j\omega) = P_1(j\omega)S_1(j\omega) + P_2(j\omega)S_2(j\omega) + P_3(j\omega)S_3(j\omega) \quad (7.10)$$

Suppose that the task is to design compensators  $P_1, P_2$  and  $P_3$  so that  $I(j\omega)$  satisfies the following conditions  $\forall\omega$ :

$$-1db \leq 20 \log_{10} |I(j\omega)| \leq 1db \quad (7.11)$$

$$-5 \text{ deg} \leq \angle I(j\omega) \leq 5 \text{ deg} \quad (7.12)$$

The QFT loop-shaping technique is used to design the following compensators:

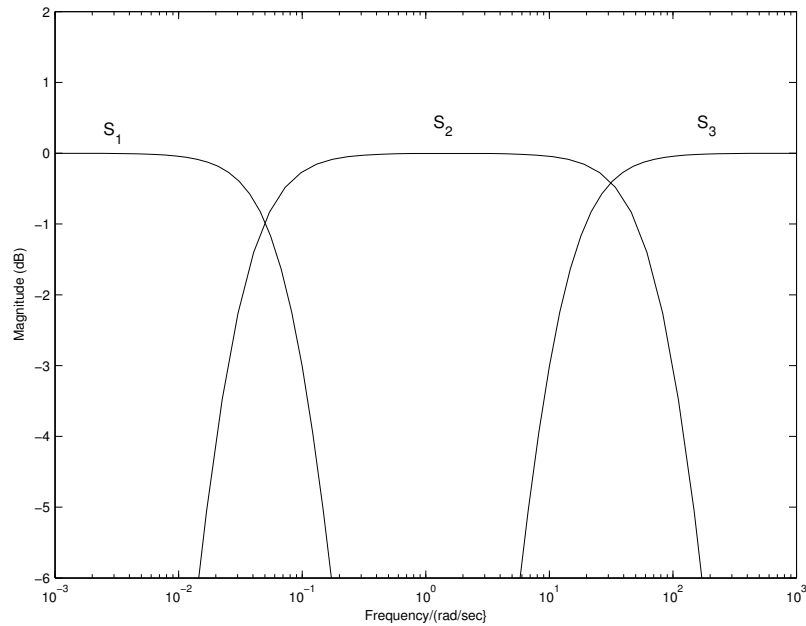


Figure 147: Magnitude Plot of Sensors,  $S_1, S_2, S_3$

$$\begin{aligned}
 P_1 &= \frac{10s + 1}{s + 1} \\
 P_2 &= \frac{0.0041667(s + 80)(s + 0.5)}{(s + 2)(s + 1)} \\
 P_3 &= \frac{s + 9}{s + 1}
 \end{aligned}$$

It should be noted that any frequency domain loop-shaping method can be used to design these compensators. Furthermore, the above compensators are not unique and similar system performance can be obtained by using another set of compensators. It usually depends on the loop-shaping skills of the designer.

The frequency response of  $I(j\omega)$  is obtained by substituting the above compensators in Equation (7.10) and plotted in Bode Diagram and Nichols Chart, which are Fig. 149 and Fig. 150 respectively. It is clear that conditions (7.11) and (7.12) are

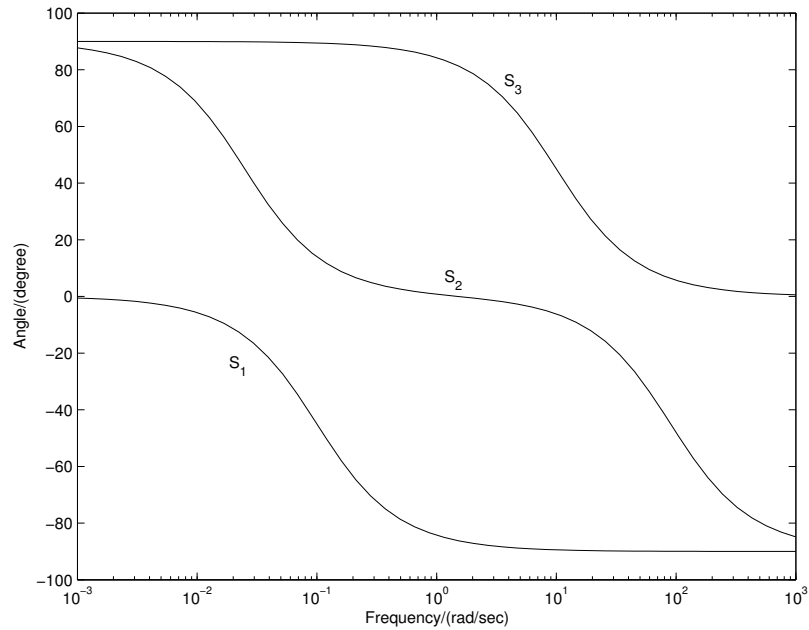
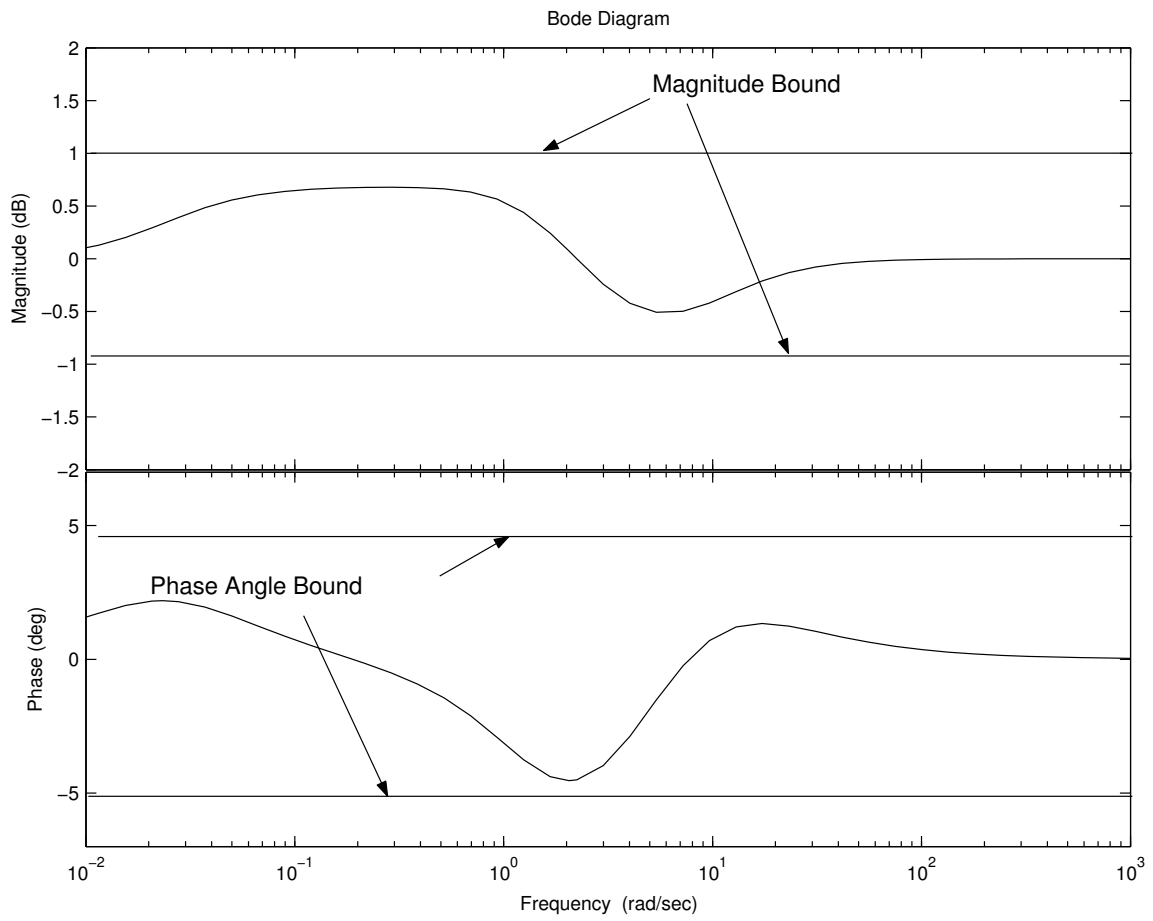


Figure 148: Phase Angle Plot of Sensors,  $S_1, S_2, S_3$

satisfied. This example is presented just to illustrate the proposed sensor array design and sensor uncertainties are not considered while designing compensators. However, the design procedure with uncertain sensor models is similar. The only difference is that conditions (7.11) and (7.12) have to be satisfied for all sensor functions in their corresponding families.

Figure 149: Bode Plot of  $I(j\omega)$



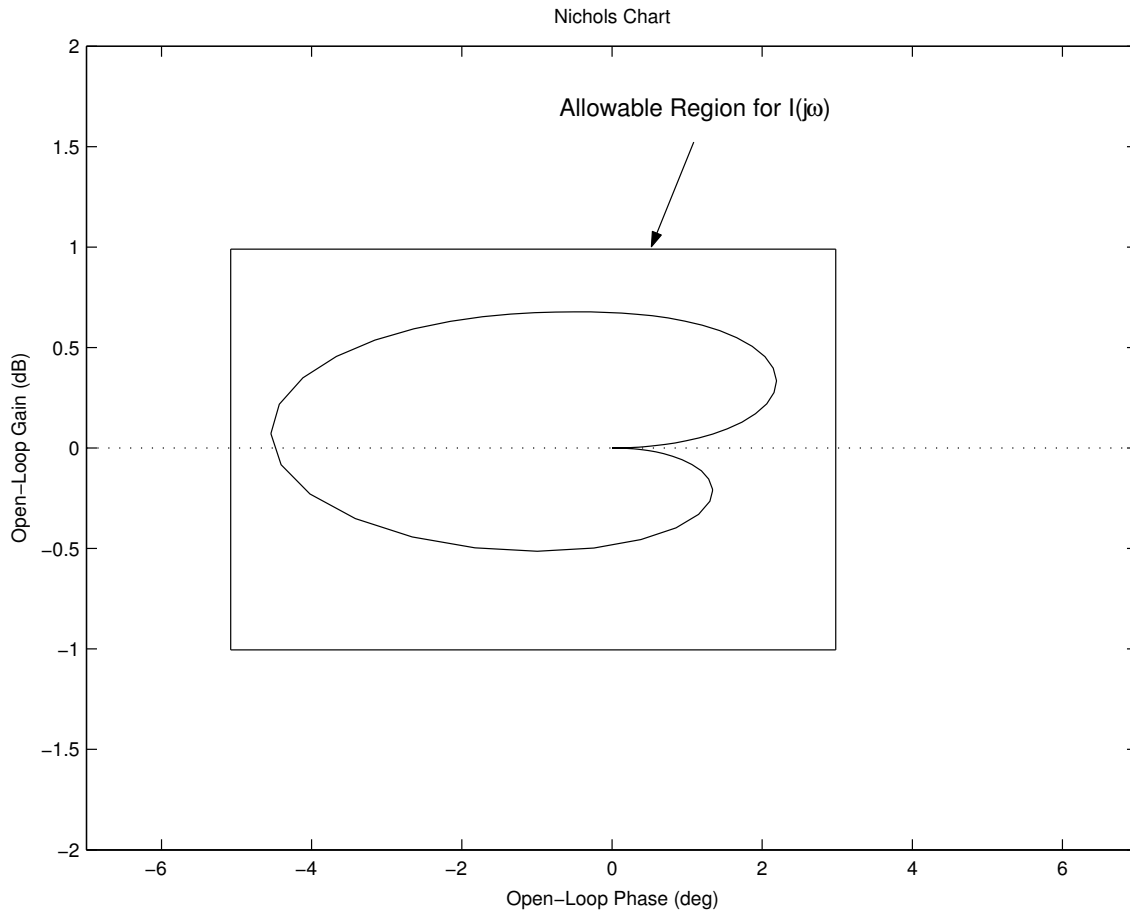


Figure 150: Frequency Response of  $I(j\omega)$  in Nichols Chart

## 2. Design of Sensor Arrays by Optimization

In this section, we present a simulation example to validate the optimization based design procedure developed in section E of chapter VI. We consider a sensor array with two sensors whose frequency responses are shown in Fig. 151.

The transfer function of the integrated system,  $I(j\omega)$ , is formulated as before.

$$I(j\omega) = P_1(j\omega)S_1(j\omega) + P_2(j\omega)S_2(j\omega) \quad (7.13)$$

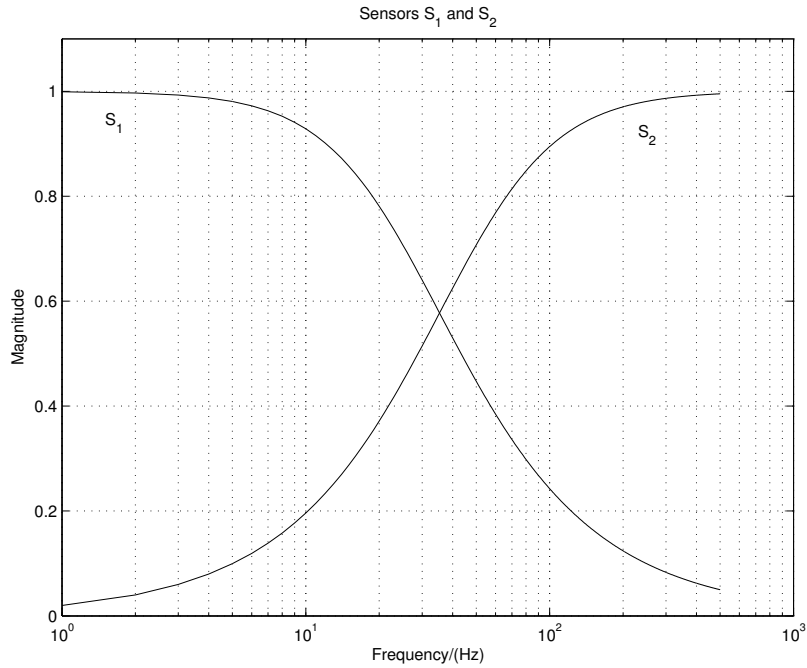


Figure 151: Frequency Responses of Sensors  $S_1$  and  $S_2$

The objective function,

$$\min_{P_1(j\omega), P_2(j\omega), \dots, P_n(j\omega)} J = \|1 - S_1(j\omega)P_1(j\omega) - S_2(j\omega)P_2(j\omega)\|, \quad (7.14)$$

is minimized subject to the constraint set,

$$\text{If } |S_1(j\omega)| > |S_2(j\omega)| \implies |P_1(j\omega)| > |P_2(j\omega)|$$

$$\text{If } |S_2(j\omega)| > |S_1(j\omega)| \implies |P_2(j\omega)| > |P_1(j\omega)|.$$

Frequency responses of resultant, optimal compensators and the function,  $I(j\omega)$  are shown in Fig. 152 and Fig. 153 respectively. At optimal conditions, function,  $I(j\omega)$ , is real and its phase angle is zero.

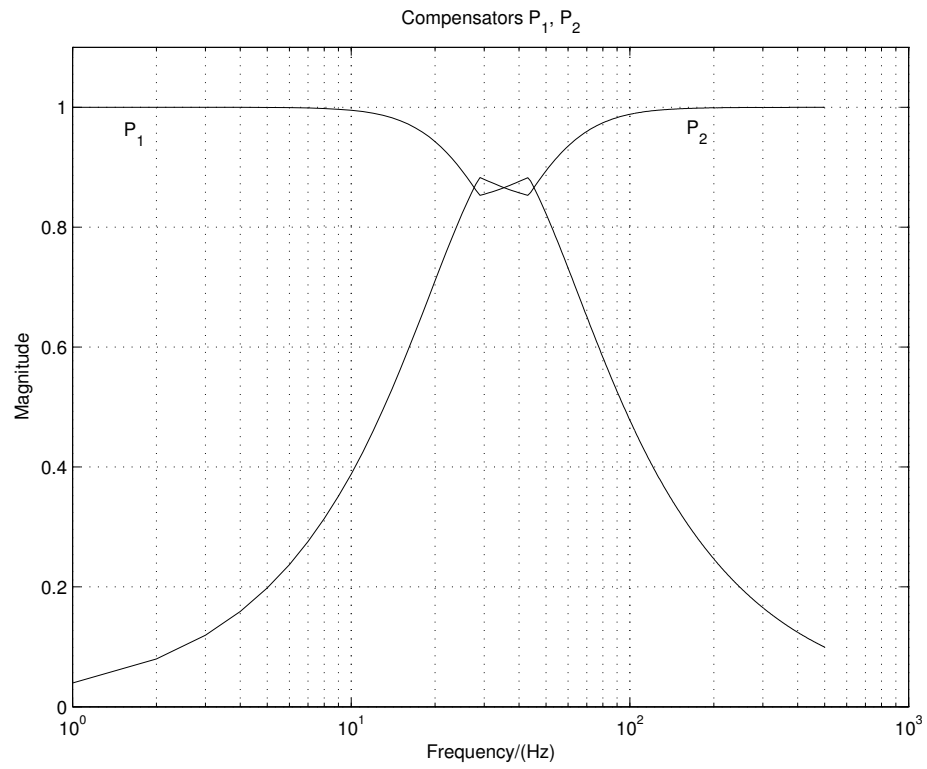


Figure 152: Frequency Responses of Compensators  $P_1$  and  $P_2$

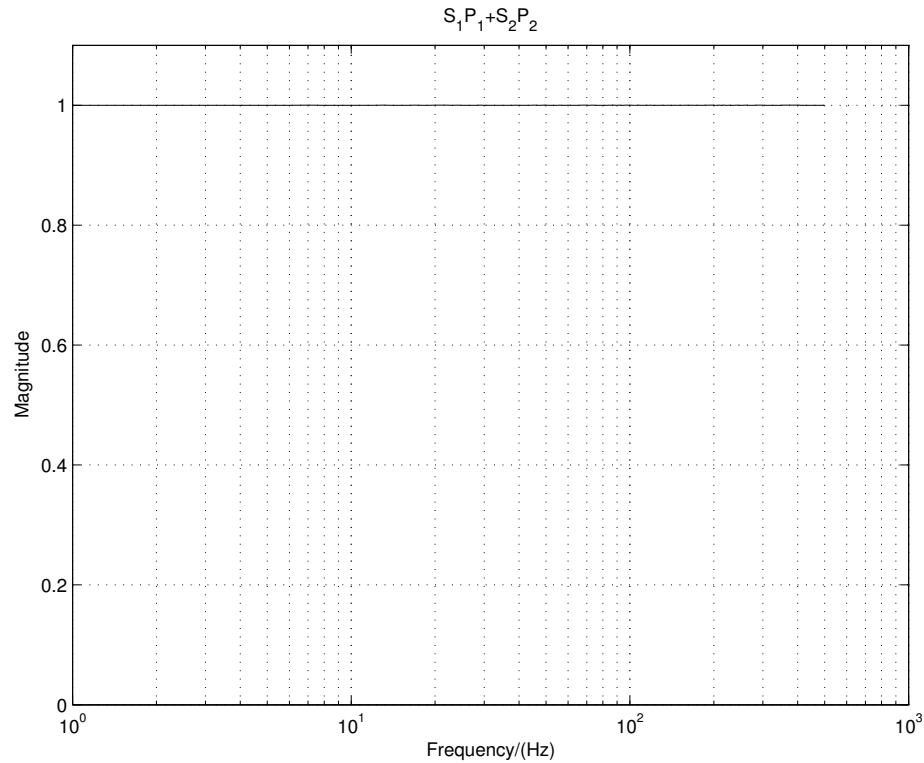


Figure 153: Frequency Response of  $I(j\omega)$

### 3. Design of Sensor Arrays from Realistic Sensor Models

The proposed approach may also be used to combine low and high frequency measurements in practice. One such situation could be velocity measurement using the accelerometer-tachometer setup shown in Fig. 154.  $n_1$  and  $n_2$  are high frequency measurement noise. The low pass filter used in channel  $S_1$  will attenuate high frequency noise,  $n_1$ . The high pass filter used in channel  $S_2$  will attenuate the integrated high frequency noise,  $\frac{n_2}{s}$ , which is of low frequency.

Suppose that the frequency responses shown in Fig. 155 characterize (sensor  $S_1$  and the low pass filter) and (sensor  $S_2$  and the high pass filter). To test how sensitive the proposed approach is to modeling errors, noise and other factors, frequency

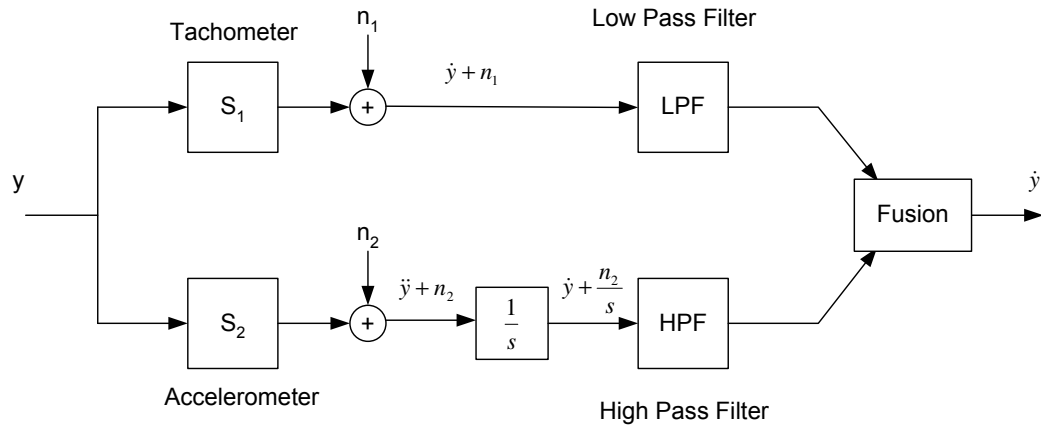


Figure 154: Fusion of Low and High Frequency Data

responses shown in Fig. 155 are used to design a two-sensor array that covers an operating bandwidth of 500 rad/sec. However, these abrupt changes are not considered while designing compensators. The non-smooth frequency responses are generated by adding random numbers to the smooth responses. The design process is carried out using the smooth sensor models. The following optimization problem is solved to design compensators  $P_1$  and  $P_2$ .

$$\min_{P_1(j\omega), P_2(j\omega)} J = \left\| 1 - \sum_{i=1}^2 S_i(j\omega) P_i(j\omega) \right\| \quad (7.15)$$

subject to

$$\text{If } |S_1(j\omega)| > |S_2(j\omega)| \implies |P_1(j\omega)| > |P_2(j\omega)|$$

$$\text{If } |S_2(j\omega)| > |S_1(j\omega)| \implies |P_2(j\omega)| > |P_1(j\omega)|$$

$$0.9 \leq |I(j\omega)| \leq 1.1$$

$\forall \omega < 500$  rad/sec, where

$$I(j\omega) = P_1(j\omega)S_1(j\omega) + P_2(j\omega)S_2(j\omega)$$

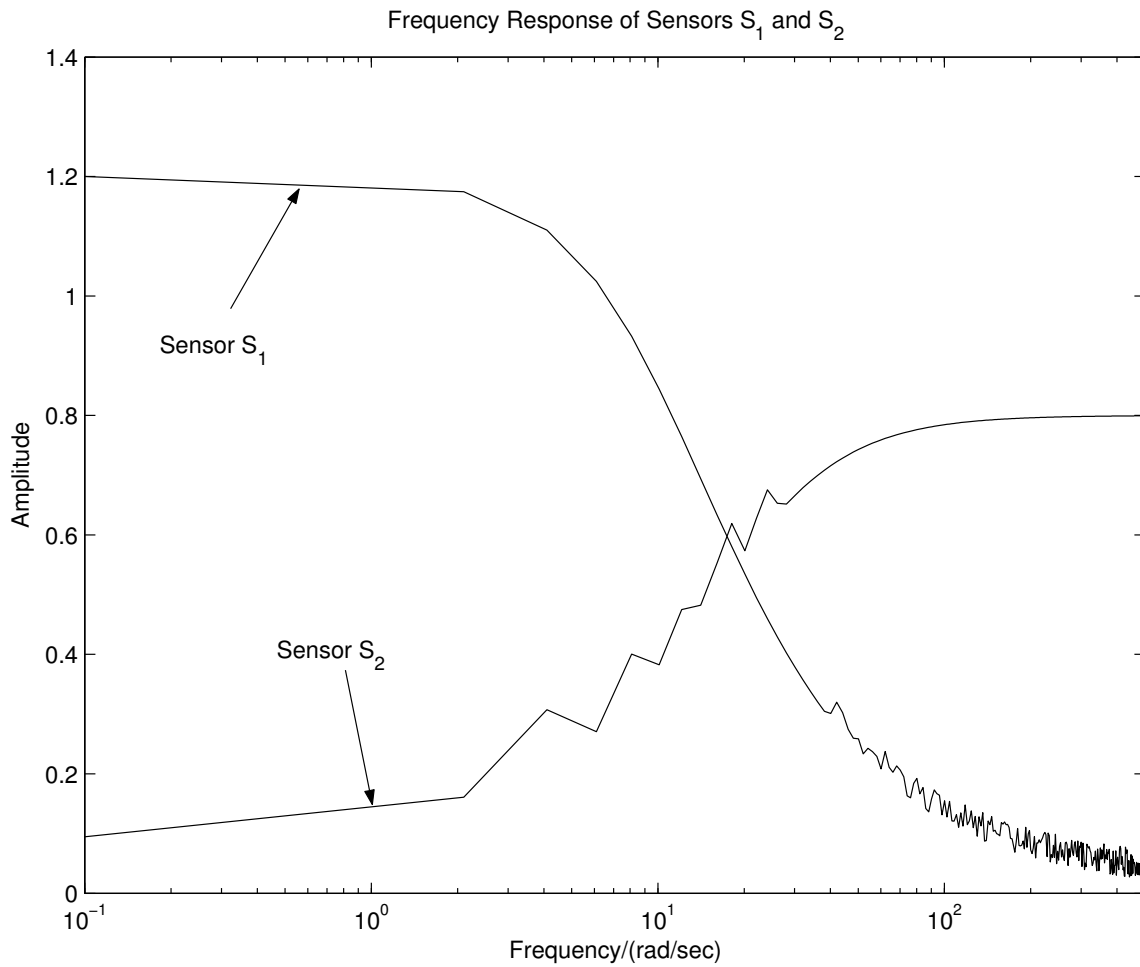


Figure 155: Frequency Responses of Realistic Sensors  $S_1$  and  $S_2$

The frequency responses of optimal compensators  $P_1$  and  $P_2$  are shown in Figures 156 and 157 respectively. The frequency response of the integrated system  $I(j\omega)$  shown in Figure 158 clearly demonstrates that the specifications are satisfied. Furthermore, it also shows that small errors due to model uncertainty and noise may be tolerable.

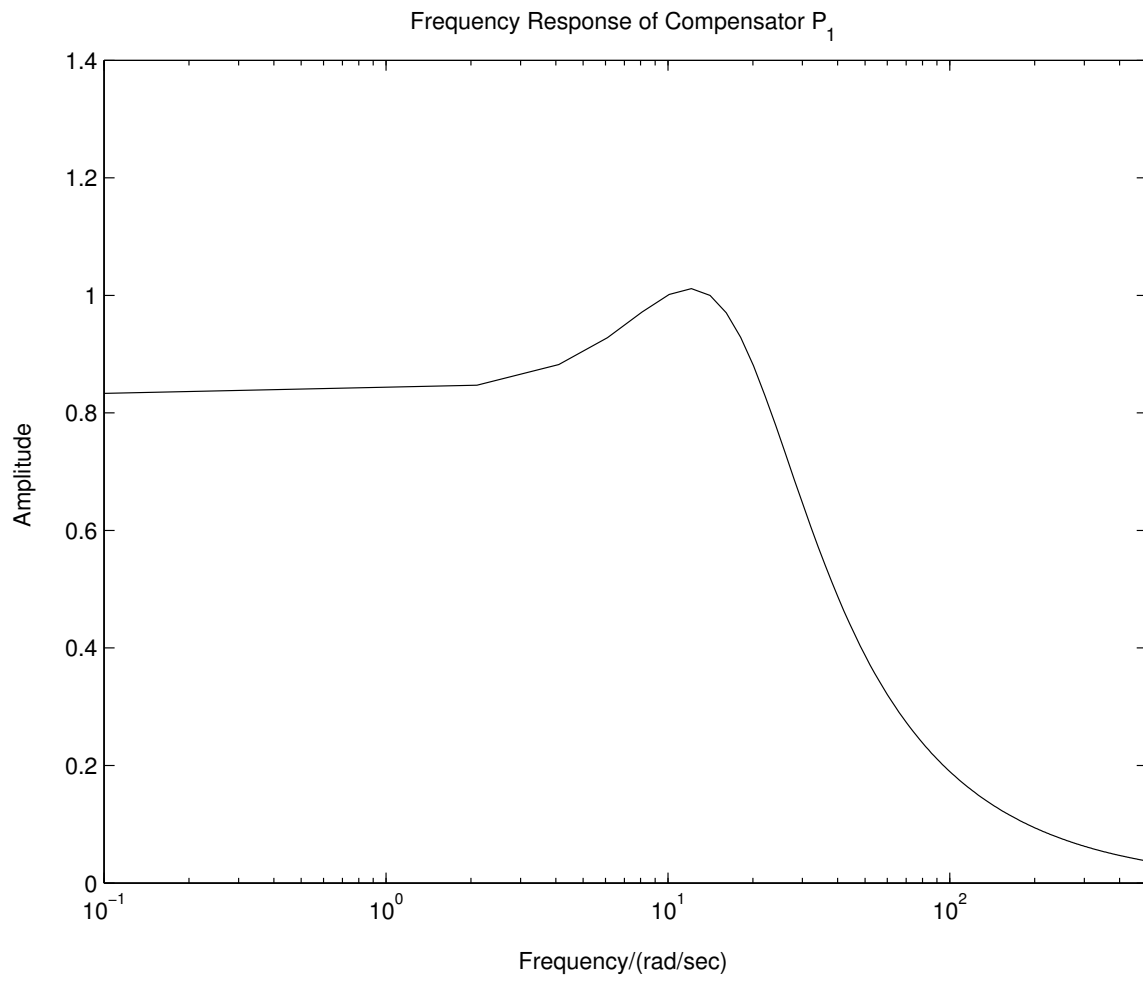


Figure 156: Frequency Response of Compensator  $P_1$

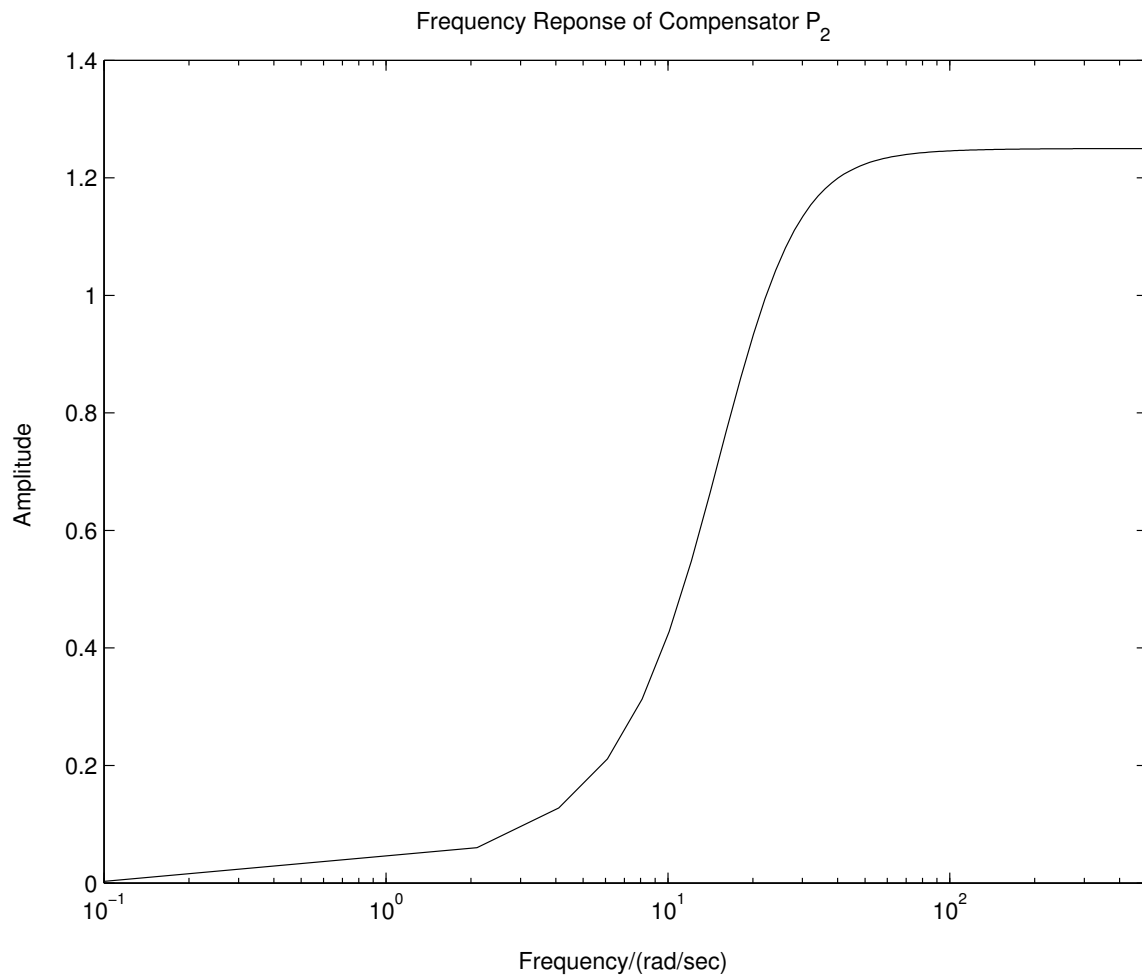


Figure 157: Frequency Response of Compensator  $P_2$



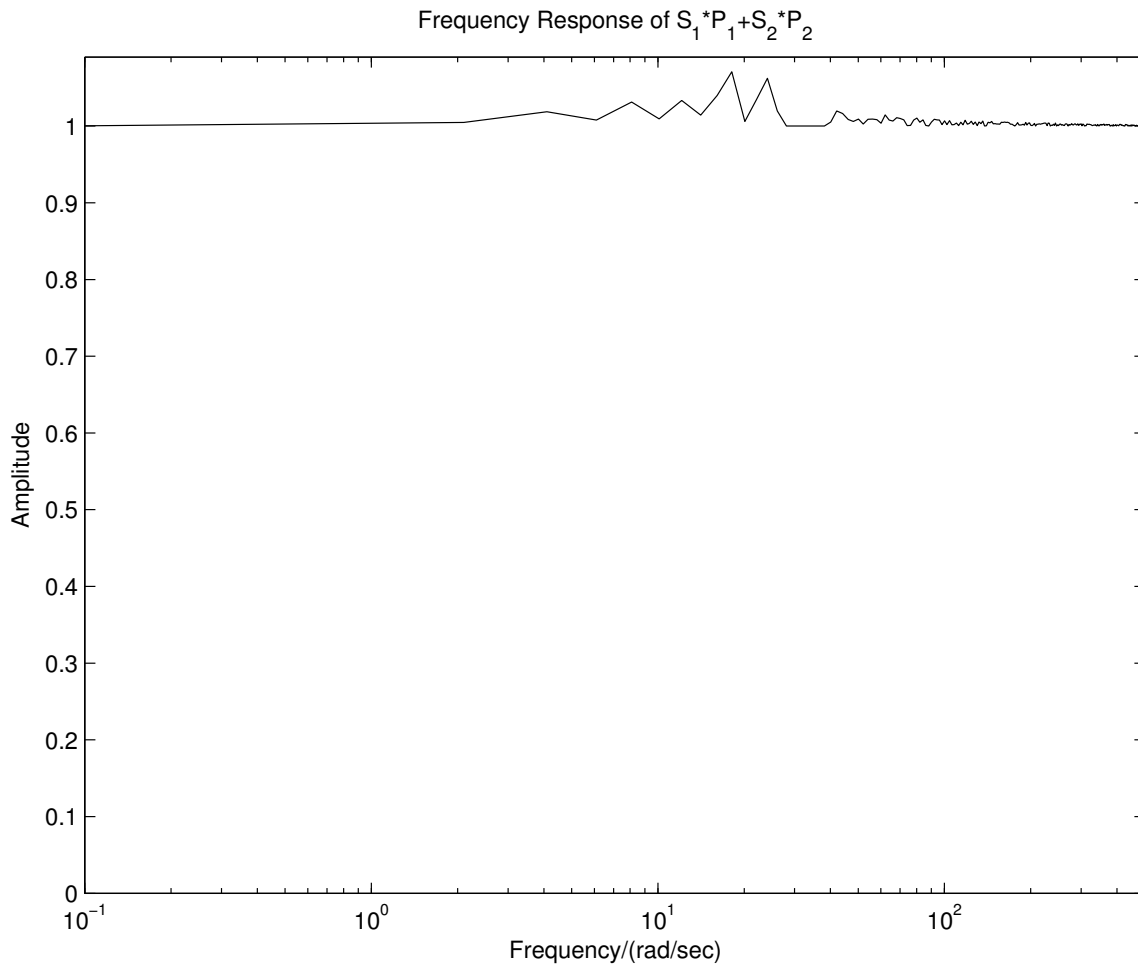


Figure 158: Frequency Response of Integrated Set up  $I(j\omega)$

#### 4. Implementation by Feedback Mechanisms

This subsection validates the implementation scheme developed in section F of chapter VI. We will illustrate how sensor arrays can be implemented by feedback mechanisms using a simulation example. Consider a two-sensor fusion problem in which a signal shown in Fig. 161 that has high as well as low frequency components is measured by two sensors, one is low frequency sensor and the other is high frequency sensor. As

this example consists of only two sensors, one stage of closed loop control is sufficient.

The Simulink model of this setup is shown in Fig. 160. The frequency spectrums of the measurements by the low and high frequency sensors are shown in Fig. 162 and Fig. 163 respectively. The following low pass filter  $F$  and the controller  $C$  have been designed to satisfy the required specifications as stated in section F:

$$F = \frac{1}{\left(\frac{s}{200} + 1\right)^4} \quad (7.16)$$

$$C = \frac{2s^2 + 20s + 2000}{s^2 + s}$$

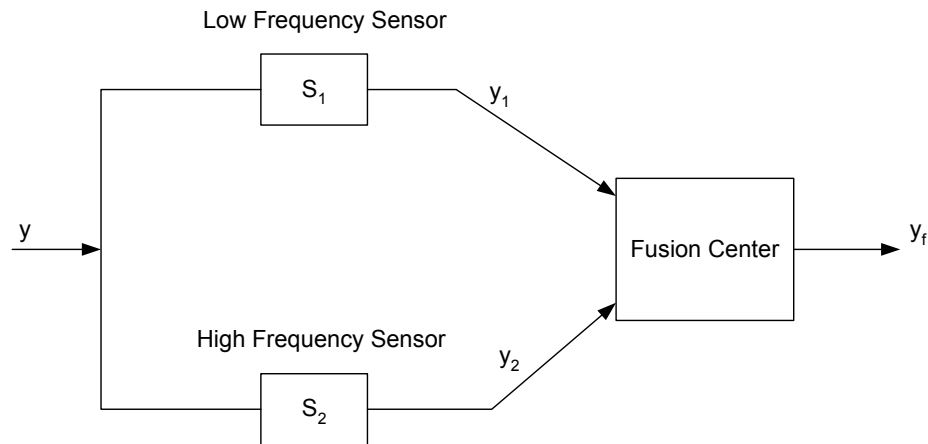


Figure 159: Sensor Fusion Setup

The output of the closed loop control system, which is the fused signal of multi-sensor data is shown in Fig. 164. Comparison of the fused data with actual data clearly demonstrates the effectiveness of this proposed scheme. Even though the fused signal is obtained with negligible error in this case, it may not be always the case. If the data to be measured have frequency components near but above the cut off frequency of the low pass filter, then these frequency components may not be

perfectly attenuated by the low pass filter, which will result in errors. These errors can be minimized but may not be completely removed, in general, by designing a low pass filter that has a very sharp cut off. However, this may cause problems in stabilizing the loop and the controller design may become very difficult. Further research is needed to clarify this issue.

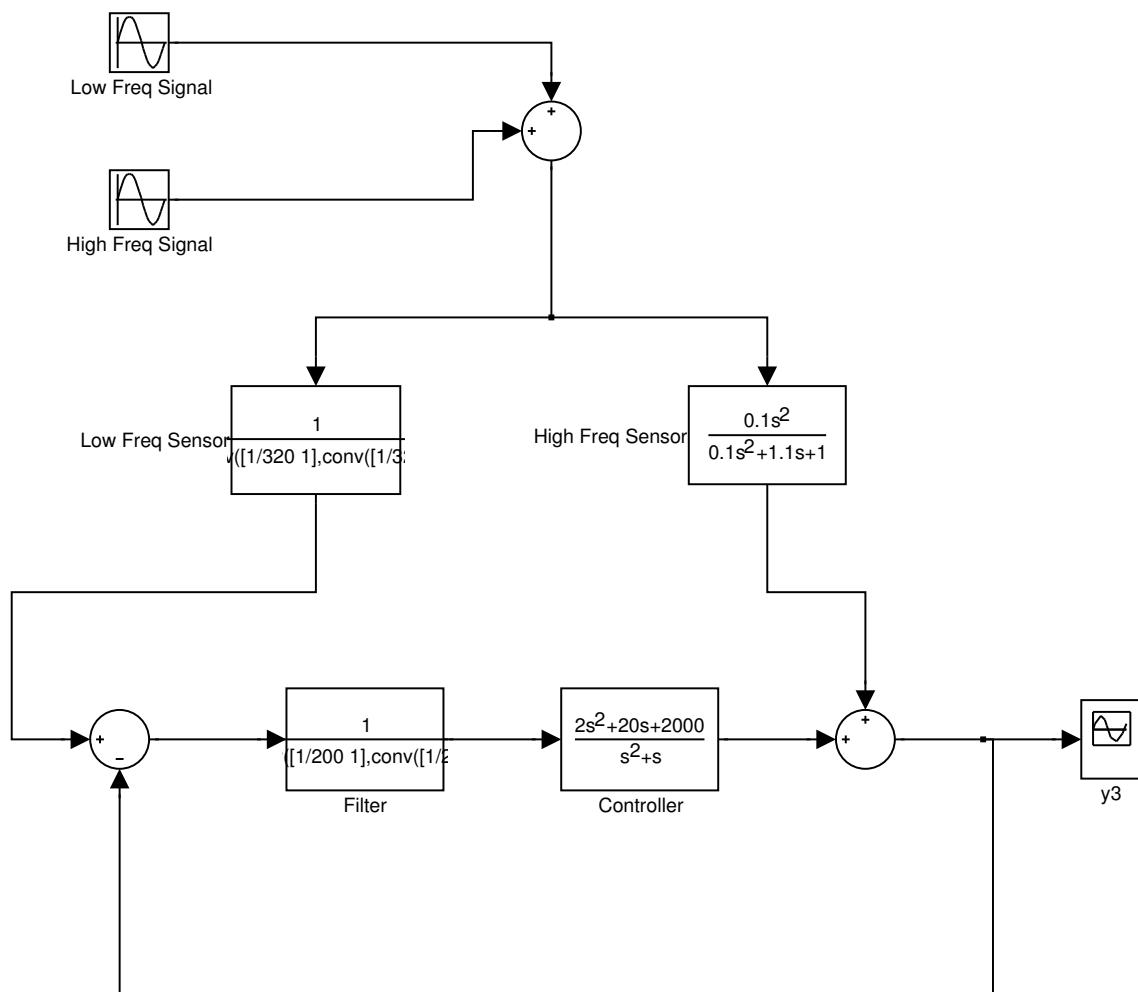


Figure 160: Multi-sensor Data Fusion Simulation Setup

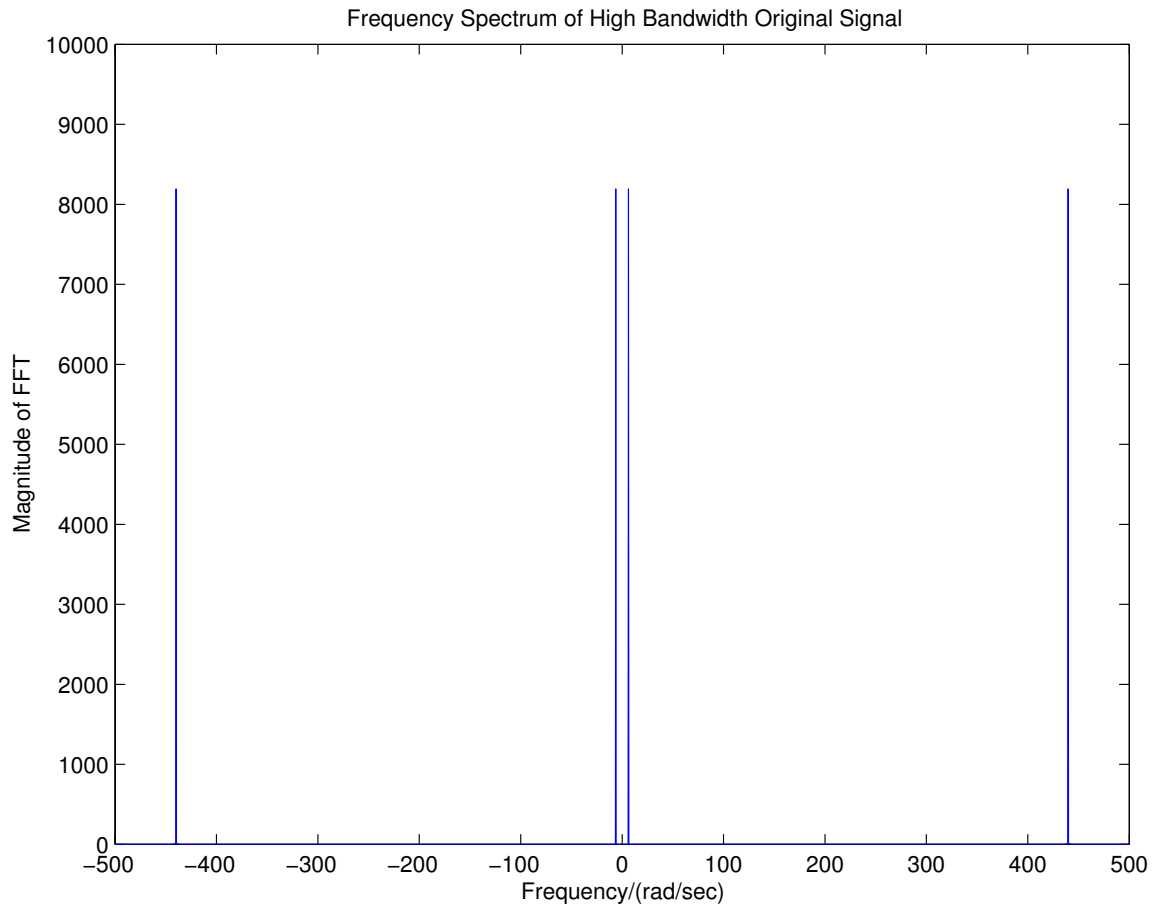


Figure 161: Original Signal Considered for Demonstration

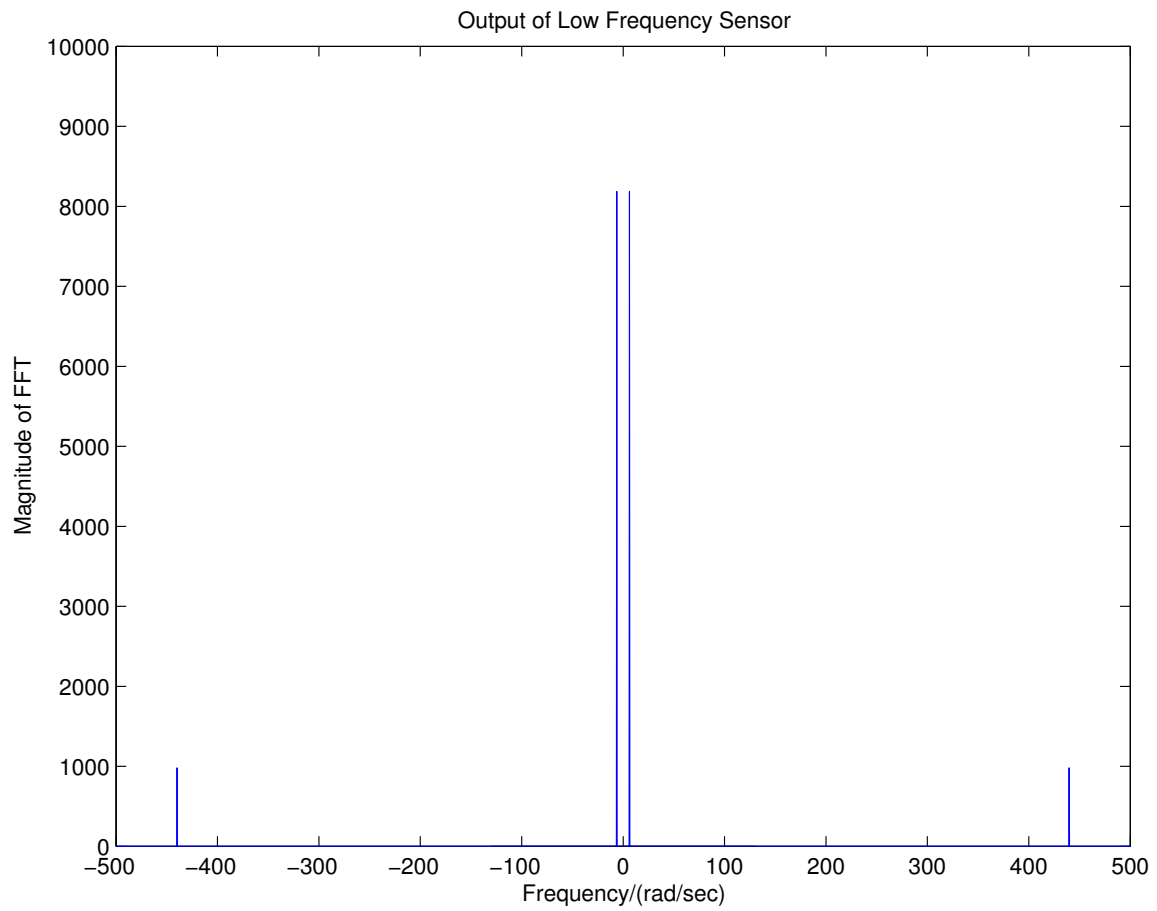


Figure 162: Low Frequency Sensor Output

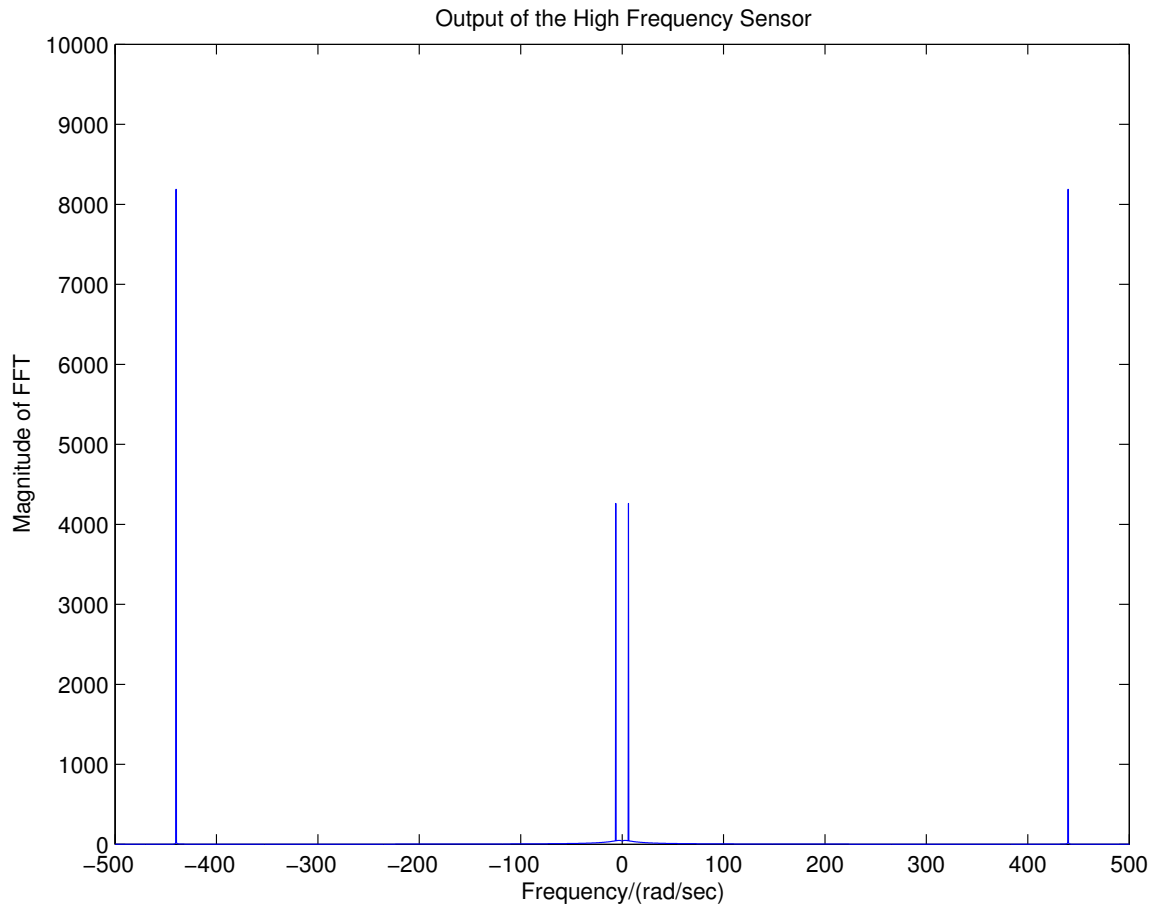


Figure 163: High Frequency Sensor Output

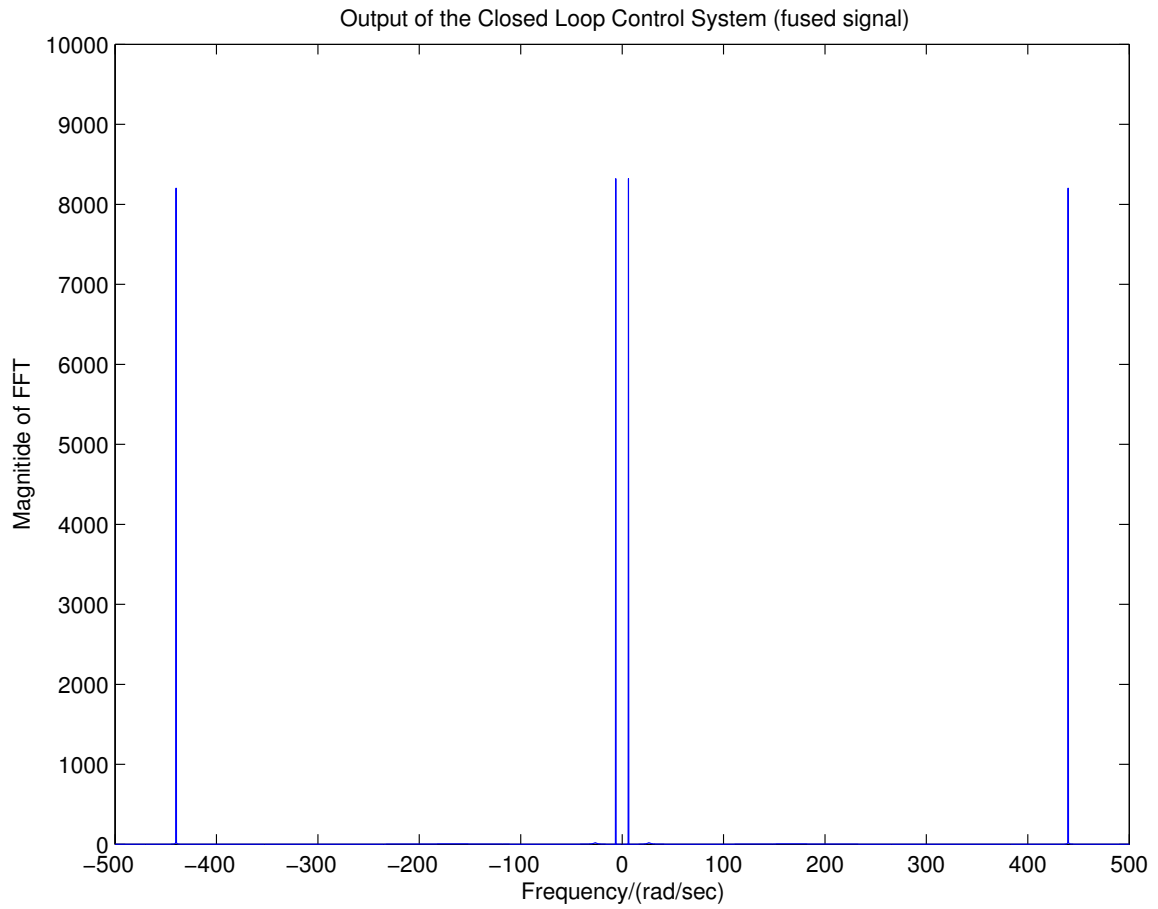


Figure 164: Fused Signal Obtained Using the Closed Loop Control

## CHAPTER VIII

### SUMMARY AND CONCLUSIONS

This dissertation is devoted to the investigation of some of the sensor related issues such as sensor nonlinearity, sensor bandwidth and sensor noise and the development of means to address them. It is demonstrated through detailed analysis the significance of the proposed research in improving reliability and accuracy of sensor measurements. It is shown that the effects of sensor nonlinearity can be reverted by conditioning the distorted sensor measurements. An efficient method that uses an array of low bandwidth pass-band sensor to attain a high operating bandwidth is proposed. In addition, several fault detection algorithms to optimize the use of sensors is proposed.

#### A. Summary and Conclusions

The problem is stated and objectives are set in chapter I. Terms used in this dissertation are defined and some important theorems are stated in chapter II. The relevant literature is reviewed to provide background information and to point out the need for further research in chapter III.

Chapter IV details the methods that have been developed to compensate the distortion caused by sensor nonlinearity. The distortion caused by sensor nonlinearity is analyzed and an efficient recursive signal recovery scheme is proposed. Some of the sufficiency conditions for the successful implementation of the proposed scheme are derived. Having shown that the proposed recursive scheme will work for certain type of sensor nonlinearities, an optimization based algorithm is proposed to treat ill-conditioned sensor nonlinearities. The results presented in Chapter VII validate performance of the signal recovery algorithms developed in this dissertation. If the characteristic of sensor function satisfies the sufficient requirements of Theorems 4



and 5 and the model of the sensor is known *a priori*, it is shown that the original signal can be uniquely recovered. It is also shown how the derived algorithm should be modified in order to obtain a solution when the gradients of the sensor function are negative.

When the sensor model is not available, the signal could still be recovered with a reasonable error bound by incorporating a model identification technique. Uniqueness of the recovered signal is solely dependent on the model identification scheme employed and the input-output data used to build the model. Identification of sensor model using the known input-output data may not always be possible. For example, if the physical quantity is temperature or pressure, it may not be possible to send “known” input data directly through the sensor. A knowledge based learning technique may be used to obtain the sensor model or the calibration curve in this case. In the examples presented in the previous chapter, an ideal low pass filter was used to filter out the high harmonics. This may not be necessary and it can be shown that a non-ideal low pass filter that satisfies the requirements of Theorems 4 and 5 can also be used in place of an ideal filter. As the ideal low pass filter is not physically realizable, this observation increases the scope of the developed scheme. According to Theorem 5, the algorithm may not converge to the expected value when the gradient of the monotonic function at any point within the working range is zero. This places a limitation on the usage of the new algorithm and the signal recovery may not be possible in this situation. However, the results show that the scheme could still be used to reduce the distortions caused by a large class of nonlinear sensors. Whenever the necessary and sufficient conditions are violated, it is shown that the algorithm converges to a solution, which is not as distorted as the sensor output. Comparison with another distortion compensation technique demonstrates the fact that the converged solution is the closest possible attainable by any available technique.

Furthermore, Some of the advantages and disadvantages of using nonlinear sensors are investigated. It is shown that whenever noise removal and wide dynamic range coverage are equally important, the use of nonlinear sensors will produce better results. Both objectives can be achieved by designing a sensor such that it has a very high slope near the origin and tapers off rapidly at  $\pm\infty$ . The weaker parts of the signal will get amplified and thus the actual sensor output can be easily distinguishable from low strength noise. It is emphasized that the successful design and implementation of nonlinear sensors simplify the task of preserving sensor linearity, which is very difficult and expensive and requires enormous effort. Furthermore, periodic maintenance and calibration may no longer be required, which is an economic incentive. With accurate sensor model, the distortion caused by monotonic nonlinearity can be completely compensated. Errors occur whenever the model is inaccurate. However, theoretical studies presented suggest that the maximum error due to model inaccuracy has a bound, which proves that algorithm is stable. It is also shown that the convergence parameter can be chosen such that the error is minimal and the algorithm is less sensitive to model uncertainty.

The iterative signal recovery scheme developed is further analyzed and several modifications needed to accommodate various anomalies are proposed. An efficient approach to recover chirp signals from distorted nonlinear sensor measurements is developed. The problem of recovering signals using a nominal sensor model instead of an accurate sensor model is investigated. Bearing in mind that successful development of such an approach will be a tremendous money-saver, several suggestions to initiate this work are provided.

Chapter V is concerned with the fusion of the distorted multiple nonlinear sensor measurements. We have taken the initiative to consider the nonlinearity as an embedded feature of a sensor. Several approaches to fuse the multi-sensor measurements

are proposed and their performance has been demonstrated by illustrative examples. It is shown that the derived fusion algorithms could efficiently extract the true information, which is hidden in the distorted multi-sensor data. It can be easily verified that if complete true information is hidden in the distorted measurements, the algorithms are capable of retrieving it to successfully reproduce the original information. Even though the exact original information is not available in the sensed data, an estimation with reasonable accuracy is possible by blending the multi-source data. If the partial blending is not possible, the sensor scheduling can be done to obtain the closest possible data. In addition, whether the original signal is recovered or not can easily be verified by checking the corresponding cost function value. If the cost function value is zero, it guarantees that the recovered signal is the original. The derived fusion procedures could also be used to compare or evaluate the performance of sensors. A faulty or redundant sensor could easily be identified by checking the optimal sensor schedule. If a particular sensor does not appear anywhere in the schedule, it is faulty or can be removed without affecting the process run. This observation has some interesting consequences. It is evident that repeatedly applying this procedure could minimize the number of sensors to be used and thus help reduce the cost of operation. The main advantage of this fusion scheme is that it could be used as a stand-alone process with no interaction with the other interconnected processes.

The main drawback of one of the fusion procedures is the increased computational load due to the combinatorial nature of solutions generated by the Branch and Bound Method. Implementing this scheme in real time looks remote at this stage and several issues need to be resolved before doing so. Though it is a time consuming process, the solution obtained is reliable and there is no other established technique available to solve this zero-one discrete optimization problem. One possible remedy to resolve this problem is to make use of faster computational resources. To avoid the use of branch

of bound technique, the fusion problem has been reformulated and two optimization based algorithms have been developed to perform the same task. In one approach, the original data is estimated from the multi-sensor measurements by partially blending the data. The relaxation of this constraint leads to the continuous optimization of the error function, which generates the optimal solution at a much faster rate than the discrete optimization. Though this fusion procedure requires that at least one of the sensor models is known *a priori*, it is noted that accurate sensor models may not be necessary to effectively fuse the sensor data. It was shown that a slight variation or error in the sensor model may not have a big impact on the fusion decision. In the other fusion approach, the fusion is done by comparing the confidence measure of each sensor reading. The main idea of this approach is to pick only the reliable data for the fusion and disregard the rest. This is done by assigning confidence measures to all available sensor data and picking the ones that lead the list of confidence measures. An optimization based approach to determine the confidence measures. This fusion procedure requires that sensor models are known *a priori*. However, as data fusion is done by comparing closeness measures of all available data, it is shown that model uncertainty or error within the pre-specified limits may not affect the sensor scheduling.

A new approach to attain a high operating bandwidth using sensor arrays is proposed in chapter VI. It is argued that the design of a single sensor of high bandwidth is not feasible both economically and practically. It is shown that the use of an array of low pass-band sensors is a cost-effective solution to attain a high operating bandwidth. The implementation issues with regard to sensor arrays are detailed and a robust multi-sensor fusion scheme using Frequency Response Methods is proposed. Sensor model uncertainties are considered while developing the implementation scheme and it is discussed that frequency domain loop-shaping techniques

can be used to solve this problem efficiently. Fusion of multi-sensor data can also be done using optimization based approaches if sensor model uncertainties are negligible. In practice, sensor models may not be readily available. This situation limits the application of the above-mentioned approaches. Further investigation of this issue yielded an approach, which utilizes feedback mechanisms to systematically combine the sensor data from the different frequency bands. This scheme does not require sensor models. However, the operating frequency bands of the sensors must be known in order to apply this method.

The techniques developed in this dissertation are further analyzed and their performance are demonstrated by experimental and simulation results in chapter VII.

Some conclusions that can be made based on this research work include:

1. The distortion caused by sensor nonlinearity can be **effectively** compensated if:
  - (a) nonlinear sensor function is monotonic
  - (b) sensor noise is of additive type, that is, sensor input is assumed to be noise-free and sensor noise enters into the picture after nonlinear transformation
2. The distortion caused by sensor nonlinearity may be **partially** compensated when the above requirements are not met.
3. When the distortion caused by nonlinearity cannot be compensated as required by specifications, the use of multiple sensors and the multi-sensor fusion will improve the accuracy of sensor measurements.
4. A high operating bandwidth can be attained by employing an array of low bandwidth pass-band sensors.

## B. Directions for Future Work

The signal recovery method developed in this dissertation is an off-line scheme and cannot be used to recover signals in real time. It was shown that with a suitable choice of the convergence parameter,  $\alpha$ , the iterative schemes given in (4.12) and (4.49) converge in a few steps. In addition, with faster computer resources, this iteration time can be further reduced. However, as time progresses the size of the signals can be very high and therefore iterative schemes may require a longer time to converge than that is expected. A good remedy to this problem is to divide the total time into several low range time segments and to solve the iterative equations in each time segment independently maintaining the continuity of signals. In this case, Short Fourier Transform or Wavelet Transform should replace Fourier Transform. A detailed investigation is necessary to explore the other related issues.

Another approach that may reduce the iteration time, is to obtain the down-sampled version of the signal first and gradually interpolate among the available samples until all samples are obtained. The process of interpolation can be devised such that the smoothing operation is done in several steps. Much work is needed to investigate this possibility.

The signal recovery scheme is developed under the assumption that sensor noise is of additive type and there will be no input noise. This simplifies the development, but seems unrealistic for some applications. As the input side of a sensor is generally inaccessible, filtering out noise is very challenging. This problem is worth investigating further.

When a signal is distorted by non-invertible sensor nonlinearities like dead-band and saturation, it is shown that the original signal may not be exactly reproduced. However, non-quadratic optimization seems to produce better results than that ob-

tained with other standard methods. The main issue with non-quadratic optimization is the existence of multiple solutions and therefore an efficient search algorithm is necessary to identify the global optimal solution. This deficiency will be clearly evident when a large scale non-quadratic optimization problem is solved with a standard software like Matlab, which prematurely terminates the search procedure and settles with most probably an incorrect local solution. In order to successfully test and implement the proposed idea, these issues have to be addressed first.

The proposed idea of using sensor arrays to attain a high bandwidth has great potential and positive benefits for many applications. It should be successful in high bandwidth applications such as flight control, altitude jitter control etc. The implementation schemes are presented just to illustrate this idea and need to be improved before applying them to solve the actual problems. For example, while designing the compensators, there was no bound or constraint enforced on the design of the compensators such as causality, order, coefficients etc. As obtaining large variations in gains are difficult to achieve on a real system, the design process should be reformulated to include these constraints.

Another issue that should be investigated further is the effect of sensor model uncertainties on overall performance of a sensor array. Though this issue is briefly discussed, a large variation of modeling errors may place a major limitation on the implementation of compensators. A systematic investigation is needed to address this issue.

The research work initiated in this dissertation opens up many avenues of exploration. Even though the problems investigated are inspired by common deficiencies found in the feedback control applications, other practitioners and researchers may find the developed tools very useful. Feedback control, signal and image processing, pattern recognition, medical sensing applications, automobile technology, manufac-

turing and control of processes, robotics and altitude jitter control are some of the areas that will directly benefit from the results of this dissertation.



## REFERENCES

- [1] J. E. Brignell and N. White, *Intelligent Sensor Systems*. Techno House, Redcliffe Way, Bristol, United Kingdom: Institute of Physics Publishing, 1996.
- [2] J. E. Brignell, "Interfacing solid state sensors with digital systems," *Journal of Phys. E. Sci. Instrum.*, vol. 18, pp. 559–565, 1985.
- [3] A. M. Tekalp and G. Pavlovic, "Image restoration with multiplicative noise: Incorporating the sensor nonlinearity," *IEEE Transactions on Signal Processing*, vol. 39, no. 9, pp. 2132–2136, 1991.
- [4] W. Martin, "High dynamic cmos image sensors," *G.I.T. Imaging and Microscopy*, pp. 26–28, 2001.
- [5] C. O. Nwagboso, Ed., *Automotive Sensory System*. New York: Chapman & Hall, 1993.
- [6] E. Udd, Ed., *Fiber Optic Sensors: An Introduction for Engineers and Scientists*. New York: John Wiley and Sons, 1991.
- [7] M. Kothari, J. G. Webster, W. J. Tompkins, J. J. Wertsch, and P. B. y Rita, "Capacitive sensors for measuring the pressure between the foot and shoe," in *Proc. Annual International Conference of the IEEE Engineering in Medicine and Biology Society*, New Orleans, LA, 1988, pp. 805–806.
- [8] M. Algrain, "Gyroless line-of-sight stabilization for pointing and tracking systems," *SPIE Optical Engineering*, vol. 33, no. 4, pp. 1255–1260, 1994.

- [9] G. C. Loney, "Design and performance of a small two-axis high-bandwidth steering mirror," *SPIE Beam Deflection and Scanning Technologies*, vol. 1454, pp. 198–206, 1991.
- [10] J. Goswami and A. K. Chan, *Fundamental of Wavelets, Algorithms and Applications*. New York: John Wiley and Sons, 1999.
- [11] H. J. Landau and W. L. Miranker, "The recovery of distorted bandlimited signals," *Journal of Mathematical Analysis and Applications*, vol. 2, pp. 97–104, February 1961.
- [12] K. Gröchenig, *Foundations of Time-Frequency Analysis*. Boston, MA: Birkhäuser, 2001.
- [13] M. D. Canon, C. D. Cullum, and E. Polak, *Theory of Optimal Control and Mathematical Programming*. New York: McGraw-Hill, 1969.
- [14] H. G. Heuser, *Functional Analysis*. New York: John Wiley & Sons, Inc., 1982.
- [15] I. W. Sandberg, "Notes on pq theorems," *IEEE Transactions on Circuits and Systems-I: Fundamental Theory and Applications*, vol. 41, no. 4, pp. 303–307, 1994.
- [16] G. D. Zames, "Conservation of bandwidth in nonlinear operations," *Quarterly Progress Report 55*, Cambridge, MA:MIT Research Laboratory of Electronics, 1959.
- [17] H. J. Landau, "On the recovery of a band-limited signal after instantaneous companding and subsequent bandlimiting," *Bell System Technical Journal*, vol. 39, pp. 351–364, March 1960.

- [18] J. Tsimbinos and K. V. Lever, "Nonlinear system compensation based on orthogonal polynomial inverses," *IEEE Transactions on Circuits and Systems: Fundamental Theory and Applications*, vol. 48, no. 4, pp. 406–417, 2001.
- [19] W. Frank, "Compensation of linear and nonlinear sensor distortions by digital post processing," in *Proc. Kongressband Sensor '95*, Nürnberg, Germany, 1995, pp. 889–892.
- [20] T. B. Bakó and T. Dabóczy, "Reconstruction of nonlinearly distorted signals with regularized inverse characteristics," *IEEE Transactions on Instrumentation and Measurement*, vol. 51, no. 5, pp. 1019–1022, 2002.
- [21] J. Scheoukens, R. Pintelon, and T. Dobrowiecki, "Linear modeling in the presence of nonlinear distortions," *IEEE Transactions on Instrumentation and Measurement*, vol. 51, no. 4, pp. 786–792, 2002.
- [22] J. Scheoukens, T. Dobrowiecki, and R. Pintelon, "Parametric and nonparametric identification of linear systems in the presence of nonlinear distortions—a frequency domain approach," *IEEE Transactions on Automatic Control*, vol. 43, no. 2, pp. 176–190, 1998.
- [23] R. W. Schafer, R. M. Mersereau, and M. A. Richards, "Constrained iterative restoration algorithms," *Proceedings of the IEEE*, vol. 69, no. 4, pp. 432–450, 1981.
- [24] D. Preis and H. Polchlopek, "Restoration of nonlinearly distorted magnetic recordings," *Journal of Audio Engineering Society*, vol. 32, no. 1/2, pp. 26–30, 1984.

- [25] S. A. White, "Restoration of nonlinearly distorted audio by histogram equalization," *Journal of Audio Engineering Society*, vol. 30, no. 11, pp. 828–832, 1982.
- [26] W. Klippel, "Modeling the nonlinearities in horn loudspeakers," *Journal of Audio Engineering Society*, vol. 44, no. 6, pp. 470–480, 1996.
- [27] J. S. Baras and A. Bensoussan, "Optimal sensor scheduling in nonlinear filtering of diffusion processes," *SIAM Journal on Control and Optimization*, vol. 27, no. 2, pp. 786–814, 1989.
- [28] *LabVIEW Measurement Manual*, 322661A-01, Austin, TX, National Instruments, 2000.
- [29] C. R. Dohrmann, "A dynamic programming approach to smoothing and differentiating data with splines," M.S. thesis, The Ohio State University, Columbus, Ohio, 1986.
- [30] P. K. Varshney, "Multisensor data fusion," *Electronics and Communication Engineering Journal*, pp. 245–253, 1997.
- [31] R. C. Luo, C. C. Yih, and K. L. Su, "Multisensor fusion and integration: Approaches, applications, and future research directions," *IEEE Sensors Journal*, vol. 2, no. 2, pp. 107–119, 2002.
- [32] R. C. Luo and K. L. Su, "A review of high-level multisensor fusion: Approaches and applications," in *Proc. IEEE International Conference on Multisensor Fusion and Integration for Intelligent Systems*, Taipei, Taiwan, 1999, pp. 25–31.
- [33] R. C. Luo and M. G. Kay, "Multi-sensor integration and fusion in intelligent systems," *IEEE Transactions on Systems, Man, and Cybernetics*, vol. 19, no. 5,

- pp. 901–931, 1989.
- [34] D. L. Hall and J. Llinas, “An introduction to multisensor data fusion,” *Proceedings of IEEE*, vol. 85, pp. 6–23, 1997.
- [35] B. V. Dasarathy, “Paradigms for information processing in multisensor environments,” *Proc. SPIE-Sensor Fusion III: 3-D Perception and Recognition*, vol. 1306, pp. 69–80, 1990.
- [36] R. R. Tenney and N. R. Sandell, “Detection with distributed sensors,” *IEEE Trans. Aerospace and Electronic Systems*, vol. AES-17, no. 4, pp. 98–101, 1981.
- [37] H. J. Kushner and A. Pacut, “A simulation study of a decentralized detection problem,” *IEEE Trans. Automatic Control*, vol. AC-27, no. 5, pp. 1116–1119, 1982.
- [38] D. Teneketzis and P. Varaiya, “The decentralized quickest detection problem,” *IEEE Trans. Automatic Control*, vol. AC-29, no. 7, pp. 641–644, 1984.
- [39] J. N. Tsitsiklis and M. Athans, “On the complexity of decentralized decision making and detection problems,” *IEEE Trans. Automatic Control*, vol. AC-30, no. 5, pp. 440–446, 1985.
- [40] Z. Chair and P. K. Varshney, “Optimal data fusion in multiple sensor detection systems,” *IEEE Trans. Aerospace and Electronic Systems*, vol. AES-22, no. 1, pp. 98–101, 1986.
- [41] I. Y. Hoballah and P. K. Varshney, “Neyman-pearson detection with distributed sensors,” in *Proc. IEEE Conf. Decision and Control*, Athens, Greece, 1986, pp. 237–241.

- [42] S. C. A. Thomopoulos and N. N. Okello, "Distributed detection with consulting sensors and communications cost," *Proc. SPIE-Sensor Fusion*, vol. 931, pp. 31–40, 1988.
- [43] L. Izzo and L. Paura, "Comments on 'optimal detection and performance of distributed sensor system'," *IEEE Trans. Aerospace and Electronic Systems*, vol. AES-25, no. 1, pp. 113–114, 1989.
- [44] A. R. Reibman and L. W. Nolte, "Optimal detection and performance of distributed sensor system," *IEEE Trans. Aerospace and Electronic Systems*, vol. AES-23, no. 6, pp. 789–797, 1987.
- [45] M. Barkat and P. K. Varshney, "Decentralized CFAR signal detection," *IEEE Trans. Aerospace and Electronic Systems*, vol. AES-25, no. 2, pp. 141–149, 1989.
- [46] V. Aalo and R. Viswanathan, "On distributed detection with correlated sensors: Two examples," *IEEE Trans. Aerospace and Electronic Systems*, vol. AES-25, no. 3, pp. 414–421, 1989.
- [47] C. C. Lee and J. J. Chao, "Optimum local decision space partitioning for distributed detection," *IEEE Trans. Aerospace and Electronic Systems*, vol. AES-25, no. 4, pp. 536–544, 1989.
- [48] K. Demirbas, "Distributed sensor data fusion with binary decision trees," *IEEE Trans. Aerospace and Electronic Systems*, vol. AES-25, no. 5, pp. 643–649, 1989.
- [49] I. Y. Hoballah and P. K. Varshney, "An information theoretic approach to the distributed detection problem," *IEEE Trans. Information Theory*, vol. IT-35, no. 5, pp. 988–994, 1989.

- [50] Z. B. Tang, K. R. Pattipati, and D. L. Kleinman, "A distributed  $m$ -ary hypothesis testing problem with correlated observations," in *Proc. IEEE Conf. Decision and Control*, Tampa, FL, 1989, pp. 562–568.
- [51] R. Krzysztofowicz and D. Long, "Fusion of detection probabilities and comparison of multisensor systems," *IEEE Trans. Systems, Man, and Cybernetics*, vol. SMC-20, no. 3, pp. 665–677, 1990.
- [52] H. Tahani and J. M. Keller, "Information fusion in computer vision using the fuzzy integral," *IEEE Trans. Systems, Man, and Cybernetics*, vol. SMC-20, no. 3, pp. 733–741, 1990.
- [53] H. Wang and L. Cai, "On adaptive multiband signal detection with the SMI algorithm," *IEEE Trans. Aerospace and Electronic Systems*, vol. AES-26, no. 5, pp. 768–773, 1990.
- [54] R. Srinivasan, "Distributed detection with decision feedback," *IEE Proceedings*, vol. 137, no. 6, pp. 427–432, 1990.
- [55] J. D. Papastavrou and M. Athans, "Distributed detection by a large team of sensors in tandem," in *Proc. IEEE Conf. Decision and Control*, Honolulu, HI, 1990, pp. 246–251.
- [56] D. Kazakos, V. C. Vannicola, and M. Wicks, "Asymptotic performance of a class of multisensor memoryless detectors," in *Proc. IEEE Conf. Decision and Control*, Honolulu, HI, 1990, pp. 2704–2709.
- [57] J. Han, P. K. Varshney, and V. C. Vannicola, "Some results on distributed nonparametric detection," in *Proc. IEEE Conf. Decision and Control*, Honolulu, HI, 1990, pp. 2698–2703.

- [58] M. Barkat and P. K. Varshney, "Adaptive cell-averaging CFAR detection in distributed sensor networks," *IEEE Trans. Aerospace and Electronic Systems*, vol. AES-27, no. 3, pp. 424–429, 1991.
- [59] M. Kam, W. Chang, and Q. Zhu, "Hardware complexity of binary distributed detection systems with isolated local bayesian detectors," *IEEE Trans. Systems, Man, and Cybernetics*, vol. SMC-21, no. 3, pp. 565–571, 1991.
- [60] E. Drakopoulos and C. C. Lee, "Optimum multisensor fusion of correlated local decisions," *IEEE Trans. Aerospace and Electronic Systems*, vol. AES-27, no. 4, pp. 593–605, 1991.
- [61] R. Mallubhatla, K. R. Pattipati, D. L. Kleinman, and Z. B. Tang, "A model of distributed team information processing under ambiguity," *IEEE Trans. Systems, Man, and Cybernetics*, vol. SMC-21, no. 4, pp. 713–725, 1991.
- [62] W. A. Hashlamoun and P. K. Varshney, "An approach to the design of distributed Bayesian decision structures," *IEEE Trans. Systems, Man, and Cybernetics*, vol. SMC-21, no. 5, pp. 1206–1211, 1991.
- [63] K. D. Donohue and N. M. Bilgutay, "OS characterization for local CFAR detection," *IEEE Trans. Systems, Man, and Cybernetics*, vol. SMC-21, no. 5, pp. 1212–1216, 1991.
- [64] J. D. Papastavrou and M. Athans, "Distributed detection by a large team of sensors in tandem," *IEEE Trans. Aerospace and Electronic Systems*, vol. AES-28, no. 3, pp. 639–653, 1992.
- [65] M. Kam, Q. Zhu, and W. S. Gray, "Optimal data fusion of correlated local decisions in multiple sensor detection systems," *IEEE Trans. Aerospace and*



- Electronic Systems*, vol. AES-28, no. 3, pp. 916–920, 1992.
- [66] C. Chui and G. Chen, *Kalman Filtering with Real-Time Applications*, ser. Springer Series in Information Sciences. New York: Springer-Verlag, 1987, vol. 17.
- [67] Y. Gao and H. F. Durrant-Whyte, “Multi-sensor fault detection and diagnosis using combined qualitative and quantitative techniques,” in *Proc. IEEE International Conference on Multisensor Fusion and Integration for Intelligent Systems*, Las Vegas, NV, 1994, pp. 43–50.
- [68] S. Cooper and H. F. Durrant-Whyte, “A frequency response method for multi-sensor high-speed navigation systems,” in *Proc. IEEE International Conference on Multi-sensor Fusion and Integration for Intelligent Systems*, Las Vegas, NV, 1994, pp. 1–8.
- [69] W. Wen and H. F. Durrant-Whyte, “Model-based multi-sensor data fusion,” in *Proc. International Conference on Robotics and Automation*, Nice, France, 1992, pp. 1720–1726.
- [70] S. J. Julier, J. K. Uhlmann, and H. F. Durrant-Whyte, “A new approach for filtering nonlinear systems,” in *Proc. American Control Conference*, Seattle, WA, 1995, pp. 1628–1632.
- [71] H. F. Durrant-Whyte and J. J. Leonard, “Navigation by correlating geomatic sensor data,” in *Proc. IEEE/RSJ International Workshop on Intelligent Robots and Systems*, Tsukuba, Japan, 1989, pp. 440–447.
- [72] C. Harris, A. Bailey, and T. Dodd, “Multi-sensor data fusion in defence and aerospace,” *Journal of Royal Aerospace Society*, vol. 162, no. 1015, pp. 229–244,

- 1998.
- [73] F. Martinerie, “Data fusion and tracking using hmms in a distributed sensor network,” *IEEE Transactions on Aerospace and Electronic Systems*, vol. 33, no. 1, pp. 11–28, 1997.
- [74] M. Stevens and J. Beveridge, “Precise matching of 3d target models to multi-sensor data,” *IEEE Transactions on Image Processing*, vol. 6, no. 1, pp. 126–142, 1997.
- [75] H. Wang, M. Kung, and T. Lin, “Multimodel adaptive Kalman filter design for manoeuvring target tracking,” *International Journal of Systems Science*, vol. 25, no. 11, pp. 2039–2046, 1994.
- [76] Y. Bar-Shalom and L. Campo, “The effect of the common process noise on the two-sensor fused-track covariance,” *IEEE Transactions on Aerospace and Electronic Systems*, vol. 22, no. 6, pp. 803–805, 1986.
- [77] Y. Bar-Shalom and T. Fortmann, *Tracking and Data Association*, ser. Mathematics in Science and Engineering Series. New York: Academic Press Inc., 1988, vol. 179.
- [78] Y. Bar-Shalom and X. Li, *Estimation and Tracking: Principles, Techniques, and Software*. Norwood, MA: Artech House, 1993.
- [79] ———, *Multitarget-Multisensor Tracking: Principles and Techniques*. Storrs, CT: YBS Publishing, 1995.
- [80] S. Shekhar, O. Khatib, and M. Shimojo, “Object localization with multiple sensors,” *The International Journal of Robotics Research*, vol. 7, no. 6, pp. 34–44, 1988.

- [81] R. O. Eason and R. C. Gonzalez, *Data Fusion in Robotics and Machine Intelligence*, M. A. Abidi and R. C. Gonzalez, Eds. New York: Academic Press, Inc., 1992.
- [82] B. R. Bracio, W. Horn, and D. P. F. Moller, "Sensor fusion in biomedical systems," in *Proc. Annual International Conference of the IEEE Engineering in Medicine and Biology Society*, vol. 3, Chicago, IL, 1997, pp. 1387–1390.
- [83] T. Kohonen, *Self-Organization and Associate Memory*. New York: Springer-Verlag, 1988.
- [84] D. L. Hall, *Mathematical Techniques in Multisensor Data Fusion*. Norwood, MA: Artech House, 1992.
- [85] S. C. A. Thomopoulos, "Data fusion system design and adaptive control," *Journal of Robotic Systems*, vol. 7, no. 3, pp. 337–372, 1990.
- [86] J. A. Stover, D. L. Hall, and R. E. Gibson, "A fuzzy-logic architecture for autonomous multisensor data fusion," *IEEE Transactions on Industrial Electronics*, vol. 43, no. 3, pp. 403–410, 1996.
- [87] A. Bloch, "Information combination operators for data fusion: A comparative review with classification," *IEEE Trans. Systems, Man, and Cybernetics*, vol. SMC-26, no. 1, pp. 52–67, 1996.
- [88] X. E. Gros, Ed., *NDT Data Fusion*. New York: John Wiley and Sons, 1997.
- [89] R. R. Murphy, "Dempster-shafer theory for sensor fusion in autonomous mobile robots," *IEEE Trans. Robotics and Automation*, vol. 14, no. 2, pp. 197–206, 1998.

- [90] S. G. Goodridge, M. G. Kay, and R. C. Luo, "Multilayered fuzzy behavior fusion for real-time reactive control of systems with multiple sensors," *IEEE Trans. Industrial Electronics*, vol. 43, no. 3, pp. 387–394, 1996.
- [91] T. A. Runkler, M. Sturm, and H. Hellendoorn, "Model based sensor fusion with fuzzy clustering," in *Proc. IEEE International Conference on Fuzzy Systems*, Anchorage, AK, 1998, pp. 1377–1382.
- [92] M. L. Wong, W. Lam, and K. S. Leung, "Using evolutionary programming and minimum description length principle for data mining of Bayesian networks," *IEEE Trans. Pattern Analysis and Machine Intelligence*, vol. 21, no. 2, pp. 174–178, 1999.
- [93] H. Bischof and A. Leonardis, "Finding optimal neural networks for land use classification," *IEEE Trans. Geoscience and Remote Sensing*, vol. 36, no. 1, pp. 337–341, 1998.
- [94] S. G. Goodridge, M. G. Kay, and R. C. Luo, "Sensor fusion and planning with perception-action network," *Journal of Intelligent and Robotics Systems: Theory & Applications*, vol. 19, no. 3, pp. 271–198, 1997.
- [95] R. Joshi and A. C. Sanderson, "Minimal representation multisensor fusion using differential evolution," *IEEE Transactions on Systems, Man, and Cybernetics-Part A: Systems and Humans*, vol. 29, no. 1, pp. 63–76, 1999.
- [96] S. Suranthiran and S. Jayasuriya, "A filtering methodology to recover signals distorted by sensor nonlinearity," in *Proc. Japan-USA Symposium on Flexible Automation*, Hiroshima, Japan, 2002, pp. 1027–1034.

- [97] —, “Filtering of signals distorted by sensor nonlinearity,” in *Proc. IFAC Conference on Mechatronic Systems*, Berkeley, CA, 2002, pp. 538–543.
- [98] —, “Signal recovery and noise removal with memory-less nonlinear sensors,” in *Proc. American Control Conference*, Denver, CO, 2003, pp. 4155–4160.
- [99] —, “Distortion analysis of memory-less nonlinear sensors,” in *Proc. International Mechanical Engineering Congress & Exposition (IMECE)*, Washington, DC, 2003.
- [100] —, “Signal conditioning with memory-less nonlinear sensors,” *Journal of Dynamic Systems, Measurement and Control*, June 2004, in press.
- [101] —, “Recovery of signals distorted by sensor nonlinearity,” *Journal of Dynamic Systems, Measurement and Control*, in press.
- [102] S. Jayasuriya and R. Langari, “Nonlinear filtering of signals exhibiting large fluctuations in strength,” in *Proc. ASME International Mechanical Engineering Congress and Exposition (IMECE)*, Atlanta, GA, Nov. 1996, pp. 159–163.
- [103] J. J. Friedmann, E. Fishler, and H. Messer, “Consistent estimation of signal parameters in non-stationary noise,” in *Proc. Tenth IEEE Workshop on Statistical Signal and Array Processing*, Pocono Manor, PA, 2000, pp. 225–228.
- [104] B. Vidaković and P. Müller, *Wavelets for Kids*. Durham, NC: Institute of Statistics and Decision Sciences, Duke University, 1991.
- [105] J. G. Proakis and D. G. Manolakis, *Digital Signal Processing*. Upper Saddle River, NJ: Prentice Hall, Inc., 1996.
- [106] S. Suranthiran, “Control with non-quadratic criteria,” M.S. thesis, University of Cambridge, Cambridge, England, December 1997.

- [107] A. N. Tikhonov and V. Y. Arsenin, *Solutions of Ill-posed Problems*. Washington, DC: V. H. Winston & Sons, 1977.
- [108] P. C. Hansen, “Numerical tool for analysis and solution of fredholm integral equations of the first kind,” *Inverse Problems*, vol. 8, pp. 849–872, 1992.
- [109] S. Suranthiran and S. Jayasuriya, “Optimal scheduling and filtering of distorted multi-sensor data,” in *Proc. ASME International Mechanical Engineering Congress & Exposition (IMECE)*, New Orleans, LA, 2002.
- [110] —, “Optimal detection of band-limited signal by multiple nonlinear sensor data fusion,” in *Proc. American Control Conference*, Denver, CO, 2003, pp. 4161–4166.
- [111] —, “Effective fusion of distorted multi-sensor data,” in *Proc. IEEE International Symposium on Intelligent Control*, Houston, TX, 2003, pp. 444–449.
- [112] —, “Optimal fusion of multiple nonlinear sensor data,” *IEEE Sensors Journal*, in press.
- [113] G. L. Nemhauser and L. D. Wolsey, *Integer and Combinatorial Optimization*. New York: John Wiley & Sons, Inc, 1988.
- [114] J. P. Ignizio, *Linear Prgramming in Single & Multiple-Objective Systems*. Upper Saddle River, NJ: Prentice-Hall, Inc., 1982.
- [115] S. Suranthiran and S. Jayasuriya, “Utilizing sensor arrays to attain high operating bandwidth,” *Journal of Dynamic Systems, Measurement and Control*, June 2004, in press.

- [116] ———, “Attaining high operating bandwidth using sensor arrays and frequency domain methods,” in *Proc. IEEE Conference on Decision and Control*, Maui, HI, 2003, pp. 4208–4213.
- [117] O. Yaniv, *Quantitative Feedback Design of Linear and Nonlinear Control Systems*. Norwell, MA: Kluwer Academic Publishers, 1999.
- [118] C. Borghesani, Y. Chait, and O. Yaniv. (2003) Qft frequency domain control design toolbox. [Online]. Available: <http://www.terasoft.com/products/qft/>
- [119] A. E. Bentley, “Pointing control design for a high precision flight telescope using quantitative feedback theory,” *International Journal of Robust and Nonlinear Control*, vol. 11, pp. 923–960, 2001.
- [120] T. D. Binnie, H. J. Weller, Z. He, and D. Setiadi, “An integrated 16/spl times/16 pvdF pyroelectric sensor array,” *IEEE Transactions on Ultrasonics, Ferroelectrics and Frequency Control*, vol. 47, no. 6, pp. 1413–1420, 2000.
- [121] A. Jeremic and A. Nehorai, “Design of chemical sensor arrays for monitoring disposal sites on the ocean floor,” *IEEE Journal of Oceanic Engineering*, vol. 23, no. 4, pp. 334–343, 1998.
- [122] F. Yalcinkaya, D. P. Atherton, H. Calls, and E. T. Powner, “Intelligent sensors: The way forward to decentralized intelligence and control,” in *Proc. UKACC Intelligent Conference on Control and Systems*, Swansea, United Kingdom, 1998, pp. 358–363.
- [123] E. T. Powner and F. Yalcinkaya, “Design of chemical sensor arrays for monitoring disposal sites on the ocean floor,” *IEEE Journal of Oceanic Engineering*, vol. 15, no. 4, pp. 19–22, 1995.

- [124] F. Yalcinkaya, E. T. Powner, and N. F. Rocks, “An intelligent multi-sensing sensor-array,” in *Proc. IEE Colloquium on Intelligent Sensors*, Leicester, United Kingdom, 1996, pp. 2/1–2/4.
- [125] D. E. Gustafson and W. C. Kessel, “Fuzzy clustering with a fuzzy covariance matrix,” in *Proc. IEEE Conference on Decision and Control*, San Diego, CA, 1979, pp. 761–766.
- [126] R. Babusha and H. B. Vebruggen, “Identification of composite linear models via fuzzy clustering,” in *Proc. European Control Conference*, Rome, Italy, 1995, pp. 1207–1212.
- [127] I. Daubechies, *Ten Lectures on Wavelets*, ser. CBMS-NSF Regional Conference Series In Applied Mathematics. Philadelphia, PA: Society for Industrial and Applied Mathematics, 1992, vol. 61.



## VITA

Suranthiran Sugathevan was born in Jaffna, Sri Lanka. He received a Bachelor of Science of Engineering First Class Honors degree from the University of Peradeniya, Sri Lanka in 1994 with a major in mechanical engineering. He received his Master of Science degree in control engineering from the University of Cambridge, England in 1997. He entered Texas A&M University in January 2001. He received his PhD in May, 2004.

From 1998 to 2000, he was in industry working mostly on hard disk drive product enhancement projects. His current research interests include controls, health monitoring and fault detection, intelligent systems, sensor arrays, sensor networks and signal processing. His permanent address is: 51  $\frac{1}{2}$ , Collingwood Place, Colombo-06, Sri Lanka.

The typist for this dissertation was Suranthiran Sugathevan.